Thermal Conversion of Deasphalted Oil at Low Temperature

by

Javier Castillo Lugo

A thesis submitted in partial fulfillment of the requirements for the degree of

Master of Science

in

Chemical Engineering

Department of Chemical and Materials Engineering

University of Alberta

ABSTRACT

Canada has one of the largest oil reserves in the world, with around 3 trillion ultimate reserves in heavy oil. Even though, one of the major difficulties that Canadian Oil sands industry has faced over time is the transportation of bitumen due to its extremely high viscosity.

Having this in mind, the concept of field upgrading process developed by Nexen Energy ULC suggests a middle thermal conversion process as the main conversion unit in the field upgrader in order to reduce the viscosity and enable to meet the pipeline transport specification. Thermal cracking of industrial deasphalted vacuum residue from the Nexen Long Lake upgrader were carried at low reaction temperature (280 - 408 °C) in order to gain a deeper understanding of the changes that heavy oil experiences during milder conversion processes. It was found that although there was not significant change in viscosity at thermal conversion reactions below 360 °C, an increase in the asphaltene content was observed even at low temperature, namely 280 °C. On the other hand, practically useful cracking conversion and viscosity reduction for upgrading was found only at 360 and 400 °C. The viscosity measured at 40 °C could be reduced by three orders of magnitude from 3720 Pa·s in the feed to 2 to 5 Pa·s in the product. The density of the product was not reduced by much, despite vacuum residue cracking conversions of 33 % at 360 °C and 45–47 % at 400 °C before the onset of coking. The liquid yield was 88–89 %. Vacuum residue conversion at 360 °C increased linearly with time, which indicated zero order kinetics. Vacuum residue conversion at 400 °C was non-zero order. This study showed that thermal cracking at 360–400 °C is better described by a rate equation with two terms. Temperature dependent differences in the maximum conversion before onset of coking, and the kinetic description of vacuum residue conversion, indicated that the equivalent residence time (ERT) description of visbreaking was an inadequate approximation of thermal conversion at 400 °C and below.

Keywords: Visbreaking, viscosity, thermal conversion, oil sands bitumen, deasphalted oil

To my grandmother…

Irida

ACKNOWLEDGEMENTS

This work would not have been possible without the support, invaluable advices, and infinite patience of my supervisor, Dr. Arno de Klerk. Thanks Arno, you have set an example of excellence to me. I will forever be indebted to you.

I extend my gratefulness to my lab group member and friends, with whom I have shared many discussions and give unconditional support. Among the many, they are Natalia Montoya, Cloribel Santiago, Isabel Penaloza, Cibele Melo Halmenschlager, Tudor Apan, and Giselle Uzcategui.

Thanks for the generous financial support from Nexen energy ULC.

I would especially like to thank my family for the love, support, and constant encouragement I have gotten over the years. In particular, I would like to thank my brother Andres for sharing many adventures together in our new home Canada. To my mother Carmen, who has always stood by my side giving me her unconditional words to keep me up along this path. To my father who taught me so many valuable lessons about life.

Finally, I would like to dedicate this thesis to my grandmother, Irida. You are my role model, you inspire me to be a better person every day, and grow without any barriers. I love you.

TABLE OF CONTENTS

LIST OF TABLES

LIST OF FIGURES

1. INTRODUCTION

1.1 Introduction

Canada has one of the largest oil reserves in the world. Bitumen, the oil part in the oil sands, is considered the heaviest fraction of petroleum. At the temperatures normally encountered in natural deposits, bitumen will not flow; in order to be moved through a pipeline, it must be heated and in some cases, diluted with a lighter oil. Bitumen contains mainly large hydrocarbon molecules classified as asphaltenes and resins, which are responsible of its high density and viscosity. In addition, it has a high content of metals, such as nickel and vanadium, and heteroatoms such as nitrogen, oxygen, and sulfur.

According to the Canadian Association of Petroleum Producers (CAPP), Canada's crude oil supply is forecasted to grow from 3.85 million barrels per day (B/D) in 2016 to 5.12 million B/D by 2030 [1], and oil sands will be the main driver for this production growth. The success of Canada's energy future relies on the ability to overcome market uncertainties. One of the major difficulties that the Canadian Oil sands industry has faced over time is the transportation of bitumen to the refineries given that bitumen deposits are located in remote areas, in northern Alberta. In addition, bitumen has an extremely high viscosity (over 10^3 Pa.s at 20 °C) which is why some form of dilution or treatment is required for it to be pumped through the pipelines.

Nowadays, dilution and upgrading are the two main strategies implemented when producing bitumen that is suitable for pipeline transport. Dilution is less capital intensive; however, it is a less-efficient and expensive way of solving this issue given that the cost of the diluent is already about 25 % higher than of light sweet crude [2], and because it reduces the effectiveness of the pipeline capacity.

Upgrading of bitumen is capital intensive and frequently associated with liquid volume loss. Over the years, a number of technologies have been developed for heavy crude and residue oil upgrading, which include processes that are based on carbon rejection, hydrogen addition and combination of both routes [3]. Carbon rejection processes represent the most common and

attractive option due to their relatively lower costs. However, carbon-rejection processes typically have a substantial reduction in liquid volume yield, since part of the crude is converted into solid coke or asphaltenes, which has little or no value in the market.

One of the cheapest processes that can be used to reduce the viscosity of heavy oil is Visbreaking. It is the oldest refining technology, which involves the mild thermal cracking of the heavy oil to reduce its viscosity to such level that it allows the products to meet fuel oil specifications [4]. Visbreaking process is conducted under temperatures of 430 to 490 °C at a short residence time, which avoids coking reactions [5]. The thermal cracking involves the decomposition of molecules to yield products that are of a lower molecular mass than the feed. The conversion of these molecules occur by homolytic bond dissociation, and resulting reactions follow free-radical chemistry. In a thermal conversion process the reactions are time and temperature dependent. However, oil sands bitumen does not follow a typical behaviour of viscosity reduction with respect to temperature and time, and the operating conditions can be less severe [4, 6].

During visbreaking, the extent of feedstock conversion and hence the decrease in viscosity is limited by coke formation [7]. Thus, if one can reduce the asphaltene content, which is postulated to be the main coke precursor in the feedstock, as well as suppress the detrimental reactions that create new asphaltenes during thermal cracking, a higher level of conversion and thereby a lower viscosity of the product can be achieved.

Asphaltenes are referred as the heaviest and most polar molecules, and are often considered to be the solubility class primarily responsible for the high viscosity of the heavy oil and bitumen, in which a high weight percentage of asphaltenes in Canadian bitumen (typically higher than 15 wt. %) interferes with its transport from the production areas due to the high viscosities seen at typical handling temperatures. The high impact on bitumen viscosity is mainly attributed to the colloidal behavior of asphaltenes to create aggregates, which cause an increase in the viscosity [8].

Dehkissia et al [8] suggest that deasphalting alone is not an efficient option for reducing viscosity to the recommended specification, since other crude constituents such as resins (polars), and polyaromatics contained in the maltenes fractions contribute to the higher viscosity of bitumen. Thus, deasphalting bitumen, eventually followed by partial upgrading through thermal treatment, would be required to allow crude oil transportation by pipeline.

There is limited information on the structure-rheology-conversion relationship of deasphalted oil (DAO), how the constituents found in the maltenes fractions contribute to the oil viscosity, as well as the creation of new asphaltenes during the thermal cracking, and on whether these constituents govern the temperature-viscosity response of DAO.

The present study examines the visbreaking unit in the BituMax^{TM} field upgrading process developed by Nexen Energy ULC (figure 1.1). According to the field upgrader concept, bitumen is initially treated so it is separated from dissolved gas, salt, water, solids and the asphaltene fraction, which is precipitated in a paraffinic solvent deasphalting unit; the product obtained is a de-asphalted or partially deasphalted oil (DAO) [9]. The degree of deasphalting depends on the type of paraffinic solvent, paraffinic solvent:heavy oil ratio, as well as the operating conditions such as temperature, pressure [5]. The low asphaltenes content heavy oil (DAO) is upgraded in a thermal cracking (visbreaking) process in order to decrease the oil viscosity to meet pipeline specifications (viscosity of < 350 cSt at 7.5 °C, density of > 19 °API (< 940 kg·m^{-3}) [2]).

The main conversion unit in the field upgrader is the thermal cracker, i.e. visbreaking unit; its performance is the main theme of this applied research work.

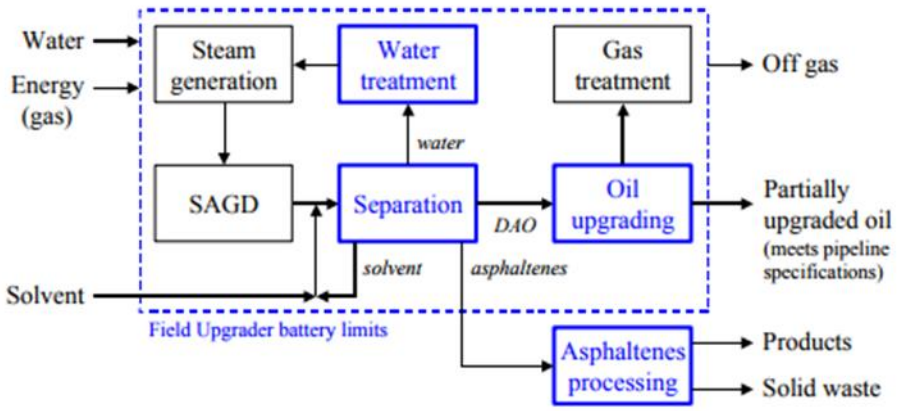

Figure 1.1. Generic process flow diagram of a Field Upgrader [9]

By deasphalting heavy oil before thermal cracking, a higher level of conversion and thereby a lower viscosity of the product can be obtained. Nonetheless, a deeper understanding on the changes that heavy oil experiences during milder conversion processes is required to better understand the antecedents of its performance at high conversion. In order to describe these changes, the time dependent conversion of DAO from the Nexen Long Lake upgrader was investigated at different temperatures in the range 280 to 400 °C. The temperature range, although lower than the intended temperature of industrial operation, was purposefully selected in order to determine the changes that occur at lower conversion. It is expected that this information would also be useful for modelling by extending the data available for modelling to lower conversion. Work related to this topic was performed by Cabrales-Navarro and Pereira-Almao, in which thermal cracking of deasphalted vacuum residue was carried out in a bench scale pilot plant at temperatures within the interval 380 - 423 °C to obtain a kinetic model of DAO upgrading.

It was also of interest to explore a temperature range of visbreaking operation between 280 °C to 400 °C with deasphalted oil, from an academic point of view, which has not been investigated in detail. Although low temperatures may not lead to a practical benefit, material processed at higher temperatures must still pass through the lower temperature range during heating. Therefore, the academic justification had some practical value as well.

Moreover, it was of great interest to understand those changes experienced in the heavy molecular-weight components during thermal cracking, which promote the formation of paramagnetic centers with stable free radicals character. Previous studies suggested that these paramagnetic centers are responsible for the association of polycondensed aromatic cores (asphaltenes) that eventually lead to phase separation and coke formation [11].

Hence, the identification and tracking of free radical species using electron paramagnetic resonance (EPR) spectroscopy will offer insights into the genesis of this species and nature of the aromatic rings condensation during thermal conversion of heavy oil.

1.2 OBJECTIVE

The objective of this study was to examine and understand the changes the industrial deasphalted heavy oil experienced over time when exposed to temperatures in the range 280 °C to 400 °C.

1.3 SCOPE OF WORK

In order to gain insight into deasphalted heavy oil thermal conversion behaviour and the changes that could be expected, it was necessary to review proper literature related to this work. The literature review facilitated an understanding on the characteristics of the feed and the mechanism by which thermal cracking takes place. A review of current process technologies used in industry (specifically visbreaking) was also conducted.

The experimental chapters will examine and discuss the conversion of deasphalted oil at different temperatures with reaction time. The thermal cracking experiments were performed in batch mode and the feed and products were characterized.

The set of experiments previously mentioned are described:

A. Storm et al [12] suggested that organized group of molecules (micelles) form and flocculate from non-asphaltenic fraction when it is heated above 285 °C, creating a microstructure conductive to coke formation at high temperature. In addition, previous studies [6][13][14] found that a reduction in temperature down to 250 °C during

visbreaking oilsands-derived bitumen bring about changes that may improve bitumen properties. Based on this, two sets corresponds to those experiments were performed at 280°C and 320 °C respectively, an initial pressure of 3 MPa and a variation of reaction time between 10 and 360 minutes. This work is shown in Chapter 3. Significant changes and a high conversion were not expected to occur due to the low temperature, and only the most reactive bonds would dissociate at those temperatures.

B. In Chapter 4 the temperature was increased to 360 °C for the third set of experiments. These experiments were conducted with an initial pressure of 3 MPa, varying the reaction time from 20 to 360 minutes. This temperature was selected for study because it represents the temperature threshold for thermal decomposition is caused to proceed at a significant rate [15].

C. Chapter 5 discusses the results obtained from visbreaking of deasphalted vacuum residue at 400°C, 3 MPa and a reaction time in the range of 10-90 minutes. This temperature was selected in order to gain understanding about the reactivity of deasphalted heavy oil (DAO), as well as the formation of pentane insoluble asphaltenes at moderate temperature, namely 400°C.

D. Chapter 6 will be the last experimental section. There will be presented a set of reactions were carried out at 408°C and 11.43 min so that there is a point of reference to account for difference in the reactor configuration and absence of steam during the micro-batch testing and the laboratory pilot testing. This enables the present study to be integrated with the proprietary industrial investigations being conducted.

Lastly, overall conclusions and recommendations for future work based on the results in all the experimental sections will be presented in Chapter 7.

Literature cited

[1] Canadian Association of Petroleum Producers. 2017 CAPP Crude Oil Forecast, Markets & Transportation [Online access]. Publication # 2017-0009. http://www.capp.ca/ publications-and-statistics/publications/303440. (accessed Aug 10, 2017)

[2] Banerjee, D. K. *Oil sands, heavy oil, & bitumen: from recovery to refinery*; PennWell Corp.: Tulsa, Oklahoma, 2012.

[3] Castaneda, L.; Munoz, J.; Ancheyta, J. Current situation of emerging technologies for upgrading of heavy oils. *Catal. Today* **2014**, 220-222, 248-273.

[4] Speight, J.G. *The chemistry and technology of petroleum*, 4th Edition; Taylor & Francis Group: Boca Raton, FL, 2007.

[5] Speight, J. G. Visbreaking: A technology of the past and the future. *Sci. Iran.* **2012**, *19*(3), 569-573.

[6] Wang, L.; Zachariah, A.; Yang, S.; Prasad, V.; De Klerk, A. Visbreaking oilsands-derived bitumen in the temperature range of 340-400 °C. *Energy Fuels* **2014**, *28*, 5014-5022.

[7] Joshi, J. B.; Pandit, A. B.; Kataria, K. L.; Kulkarni, R. P.; Sawarkar, A. N.; Tandon, D.; Ram, Y.; Kumar, M. M. Petroleum residue upgrading via visbreaking: A review. *Ind. Eng. Chem. Res.* **2008**, *47*, 8960-8988.

[8] Dehkissia, S.; Larachi, F.; Rodriguez, D.; Chornet, E. Characterization of Doba–Chad heavy crude oil in relation with the feasibility of pipeline transportation. *Fuel* **2004**, *83*(16), 2157-2168

[9] De Klerk, A.; Reques, N. G. Z.; Xia, Y.; Omer, A. A. (Nexen Energy ULC). Integrated central processing facility (CPF) in oil field upgrading (OFU). U.S. Patent 2014/0138287, May 22, 2014.

[10] Cabrales-Navarro, F. A.; Pereira-Almao, P. Reactivity and comprehensive kinetic modeling of deasphalted vacuum residue thermal cracking. *Energy Fuels* **2017**, *31*(4), 4318-4332.

[11] Yen, T. F.; Erdman, J. G.; Saraceno, A. J. Investigation of the nature of free radicals in petroleum asphaltenes and related substances by electron spin resonance. *Anal. Chem.* **1962**, *34*(6), 694-700.

[12] Storm, D. A.; Barresi, R. J.; Sheu, E. Y.; Bhattacharya, A. K.; De Rosa, T. F. Microphase behavior of asphaltic micelles during catalytic and thermal upgrading. *Energy Fuels* **1998**, *12*(1), 120-128.

[13] Wang, L. Low Temperature Visbreaking. MSc Thesis, University of Alberta, Edmonton, AB, Canada, 2013.

[14] Yañez Jaramillo, L. M. Visbreaking of Oilsands Bitumen between 150 and 300 ˚C. MSc Thesis, University of Alberta, Edmonton, AB, Canada, 2016.

[15] Speight, J. G.; Ozum, B. *Petroleum refining processes*; Marcel Dekker, Inc.: New York, 2001, p. 348.

2. LITERATURE REVIEW

2.1 Introduction

Nowadays, demand of lighter liquid oils is increasing, while crude oil becomes heavier. That have been forcing the petroleum industry to combine conventional refining with the production and use of heavy and ultra-heavy crude oils, bitumen, and residuum. Heavier grades of crude including bitumen are among the world's largest resources with estimated reserves of 600 billion barrels even when considering only Venezuela Orinoco belt and Canada Athabasca bitumen [1].

Since this thesis deals with the conversion of material obtained from oilsands bitumen, the characteristics of bitumen and deasphalted heavy oil derived from bitumen will be reviewed. Then the second topic that will be reviewed is the chemistry associated to thermal conversion of heavy oil. The last topic that will be reviewed is visbreaking, which it is the conversion process that is studied in this work.

2.2 Geographic location of Canadian oilsands deposits

Oil sand is defined as a naturally occurring mixture of sand, clay or other minerals, water and bitumen. The oil sands reserves can be found in several locations around the world, including Venezuela, the United States and Russia, and one of the largest deposits lie in northeastern Alberta-Canada [2]. According to the Canadian Energy Research Institute (CERI), Canada has a remaining oil reserve of 168 billion barrels, 97 per cent of which are bitumen deposits located in the oil sands of Alberta [3]. Three main deposits can be distinguished: Athabasca (Wabasca), Cold Lake, and Peace River. The Athabasca deposit, which is the largest one, cover around 46,800 km^2 (about the size of Belgium), and is located in the northeastern part of Alberta [4]. The present investigation was conducted with deasphalted oil obtained from bitumen produced at the Nexen Long Lake site.

In the Canadian oil sands, the total percentage of bitumen plus water remains fairly constant between 15 - 20 wt. %, and the remainder is made up of quartz and clay [2]. As the bitumen content increases, the water content decreases by the same ratio.

Figure 2.1 shows a hypothetical microstructure for Athabasca oil sands presented in [5], a thin water layer can be found between the quartz and bitumen. The amount of water retained in the layer cannot be reduced and it mostly represents less than 5% of the total water. In addition, Takamura suggests that the stability of this layer come from the resultant pressure by repulsive and attractive forces, as a result of the electrical double layer and London-Van der Waals interactions [5]. This study employed the bitumen after separation from the water and mineral matter.

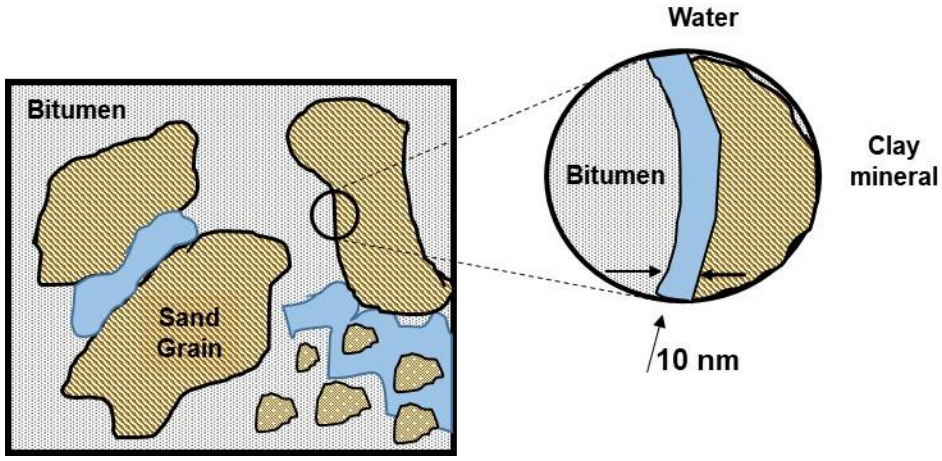

Figure 2-1. The oil sand microstructure. Modified from [5].

2.3 Composition of bitumen

Bitumen, which is the oil part in oil sands, has an API gravity less than 10 and a viscosity above 10.000 cP at reservoir conditions [2]. It is considered the heaviest fraction of petroleum and is practically a solid at room temperature. Bitumen is a complex mixture of hydrocarbons that is composed primarily of two elements, carbon and hydrogen, along with considerable amounts of nitrogen, oxygen and sulfur, as well as trace concentrations of metals (V, Ni, Fe, etc.), and minerals [4].

This heavy oil fraction contain mainly large hydrocarbon molecules known as asphaltenes and resins, which carries significant quantities of sulphur, nitrogen and metals that makes processing difficult. Furthermore, bitumen have been considered a complex material that comprises more than thousands of different molecules with broad ranges of molar masses [6]. Thus,

characterization is not possible on a molecular basis so bitumen has been characterized by fractions to make the understanding a little easier.

2.3.1 Chemical composition by distillation

Conventional crude oil and bitumen are frequently characterized by its boiling fractions since it indicates how much of the material can be fractionated. In a conventional oil refinery, the first two steps are atmospheric distillation followed by vacuum distillation. In the case of bitumen, about 50% of a barrel consists of material with boiling point > 524°C that cannot be recovered by atmospheric and vacuum distillation combined [2]. This unrecovered material is called vacuum residue, and it has a higher concentration of asphaltene and resins, as well as heteroatoms (nitrogen, oxygen, sulfur) and metals such as vanadium and nickel in the bitumen [7].

As reference along this work, the most frequently employed terms for distillation fractions in oil refinery processing are shown in Table 2-1.

Table 2-1. Common ranges for distillation fractions in oil refinery [7]

	Temperature range [°C]
Naphtha	IBP(1) - 177
Middle distillate	177 - 343
Gas oil	343 - 524
Vacuum residue	> 524

(1) IBP: Initial boiling point, commonly about 35 °C

2.3.2 SARA fractions

One of the most common methods to characterize bitumen is to divide the constituents into four fractions – namely, saturates, aromatics, resins, and asphaltenes. Each relative fraction can be separated from one another, and impart unique characteristics to the crude oil [4]. This procedure is described in ASTM D-2007 [8], and it is based on the solubility and adsorption of each fraction.

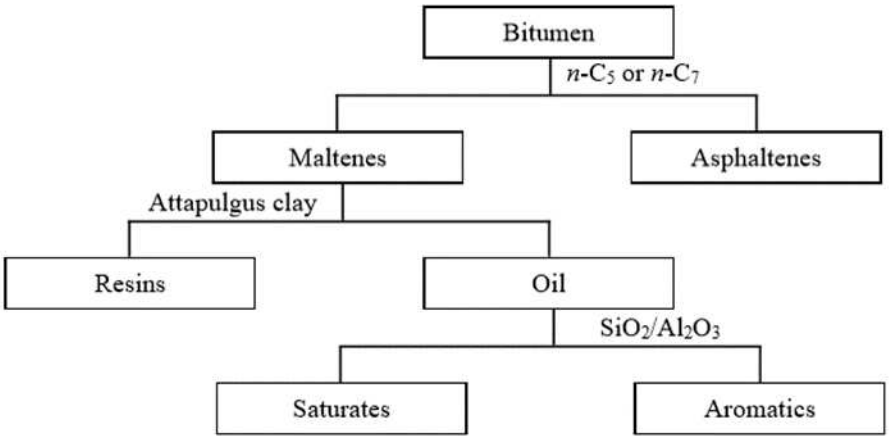

Figure 2-2. SARA fractionation.

Asphaltenes are separated as the first step in the class fractionation of bitumen and heavy oil. It is accomplished by solvent precipitation using a low-molecular weight alkane – namely, *n*-pentane or *n*-heptane, as precipitant. More details about the procedure for asphaltenes precipitation can be found in ASTM D6560-12 [9]. In this work asphaltenes were determined using *n*-pentane only. Two fractions is obtained from *n*-pentane precipitation, one corresponds to asphaltenes (precipitate) and the other one is named maltenes (*n*-pentane soluble). The precipitate obtained using *n*-pentane is a brown-to-black powdery and amorphous solid material.

It is worth highlighting that the apparent solubility of asphaltenes in the solvent increase with the molecular weight of the naphtha range paraffinic solvent used and therefore, from a given bitumen, the weight of the pentane insoluble material is greater than the *n*-heptane insoluble material.

Using chromatography, the *n*-pentane soluble fraction (maltenes) can further be separated. High surface area chromatographic materials such as Fuller's earth, Attapulgus, alumina and silica gel have been used for this objective [7]. The fraction of oil adsorbed from a solution of the *n*-pentane soluble by an Attapulgus clay or silica gel is called resins and the fraction not adsorbed is called oils. Oils may be fractionated into aromatics and saturates. For this purpose, a silica/alumina column from the *n*-pentane solution have been used; oil absorbed is called

aromatics and the non-adsorbed fraction is called saturates [10]. In this study only the asphaltenes fraction was determined, because fluidity was of interest and the asphaltenes may affect fluidity.

According to Strausz et al [4], Alberta bitumen contains pentane insoluble material (asphaltene) in an order of 14-20 wt. % range. Meanwhile, resins comprises the largest class fraction, reaching up to almost 50 wt. % in bitumen. In the Table 2-2 is shown the typical class composition of Alberta oil sand bitumen.

Table 2-2. Typical class compositions of Alberta oil sand bitumen [4]

Saturates	15-21 wt.%
Aromatics	18-19 wt.%
Resins	44-48 wt.%
Asphaltenes	14-20 wt.%

2.4 Proton nuclear magnetic resonance (^{1}H NMR) spectroscopy

Proton Nuclear Magnetic Resonance (^{1}H NMR) spectroscopy is an analytical technique which allows one to obtain information about hydrogen distribution within the structure of molecules based on the atomic nuclei response to magnetic fields [10]. This technique has been extensively used in the structural analysis of petroleum fractions, providing a direct measure as hydrogen distribution associated to the aromatic and aliphatic carbon.

Based on data presented by Sharma et al [11], Yen et al [12], and Hauser et al [13], some regions can be identified in ^{1}H NMR spectra (see figure 2-3). In a typical ^{1}H NMR spectra of vacuum residue and their deasphalted fraction, two main regions can be clearly distinguished; a region in the spectra that correspond to 0.4 to 4 ppm which is associated to the aliphatic hydrogen and a region between 6 and 9 ppm which is related with aromatic and phenolic hydrogens [11]. In addition, three main peaks can be detected in the aliphatic region of the spectra [12]. The first one, region between 0.4 and 1.1 ppm, is associated with methyl hydrogens from straight-chain alkanes, referred to as primary aliphatic in Figure 2.3. Next to them, a second peak is observed,

in the region between 1.1 and 2 ppm, and it can be related to methylene hydrogen of alkyl chains (secondary aliphatic). The last peak, region correspond to 2 to 4 ppm, is mainly referred to α-methyl and α-methylene substitution (benzylic hydrogen).

Additionally, a peak is observed between 5 and 5.5 ppm (ca. 5.3 ppm) which corresponds to the solvent used (methylene chloride) for the sample preparation [14].

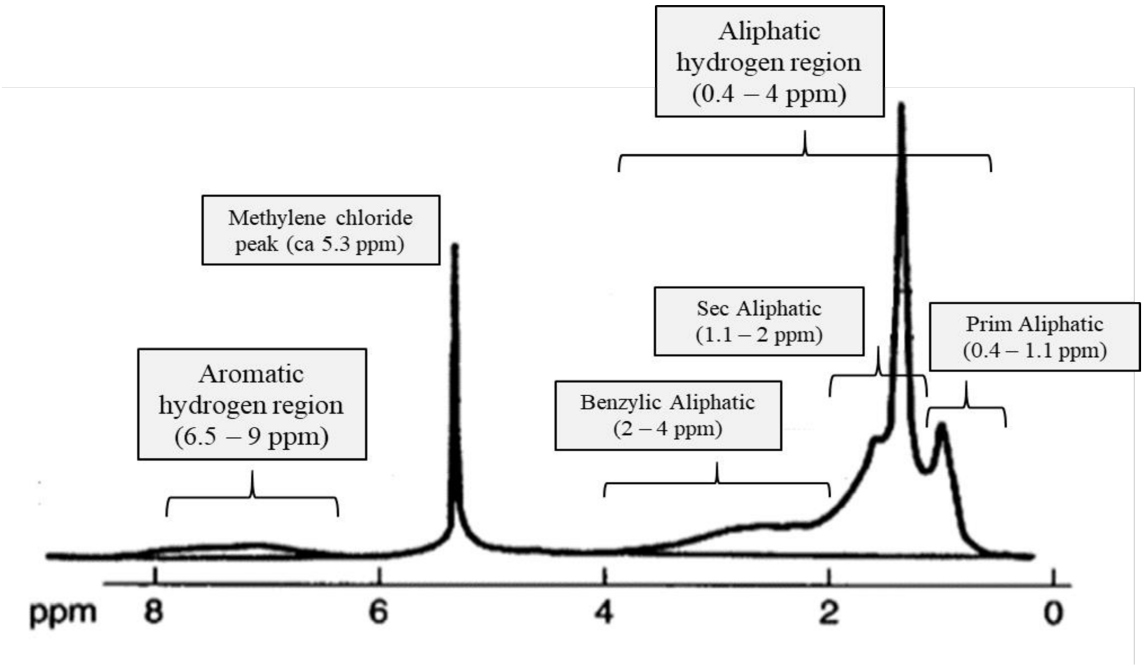

Figure 2-3. Proton NMR spectra obtained for an Asphaltene petroleum fraction. Modified from [15]

The identification of these hydrogen types could be used to determine the ratio between aliphatic and aromatic hydrogen. Thus, any changes experienced in chemical environment of the hydrogen of bitumen during thermal conversion may be identified by the change in the ^{1}H NMR spectra.

2.5 Electron Paramagnetic Resonance

Electron paramagnetic resonance (EPR) or electron spin resonance (ESR) is a spectrometric technique used to study chemical species that contains one or more unpaired electrons [16]. In this technique, a magnetic and microwave field are applied to samples that have paramagnetic species, causing the electrons to line up with the magnetic field and absorb energy, elevating

them to a higher energy level [17]. This absorption of microwave radiation is commonly recorded as first derivative curve, from which it is possible to identify unpaired electron species as well as determine spin concentrations.

The number of unpaired spins per gram of material (Ng) and the effective g factor are the most frequently reported parameters obtained by EPR measurements. The g-factor is a measure of the center of free radical absorption on the ESR spectra, which it is constant characteristic of the spin system and has been considered to be affected by the chemical neighborhood of the unpaired electron [17].

In bitumen and crude oils, two kinds of species have been found in the EPR spectrum; organic free radicals and vanadium complexes (VO^{2+}) [18-21]. These are overlapped in the same magnetic field range, as shown in the figure 2-4, being identified by the number of peaks and their location. Organic free radicals usually exhibit an intense single peak, absorbing around 3400 gauss on the electromagnetic X band (9.7 GHz) (g-values between 1.99 – 2.01) [18]. In the case of vanadyl complex (VO^{2+}), a signal with multiple peaks is generated. This spectra is typically comprised by sixteen anisotropic peaks, being eight peaks for the direction parallel, and eight peaks for the direction perpendicular to the applied magnetic field [17].

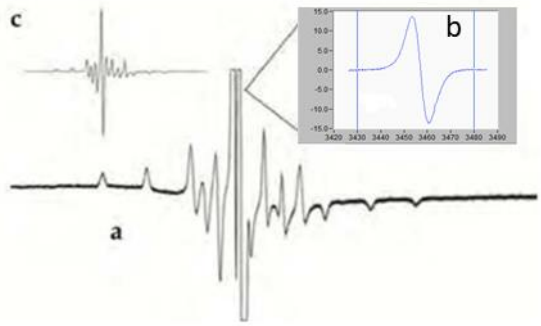

Figure 2-4. a) EPR spectrum for Brazilian crude oil b) Signal of organic free radical c) Spectrum for vanadium VO^{2+} complex. Modified from [17]

Previous study reported samples of Athabasca and Cold Lake bitumen contain slightly more than 1 x 10^{17} spins/g, and their derived asphaltenes gave an organic free radical concentration slightly over 1 x 10^{18} spins/g [20]. It was also observed in the above study [20], that the spin concentration varies in the order asphaltene > heavy resins > light resins > maltenes. Another

observations was that the Ng values for maltenes was 0.3 x 10^{17} spins/g, which is one order of magnitude lower than asphaltenes values.

In an early study, Athabasca asphaltene was separated according to molecular weight (MW) fractions by GPC, and it was found that the spin concentration of free radicals increase with increasing MW of the fraction, at the same time, the g-values decrease [22].

Furthermore, EPR g-values, in a variety of bituminous materials, were correlated with the heteroatomic contribution (S, N, and O), and a linear correlation was found [23]. The g-values increase at increasing heteroatoms content. This suggest that sulfur, nitrogen and oxygen atoms may play a key role in the structure of free radicals.

The same behavior was observed by Scotti and Montanari [24] and Guedes et al [25], using Colombian crude oil, and Brazilian and Arabian crude oils respectively. In addition, Scotti & Montanari reported that free radical concentration of seven asphaltenes showed a proportionality with their aromatic carbon fraction [24].

Several stable free radical structures have been proposed [4], from which Gomberg in 1900 was the first to observe a coloured triphenylmetthyl radical in equilibrium. The stability of this radical lies with the presence of three bulky benzene rings [16]. These effectively shield the central carbon atom supporting the lifetime of radicals and slow down any reactions.

Yen and co-workers also proposed structures based on gaps or holes in aromatics clusters that result when heteroatoms such as oxygen, nitrogen, and sulfur cannot form as many bonds as carbon [26].

Although the nature of this type of radicals has not yet been completely established, previous studies suggest that free radical sites of these materials are associated with the aromatics moieties of the bitumen skeleton, which are stabilized by the resonance of the delocalized π-system in the asphaltic structure.

In addition, Yen et al. suggests that free radical species may contribute to the tendency toward micelle formation by interactions between π- π electronic clouds of adjacent molecules, thereby prompting the aggregation in the petroleum asphaltenes [26]. This tendency to aggregate in the asphaltic structure will enhance the stability of the free radical itself by the shielding provided by other aromatic compounds in the aggregate. Thus, the free radical will remain caged by asphaltenes, protecting these reactive species from hydrogen transfer and other reactions [27].

On the other hand, the identification and tracking of free radical species using EPR technique will help to obtain more information about the behavior of this species during thermal conversion of deasphalted heavy oil.

2.6 Fourier transform infrared (FT-IR) spectroscopy

Infrared spectroscopy has been considered an useful tool to identify chemical functional groups present in petroleum compounds. In this spectroscopic technique, an incident light is passed through a sample, from which some light is absorbed by the covalent bonds in molecules and some passes through (is transmitted) [10]. Each type of bond will absorb the light with a different intensity and frequency, this makes the chemical functionalities identification possible. Infrared spectra can be shown either as percent transmittance or as absorptivity versus wavenumber (cm^{-1}) [10]. The resulting signal is a spectrum representing a molecular 'fingerprint' of the sample.

Some important peaks have been identified by previous literature in the bitumen FTIR spectra. The stretch of the methyl C-H bond (β or further away from the aromatic ring) could be observed at ~ 2970 cm^{-1} or 2872 cm^{-1} depending on the asymmetric or symmetric stretch respectively. These bands suggest the aliphatic nature of those functional group [28]. In addition, the ratio of the band at 1602 cm^{-1} (aromatic C═C stretching) to that at 2970 cm^{-1} or 2872 cm^{-1} (aliphatic hydrogen–carbon stretching) in methylene groups is a good relative measure for the aromaticity of a sample [10].

Moreover, the 700 to 900 cm^{-1} region can also confirm the aromatic characteristic due to a group of peaks that can be found associated to the ring bending vibration of one isolated aromatic C-H

bond (870 cm^{-1}), two or three adjacent aromatic C-H bonds (815 cm^{-1}) and four aromatic adjacent aromatic bonds (745 cm^{-1}) [11].

Another feature emerging in the 700-900 cm^{-1} region, it is the 720 -725 cm^{-1} peak associated to alkyl side chains possessing four and more methylene groups attached to aromatic rings [11]. In addition, the peaks at 1375 and 1456 cm^{-1} associated to symmetrical and asymmetrical bending vibration of the C-H bonds confirm the methyl and methylene groups in aliphatic chains [10].

Sulfur compounds as sulfoxides can be detected in the liquid products through the peak at 1030 cm^{-1}, a characteristic peak for the stretching of S=O bond [29].

Based on this information, previous studies [11] [14] [30] have suggested average structural parameters based on ratios the ratios of adsorption values of the specific FTIR bands in order to characterize bitumen and their fractions, as well as track changes during thermal conversion. More specifically, the ratio of aromatics C=C bonds to aliphatic methylene bonds stretching intensity [measured as the ratio of 1600 cm^{-1}/ 2853 cm^{-1} band] would aid to confirm the occurrence of the addition reactions and increase in the aromaticity of the product during thermal conversion. In addition, the intensities ratios of the absorption frequencies of methylene and methyl groups from IR spectra, between 1375 and 1460 cm^{-1}, give a measure of the chain length and/or degree of branching [11]. This latter ratio, in conjunction with the ^{1}H NMR data may help to detect the dealkylation and/or reduction in the alkyl chain length during thermal treatment of the deasphalted vacuum residue (DAO).

2.7 Density

Density is one of the most common and important properties of petroleum reported, and it is defined as mass per unit volume of a substance. Density is temperature dependent, and it will vary according to bitumen composition. Many factors such as aromaticity, molecular weight, asphaltene content, hydrogen content, and presence of heteroatoms (S, N, and O) will affect bitumen density. In the case of hydrogen content, the density will increase as the hydrogen content in the material decrease.

Two density-related properties of petroleum and petroleum products are often used: (i) specific gravity and (ii) American Petroleum Institute (API) gravity.

Specific Gravity (SG) and API gravity can be calculated through Equation (1) and (2) respectively.

$$\text{SG} = \frac{\rho_{oil}}{\rho_{water}} \qquad (1)$$

$$API = \frac{141.5}{SG\ of\ oil\ at\ 15.6\ °C} - 131.5 \qquad (2)$$

The density of bitumen is typically close to 1000 kg/m^3 at standard condition of 15 °C, where its subfractions may have higher or lower densities than the starting bitumen [31]. Since the density of the material is a function of its molecular composition, the density of the vacuum residue fraction is higher than the bitumen.

On the other hand, the density of bitumen decreased linearly with increasing temperature at a constant pressure [32].

2.8 Viscosity

Viscosity can be defined as the resistance of a fluid to flow when a shearing force is applied. Like density, viscosity is affected by temperature. As temperature decreases, viscosity increases. Viscosity is a very important property in industries where transportation of material through pipeline is essential. Efficient bitumen transportation is a constant industrial challenge and viscosity reduction is vital to enable transportation.

The most frequently employed units for viscosity are centipoise (cP) and, for kinematic viscosity, centistokes (cSt), which is defined as the viscosity, in cP, divided by the specific gravity. In the metric system, viscosity is represented by the units of millipascal-seconds (mPa·s).

Canadian bitumen is characterized by an extremely high viscosity, typically of the order 10^4 mPa.s (cP) at 40 °C [4]. As stated before, the viscosity of heavy oil is rely on temperature. In the Figure 2-5 is shown the viscosity-temperature trend for different types of bitumen from Alberta.

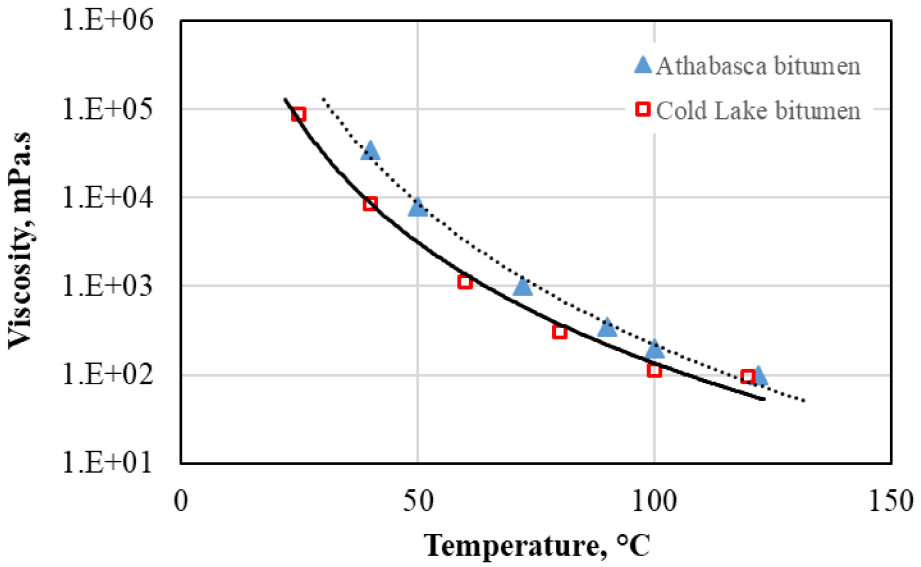

Figure 2-5. Viscosity-Temperature data for Alberta bitumens. Data from Gray et al. [33]

Moreover, the viscosity of a bitumen or heavy oil is dramatically affected by the presence of solvent material and low-boiling distillate fractions. As it is exhibited in Figure 2-6, the viscosity of a bitumen, heavy oil and crude oil could decrease by orders of magnitude by increasing their fraction boiling below 350 °C [33].

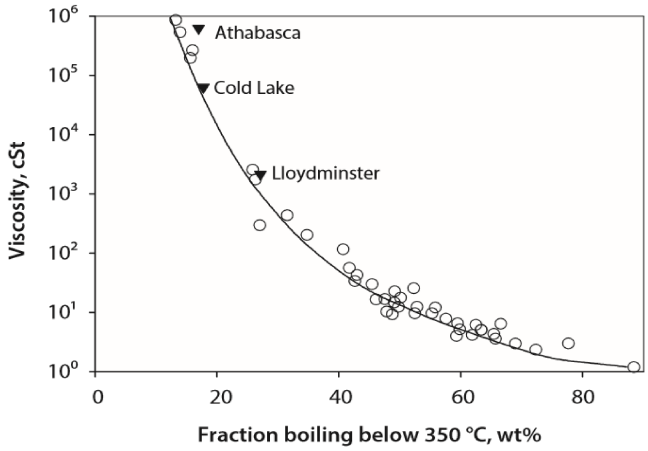

Figure 2-6. Viscosity – low boiling distillate fraction relationship for heavy oil (used with permission) [33]

Conversely, previous studies suggests that the asphaltene content affect the viscosity of heavy oil. Argilliere et al. [34] evaluated the impact of asphaltene concentration over the viscosity of heavy oil, and it was found that the viscosity was closely constant until reaching an asphaltene

concentration of 10 wt. %, after which the addition of more asphaltene resulted in a sudden increase in viscosity (see Figure 2-7). This behaviour was associated to the interaction of the aggregated asphaltenes in suspension at high concentration.

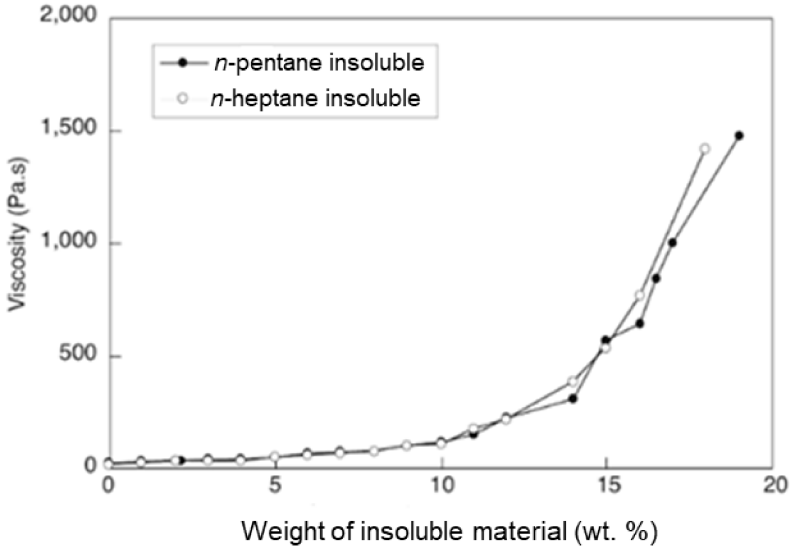

Figure 2-7. Viscosity for heavy crude oil with different asphaltene concentration. Modified from [34]

Based on above mentioned, the characterization of the liquid product through measuring the chemical composition by SIMDIS and asphaltene content, will aid to understand the changes over viscosity during thermal treatment at low temperature.

2.9 Refractive index

The refractive index of a material is defined as the ratio of the velocity of light in a vacuum to the velocity of light in this material. For compounds with similar molecular weight, this value increases in the order; paraffin, naphthenic, and aromatic. Thus, high values are related with aromatic compounds. Based on this, refractive index may be used as an indicator of the chemical changes taking place during thermal conversion of heavy oil [7].

2.10 Elemental composition

Elemental composition is one of the most common method employed to evaluate the general nature of the feedstock, and changes its main elements through the determination of the

percentages by weight of carbon, hydrogen, nitrogen, sulfur, and oxygen. Moreover, the atomic ratios of diverse elements to carbon (i.e., H/C, N/C, S/C, and O/C) are often utilized to evaluate the overall character of the feedstock [10].

In the case of Alberta bitumens and their vacuum residue, the hydrogen to carbon (H/C) molar ratios are found in the narrow range of 1.50 and 1.40, respectively [31]. Deasphalted oil (DAO) has values of (H/C) molar ratio close to their original bitumen, meanwhile the asphaltene fraction have been reported (H/C) molar ratio around to 1.0 [35].

The H/C molar ratio is commonly obtained in order to evaluate the hydrogen deficiency of the feedstock and provide information on the types of reaction taking place during visbreaking [36].

The characterization of the liquid product through the H/C molar ratio and ^{1}H NMR data, will help to track the aromaticity of the product during thermal treatment at low temperature. Moreover, Stravtiev et al. [37] investigated the characteristics of 36 vacuum residue oil and their deasphalted oil fractions, suggesting that hydrogen content and H/C atomic ratio of the vacuum residue oil and DAO fractions strongly correlate with their density measured at 20 °C.

Furthermore, sulfur and nitrogen are present in a diversity of the organic components in the bitumen, being concentrated in the vacuum residue. The sulfur is present in two main forms; thiophene (associated to aromatic rings) and aliphatic sulfides [31]. The thiophenic sulfur species contains in the petroleum and bitumen are resistant to thermal conversion, and hydrogenation using catalyst is required.

A previous study [38] have reported that thiophenic sulfur species constitute 55 mol % of total sulfur in the deasphalted oil from Cold Lake bitumen.

Nitrogen species are found in bitumen in two main forms; the non-basic derivatives of pyrrole and the basic derivatives of pyridine [31]. Both types of nitrogen are highly resistant to removal by thermal treatment.

In the case of oxygen content, a wide range of values was reported (from 0.2 wt. % to 4.5 wt. %) since this content is estimated by difference, and it is susceptible to the accumulation of all the error in the other elemental data [10].

2.11 Microcarbon residue

An important parameter for upgrading of bitumen is the coke-forming tendency of the feedstock during a thermal or catalytic process. This characteristic is usually determined in the resid fraction of the heavy oil and bitumens. The microcarbon residue is obtained by measuring the amount of solid residue after pyrolizing a sample under controlled conditions in the absence of oxygen [10]. Three methods of measurement the carbon residue are commonly employed in the oil industry; conradson carbon residue (CCR), ramsbottom carbon residue (RCR), microcarbon residue (MCR). The main differences among each method are in the details of the apparatus and heating conditions [31].

A typical value for microcarbon residue (MCR) in Athabasca bitumen is around 13.6 wt. %. Moreover, the high molecular weight material responsible for the coke formation tendency mainly remains in the vacuum residue fraction (524 °C+) which typically contains a MCR value of approximately 28 wt. % [31].

Furthermore, the asphaltene fraction typically show a higher MCR than any other fraction in the vacuum residue, but the non-asphaltene fraction still contribute to the overall MCR. Brons et al. [38] reported data for deasphalted oil fractions separated using light hydrocarbons solvents (*n*-butane, isobutane, and propane) that show all of these fall in a 2-3 wt. % CCR range.

Additionally, the microcarbon residue content has been correlated in the past with hydrogen content and H/C atomic ratio in the oil fraction. It has been reported in previous literature [37] that the hydrogen content and H/C atomic ratio increase as the microcarbon residue content decrease.

2.12 General aspects of thermal cracking in partial upgrading of heavy oil

2.12.1 Chemistry of thermal cracking

The thermal cracking follows free radical chemistry, and involves a radical chain processes based on three basic steps; initiation, propagation and termination.

Initiation. Free radicals are formed through homolytic cleavage of thermodynamically favorable bonds, more likely the carbon-sulfur or carbon-carbon. When large molecules undergo thermal cracking, the breakage of the weakest bond (the lowest dissociation energy) in the chain proceeds first.

$$R - R_i \longrightarrow R^* + R_i^*$$

$$\text{Example; } C_2H_6 \longrightarrow CH_3^*$$

Thermodynamics governs breakage of bonds and typical bond dissociation energies required for cleavage of bonds in non-radical molecules are shown in Table 2-3. This energy give an indication of the difficulty of breakage, from which cleavage of carbon-carbon, carbon-sulphur and carbon-hydrogen bonds are commonly present in the upgrading of oil sands bitumen.

Table 2-3. Bond dissociation energies [31]

Chemical bond	Energy, kJ/mol
C-C (aliphatic)	344 ± 4
C-H (primary)	411 ± 4
C-H (secondary)	398 ± 4
C-H (aromatic)	464 ± 8
C-S	307 ± 8
C-N	342 ± 8
C-O	344 ± 4

As it is shown in Table 2-3, the carbon-carbon (C-C) bonds in the aromatic ring are much stronger than the aliphatic bonds, and it is due to the resonance stabilization energy associated to the ring which make those bonds unbreakable at normal process temperatures (<600 °C) unless the aromatic character is first destroyed by hydrogenation.

The energies required to break these chemical bonds and create free radicals are so high that this free radicals species are never found in high concentrations [31]. Moreover, the free radical reaction is a chain reaction process where the initiation step is very important; once the free

radical species are created, they can go further through many cycles of the propagation reactions which have lower energy barrier than of bond dissociation [31].

In addition, the kinetic of this reaction increases in rate at higher temperatures, being more significant after 410 °C [7].

Propagation. During this step several types of reactions take place.

Hydrogen abstraction

$$\beta_i{}^* + R_iH \longrightarrow \beta_iH + R_i{}^*$$

Example; $CH_3{}^* + C_2H_6 \longrightarrow CH_4 + C_2H_5{}^*$

β-Scission

$$\beta_i\text{- C-C - R}^* \longrightarrow \beta_i\text{ – C}^* + \text{R=C}$$

Example; $CH_3\text{-}CH_2\text{-}CH_2\text{-}CH_2\text{-}CH_2{}^* \longrightarrow CH_3\text{-}CH_2\text{-}CH_2{}^* + CH_2\text{=}CH_2$

Radical Addition

$$R_i{}^* + \text{C=C – Rj} \longrightarrow \text{Ri-C-C}^*\text{- Rj}$$

Example; $CH_3{}^* + CH_2\text{=}CH_2 \longrightarrow CH_3\text{-}CH^*\text{-}CH_3$

Radical rearrangement

$$\text{R}^* \text{ - C-C- } \beta_i \longrightarrow R_j{}^*$$

Example; $CH_3CH_2CH_2CH_2{}^* \longrightarrow CH_3CH_2\,(CH\,^*)\,CH_3$

Where $R - R_i$ represents bitumen/heavy oil, and R_i and R_i are alkyl groups containing chains of carbon atoms maybe branched (i.e. Methyl, ethyl, etc.). R^*, $R_i{}^*$, $\beta_i{}^*$, and $Rj\,^*$ are alkyl radicals. $R - C = C$ represents olefins.

- Hydrogen abstraction or metathesis. Once the free radical is created, the molecules of their surrounding can be activated via H-transfer reactions in order to favour the formation of the most stable radical species, which for alkyl free radicals is in the following order: tertiary > secondary > primary [31].

- Decomposition of the free radicals in olefins (β-Scission). This reaction is characterized by the breaking or scission of a C-C bond in the β position to the radical centre (that is, two carbons away) to create an olefin and new free radical with lower molecular weight [11].
- Isomerization and cyclization reactions (radical rearrangement). This type of reactions can occur depending on the structure of the hydrocarbon molecules and the type of free radical created.
- Radical addition or condensation reactions. Aromatic compounds in the feed have a high tendency to undergo this type of reactions that lead to coke formation through creation of high polyaromantic compounds. The asphaltenes are primarily subject to this reaction.

Secondary reactions can happen to the products created during the first pass via all the previous reactions. It is worth noting that although the propagation reactions take place, the primary initiation reactions continue as well.

Termination. The thermal cracking reactions terminate by recombination of two free radical to form a new bond.

$$Ri^* + Rj^* \longrightarrow Ri\text{-}Rj$$

$$\text{Example; } CH_3\text{-}CH_2^* + CH_3^* \longrightarrow CH_3\text{-}CH_2\text{-}CH_3$$

It is also possible a termination step by disproportionation of radicals;

$$Ri^* + Rj^* \longrightarrow RiH + RjH$$

$$\text{Example; } CH_3\text{-}CH_2^* + CH_3\text{-}CH_2^* \longrightarrow 2\,(CH_2{=}CH_2)$$

Although each step in a free-radical chain reaction look simple, the overall network of reactions is complicated since there is more than one reaction occurring at the same time, especially for a complex material such as bitumen. Moreover, Gray [31] suggests that the overall network of reactions is affected if thermal cracking is taking place in liquid or vapour phase.

Kissin suggests [39] that bimolecular reactions such as hydrogen transfer and radical addition are favoured over β-Scission when thermal cracking occurs in the liquid phase since the density of the reacting species is higher. This may suggest that during the thermal cracking of bitumen at

low temperature, the olefin levels in the product is reduced due to the olefins being involved in the addition reactions.

In addition, the occurrence of hydrogen transfer is a very important reaction during the thermal cracking process in order to help controlling the addition reactions between condensed aromatic rings that it will lead to coke formation.

Nevertheless, coke formation requires that some portion of the oil becomes insoluble first through the formation of a second phase. This liquid second phase is called mesophase and is composed by highly aromatic compounds (asphaltenes) generated from combinations of reactions during thermal cracking of bitumen that increase aromatic carbon content (side chains cracking on aromatic rings and dehydrogenation of hydroaromatics through β-Scission / Hydrogen abstraction reactions), increase molar mass (addition reactions), or both [31].

The onset of coking or induction time in the thermal conversion of heavy oil is defined by the period of time which molecules this second phase becomes completely insoluble in that phase, leading to coke formation.

2.13 Visbreaking

Visbreaking can be defined as a mild thermal cracking process, and it was originally developed to reduce the vacuum residue oil viscosity in order to meet the fuel oil specifications. It is considered one of most economical and low severity thermal conversion process which has made it widely used around the world where there are markets for fuel oil.

In the context of bitumen partial upgrading, the primary aim is to reduce the viscosity and enable to meet the pipeline transport specification without the addition of a solvent.

A typical visbreaking feed material in oil refineries are atmospheric and vacuum residue fraction, and the operation is conducted at 430 – 490 °C and 0.5-1.2 MPa with short residence times (1-15min), which avoids coking reactions [7]. From the point of view of bitumen partial upgrading, deasphalted heavy oil is suggested as visbreaking feed material.

The thermal cracking involves the decomposition of molecules to yield products that are of a lower molecular mass than the feed. The conversion of these molecules occur by homolytic bond dissociation, and resulting reactions follow free-radical chemistry. Visbreaking reactions are purely thermal cracking reactions and mainly depend on parameters such as; feed properties, pressure, temperature and residence time [40].

Eshraghian and Husein [41] suggest that the effect of pressure on thermal cracking of vacuum residue oil depends the operating temperature, and as the pressure is increased at low reaction temperature (400 °C), a more stable material is produced since the rate of the radical rearrangement reactions is increased during thermal cracking.

During visbreaking, the percent conversion of the feed to product (defined as; conversion: Mass $_{\text{feed >524 °C boiling point fraction}}$ − Mass $_{\text{product >524 °C boiling point fraction}}$)/ (Mass $_{\text{feed >524 °C}}$) x 100 [31]) is limited by the onset of coking in order to avoid the coke formation on the internal surface of the furnace tubes. A second limitation of visbreaking is the stability of the liquid products, which it is defined as their capacity to maintain the asphaltenes in suspension [31]. Moreover, Yan suggests that the coke-forming tendency as well as the onset of asphaltene precipitation depends on the feedstock properties, where one of the most important characteristic is the initial asphaltene content [42].

Rahimi et al. [43] reported that a conversion between 10-20 wt. % of heavy material in the bitumen can be achieved in typical visbreaking conditions at low to moderate severities without significant coke formation. In the case of thermal conversion of deasphalted vacuum residue at temperature between 380-423 °C, Cabrales-Navarro and Pereira-Almao [44] reported conversions of hydrocarbon (> 560 °C boiling point fraction) around 40 %.

There is two type of configuration for Visbreaking;

a) Coil Visbreaking: The coil type process achieves conversion by high temperature operation in the furnace (473 °C to 500 °C) for a usually about 1-3 minutes. [40] The process scheme of coil visbreaking is seen in Figure 2-8.

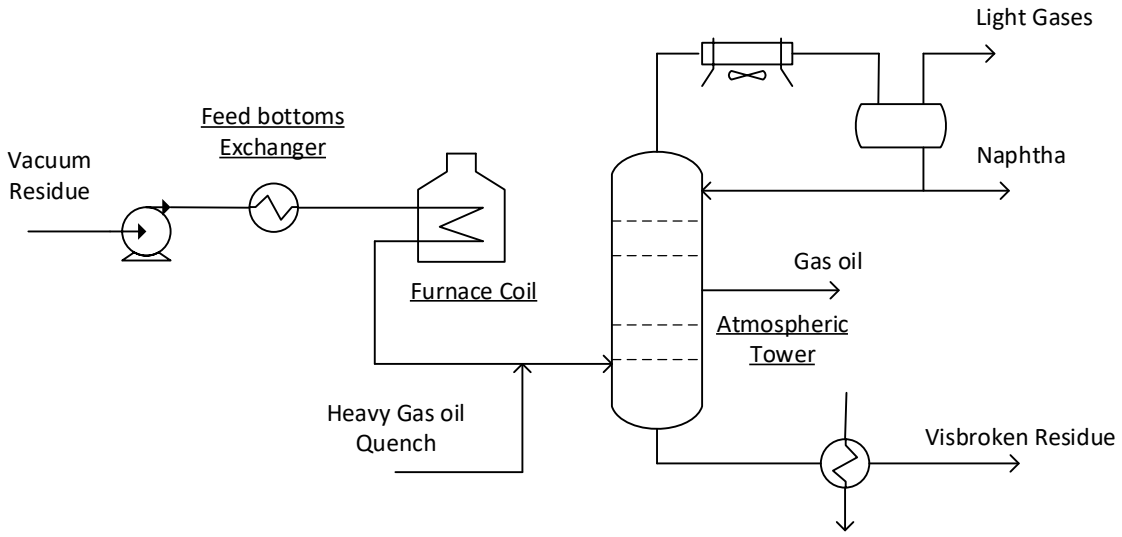

Figure 2-8. Process scheme of a coil visbreaking [40]

b) Soaker Visbreaking: This type uses a soaking chamber to complete the conversion initiated in the furnace, hence relatively lower temperature operation (427 °C to 433 °C) and longer reaction times are required. [40] The process scheme of soaker visbreaking is seen in Figure 2-9.

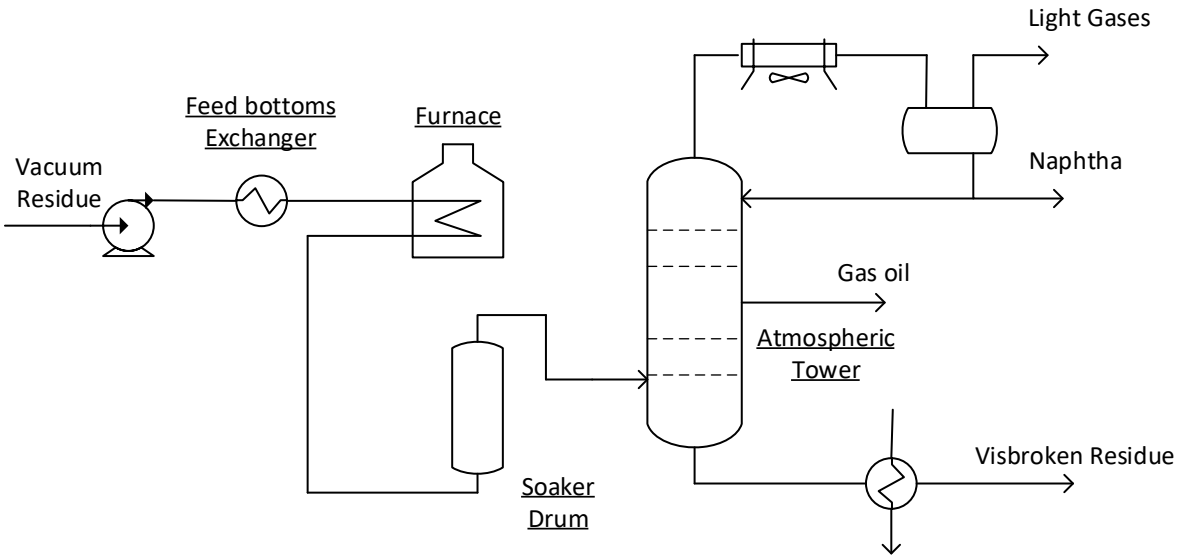

Figure 2-9. Process scheme of a soaker visbreaking [40]

At the typical visbreaking conditions (Temperature > 430 °C), the two different types of visbreaking may generate similar product yields and properties at the same level of conversion, with the only difference that the soaker operation has the advantage of lower energy consumption and longer run times before having to shut down to remove the coke from the furnace tubes. Although each type of configuration could yield a liquid product at the level of conversion that share some generic properties such as density, H/C molar ratio; each product have different inner properties caused by the chain-reaction mechanism along the reaction time.

The time-temperature relationship during thermal conversion of heavy oil at low temperature (<400 °C) is not completely clear, as well as there is limited open literature on the structure-rheology-conversion relationship of deasphalted oil (DAO).

2.14 Relevance of applied investigation of the thermal conversion of deasphalted oil to the present work

Oil sands bitumen is characterized by its high viscosity which is mainly a consequence of its composition, from which the high content of heavy molecular compounds – namely asphaltenes and resins are mainly responsible.

It is also known that asphaltenes and aggregates formed by asphaltenes are not only precursors for coke formation that limits conversion during visbreaker operation, but are also suspected to contribute to increased viscosity as it was mentioned in the section 2.9.

By performing a deasphalting step before thermal cracking in the Field Upgrader, a higher level of conversion can be reached and thereby a partially upgraded bitumen with higher content of lighter fractions.

Nonetheless, to understand those changes at high conversion of deasphalted oil, a better understanding of the performance at milder conversion is necessary.

Based on this, the time dependent conversion of industrial deasphalted vacuum residue (DAO) from the Nexen Long Lake upgrader was investigated at different temperatures in the range 280 to 400 °C.

This temperature range is below the intended operation temperature in the thermal cracker and was selected specifically to provide some insights about the changes taking place at lower conversion.

Literature cited

[1] Bauquis, P. R. A reappraisal of energy supply and demand in 2050. *Oil & Gas Science and Technology* **2001**, *56* (4), 389–402.

[2] Banerjee, D. K. *Oil sands, heavy oil, & bitumen: from recovery to refinery*; PennWell Corp.: Tulsa, Oklahoma, 2012.

[3] Canadian Energy Research Institute (CERI). Canadian economic impacts of new and existing oil sands development in Alberta, 2014, Calgary, Alberta, Canada. http://www.ceri.ca/images/stories/CDN_Economic_Impacts_of_New_and_Existing_Oil_Sands_Development_in_Alberta_-_November_2014_-_Final.pdf.

[4] Strausz, O. P.; Lown, E. M. *The chemistry of Alberta oil sands, bitumens and heavy oils*; Alberta Energy Research Institute: Calgary, 2003.

[5] Takamura, K. Microscopic structure of Athabasca oil sand. *Can. J. Chem. Eng.* **1982**, 60, 538.

[6] Wiehe, I. A. Tutorial on resid conversion and coking, Proc. 2nd Intl. Conf. on refinery processing, AIChE 1999 Spring National Meeting, Houston, TX, March 14-18, 499-505.

[7] Speight, J. G. *The chemistry and technology of petroleum;* CRC press: Boca Raton, 2014.

[8] ASTM D2007-11. *Characteristic groups in rubber extender and processing oils and other petroleum derived oils by the clay-gel absorption chromatography method*; ASTM: West Conshohocken, PA, 2016.

[9] ASTM D6560-12: *Standard test method for determination of asphaltenes in crude petroleum and petroleum products*; ASTM: West Conshohocken, PA, 2012.

[10] Speight, J. G. *Handbook of Petroleum Product Analysis*; John Wiley & Sons: Boca Raton, 2015.

[11] Sharma, B. K.; Tyagi, O. S.; Aloopwan, M. K. S.; Bhagat, S. D. Spectroscopic characterization of solvent soluble fractions of petroleum vacuum residues. *Pet. Sci. Technol.* **2000**, 18, 249-272.

[12] Yen, T. F.; Wu, W. H.; Chilingar, G. V. A study of the structure of petroleum asphaltenes and related substances by proton nuclear magnetic resonance. *Energy Sources*, **1984,** 7(3), 275-304.

[13] Hauser, A.; AlHumaidan, F.; Al-Rabiah, H.; Halabi, M. A. Study on thermal cracking of Kuwaiti heavy oil (vacuum residue) and its SARA fractions by NMR spectroscopy. *Energy Fuels* **2014**, *28* (7), 4321-4332.

[14] Dehkissia, S.; Larachi, F.; Rodrigue, D.; Chornet, E. Characterization of Doba–Chad heavy crude oil in relation with the feasibility of pipeline transportation. *Fuel* **2004**, *83*(16), 2157-2168.

[15] Huc, A. Y. *Heavy crude oils, from geology to upgrading: an overview*; Editions Technip: Paris, 2011.

[16] Parsons, A. F. *An introduction to free radical chemistry*; Wiley-Blackwell: United Kingdom, 2000, p. 16.

[17] Piccinato, M. T.; Guedes, C. L. B.; Di Mauro, E. Crude oil by EPR. *In crude oil emulsions-composition stability and characterization*; InTech; Manar El-Sayed Abdel-Raouf *Eds;* Brazil; 147-168.

[18] Humphrey, B. J. *Electron paramagnetic resonance on asphaltic materials (No. NMERI-WA5-10-(SS-5.01))*; rep.; New Mexico Engineering Research Institute: New Mexico, 1987.

[19] Elofson, R. M.; Schulz, K. F.; Hitchon, B. Geochemical significance of chemical composition and ESR properties of asphaltenes in crude oils from Alberta, Canada. *Geochim. Cosmochim. Acta* **1977**, *41*(5), 567-580.

[20] Schultz, K. F.; Selucky, M. L. ESR measurements on asphaltene and resin fractions from various separation methods. *Fuel* **1981**, *60*(10), 951-956.

[21] Chilingarian, G. V. *Bitumens, asphalts, and tar sands, Volume 7;* Ed.; Elsevier, 2011.

[22] Adams, J.; Altgelt. K.; LeTourneau, L.; Lindeman, P. Free radical concentration in gel permeation fractions of asphaltenes from different crude oils. *Am. Chem. Soc. Div. Petrol. Chem. Preprints* **1966**, 11, B-140.

[23] Yen, T. F.; Sprang, S. R. Contribution of ESR analysis toward diagenic mechanisms in bituminous deposits. *Geochim. Cosmochim. Acta* **1977**, *41*(8), 1007-1018.

[24] Scotti, R.; Montanari, L. Molecular structure and intermolecular interaction of asphaltenes by FT-IR, NMR, EPR. In *Structures and Dynamics of Asphaltenes*; Mullins, O. C., Sheu, E.Y. Eds.; Springer: Boston, **1998**; 79-113.

[25] Guedes, C. L. B.; Di Mauro, E.; Mangrich, A. S.; Ramoni, M.; Antunes, V. Study of the photodegradation of oil by electronic paramagnetic resonance. *Cienc.-Tec.-Pet., Sec. Quim.* **2001**, *3*, 145-154.

[26] Yen, T. F.; Erdman, J. G.; Saraceno, A. J. Investigation of the nature of free radicals in petroleum asphaltenes and related substances by electron spin resonance. *Anal. Chem.* **1962**, *34*(6), 694-700.

[27] Mujica, V.; Nieto, P.; Puerta, L.; Acevedo, S. Caging of molecules by asphaltenes. A model for free radical preservation in crude oils. *Energy Fuels* **2000**, *14* (3), 632-639.

[28] Karlsson, R.; Isacsson, U. Application of FTIR-ATR to Characterization of bitumen rejuvenator diffusion. *J. Mater. Civ. Eng.* **2003**, *15* (2), 157-165.

[29] Silverstein, R. M.; Webster, F. X.; Kiemle, D. J.; Bryce, D. L. *Spectrometric identification of organic compounds*; John Wiley & Sons: New York, 2014**.**

[30] Liang, W.; Que, G.; Chen, Y.; Liu, C. Chapter 10 Chemical composition and characteristics of residues of chinese crude oils. *Developments in Petroleum Science Asphaltenes and Asphalts, 2* **2000**, 281–304

[31] Gray, M. R. Upgrading oilsands bitumen and heavy oil; The University of Alberta Press: Edmonton, 2015.

[32] Kariznovi, M.; Nourozieh, H.; Abedi, J. Measurement and correlation of viscosity and density for compressed Athabasca bitumen at temperatures up to 200ºC. *Journal of Canadian Petroleum Technology* **2014**, *53* (06), 330–338.

[33] Ancheyta, J. *Modeling of processes and reactors for upgrading of heavy petroleum;* CRC Press: Boca Raton, 2013.

[34] Argillier, J.-F.; Coustet, C.; Henaut, I. Heavy oil rheology as a function of asphaltene and resin content and temperature. *Proceedings of SPE International Thermal Operations and Heavy Oil Symposium and International Horizontal Well Technology Conference* **2002**.

[35] Avid, B.; Sato, S.; Takanohashi, T.; Saito, I. Effect of *n*-pentane and *n*-heptane insolubles on the pyrolysis of vacuum residue. *Energy & Fuels* **2006**, *20* (6), 2475–2477.

[36] Kapoor, M. P.; Kothiyal, V.; Singh, I. D. Compositional and structural studies of visbroken residues. *Fuel Sci. Technol. Int.* **1993**, 11 (7), 975-989.

[37] Stratiev, D.; Shishkova, I.; Tsaneva, T.; Mitkova, M.; Yordanov, D. Investigation of relations between properties of vacuum residual oils from different Origin, and of their deasphalted and asphaltene fractions. *Fuel* **2016**, 170, 115–129.

[38] Brons, G.; Yu, J. M. Solvent deasphalting effects on whole Cold Lake bitumen. *Energy Fuels* **1995**, 9 (4), 641–647.

[39] Kissin, Y. V. Free-radical reactions of high molecular weight isoalkanes. *Industrial and Engineering Chemistry Research*. **1987**, 26 (8), 1633–1638.

[40] Gary, J. H.; Handwerk, G. E.; Kaiser, M. J. Petroleum refining: Technology and Economics, 5th Ed. CRC Press: Boca Raton, FL, 2007.

[41] Eshraghian, A.; Husein, M. M. Thermal Cracking of Athabasca VR and Bitumen and Their Maltene Fraction in a Closed Reactor System. *Fuel* **2017**, 190, 396–408.

[42] Yan, Y. T. Characterization of visbreaker feeds. *Fuel* **1990**, 69 (8), 1062–1064.

[43] Rahimi, P. M.; Gentzis, T. The Chemistry of Bitumen and Heavy Oil Processing. In *Practical Advances in Petroleum Processing;* Hsu C.S.; Robinson P.R. Eds; Springer, New York, NY**, 2006**; Volume 2, 597–634.

[44] Cabrales-Navarro, F. A.; Pereira-Almao, P. Reactivity and Comprehensive Kinetic Modeling of Deasphalted Vacuum Residue Thermal Cracking. *Energy Fuels* **2017**, 31(4), 4318-4332.

3. THERMAL CONVERSION OF DEASPHALTED OIL BELOW 320 °C

3.1 Introduction

As stated in the first chapter, when a thermal conversion process such as visbreaking is applied to oil sands bitumen as method to decrease viscosity, lower temperatures provided interesting results [1][2][3]. By operating at temperature as low as 250 °C during visbreaking oilsands-derived bitumen, there was reported a significant improvement in the bitumen properties in which the viscosity of the products decreased by two to three orders of magnitude compared with the raw bitumen.

On the other hand, it is well known that in all thermal cracking processes (operated above the normal operating temperature of 430 °C), the reactions are time and temperature dependent, and there is a trade-off relationship between reaction temperature and processing time [4]. Although Wang et al. [2] suggested that thermal conversion of bitumen at low temperature (below 400 °C) fails to follow the inverse relationship between process time and reaction temperature since there is limited amount of reactions where the activation energy requirement is met. The homolytic scission which required lowest activation energy occurred first, giving an improvement in selectivity and product quality beyond that predicted from typical visbreaking operating experience at higher temperatures.

In addition, Yañez et al. [3] suggested that viscosity changes in the thermal conversion of bitumen at low temperature (between 250 °C and 300 °C) are not monotonous and reaction time significantly affects products in a more important way.

Based on what it was mentioned before and the limited information on the structure-rheology-conversion relationship of deasphalted oil (DAO), thermal conversion of deasphalted oil at operating temperature of 280 and 320 °C were investigated in order to obtain a deeper understanding of the changes that heavy oil experiences during milder conversion processes at low temperature.

3.2 Experimental Section

3.2.1 Materials

Deasphalted vacuum residue oil from the Nexen Long Lake upgrader was used for the thermal conversion reactions. The deasphalted oil was characterized and the characterization is shown in Table 3-1.

Table 3-1. Characterization of Long Lake DAO.

Description	Long Lake DAO	
	x	s
Density @ 20 °C [kg/m^3]	1057.3	3.6
Mass with B.P < 524 °C [wt. %]	10.5	0.5
Microcarbon residue [wt. %]	7.5	0.8
Pentane insoluble [wt. %] [a]	6.6	0.2
Elemental Analysis [wt. %][b]		
H	9.90	0.06
C	83.39	0.40
N	0.58	0.03
O [b]	0.60	0.10
S	5.61	0.10
Vanadium [ppm]	60	2
Nickel [ppm]	33	1
Viscosity at 50 °C [Pa.s] [c]	600	13.4
Refractive index @ 20 °C	1.5921	0.0001

a. *n*-pentane insoluble 40:1 solvent: DAO ratio
b. Mineral matter free; mineral matter content 0.4 ± 0.1 wt. % feed
c. Oxygen was determined by difference
d. Shear rate: 10 [1/s]

The configuration of the OrCrude™ unit of the Nexen Long Lake upgrader is shown in Figure 3-1. The bitumen-water mixture that is recovered from SAGD process is mixed with diluent to separate the water (step not shown in Figure 3-1) to produce a diluted bitumen that is the feed to the process. The diluted bitumen is combined with cracked products from the visbreaker, which

is then fractionated by atmospheric and vacuum distillation to obtain different distillation cuts. The residue fraction from distillation is solvent deasphalted using *n*-pentane to produce the deasphalted vacuum residue oil (VR DAO) that serves as the feed material to the coil-type visbreaker in the upgrader facility. This is the VR DAO that was employed in this study. Of importance to this work is that the VR DAO contains both straight run and recycled cracked material.

It is important to mention that the presence of recycled cracked material in the feed will impact the product quality obtain after thermal conversion. Japanwala reported that this recycle stream is rich in polynuclear aromatic compounds with high content of heteroatoms (nitrogen and sulfur) which it will deteriorate the quality of the product obtain after thermal conversion [5].

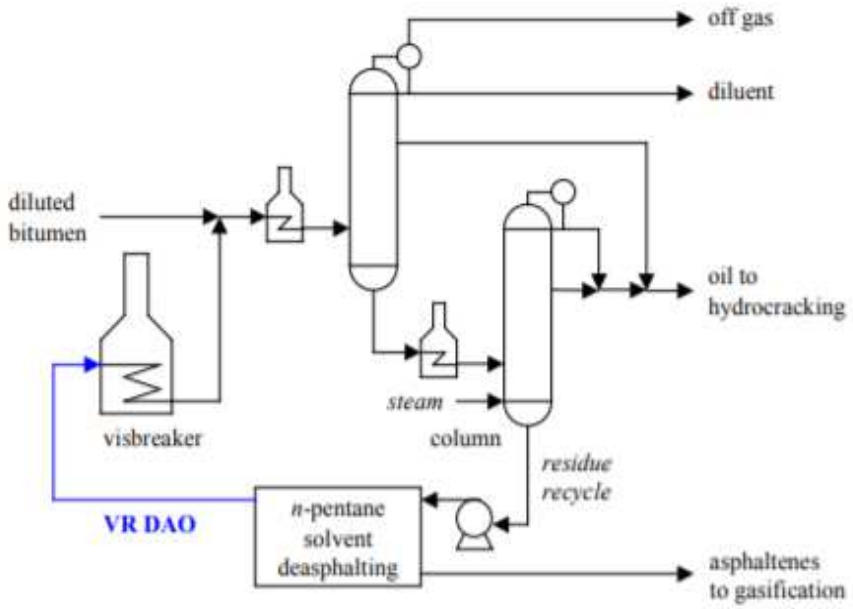

Figure 3-1. The OrCrude™ and visbreaker unit configuration at the Nexen Long Lake upgrader. The VR DAO stream is indicated in blue.

Other chemicals, cylinder gases and calibration substances employed in this work are listed in Table 3-2.

Table 3-2. List of chemicals, cylinder gases and calibration substances.

Compound	Formula	CASRN [a]	Mass Fraction purity [b]	Supplier
Chemicals				
n -pentane	C_5H_{12}	109-66-0	1.00	Fisher Scientific
toluene	C_7H_8	108-88-3	1.00	Fisher Scientific
dichloromethane	CH_2Cl_2	75-09-2	1.00	Fisher Scientific
carbon disulfide	CS_2	75-15-0	1.00	Fisher Scientific
d -chloroform	$CDCl_3$	865-49-6	0.9996 [c]	Sigma - Aldrich
Cylinder gases				
nitrogen	N_2	7727-37-9	0.99999 [d]	Praxair
Calibration substances				
4-hydroxy-2,2,6,6-tetramethyl-1-piperidine -1-oxyl (TEMPOL)	$C_9H_{18}NO_2$	2226-96-2	0.98	Alfa Aesar
reference material 5010	-	-	-	Supelco
polywax 655	-	-	-	Agilent

[a] CASRN = Chemical Abstracts Services Register Number
[b] Minimum purity of the material guaranteed by the supplier; material was not further purified
[c] Deuterated content
[d] Mole fraction purity

3.2.2 Equipment and Procedure

The experiments were carried out in a batch reactor system; a scheme is shown in Figure 3-2. The setup was built using Swagelok 316 stainless steel tubing and fittings. A fluidized sand bath (An Omega Fluidized Bath FSB-3) was employed to heat and maintain the reaction temperature constant. The reactor temperature was monitored and indirectly controlled by adjusting the temperature of the heated fluidized sand bath. These thermal cracking experiments were carried out in 15-mL stainless steel batch micro reactors.

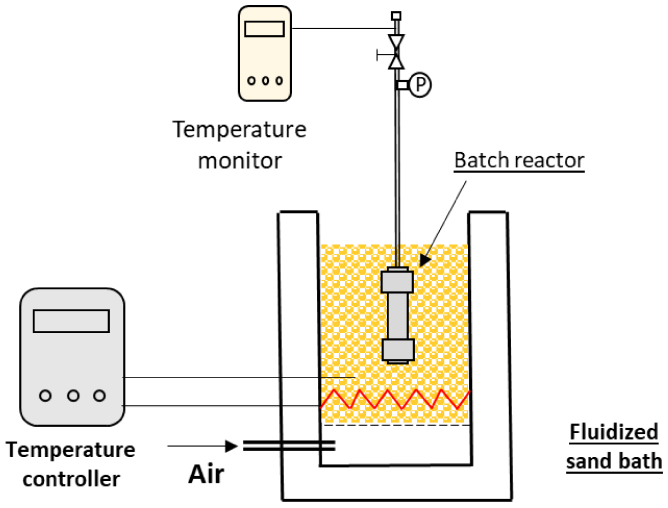

Figure 3-2. Batch reactor system used for thermal conversion reactions

Before the reaction, the microreactor was pressurized with nitrogen to 5 MPa, then purged and pressurized at 3 MPa, respectively. Reactions were conducted at 280, and 320 degree Celsius respectively (internal reactor temperature) meanwhile residence time was varied between 1 to 360 min. The reaction time starts when the temperature is reached and a typical heat-up time is 6 min. For each experiment, around 12 grams of Long Lake deasphalted oil were used. DAO samples were previous heated during 30 minutes at 100 °C using a Fisher Scientific Isotemp hot plate to pour them into the microreactors.

After reaction, reactors were cooled down until atmospheric temperature, weighed, and depressurized. Light products plus nitrogen were collected in a gas bag and analyzed afterwards. Reactors were weighed again in order to determine the mass of the gaseous products based on the difference between the pressurized and depressurized reactor, and then gas chromatography analysis was used to obtain the amount of N_2 so that the gas make could be calculated.

The products in the reactor were initially removed using a manual tool (between 5 to 7 grams were recovered) and then the remaining were dissolved using methylene chloride in a ratio of 1:40 as solvent and removed from the reaction system. The remaining product removed with methylene chloride was vacuum filtered using a 0.22 μm filter to determine the solid content. Liquid products were heated at 45 °C under atmospheric pressure inside a fume hood for one week.

A Fischer Scientific Isotemp hot plate was used to evaporate the solvent. Then, the sample was kept at room temperature during a week to remove the excess of solvent. The solids obtained from the filtration step were dried inside the fumehood for 2 days to evaporate all the methylene chloride and weighed at room temperature. Solid samples were weighed using Mettler Toledo XS 105 analytical balance (120 g capacity with 0.0001 g readability).

The manually recovered product was weighed, stored, and kept at a nitrogen atmosphere. This fraction was used to determine viscosity, simulated distillation, and free radical concentration in the product. After analysis, the sample was dissolved in methylene chloride and filtered using a 0.22 μm filter to determine the total amount of solid in the product. All solids obtained were also dried inside the fumehood for 2 days to evaporate all the methylene chloride and weighed employing the same Mettler Toledo XS 105 analytical balance mentioned previously.

Material balance closure was typically within 97 to 102 wt. %. All the experiments were performed in triplicate and results were reported as an average with one sample standard deviation.

3.2.3 Analysis

Identification of the gaseous product was performed using an Agilent 7820A gas chromatography (GC) equipped with both flame ionization (FID) and thermal conductivity (TCD) detectors. A Hay Sep R column, 2.44 × 0.003 m (8 ft × ⅛ inch) was employed to achieve the separation. Helium was the carrier gas with flow of 25 $mL \cdot min^{-1}$. The injector temperature was set at 200 °C. The temperature program employed started at 70 °C, held isothemally for 7 minutes then the temperature was raised to 250 °C with 10 $°C \cdot min^{-1}$ ramp and then maintained isothermally for 2 minutes, followed by ramping at 30 $°C \cdot min^{-1}$ to 300 °C and holding for 8 minutes.

The DAO and liquid products were weighed using Mettler Toledo ML 3002 balance (3200 g capacity with 0.01 g readability) to determine the yields and mass balance closure.

Viscosity measurements were obtained using an Anton Paar RheolabQC viscometer. A concentric cylinder CC17/QC-LTC measuring cup was employed, its internal diameter is 16.664 mm and

24.970 mm length. An average of 4 g of the samples was employed for analysis. Viscosity measurements were carried out at three different temperatures: 40, 50 and 60 °C. The temperature was controlled by a Julabo F25-EH circulating heater/chiller, maintaining the temperature constant to within ±0.2 °C. The samples were measured at a constant shear rate of 10 s^{-1} for all the temperatures except 40 °C (shear rate $1s^{-1}$).

Refractive index was measured using an Anton Paar Abbemat 200 refractometer and determined relative to air using the sodium D-line (589 nm). The equipment was factory calibrated with official standards, with an accuracy of ± 0.0001 nD. The calibration was not experimentally verified. Refractive index was determined at different temperatures, namely 40, 50 and 60 °C and the accuracy of the temperature control was 0.05 °C.

Elemental analysis was made on a thermo Scientific Flash 2000 CHNS-O Organic Elemental analyzer.

^{1}H Nuclear Magnetic Resonance (NMR) spectra were determined in a Nanalysis 60 MHz NMReady –60 spectrometer. For the analysis, 0.15 g of the sample were dissolved in 0.7 mL deuterated chloroform and placed in 5mm NMR tubes. The analysis was performed using the following conditions: 0-12 ppm; number of scans for sample: 32; the scan delay was 20 seconds; and 4096 points were recorded per scan. Mnova NMR software was used to analyze all spectra obtained. Each spectrum was baseline corrected using a multipoint baseline correction method. Peak integration was made manually on the baseline corrected spectrum using aliphatic and aromatic hydrogen ranges.

Liquid products were analyzed using an Agilent 7890B gas chromatograph outfitted with flame ionization detector (FID) in order to determine the boiling point distribution through a temperature of 720 ºC (*n*-C_{100}) of crude oils and its residues following the Standard Test Method for Boiling Point Distribution of Samples with Residues Such as Crude Oils and Atmospheric and Vacuum Residues by High Temperature Gas Chromatography (ASTM D7169 – 11 [6]). This method enables the use of simulated distillation to analyze samples that do not elute completely from the chromatographic system. Samples were prepared in CS_2 with a dilution factor of 100, using 0.100

grams of liquid product on a 10 mL volumetric flask. As external standard, reference material 5010, ASTM D6352/D7169, Supelco was used to determine the detector response factor which is used to calculate the amount of sample recovered. Retention time calibration mixture 655 was employed as standard to develop a retention time versus boiling point curve, hence the boiling point distribution can be calculated up to the recovered amount. The standard 655 was prepared using 50 mg of Polywax 655, 50 µL of the boiling point calibration sample #1 kit (Agilent technologies Part. No. 5080-8715) diluted in CS_2 on a 10 mL volumetric flask. Blank subtraction was made automatically at the end of the run by the software OpenLab GC Agilent Technologies, in which three blanks (CS_2) at the beginning of the sequence, as well as a blank was run after each standard or sample injection to verify the absence of carryover from previous samples.

Fourier transform infrared (FT-IR) spectra of the sample were obtained using an ABB MB3000 spectrometer equipped with a MIRacle™ Reflection Attenuated Total Reflectance (ATR) diamond crystal plate and pressure clamp. The infrared used a deuterated triglycine sulfate (DTGS) detector. The 29 spectra were obtained at a resolution of 4 cm^{-1} as the average of 120 scans over the spectral region 4000-600 cm^{-1}.

The asphaltenes content was measured using as reference the ASTM D6560-12 [7] standard test method for separating asphaltenes from crude oil. The standard method was modified using the following parameters; *n*-Pentane was employed as the standard precipitant. For this work, 2 grams of liquid product was mixed with 80 mL of *n*-pentane (*n*-C_5) in a 250 mL Erlenmeyer and stirred for 1 h. Samples were left inside the fumehood overnight, then they were filtered in a vacuum system using a 0.22 µm milipore filter. Solid samples were maintained inside the fumehood for 2 days to evaporate all the *n*-pentane.

Density measurements were made using a 5 mL (+/- 0.03) Thomas Specific gravity bottle (glass pycnometer – Gay-Lussac type), provided with capillary glass stopper ground to flat-sided point for take-off of overflow. Measurements were performed following the standard test method for Density of Semi-Solid Bituminous Materials (ASTM D 70 – 09 [8]). Since the volume of the pycnometer is constant, determinations made are based on the weight of empty and filled pycnometer. An analytical Mettler Toledo XS 105 balance (120 g capacity with 0.0001 g

readability) was used. For the analysis, 2 g of heavy oil was employed and then the pycnometer was filled completely using de-ionized water. Density was determined at two different temperatures, namely 20 and 40 °C. For this, the pycnometer was immersed in a water bath for 10 minutes and the temperature was controlled by a Julabo F25-EH circulating heater/chiller, maintaining the temperature constant to within ±0.2 °C. A sample of the calculation is shown in the appendix A.

The electron spin resonance (ESR) spectra of the samples were obtained using an Active Spectrum' Micro ESR TM Electron Spin Resonance Spectrometer operating a nominal frequency 9.7 GHz, with a micropower level sufficiently low to avoid saturation effects (10 mW). The micro-ESR spectrometer contains an internal cooling device designed to hold the sensor at the fixed temperature, ensuring uniformity of results. High precision 5 mm diameter quartz tubes, Wilmad labGlass Part No. 701-PQ-7, were used for quantitative analysis. The samples were diluted at 30 wt. % in toluene to pour them into the sample tubes; 0.25 g of the sample were dissolved in 0.67 mL of toluene. The diluted sample was filtered out using a disposable Millex-GP syringe filter, pore size 0.22 μm. The analysis was performed using the following conditions: Starting sweep field; 3200 G; microwave power: 10mW; coil amplitude percentage: 100%; number of scans for sample: 5; 162.8 seconds was the average scan time and 4096 data points were recorded per scan. The spectra were analyzed and baseline corrected using Active Spectrum software. The free radicals concentration in all samples were calculated by comparison of the double integrated intensity with a calibration curve built using 4-hydroxy TEMPO, free radical (98+%) at different concentrations diluted in toluene (Figure 3-3).

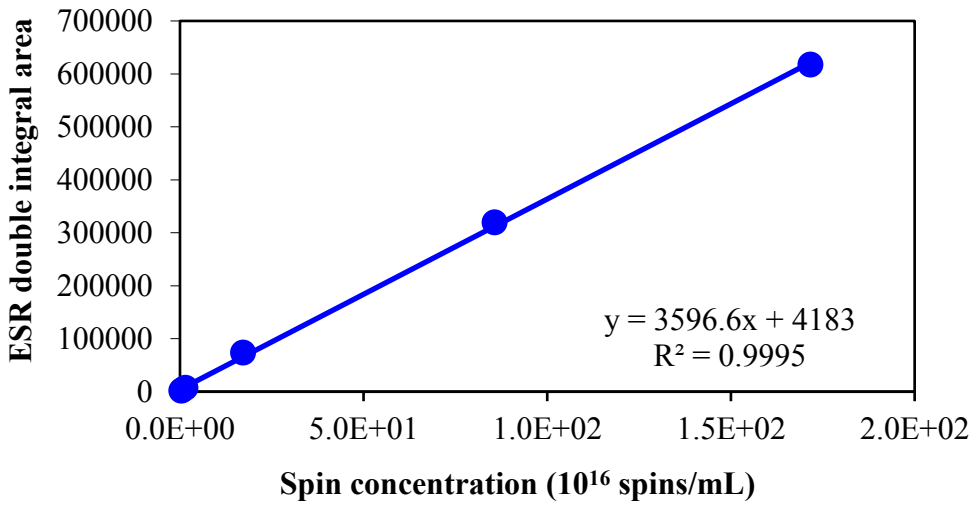

Figure 3-3. Calibration curve double integral area vs free radical concentration; built using 4-hydroxy TEMPO, free radical (98+ %) at different concentrations diluted in toluene

Solid obtained from the reactions were analyzed using a Carl Zeiss Discovery V.20 stereomicroscope to visually distinguish the solids obtained at different reaction times. This lens has a zoom range of 20:1, and it is capable of a magnification of 345X. The camera resolution was up to 1000 {line pairs (LP)}/mm. A resolution of 10 lines per millimeter implies 5 dark lines alternating with 5 light lines or 5 line pairs per millimeter (5LP/mm). Images were recorded using reflected light at 7.5X magnification.

Solids product samples were additionally analyzed using a Zeiss Sigma 300 VP field emission scanning electron microscope (FE-SEM). The equipment is equipped with 4 different detectors (cathodoluminescence, an in-lens electron, secondary and backscattered electron detectors) and a Bruker energy dispersive X-ray spectroscopy (EDS) system with dual silicon drift detectors each with an area of 60 mm^2 and a resolution of 123 eV so that images of the particles, surfaces and nanostructures could be generated and analyzed. It has a resolution of 10 nm and could be operated at variable pressure and high vacuum modes. Samples must be coated with either gold or carbon before being analyzed. The samples of the solid particles from thermal conversion reaction were prepared for scanning electron microscopy (SEM) by being sputter-coated with carbon.

3.3 Results

As part of the study to understand the changes that took place during this mild thermal treatment. Products were characterized and analyzed. The three phases influenced each other; however, this work is mainly focused on those changes related to the liquid phase products.

3.3.1 Material Balance

The reaction products were obtained under these conditions: 280 and 320 °C, an initial pressure of 3 MPa N_2 and reaction time varying from 1 to 360 minutes. The reaction time of 0 min corresponds to deasphalted vacuum residue sample (i.e. feed not exposed to temperature). The mass of each phase was determined individually. The overall material balance (Table 3-2) and the product yields of each phase at 280 °C (Table 3-3) and 320 °C (Table 3-5) were obtained for experiments that were performed in triplicate. In all experiments, the average material balance closed to within 2 %, i.e. material balance was between 98 and 102 %.

Table 3-3. Mass balance for thermal conversion at 280 and 320 °C for different reaction times

Balance Material [wt. %][a]		
Reaction temperature: 280 °C		
Reaction time [min]	**x**	**s**
10	100.25	1.12
20	99.89	0.55
30	99.13	1.21
45	100.13	0.91
60	100.13	0.35
90	99.39	1.05
120	99.78	1.57
240 [b]	100.00 [b]	--
Reaction temperature: 320 °C		
20	99.71	1.45
45	100.28	0.39
60	100.20	0.29
90	99.65	1.04
120	100.02	0.14
240	100.32	1.43
360 [b]	99.68 [b]	--

[a] Average (x) and sample standard deviation (s) of three experiments are reported
[b] Single sample was performed at this condition

Table 3-4. Product yield (wt. %) for thermal conversion at 280 °C for different reaction times

Material Balance [wt. %][a]						
Reaction temperature: 280 °C						
Time [min]	**Gas**		**Liquid**		**Solid**	
	x	**s**	**x**	**s**	**x**	**s**
10	0.24	0.06	99.18	0.18	0.69	0.11
20	0.06	0.04	99.39	0.15	0.55	0.19
30	0.46	0.06	99.16	0.30	0.38	0.30
45	0.16	0.01	99.22	0.19	0.61	0.20
60	0.15	0.01	99.35	0.29	0.50	0.29
90	0.34	0.25	99.11	0.58	0.55	0.33
120	0.30	0.35	99.02	0.34	0.46	0.16
240[b]	2.35	--[b]	96.97	--[b]	0.68	--[b]

[a] Average (x) and sample standard deviation (s) of three experiments are reported
[b] Single sample was performed at this condition

After reaction, some observations were made during the phase separation. A small amount of gaseous products were obtained within the first 120 minutes of reaction (< 1wt. %), mostly methane, H_2S and CO_2. Gaseous products contain some H_2S, which was expected due to the elemental analysis of the feed.

Table 3-5. Product yield (wt. %) for thermal conversion at 320 °C for different reaction times

Material Balance [wt. %][a]						
Reaction temperature: 320 °C						
Time [min]	**Gas**		**Liquid**		**Solid**	
	x	**s**	**x**	**s**	**x**	**s**
20	1.10	0.20	97.97	0.37	0.90	0.24
45	0.48	0.45	98.91	0.28	0.61	0.18
60	1.13	0.66	98.18	0.71	0.69	0.12
90	1.21	0.80	98.35	0.79	0.45	0.07
120	1.25	0.19	98.31	0.14	0.59	0.09
240	6.15	0.56	92.94	0.91	0.91	0.35
360[b]	6.44	--	93.05	--	0.50	--

[a] Average (x) and sample standard deviation (s) of three experiments are reported
[b] Single sample was performed at this condition

At 280 °C, as the time increased from 0 min to 90 min, the yields of gas, solid, and liquid stayed nearly constant. After 240 min, there is an increase in the amount of gases generated in which the gas yield raise to 2.35 wt. %.

In the case of reaction at 320 °C, the liquid yield remains fairly constant up to 120 min. Thus, from 240 min to 360 min, the yield of liquid decreased from 98.3 to 92.9 wt. % as the yield of gas increased. There is not significantly increase compare with the solid content in the feed (DAO) during the time reported. The yield of gas increased within the first 20 min, showing that a considerable amount of gases are generated from the beginning.

Filtration of liquid products took a long time before solids were obtained and this was found for all experiments. It is likely that the solids in the feed were very fine, which was later confirmed by microscopy.

3.3.2 Product characterization

3.3.2.1 Viscosity

In the light of support for the industrial development of a process for the partial upgrading of oil sands bitumen in smaller facilities closer to the point of bitumen recovery, the first and probably the main product property of this work is the viscosity measurements.

Every measurement was performed at 3 different temperatures (40, 50 and 60 °C), but shear rate was kept constant at 10 s^{-1} for all the temperatures except 40 °C (shear rate 1s^{-1}). These results are reported in Table 3-6 and Table 3-7 for reaction temperature at 280 °C and 320 °C respectively.

Table 3-6. Viscosity data to thermal conversion products under 280 °C and initial pressure 3 MPa

	Time reaction [min]								
	0	**10**	**20**	**30**	**45**	**60**	**90**	**120**	**240**
	Viscosity [Pa.s]								
Measured Temperature: 60 [°C]									
Average	131.2	118.8	115.0	121.3	113.0	122.5	119.8	118.6	111.5
Std. dev.	3.8	2.5	8.2	3.8	2.7	3.4	4.6	5.8	--[a]
Measured Temperature: 50 [°C]									
Average	600.0	506.6	522.1	542.5	486.2	547.6	526.4	534.9	497.8
Std. dev.	13.4	59.5	44.3	15.8	31.0	15.3	34.3	42.0	--[a]
Measured Temperature: 40 [°C]									
Average	3718.5	3413.7	3193.6	3417.7	3660.6	3447.7	3210.2	3219.5	3040.0
Std. dev.	293.9	313.0	261.8	99.7	140.6	96.2	521.8	363.9	--[a]

[a] Single sample was performed at this condition

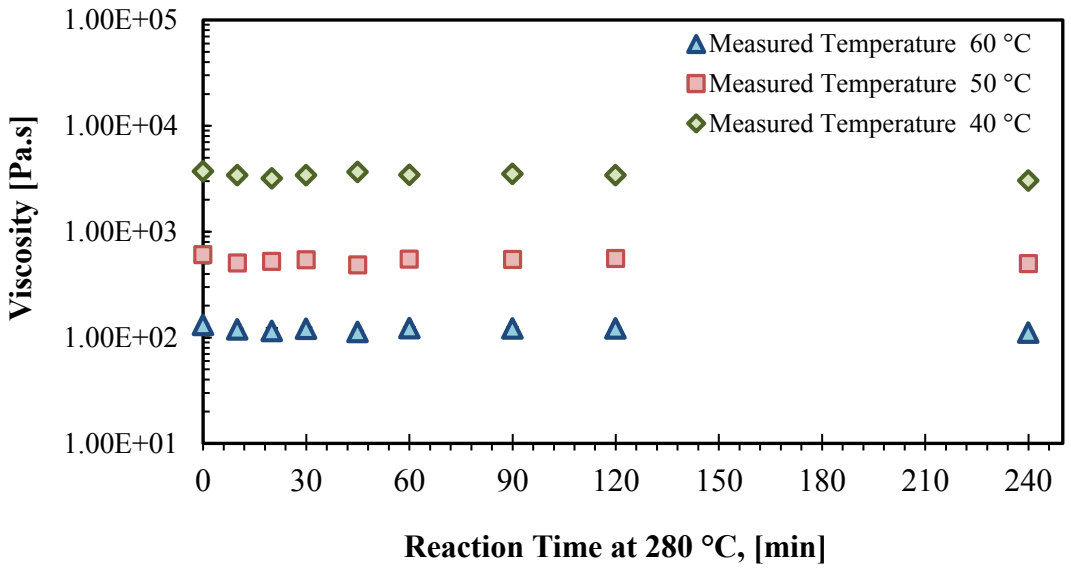

Figure 3-4. Viscosity of thermal conversion products obtained under 280 °C, initial pressure of 3 MPa and reaction time varying between 1 and 240 minutes. Measurements were performed at different temperatures

After thermal treatment at 280 °C, the viscosity of the products is observed fairly constant along the time reported in this work (Figure 3-4).

Table 3-7. Viscosity data to thermal conversion products under 320 °C and initial pressure 3 MPa

	Time reaction [min]							
	0	**20**	**45**	**60**	**90**	**120**	**240**	**360**
	Viscosity [Pa.s]							
Measured Temperature: 60 [°C]								
Average	131.2	88.2	80.7	71.9	55.8	66.8	40.9	42.6
Std. dev.	3.8	2.5	8.2	3.8	2.7	3.4	4.6	--[a]
Measured Temperature: 50 [°C]								
Average	600.0	355.1	303.0	302.6	196.5	234.8	148.7	156.0
Std. dev.	13.4	9.2	39.4	25.6	1.8	55.2	14.7	--[a]
Measured Temperature: 40 [°C]								
Average	3718.5	2165.1	1820.6	1732.2	1190.3	1219.8	746.7	777.2
Std. dev.	293.9	87.3	235.9	146.3	10.7	357.3	170.2	--[a]

[a] Single sample was performed at this condition

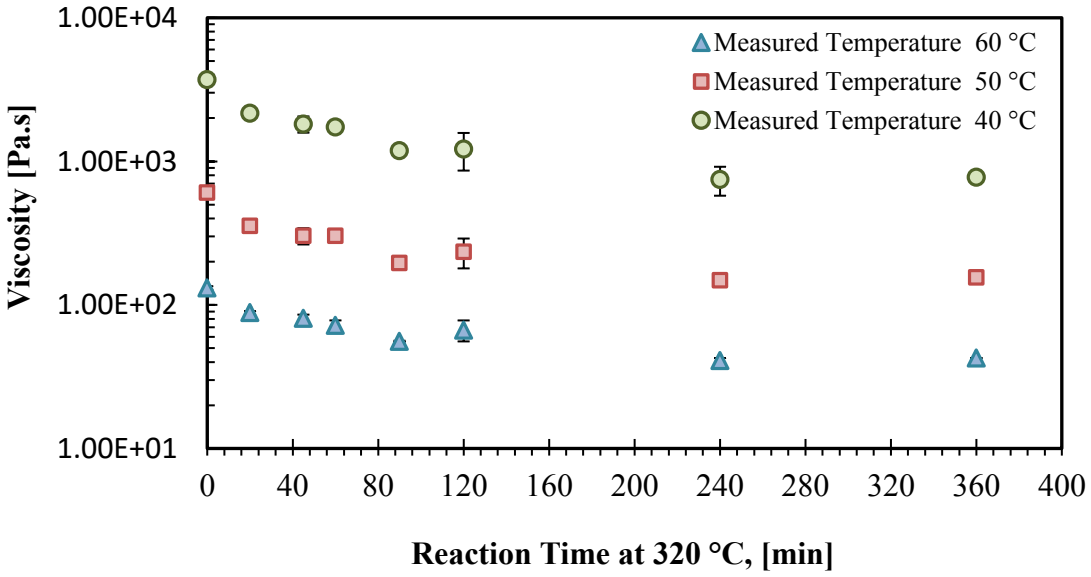

Figure 3-5. Viscosity of thermal conversion products obtained under 320 °C, initial pressure of 3 MPa and reaction time varying between 1 and 360 minutes. Measurements were performed at different temperatures

As listed in the characterization of Nexen Long Lake DAO in Table 3-1, the viscosity of deasphalted vacuum residue oil is about 600 Pa.s at 50 °C. In the case of thermal conversion at 320 °C, as the reaction time increases, a decrease in viscosity compared to was observed up to 240 min. As a result, the viscosity measured at 40 °C was reduced by about 5 times (half order of

magnitude) compared to the value of DAO from 0 min to 240 min without coke formation. Afterward, the viscosity increased slightly from 745 Pa.s to 777 Pa.s at 40 °C, although there was no increase in the coke yield from 240 min to 360 min (Figure 3-5).

It is noteworthy to mention that these samples were analyzed as recovered directly from the reactor, without any solvent being added. This data therefore represents 'true values', unless there is a natural segregation due to inhomogeneity and that samples must be homogenized to get a representative sample.

3.3.2.2 Refractive index

The refractive index of every sample was determined at 5 different temperatures (20, 30, 40, 50 and 60 °C), and in Table 3-8 and Table 3-9 is reported the values at 280 °C and 320 at different reaction times. Furthermore, Figure 3-6 and Figure 3-7 shows the refractive index at 280 and 320 °C versus time in order to identify variation of this property over reaction time.

Table 3-8. Refractive Index measurements performed on liquid products after thermal conversion at 280 °C and initial pressure 3 MPa reaction

	Temperature [°C]	**Time reaction [min]**								
		0	**10**	**20**	**30**	**45**	**60**	**90**	**120**	**240**
		Refractive index [nD]								
Average	20	1.5921	1.5909	1.5919	1.5916	1.5923	1.5934	1.5935	1.5928	1.5961
Std. dev.		0.0001	0.0006	0.0010	0.0008	0.0006	0.0007	0.0028	0.0010	--[a]
Average	30	1.5883	1.5871	1.5872	1.5879	1.5885	1.5897	1.5896	1.5891	1.5924
Std. dev.		0.0000	0.0025	0.0025	0.0009	0.0006	0.0007	0.0027	0.0009	--[a]
Average	40	1.5846	1.5834	1.5835	1.5841	1.5848	1.5860	1.5860	1.5853	1.5887
Std. dev.		0.0001	0.0026	0.0025	0.0008	0.0006	0.0007	0.0029	0.0009	--[a]
Average	50	1.5808	1.5797	1.5798	1.5805	1.5810	1.5814	1.5822	1.5816	1.5851
Std. dev.		0.0001	0.0026	0.0024	0.0008	0.0006	0.0009	0.0031	0.0009	--[a]
Average	60	1.5773	1.5761	1.5760	1.5769	1.5774	1.5777	1.5783	1.5780	1.5815
Std. dev.		0.0001	0.0027	0.0024	0.0006	0.0005	0.0008	0.0033	0.0010	--[a]

[a] Single sample was performed at this condition

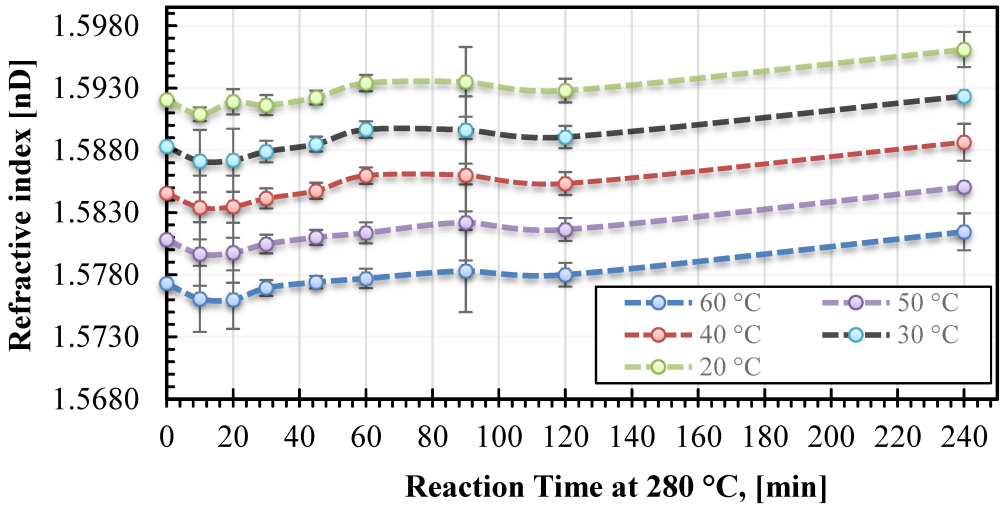

Figure 3-6. Refractive Index results for Thermal Conversion Products at 280 °C, initial pressure of 3 MPa and different reaction times: Refractive index vs Time

At 280 °C, it is exhibited a slightly increase of the index of refraction along time until reaction time reach 60 minutes, after which the index refractive remains constant up to 120 minutes to then continually increase after 240 min (Figure 3-6). This behavior is an indication of the liquid product is being mildly more aromatic.

Table 3-9. Refractive Index measurements performed on thermal conversion products after 320 °C and initial pressure 3 MPa reaction

	Temperature [°C]	Time reaction [min]							
		0	20	45	60	90	120	240	360
		Refractive index [nD]							
Average	20	1.5921	1.5910	1.5889	1.5903	1.5909	1.5910	1.5931	1.5948
Std. dev.		0.0001	0.0019	0.0011	0.0026	0.0019	0.0014	0.0005	--[a]
Average	30	1.5883	1.5872	1.5851	1.5864	1.5871	1.5872	1.5893	1.5910
Std. dev.		0.0000	0.0028	0.0011	0.0028	0.0019	0.0015	0.0006	--[a]
Average	40	1.5846	1.5832	1.5812	1.5824	1.5833	1.5834	1.5856	1.5873
Std. dev.		0.0001	0.0030	0.0012	0.0028	0.0020	0.0015	0.0005	--[a]
Average	50	1.5808	1.5793	1.5774	1.5785	1.5795	1.5796	1.5818	1.5835
Std. dev.		0.0001	0.0032	0.0012	0.0030	0.0021	0.0016	0.0006	--[a]
Average	60	1.5773	1.5756	1.5735	1.5746	1.5754	1.5759	1.5782	1.5800
Std. dev.		0.0001	0.0033	0.0013	0.0032	0.0026	0.0016	0.0005	--[a]

[a] Single sample was performed at this condition

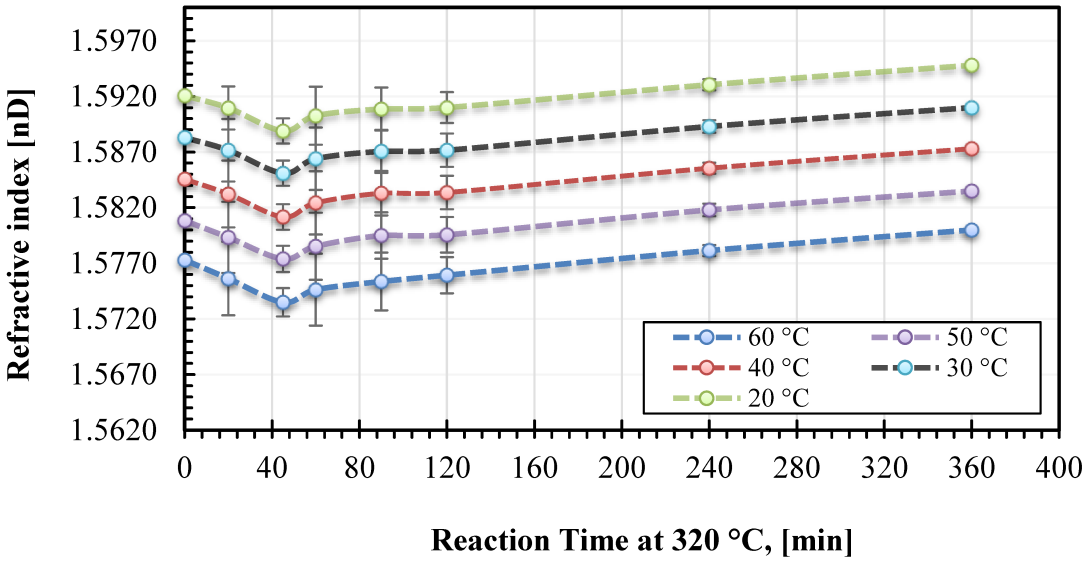

Figure 3-7. Refractive Index results for Thermal Conversion Products at 320 °C, initial pressure of 3 MPa and different reaction times: Refractive index vs Time

From the Figure 3-7, it can be observed that there is a slightly decrease of the index of refraction along time until reaction time reach 45 minutes, after which it is followed by an increase in the measurement. These behavior align with the others measured variables such as viscosity, H/C ratio, ^{1}H NMR, *n*-pentane insoluble material.

In addition, it is shown that the index of refraction maintain the tendency along time at different measured temperature.

3.3.2.3 Liquid boiling point distribution (SimDist)

The liquid boiling point distribution of the thermal conversion products at 280 °C and 320 °C was determined, and it is presented in figure 3-8 and figure 3-9. The results of this analysis are shown in the following way: Temperature vs weight percent distilled.

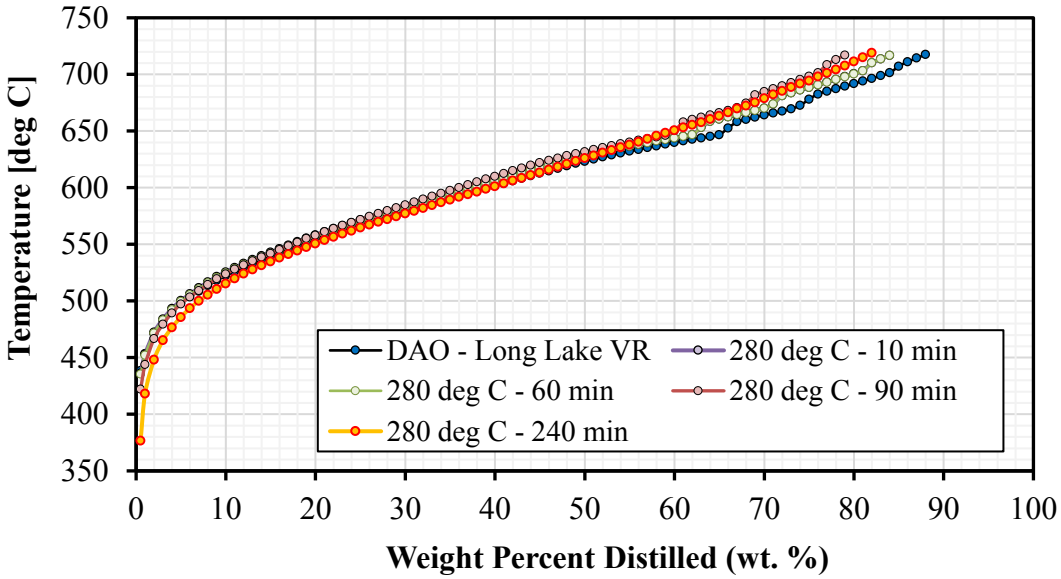

Figure 3-8. Liquid boiling point distribution of liquid products after thermal conversion at 280 °C, initial pressure of 3 MPa at different reaction times

At 280 °C, there is not a significantly generation of light products, but also some heavy compounds are generated. This pattern correspond with others measured variables such as viscosity, H/C ratio, refractive index.

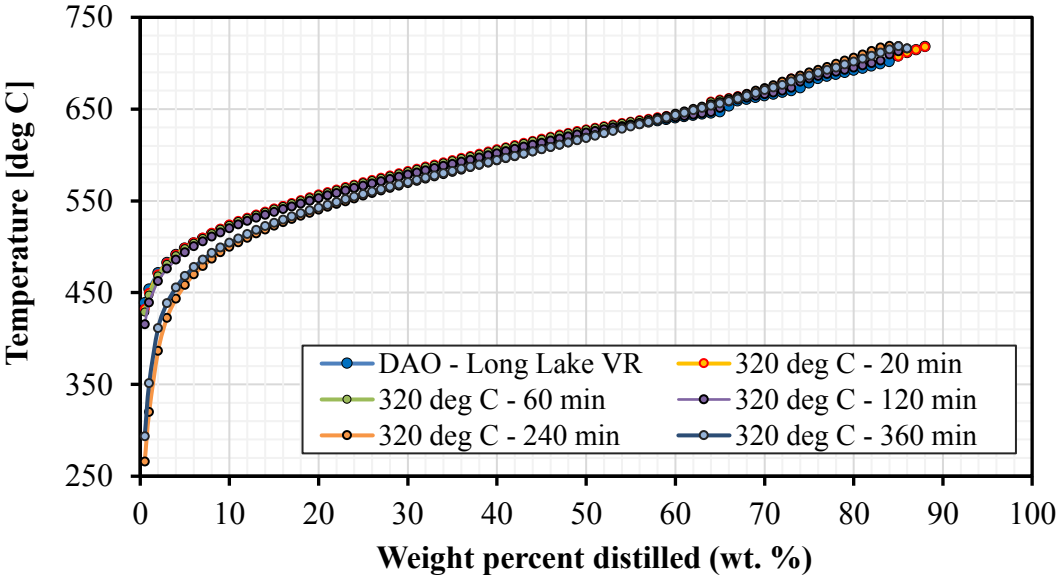

Figure 3-9. Liquid boiling point distribution of liquid products after thermal conversion at 320 °C, initial pressure of 3 MPa at different reaction times

In the case of reaction at 320 °C, the liquid boiling point distribution fairly constant up to 120 minutes. Afterward, from 240 min to 360 min, there is an increase in the amount of light boiling point compounds (BP < 524 °C).

3.3.2.4 Elemental analysis

Elemental analysis of the products and deasphalted vacuum residue oil were obtained in order to track changes in the products such as hydrogen disproportionation. These results are reported in Table 3-10 and Table 3-11 for reaction temperature at 280 °C and 320 °C respectively.

Table 3-10. Elemental analysis in wt. % of thermal conversion products after 280 °C, initial pressure of 3 MPa at different reaction times

Elemental analysis [wt. %][a]								
Reaction temperature: 280 °C								
Time [min]	**C**		**H**		**N**		**S**	
	x	**s**	**x**	**s**	**x**	**s**	**x**	**s**
0	83.35	0.31	9.88	0.05	0.58	0.03	5.59	0.12
10	82.56	0.35	9.78	0.04	0.59	0.01	5.60	0.07
20	82.28	0.69	9.78	0.06	0.58	0.01	5.81	0.20
30	83.03	0.34	9.84	0.02	0.55	0.03	5.65	0.08
45	83.26	0.51	9.77	0.02	0.56	0.01	5.47	0.04
60	82.40	0.54	9.77	0.05	0.57	0.01	5.72	0.03
90	82.63	0.08	9.81	0.01	0.59	< 0.01	5.78	0.14
120	82.55	0.30	9.80	0.04	0.59	< 0.01	5.82	0.13

Table 3-11. Elemental analysis in wt. % of thermal conversion products after 320 °C, initial pressure of 3 MPa at different reaction times

Elemental analysis [wt. %][a]								
Reaction temperature: 320 °C								
Time [min]	**C**		**H**		**N**		**S**	
	x	**s**	**x**	**s**	**x**	**s**	**x**	**s**
0	83.35	0.31	9.88	0.05	0.59	0.03	5.59	0.12
20	82.28	0.06	9.77	0.04	0.58	0.01	5.60	0.06
45	82.50	0.04	9.79	0.01	0.58	< 0.01	5.65	0.08
60	83.19	0.05	9.84	< 0.01	0.59	< 0.01	5.63	0.09
90	82.88	0.38	9.81	0.03	0.56	0.04	5.60	0.07
120	83.13	0.15	9.82	0.05	0.59	< 0.01	5.57	0.04

[a] Average (x) and sample standard deviation (s) of three experiments are reported

In addition, the hydrogen/carbon molar ratio of the thermal conversion products at 280 °C and 320 °C were calculated, it is presented in Figure 3-10 and Figure 3-11, respectively.

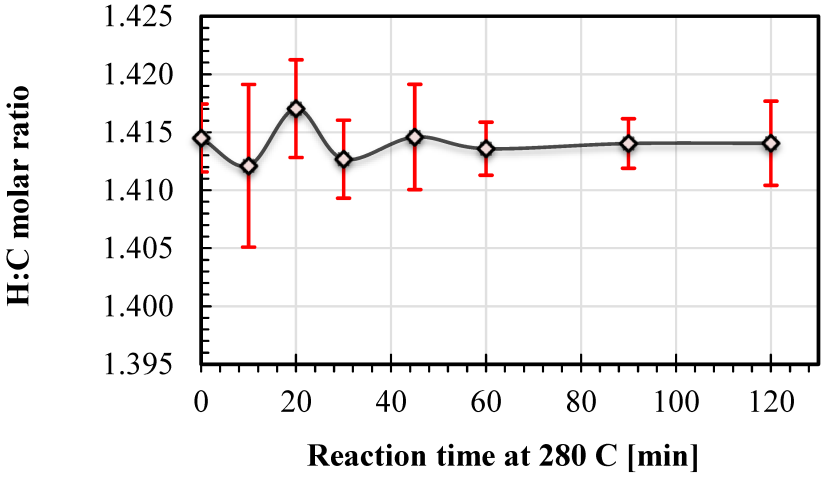

Figure 3-10. Hydrogen/carbon molar ratio of thermal conversion products after 280 °C, initial pressure of 3 MPa at different reaction time

After thermal treatment at 280 °C, as a previous measured variable, the H/C molar ratio of the products is observed fairly constant along the time reported in this work.

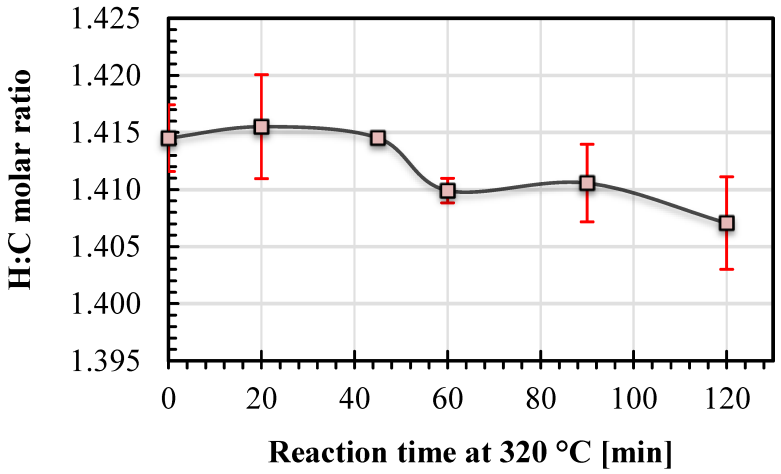

Figure 3-11. Hydrogen/carbon molar ratio of thermal conversion products after 320 °C, initial pressure of 3 MPa at different reaction time

From Figure 3-11, it can be seen that the H/C molar ratio maintain fairly constant until reach 45 minutes at 320 °C, afterward the ratio decreases along time. This change coincides with the change in the refractive index (Fig 3-7).

3.3.2.5 Proton nuclear magnetic resonance ^{1}H NMR

Proton NMR analysis was employed to estimate aliphatic and aromatic content and observe how its proportions change under different reaction conditions. In Figure 3-12 and Figure 3-13, it is presented a) the NMR spectra of thermal conversion products in order to identify all the structural changes of the DAO if there is any change, and b) the aliphatic hydrogen content of thermal conversion products against reaction time to enable tracking any change related with the aliphatic content at 280 and 320 °C

In order to convert the NMR data to obtain the aliphatic hydrogen content, some regions can be identified in based on data presented by Sharma et al [9], Yen et al [10], and Hauser et al [11]. A typical ^{1}H NMR spectra of vacuum residue and their deasphalted fraction shows a clear distinction between hydrogen associated to aliphatic and aromatic carbons, in which the main region in the spectra correspond to 0.4 to 4 ppm refers to the aliphatic hydrogen and between 6 and 9 ppm this peak is related with aromatic and phenolic hydrogens [9].

Moreover, a peak was found between 5 and 5.5 ppm (ca. 5.3 ppm) which corresponds to the solvent used (methylene chloride) for the sample preparation. This shift value was also reported and attributed to methylene chloride by Dehkissia et al [12].

Mnova NMR software was used the determination of peak area based on the hydrogen ranges mentioned before, and methylene chloride shift was ignored for the calculations purpose.

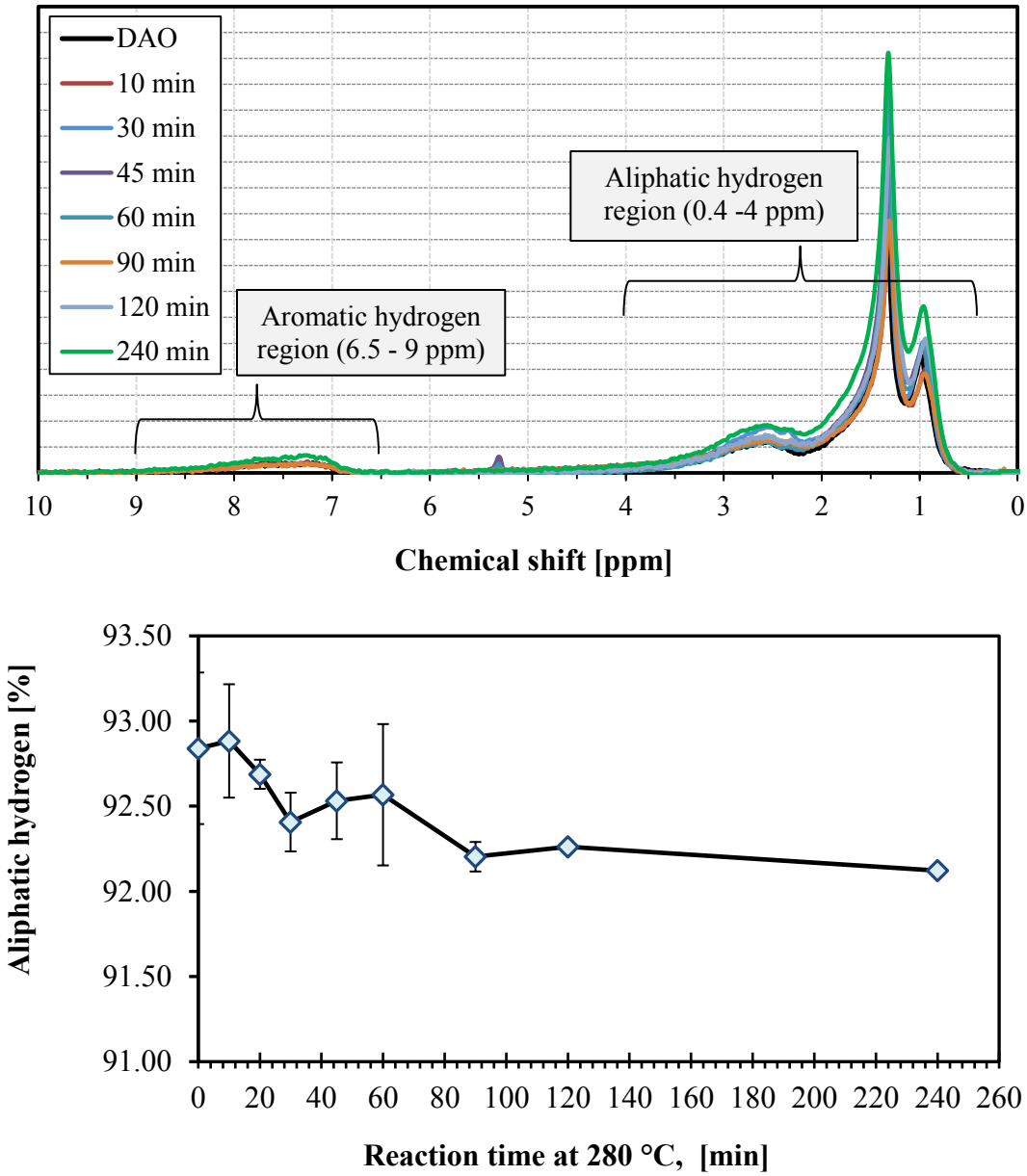

Figure 3-12. Proton NMR results of thermal conversion products after 280 °C, initial pressure of 3 MPa and different times; a) ^{1}H NMR spectra b) % Aliphatic hydrogen vs Time

At 280 °C, there is a decrease in the aliphatic hydrogen content along time until reach 90 minutes, subsequently the measured variable remains constant up to 240 min.

In the case of reaction at 320 °C, the aliphatic hydrogen content decrease constantly along time until reaction time reach 240 minutes. Afterward, from 240 min to 360 min, there is an increase in

the aliphatic hydrogen content remains constant around 92 wt. %. This behavior is aligned with others measured variables such as refractive index, pentane insoluble material.

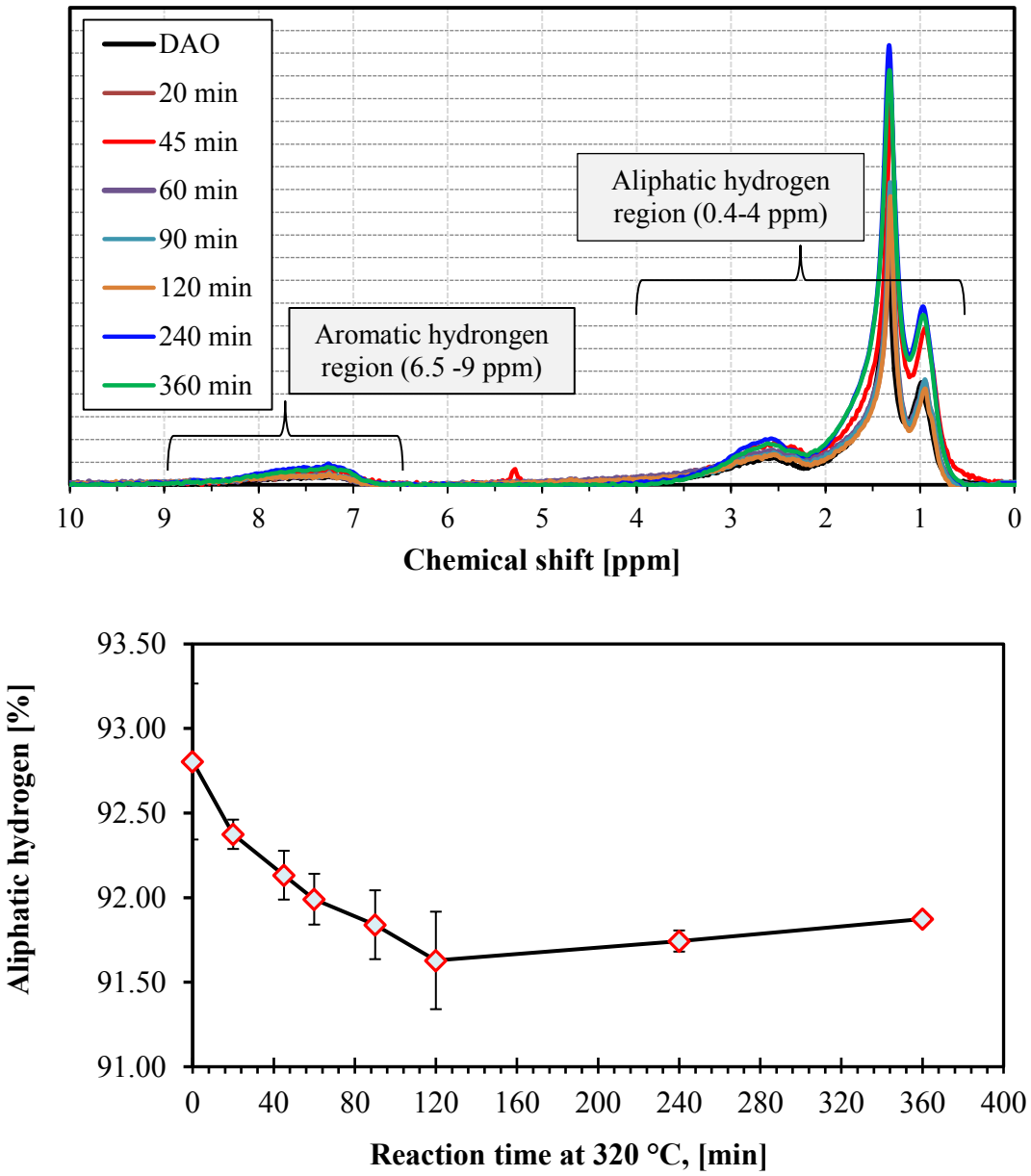

Figure 3-13. Proton NMR results of thermal conversion products after 320 °C, initial pressure of 3 MPa and different times; a) ^{1}H NMR spectra b) % Aliphatic hydrogen vs Time

3.3.2.6 Pentane insoluble material (Asphaltene content)

Asphaltenes are the highest-molecular-weight fraction of petroleum and they can be defined as the amount of compounds which are insoluble using *n*-pentane as solvent following ASTM D6560-12

[7]. The *n*-pentane precipitated asphaltenes content was determined, it is listed in Table 3-12 and Table 3-13. Moreover, Figure 3-14 and Figure 3-15 shown the *n*-pentane content in the thermal conversion products versus time at 280 °C and 320 °C respectively, in order to illustrate and identify variation of this property over reaction time.

Table 3-12. Pentane insoluble content in wt. % of thermal conversion products after 280 °C, initial pressure of 3 MPa and different times

	Time reaction [min]							
	0	**10**	**30**	**45**	**60**	**90**	**120**	**240**
	***n*-Pentane insoluble [wt. %]**							
Average	6.56	7.59	8.61	8.59	9.01	9.36	9.28	9.47
Std. dev.	0.15	0.38	1.03	0.84	1.32	0.39	1.44	--[a]

[a] Single sample was performed at this condition

Table 3-13. Pentane insoluble content in wt. % of thermal conversion products after 320 °C, initial pressure of 3 MPa and different times

	Time reaction [min]							
	0	**20**	**45**	**60**	**90**	**120**	**240**	**360**
	***n*-Pentane insoluble [wt. %]**							
Average	6.56	8.37	7.97	8.02	8.89	9.01	8.13	8.15
Std. dev.	0.15	0.44	0.40	0.61	0.71	0.26	0.75	--[a]

[a] Single sample was performed at this condition

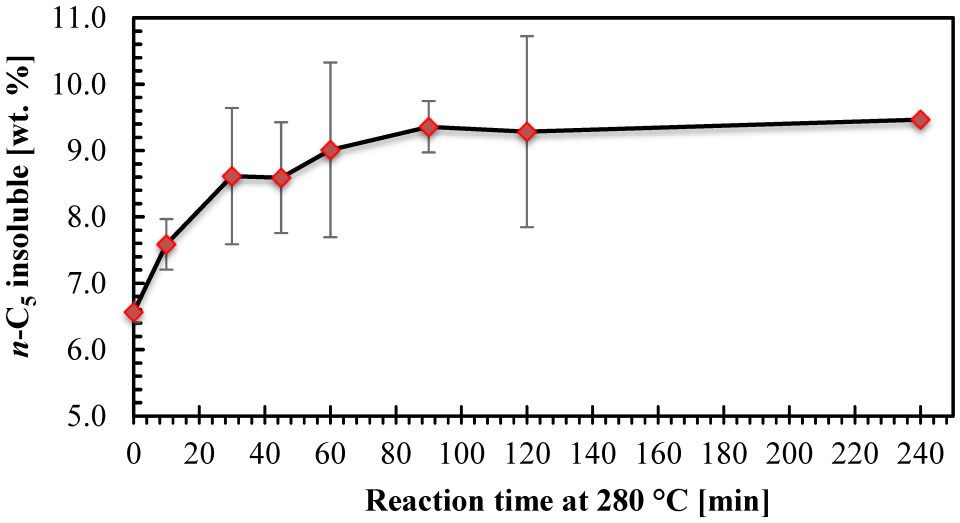

Figure 3-14. Pentane insoluble content of liquid products after thermal conversion at 280 °C, initial pressure of 3 MPa and different times

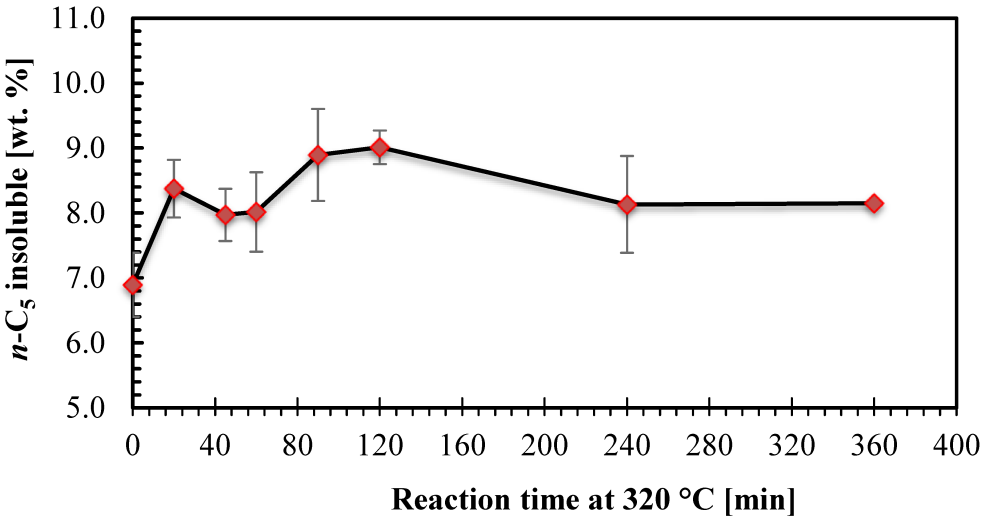

Figure 3-15. Pentane insoluble content of liquid products after thermal conversion at 320 °C, initial pressure of 3 MPa and different times

From Figure 3-14 and Figure 3-15, there was observed that the increase in asphaltenes content was not just a high temperature process, but took place also at the lowest temperature investigated, namely 280 °C and 320 °C.

3.3.2.7 FT-IR spectroscopy

FT-IR spectroscopy allow it to detect the presence of chemical groups in materials. In the case of raw deasphalted oil, as bitumen, it is a complex mixture that contains many compounds, thereby this method help to support and confirm hypothesis about changes during the thermal conversion. In Figure 3-16 and Figure 3-17, the spectrum for every reaction time was plotted.

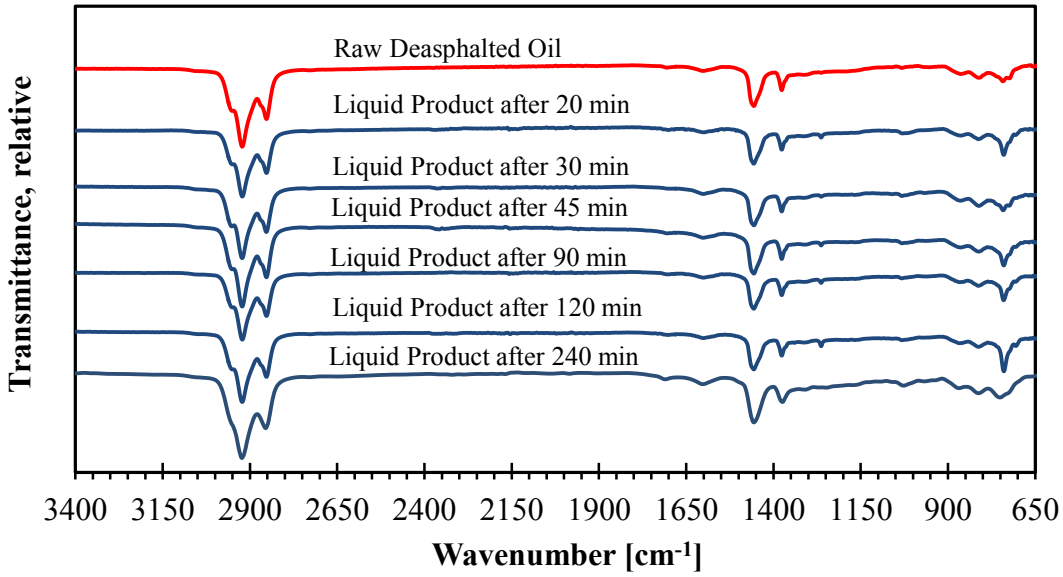

Figure 3-16. FTIR spectra of thermal conversion products after 280 °C, initial pressure of 3 MPa and different reaction times

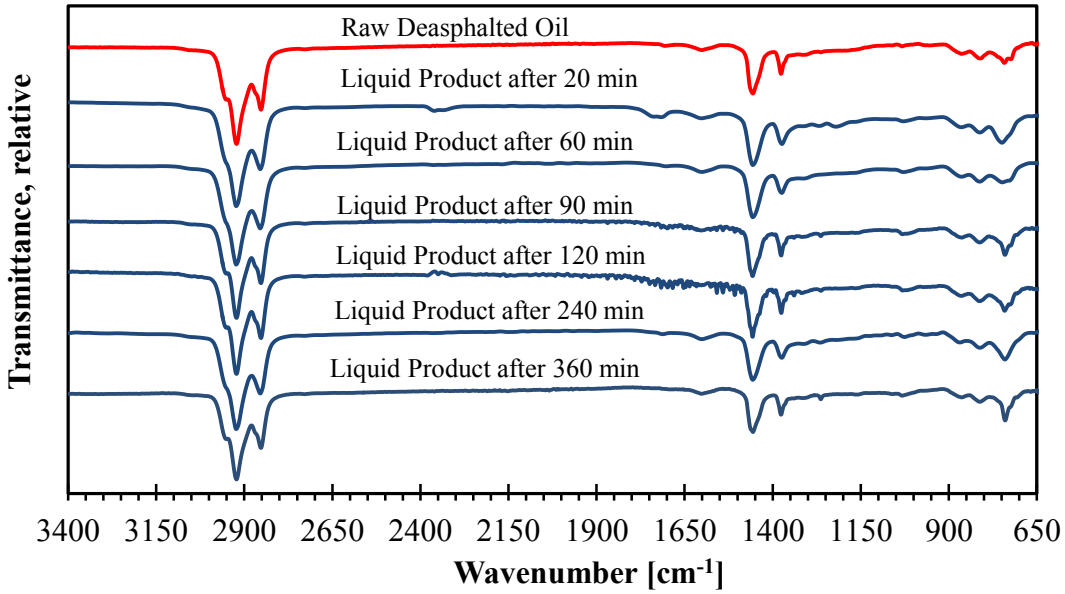

Figure 3-17. FTIR spectra of thermal conversion products after 320 °C, initial pressure of 3 MPa and different reaction times

3.3.2.8 Electron spin resonance (ESR) spectroscopy

The electron spin resonance (ESR) spectra of the liquid products and deasphalted vacuum residue oil were obtained in order to track the free radical species, mainly focused on organic radicals, and thus offer insights into the genesis of this species and nature of the aromatic rings addition during

thermal conversion of heavy oil. The ESR spectra were recorded as first derivative curves, and it is shown in Figure 3-18 and Figure 3-19.

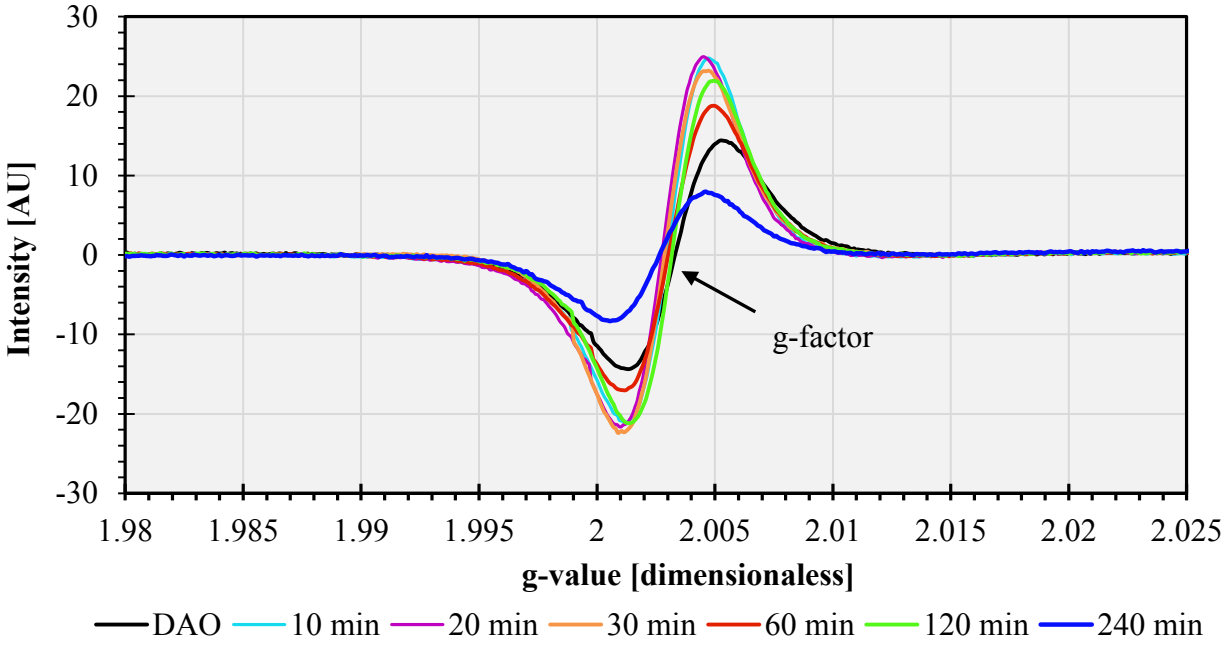

Figure 3-18. ESR spectra of DAO and thermal conversion products after 280 ˚C, initial pressure of 3 MPa and different reaction times

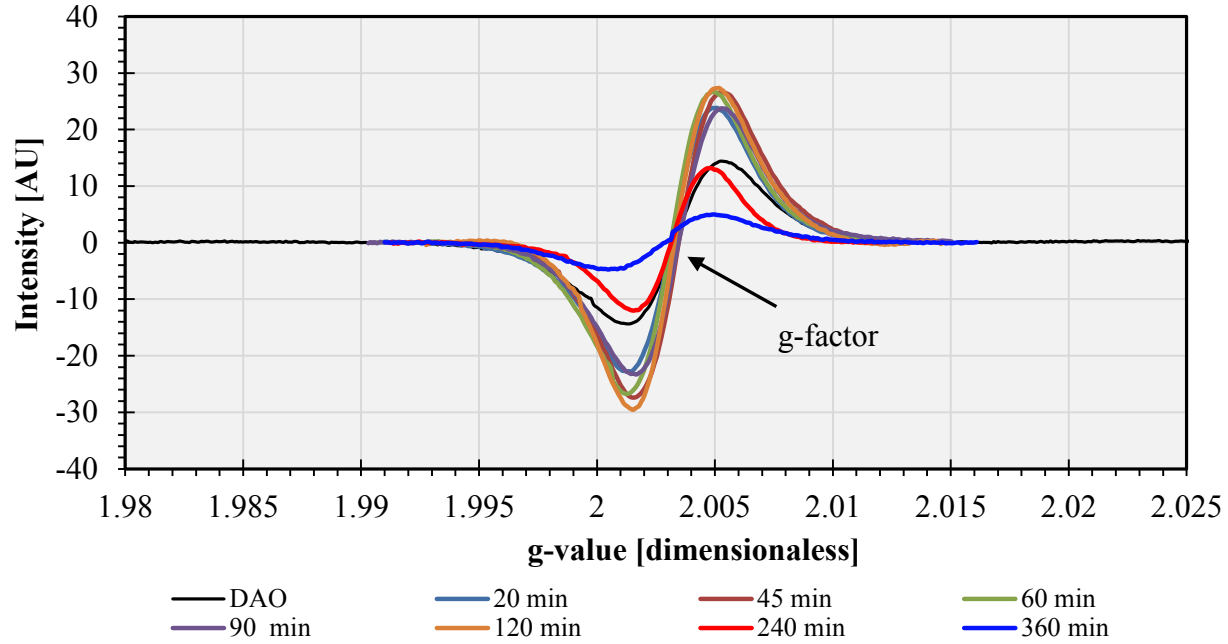

Figure 3-19. ESR spectra of DAO and thermal conversion products after 320 °C, initial pressure of 3 MPa and different reaction times

As shown Figure 3-18 and Figure 3-19, a single peak between g-values of 1.99-2.01 (magnetic field absorption between 3440 - 3470 gauss) is easily identified. As mentioned previously in Chapter 2, this intense single peak in the ESR spectra of petroleum fractions correspond to the presence of organic free radicals.

In the case of vanadium complexes (VO^{2+}) species, there is not well-defined peaks detected in the spectra due to the low vanadium content in the feed (around 60 ppm) and the dilution factor used in this work. However, Figure 3-20 presents the ESR spectra of DAO at two different concentrations diluted in toluene in order to illustrate the presence of peaks associated to vanadium complexes (VO^{2+}).

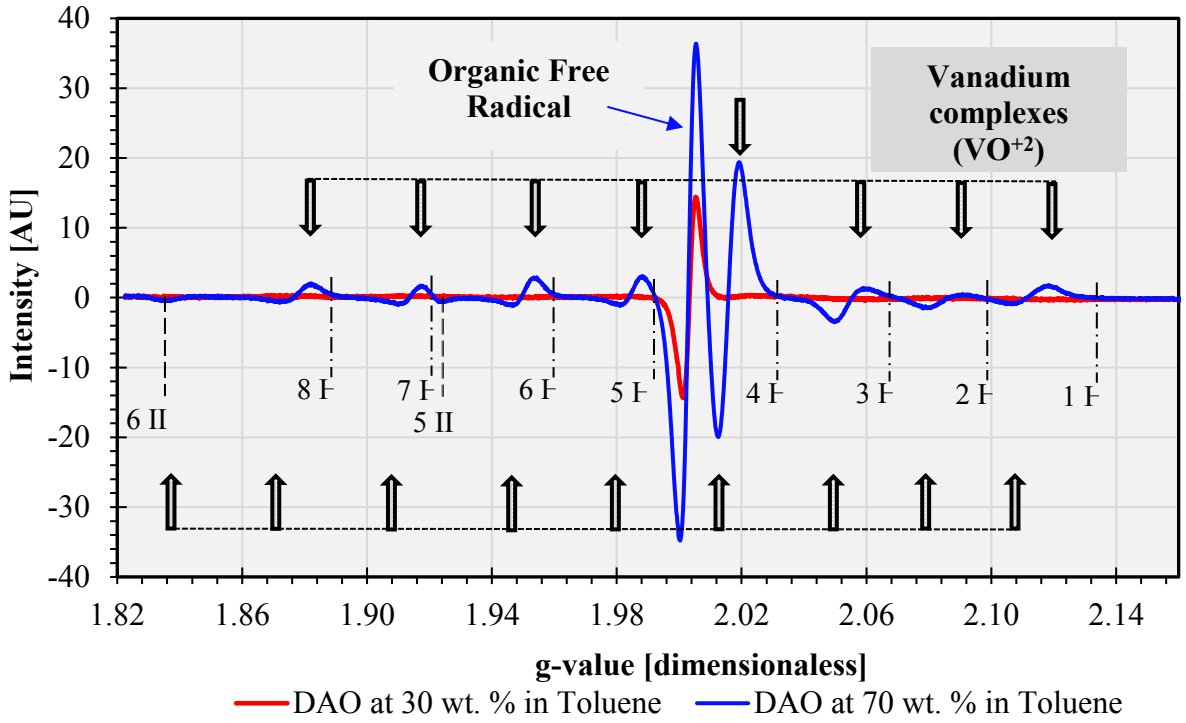

Figure 3-20. ESR spectra of Nexen deasphalted vacuum residue oil (DAO) at two different percent of dilution in Toluene

In the Figure 3-20, is shown some of the peaks associated to the anisotropic character of vanadyl complex, based on the data reported by Yen et al [13]. In addition, a particular feature can be distinguished on the figure, where the peaks related to the line N° 4 (4 I) of the hyperfine structure corresponding to the perpendicular orientation of magnetic axe of the vanadyl complex disappear

completely at 30 wt. % dilution in toluene, showing that there may not be a linear correlation between vanadium peak intensity and dilution factor. It has been suggested by previous studies [13] [14] that some vanadium complexes (VO^{+2}) could be trapped between sheet of aromatic molecules, and by increasing temperature or dilution, the observed "bound" vanadium can be shifted toward the free type and thus it generates changes in the vanadium spectra.

In the other hand, the organic free radicals concentration in all the samples were calculated by comparison of the double integrated intensity against the calibration curve built using 4-hydroxy TEMPO (see Figure 3-3). The number of unpaired spins per gram and g-factors of the thermal conversion products at 280 °C and 320 °C were calculated, it is presented in Table 3-14 and Table 3-15 respectively. In addition, the Figure 3-21 and Figure 3-22 shows the organic free radical concentration of thermal conversion products versus time at 280 °C and 320 °C respectively, so as to identify variation of this property over reaction time.

Table 3-14. ESR Parameters of thermal conversion products after 280 °C, initial pressure of 3 MPa and different reaction times

Time [min]	Double integrated intensity Area		Calculated organic free radical concentration [spins/g]		g-factor	
	x	s	x	s	x	s
0	14269	833	1.30×10^{17}	8.10×10^{15}	2.0032	0.0002
10	15918	795	1.46×10^{17}	7.72×10^{15}	2.0030	0.0001
20	16865	1187	1.55×10^{17}	1.15×10^{15}	2.0032	0.0003
30	18298	950	1.69×10^{17}	9.23×10^{15}	2.0030	0.0003
60	17139	1229	1.57×10^{17}	1.19×10^{15}	2.0032	0.0002
120	16516	1266	1.51×10^{17}	1.23×10^{15}	2.0033	0.0001
240	10551	--[a]	9.34×10^{16}	--[a]	2.0028	--[a]

[a] Single sample was performed at this condition

As listed in Table 3-14, the calculated organic free radical concentration at reaction time of 0 min correspond to deasphalted vacuum residue sample. The organic free concentration obtained for Nexen DAO samples agree within the same order of magnitude with the values reported by previous study for Athabasca and Cold Lake bitumens, in which values in the order of 1×10^{17} spins/ g [15].

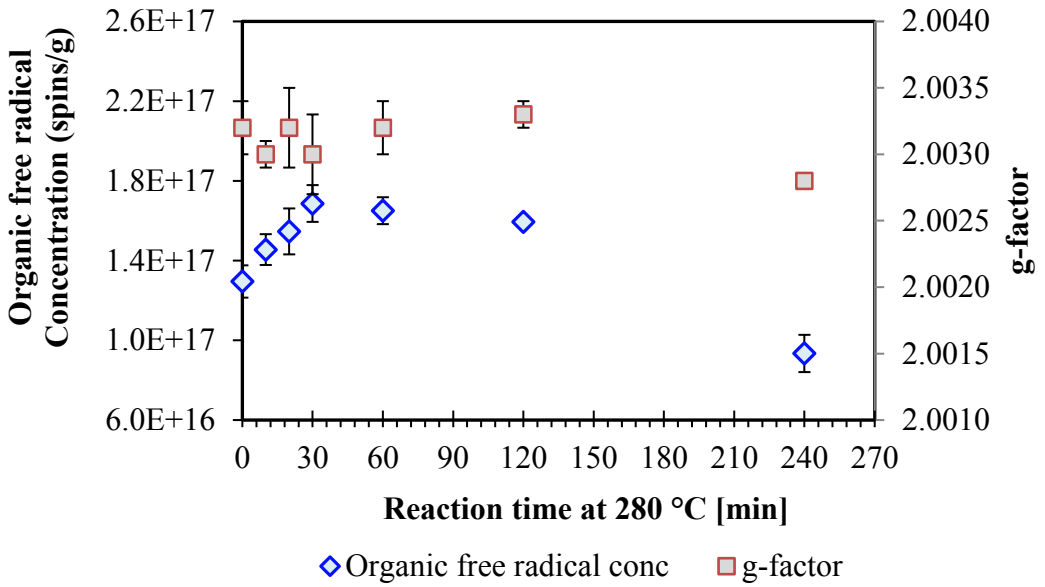

Figure 3-21. Organic free radical concentration and g-factors of thermal conversion products after 280 °C, initial pressure of 3 MPa and different reaction times

Table 3-15. ESR Parameters of thermal conversion products after 320 °C, initial pressure of 3 MPa and different reaction times

Time [min]	Double integrated intensity Area		Calculated organic free radical concentration [spins/g]		g-factor	
	x	s	x	s	x	s
0	14269	833	1.30×10^{17}	8.10×10^{15}	2.0032	0.0002
20	17355	1378	1.59×10^{17}	1.33×10^{16}	2.0031	0.0002
45	16599	740	1.52×10^{17}	7.19×10^{15}	2.0029	0.0005
60	17731	307	1.63×10^{17}	2.98×10^{15}	2.0029	0.0004
90	16488	322	1.51×10^{17}	3.12×10^{15}	2.0032	0.0001
120	18002	1546	1.56×10^{17}	1.31×10^{16}	2.0027	0.0004
240	11219	36	9.99×10^{16}	3.51×10^{14}	2.0032	0.0001
360	9663	--[a]	8.48×10^{16}	--[a]	2.0028	--[a]

[a] Single sample was performed at this condition

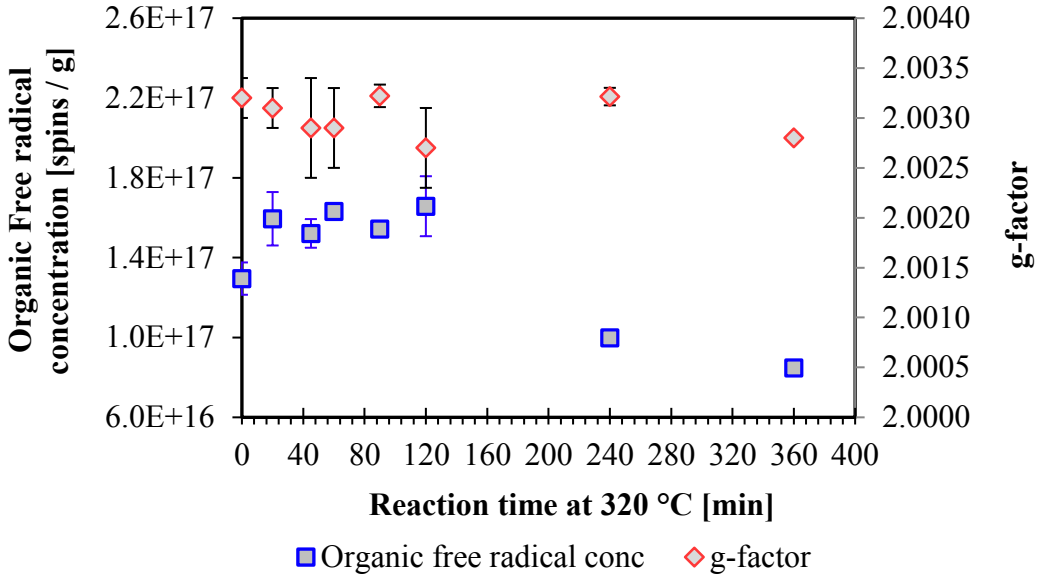

Figure 3-22. Organic free radical concentration of thermal conversion products after 320 °C, initial pressure of 3 MPa and different reaction times

The g-factor, a measure of the center of free radical absorption, obtained from the thermal conversion of DAO below 320 °C fall in the narrow range of 2.0027-2.0036, which agree with the values reported for asphaltenes fractions obtained from bitumens by literature [13]. In addition, it was expected that some trend in g-factors would be apparent as the nature of the free radical should change with increasing the aromaticity. Although, g-factors did not show any marked change along the reaction time.

3.3.2.9 Density

Density measurements of the liquid products and deasphalted vacuum residue oil were determined at two different temperatures, namely 20 and 40 °C. Samples must be heated up before being injected in the pycnometer. Density measurements are reported in Table 3-16 and Table 3-17 for thermal conversion products after reaction at 280 °C and 320 °C respectively.

Table 3-16. Density measurements performed at two different temperatures: 20 and 40 °C to thermal conversion products after reaction at 280 °C

	Temperature [°C]	Time reaction [min]								
		0	10	20	30	45	60	90	120	240
		Density [kg/m^3]								
Average	20	1057.3	1062.4	1063.8	1060.7	1064.5	1066.3	1062.2	1066.6	1067.9
Std. dev.		3.6	5.6	3.5	4.9	3.3	4.84	0.8	1.1	--[a]
Average	40	1049.8	1054.9	1056.2	1055.6	1057.0	1056.3	1055.7	1059.4	1061.3
Std. dev.		4.7	5.5	3.5	2.7	3.2	8.8	2.6	1.6	--[a]

[a] Single sample was performed at this condition

In addition, the average density versus reaction time is presented in Figure 3-23 and Figure 3-24 in order to reveal any change in the liquid product along the time.

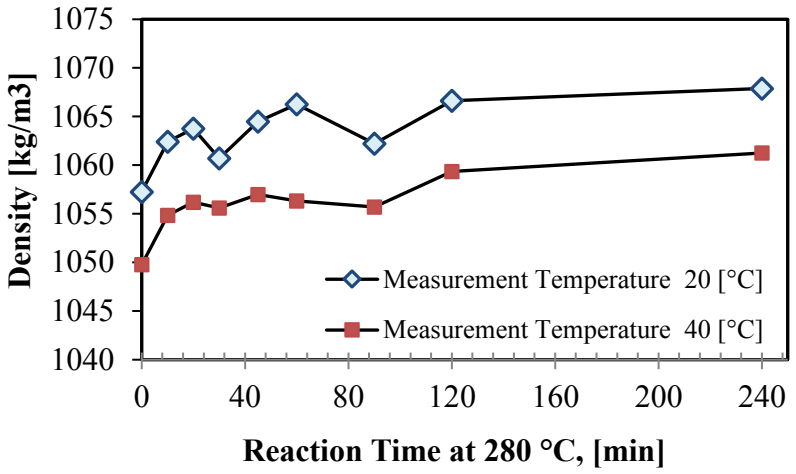

Figure 3-23. Density of thermal conversion products obtained under 280 °C, initial pressure of 3 MPa and different reaction times

In the case of reaction at 280 °C, it is shown a slight increase in the density of the products along the time; in which a maximum density measurement is observed after 240 minutes reaction. Although, it could be considerable constant since the variation of density over the time fell with the pretty narrow range (around 1% compared to initial DAO).

Table 3-17. Density measurements performed at two different temperatures: 20 and 40 °C to thermal conversion products after reaction at 320 °C

	Temperature [°C]	Time reaction [min]							
		0	20	45	60	90	120	240	360
		Density [kg/m^3]							
Average	20	1057.3	1040.4	1041.4	1041.2	1033.3	1033.1	1041.4	1080.1
Std. dev.		3.6	14.6	1.5	12.1	0.90	3.69	--[a]	--[a]
Average	40	1049.8	1036.4	1032.0	1032.9	1026.2	1026.1	1035.3	1068.3
Std. dev.		4.7	17.1	3.0	6.7	10.6	10.6	--[a]	--[a]

[a] Single sample was performed at this condition

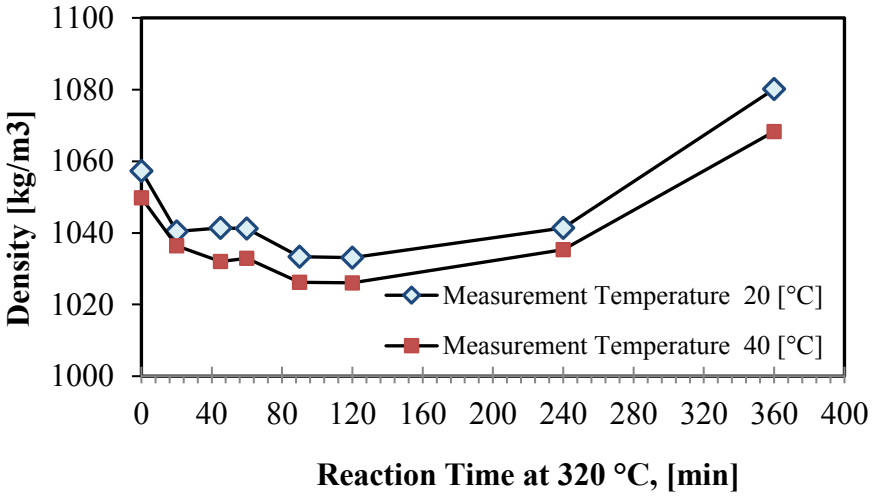

Figure 3-24. Density of thermal conversion products obtained under 320 °C, initial pressure of 3 MPa and different reaction times

At 320 °C, there is a decrease in the density of the products along the time until reach 120 minutes of reaction time, showing that some compounds with lighter molecular weight are generated from the thermal conversion reaction. After 120 minutes, there is an increase in the density of the liquid product.

At 360 minutes, there is a considerable increase in the density of the liquid product reaching a value which is higher than the initial DAO density. Although, the thermal conversion reaction at this specific conditions were performed once, the value agree with refractive index measurement

and gas yield which suggests a decrease of the hydrogen content in the liquid product and thus an increase in the density value.

3.3.2.10 Gas Chromatography

Gas products associated the thermal conversion reactions were collected in a gas bag and injected in the gas chromatograph to be analyzed. The gaseous product analyses are summarized in Table 3-18 and Table 3-19 for thermal conversion reactions at 280 and 320 °C, which presents the mole concentration obtained for every compound between C1 to C6 in the sample.

Table 3-18. Gas products associated to thermal conversion of DAO after reaction at 280 °C and initial pressure 3 MPa

Reaction time at 280 °C; Gas product chromatography								
Compounds	**10 min**	**20 min**	**30 min**	**45 min**	**60 min**	**90 min**	**120 min**	**240 min**
				[mole %]				
Methane	0.38	0.47	1.43	0.28	0.32	0.05	0.75	3.51
Ethylene	--	--	--	--	--	--	--	0.14
Ethane	0.19	--	--	--	--	--	--	0.53
Propylene	--	--	--	--	--	--	--	0.08
Propane	0.23	--	--	--	--	--	0.35	0.61
Iso-butane	0.04	--	--	--	--	--	0.25	0.40
n-Butane	--	--	0.07	--	--	--	--	0.01
cis-2 Butane	0.10	--	--	--	0.33	--	--	0.29
Iso-pentane	0.19	--	0.64	--	0.17	--	0.50	9.36
n-pentane	0.08	--	--	--	--	--	--	0.38
Iso-hexane	--	--	0.40	0.40	--	--	--	--
n-Hexane	--	--	--	--	--	0.00	--	--
H_2S	-- [a]	-- [a]	-- [a]	-- [a]	-- [a]	0.73	-- [a]	0.05
CO_2	0.01	0.07	--	--	--		0.05	
N_2	98.80	99.46	97.34	99.13	99.17	97.79	98.09	84.61
Total	**100.00**	**100.00**	**100.00**	**100.00**	**100.00**	**100.00**	**100.00**	**100.00**

[a] H_2S was observed at very low concentration

Table 3-19. Gas products associated to thermal conversion of DAO after reaction at 320 °C and initial pressure 3 MPa

Reaction time at 320 °C; Gas product chromatography							
Compounds	**20 min**	**45 min**	**60 min**	**90 min**	**120 min**	**240 min**	**360 min**
[mole %]							
Methane	0.25	0.24	1.29	1.38	2.39	8.80	4.88
Ethylene	--	--	0.04	0.04	--	0.37	0.24
Ethane	--	--	0.25	0.39	--	3.57	2.25
Propylene	--	--	0.12	0.24	1.08	0.79	0.73
Propane	--	0.12	0.66	1.00	--	4.64	3.00
Iso-butane	--	--	0.05	0.29	1.73	0.46	0.21
n-Butane	--	--	0.11	0.26	0.34	1.09	0.76
cis-2 Butane	0.56	--	0.83	0.63	0.61	3.13	2.44
Iso-pentane	1.40	--	2.30	1.88	0.55	2.23	1.56
n-pentane	1.30	--	0.17	0.47	0.14	9.48	2.65
Iso-hexane	--	--	0.27	0.04	0.48	1.42	3.50
n-Hexane	--	--	0.13	0.33	--	2.60	4.93
H_2S	-- [a]	-- [a]	0.03	-- [a]	0.05	0.42	0.22
CO_2	0.04	0.01	0.04	0.04	0.03	0.10	0.03
N_2	96.45	99.62	93.71	93.00	92.61	60.89	72.62
Total	**100.00**	**100.00**	**100.00**	**100.00**	**100.00**	**100.00**	**100.00**

[a] H_2S was observed at very low concentration

Measurements of gas evolution at moderately low temperatures provided a key to the detection and monitoring of chemical changes which take place in the deasphalted heavy oil.

Although, a rigorous tracking and interpretation in the evolution of the each compound along the reaction time is not possible due to the use of gas bag for collecting the samples. This sampling method is a poor technique for collecting and analysis of gaseous compounds generated from batch reactor systems, and it is reflected in the data presented in the Table 3-18 and Table 3-19.

3.3.2.11Solid content

After reactions took place, liquid products were diluted with methylene chloride to help with the recovering and filtering steps. Solid are separated from the solvent-liquid product solution through a vacuum filtration system. A milipore filter paper of 0.22 um was used and samples were left inside the fumehood for 2 days to dry. In Figure 3-25 and Figure 3-26, it is shown images of the solids obtained after thermal conversion at 280 and 320 °C. The total solid content obtained after thermal conversion were reported as part of the material balance (see Table 3-3 and Table 3-5).

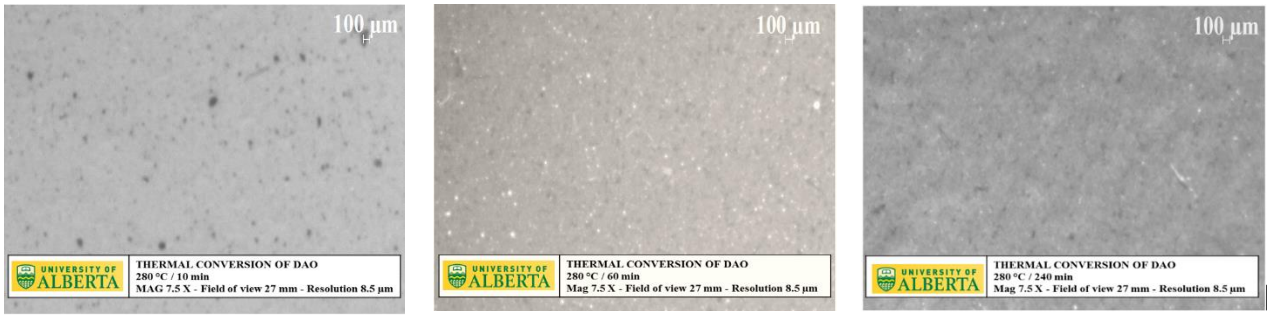

Figure 3-25. Images taken of 10 min, 60 min and 240 min reaction solids in StereoMicroscope V.20. Reaction conditions: 280 °C and 3 MPa (Mag 7.5x / Field of view 27 mm / Res 8.5 µm)

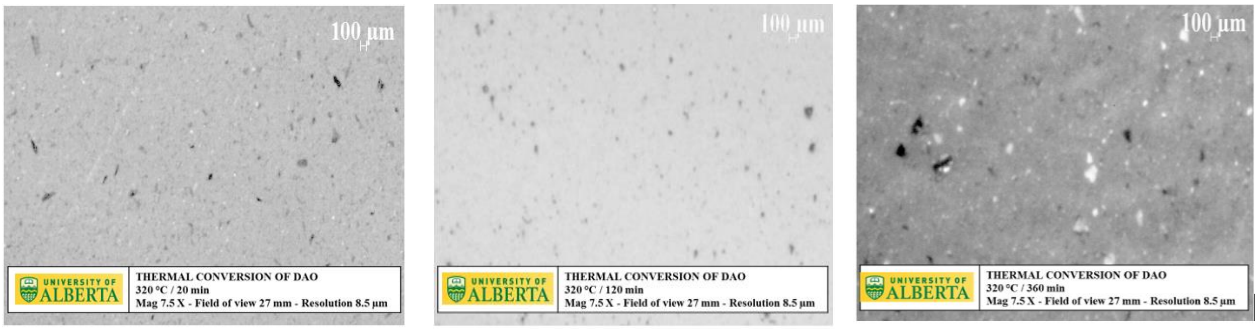

Figure 3-26. Images taken of 20 min, 120 min and 360 min reaction solids in StereoMicroscope V.20. Reaction conditions: 320 °C and 3 MPa (Mag 7.5x / Field of view 27 mm / Res 8.5 µm)

From the images, it was observed under the microscope that fine solids smaller than 200 microns were found for all the experiments, excepting for the images taken of 360 min reaction at 320 °C where some solids within 200 – 300 micron range were obtained from the filtration of the thermal conversion product.

In addition, some pictures were taken using a field emission scanning electron microscope (FE-SEM) to show how solids change along the reaction time.

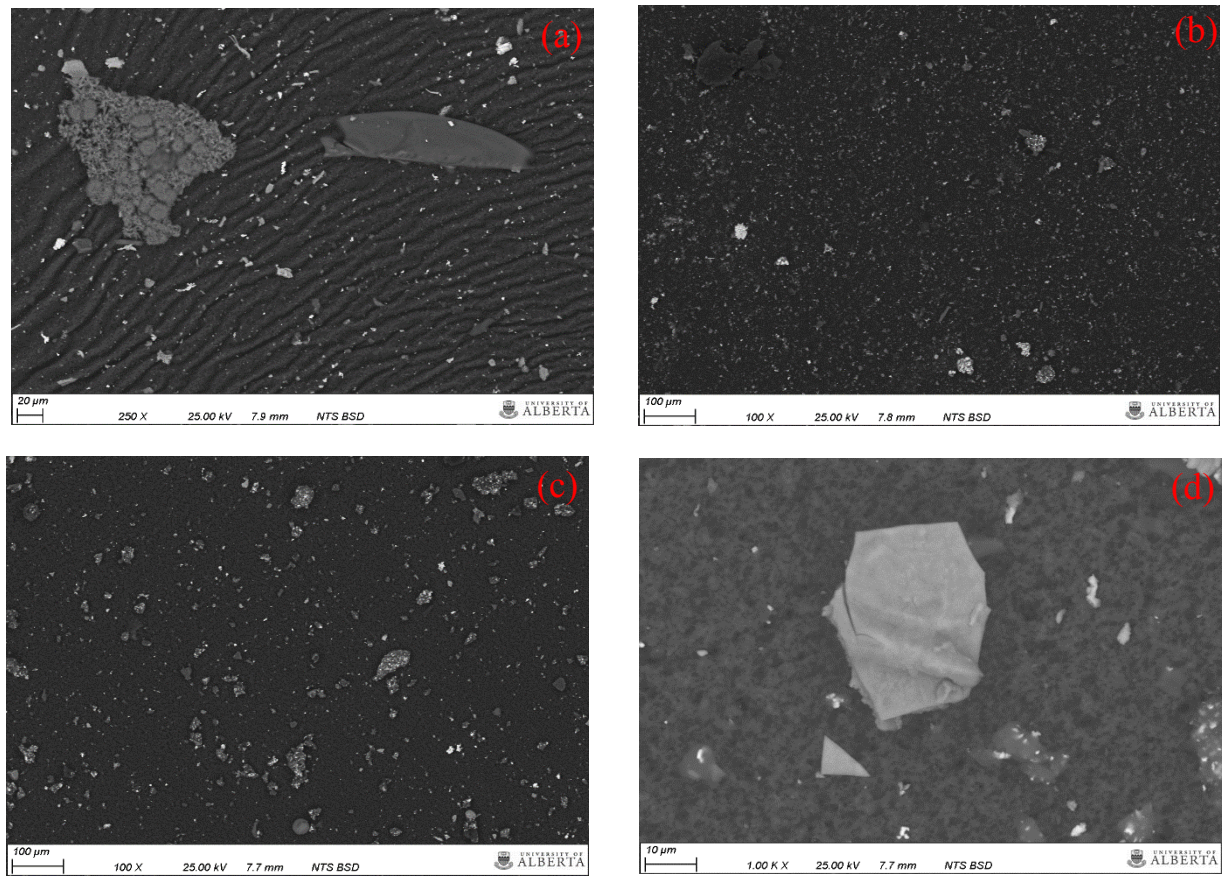

Figure 3-27. Images taken of 10 min (a), 60 min (b), and 240 min (c) (d) reaction solids in SEM. Reaction conditions: 280 °C and 3 MPa

Figure 3-27 shows the SEM images taken to some of the solid samples collected after reaction. As previously mentioned, fine solids with irregular shape smaller than 100 microns and with no evidence of any coalescence were observed under the microscope. In accordance with the results of X-ray dispersive analysis (EDX), it showed primarily the presence of Si, Fe, S, Ca, and Al. The EDX results are shown in the appendix B. Those elements are mainly associated to mineral matter (see Figure 3-26a and Figure 3-26d) typically found in the oil sands bitumen such as quartz (Si), calcite (Ca), pyrite (Fe, S), and clay minerals (Al, Si) [16].

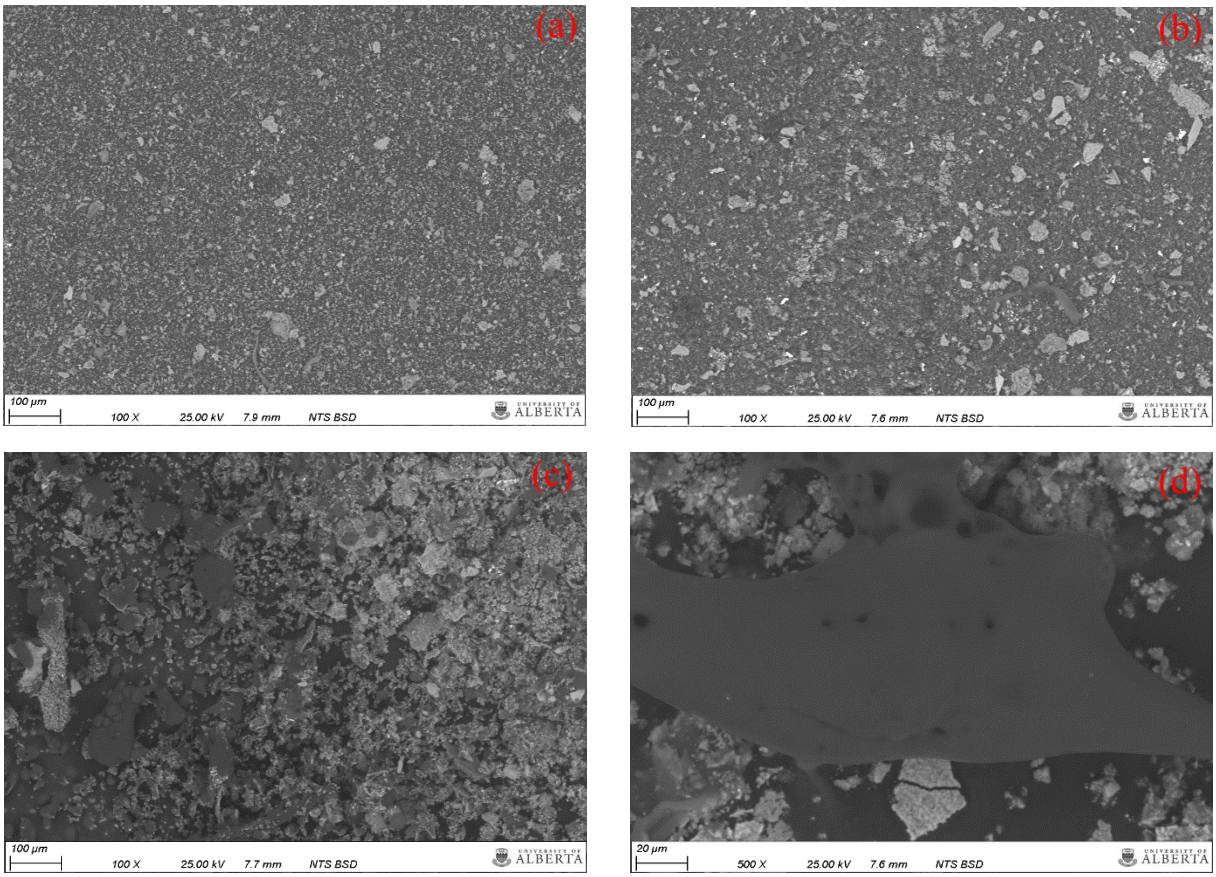

Figure 3-28. Images taken of 20 min (a), 120 min (b) and 360 min (c) (d) reaction solids in SEM. Reaction conditions: 280 °C and 3 MPa

In the case of reaction solids obtained at 320 °C, different morphology in the particles was observed after 360 minutes of reaction (see Figure 3-28). Some particles exhibited greater opacity and brittle shape composed with smaller rounded particles tending toward spherical (see Figure 3-28c and Figure 3-28d). The SEM-EDX spectra showed the predominately presence of carbon, iron and sulfur in this particles.

3.4 Discussion

Limited information is available in the open literature for DAO thermal cracking. To obtain an insight into the thermal cracking behavior of deasphalted oil – characterization of chemical structure of petroleum heavy oil may provide useful information to promote their effective utilization, since the structural variation may affect their reactivity.

3.4.1 Viscosity reduction and crackability of deasphalted oil at low temperature

Thermal cracking reactions at high temperature (greater than 430 °C) are well known to follow a trade-off relationship between reaction temperature and processing time [4]. On the other hand, it is suggested that viscosity reduction via visbreaking substantially increases with an increase in the extent of conversion for a given feedstock with specific characteristic properties [17]. The term of crackability is defined as the extent of this permissible conversion of a determined feed within which it is stable and has no coke yield [18]. Moreover, previous studies have shown that the stability and crackability of the feed improve with a decrease in the content of asphaltene [19].

In the case of the feed used in this work, as it listed in Table 3.1, the industrially deasphalted DAO contained 6.6 ± 0.5 wt. % *n*-pentane insoluble material as determined by precipitation at 40:1 solvent:DAO ratio in the laboratory. The DAO is therefore not completely asphaltenes-free. Despite the presence of some asphaltenes, the DAO had a microcarbon residue content of 7.5 wt. %.

At 280 °C, it was found no significant change in viscosity and conversion (material with boiling point below 524°C) since there is limited amount of energy to overcome the activation energy barrier for chemical reactions. Only thermal reactions with the low homolytic bond dissociation energy can occur, or reactions that have a low activation energy barrier, such as hydrogen transfer. Although, temperature can always affect heavy oil behavior and cause some small changes in microstructure that it will be discussed below.

In the case of thermal conversion at 320 °C, as the reaction time increases, a decrease in viscosity compared to the initial deasphalted oil was observed up to 240 min. However, it was observed for a decrease in viscosity by about half order of magnitude, there was not remarkable change in the amount of material in the liquid product with boiling point below 524 °C. The conversion to lighter material was less than 6 wt. %. Thus, it is likely that most of this decrease in viscosity can be attributed to deaggregation and molecular rearrangement [1, 3].

Moreover, Brauch et al. reported that feeds with high viscosity and high sulfur content (greater than 1 wt. %) experience high viscosity reduction via visbreaking, as a result of cross-linking

within different components by weak bonds that can easily break, as compared to the feeds with lower starting viscosity [20]. As it is reported in Table 3.1, the sulfur content in the deasphalted oil is around 5.6 wt. %. Furthermore, Gray suggested that the facile rupture of sulfide bonds in heavy oil is a major mechanism in the thermal cracking of high-molecular weight components, and it is always followed by the evolution of hydrogen sulfide, even at temperature as low as 250 °C [4]. These approaches are in accord with the observation that hydrogen sulfide was present among gaseous products even at 280 °C (see Table 3-18 and Table 3-19)

After 240 minutes, the viscosity remains slightly constant 745 ± 170 Pa.s vs 777 Pa.s after 360 min. This might be due to the formation of heavy components that counteracts any additional viscosity reduction in the product. Therefore, 240 min was considered to be a break-down point in processing time at 320 °C since before reaching 240 min, the viscosity reached its minimum value and at 240 min, coke formation initiated.

3.4.2 Effects of hydrogen disproportionation

In the thermal conversion of vacuum residue derived from bitumen, hydrogen disproportion is a greatly favorable reaction as a result of the abundancy of weak C–H bonds in the hydro aromatics, alkyl side chains, and alkyl bridges that are common in such residues [21]. In addition, Speight [22] and Sharma et al [9] suggested that the deasphalted heavy oil is the most thermally labile fraction of the bitumen, with more than 60 % of all carbon and 90 % of hydrogen atoms located in saturated positions. Similar values of aliphatic hydrogen content were obtained from ^{1}H NMR results for Nexen DAO samples, and it shown in Figure 3-12 and Figure 3-13.

From Figure 3-12 and Figure 3-13, it is remarkable that some change in the distribution of aliphatic hydrogen content is occurring, which is evidence of hydrogen transfer or hydrogen disproportionation taking place also at the lowest temperature investigated, namely 280 °C.

In order to obtain more information about those change, some regions can be identified in Figure 3-12a and Figure 3-13a based on data presented by Sharma et al [9], Yen et al [10], Hauser et al [11]. Based on the literature mentioned, the main region in the spectra correspond to 0 to 4 ppm refers to hydrogens associated to the aliphatic carbons and between 6 and 9 ppm this peak is related

with aromatic and phenolic carbons. In the aliphatic region of the spectra, three main peaks can be detected. The first one, region between 0.4 and 1.1 ppm, is associated with methyl hydrogens from straight-chain alkanes, referred as primary aliphatic in Figure 3-29 and Figure 3-30. Next to them, a second peak is observed, region between 1.1 and 2 ppm, and it can be related to methylene and methine hydrogen of alkyl chains (secondary aliphatic). The last peak, region correspond to 2 to 4 ppm, is mainly referred to α-methyl and α-methylene substitution (benzylic hydrogen) [9].

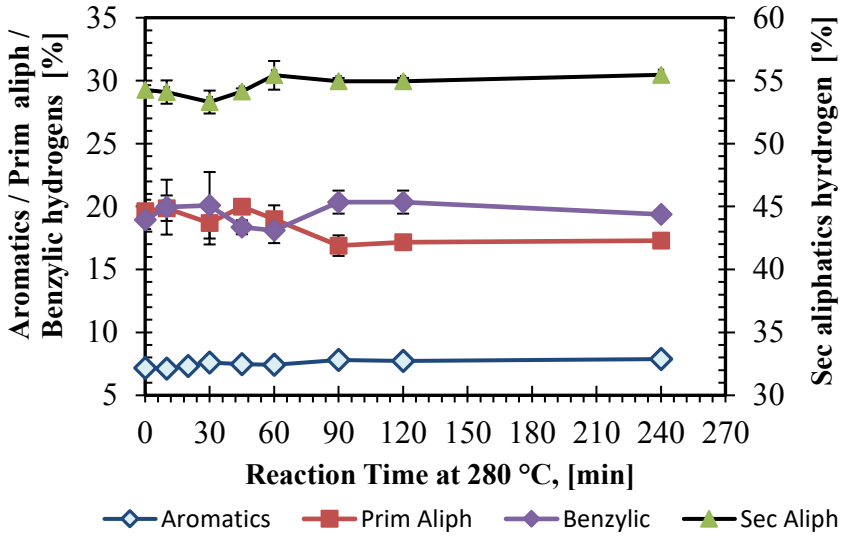

Figure 3-29. Area under the curve extracted from the NMR spectra, comparing the amount of the type of proton found in the thermal conversion liquid product after 280 °C reaction

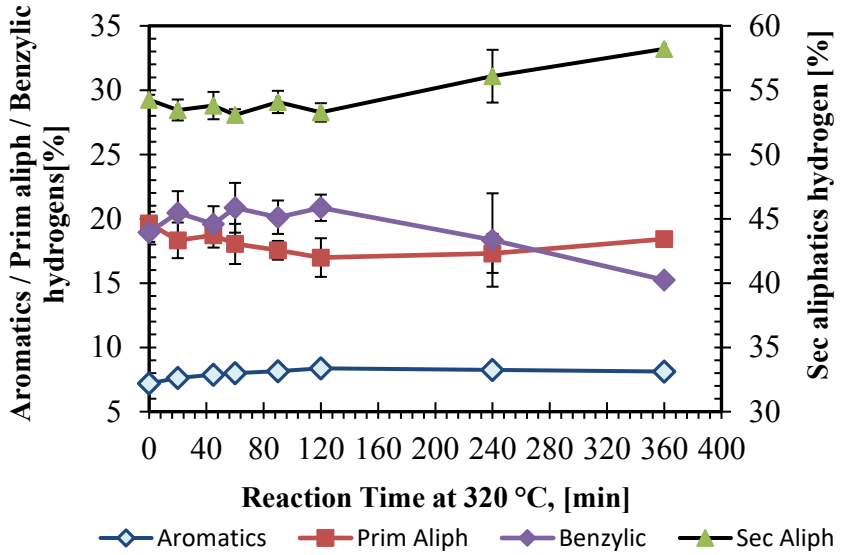

Figure 3-30. Area under the curve extracted from the NMR spectra, comparing the amount of the type of proton found in the thermal conversion liquid product after 320 °C reaction

In the Figure 3-29, it is shown that the amount of primary aliphatic decreased by 14 % relative to that feed after 90 minutes reaction meanwhile the amount of secondary and benzylic remained almost constant. This could indicate the high thermolability of side chains associated to polycondensed aromatics rings and prevalence of dealkylation reactions, even a low temperature.

At 320 °C, the amount of primary aliphatic also presented a drop during the first 120 minutes reaction while the amount of secondary remained barely constant. Moreover, the amount of secondary aliphatic and aromatic hydrogen showed an increase that it may be associated to an increase in the proportion due to primary aliphatic reduction. After 120 minutes reaction, a decrease in the amount of benzylic hydrogen is observed in the liquid product. This behavior is consisted with the typical bond dissociation energies where dealkylation of the aromatics and resins will result first (C_{ar} -C_{ali}, BDE: 89 kcal mol^{-1}) with parallel dehydrogenation of the naphthenic rings (C-H_{sec}, BDE: 95 kcal mol^{-1}) [21].

The prevalence of dehydrogenation of naphthenic rings to aromatics after 120 minutes may explain why there is not additional viscosity reduction with more time, as it is shown in the Figure 3-5.

Moreover, the occurrence of this structural changes during thermal treatment at 320 ° C, side chain fragmentation and dehydrogenation reactions result in a rise in the aromaticity of the liquid product. The trend in aromaticity was further corroborated by liquid product analysis, such as H:C ratio, refractive index, and *n*-pentane insoluble material which suggest that some compounds with higher molecular weight and lower hydrogen content were created (asphaltenes).

This finding might also explain the increase in the density in the liquid product observed after 240 min (see Figure 3-24) since an increase in the amount of high molecular weight will cause an increasing in density. It is well known that density is affected by size and composition of its components and an increase in the average boiling point and molar mass also is accompanied by an increment in the density values [21]. Density will also increase when the hydrogen content decreases [22].

In addition, there is a considerable increase in the amount of gases generated after 120 min, whereas the gas yield raised from 1.25 to 6.15 wt. %. This further support the increase in aromaticity and density in the liquid product due to the loss of hydrogen to gaseous products in the form of light hydrocarbons (C_1-C_5).

3.4.3 FT-IR Hints

In order to obtain more information about the changes that heavy oil experiences during milder conversion processes, FT-IR spectroscopy was employed since it could be considered a useful tool for identifying certain groups of compounds. Over the wavenumber range in a FT-IR spectrum, certain groups of atoms give rise to bands at or near the same wavenumber to indicate bonds interactions [23]. In addition, two important areas for a preliminary analysis of a FT-IR spectrum are the regions 4000-1300 and 900-650 cm^{-1}, in which the high wavenumber region of the spectrum show characteristic stretching frequencies for important functional groups [23][24].

In the Figure 3-16 and Figure 3-17, the FT-IR spectrum is presented for different thermal conversion products. As many organic molecules, the raw deasphalted oil shows two peaks around 2923 cm^{-1} and 2853 cm^{-1} corresponding to the asymmetrical and symmetrical stretching of methylene groups in aliphatic chains [23]. On the other hand, the presence of methyl groups is confirmed by the appearance of the left side shoulders at 2943 and 2872 cm^{-1}.

In addition, the peaks at 1375 and 1456 cm^{-1} associated to symmetrical and asymmetrical bending vibration of the C-H bonds confirm the methyl and methylene groups in aliphatic chains.

On the other hand, the FT-IR spectrum of the all samples shown a group of peaks between 900 and 700 cm^{-1} that are associated with out-of plane C-H and ring bending vibration of one isolated aromatic C-H bond (870 cm^{-1}), two or three adjacent aromatic C-H bonds (815 cm^{-1}) and four aromatic adjacent aromatic bonds (745 cm^{-1}) [9]. The peak at ~1600 cm^{-1} is also related to the stretching of C=C bond in a ring structure of aromatics, which in conjunction with an increase of the peak at 745 cm^{-1} suggest a rise in the aromaticity of the products along the reaction time at 280 and 320 °C, as well as suggest the creation of new asphaltenes.

Another feature emerging in the 700-900 cm^{-1} region, it is the 720 -725 cm^{-1} peak ascribed to alkyl side chains possessing four and more methylene groups attached to aromatic rings [9].

Sulfur compounds as sulfoxides can be observed in the liquid products through the peak at 1030 cm^{-1}, a characteristic peak for the stretching of S=O bond [23].

Based on this information, the ratio of aromatics C=C bonds to aliphatic methylene bonds stretching intensity [measured as the ratio of 1600 cm^{-1}/ 2853 cm^{-1} band] vs reaction time was plotted in Figure 3-31. The increase observed in aromatic: aliphatic methylene ratio along the reaction time to both temperature, namely 280 and 320 °C, suggest an increase in the aromatic content due to condensation reaction. This pattern correspond with others measured variables such as refractive index, ^{1}H NMR, and *n*-pentane insoluble content.

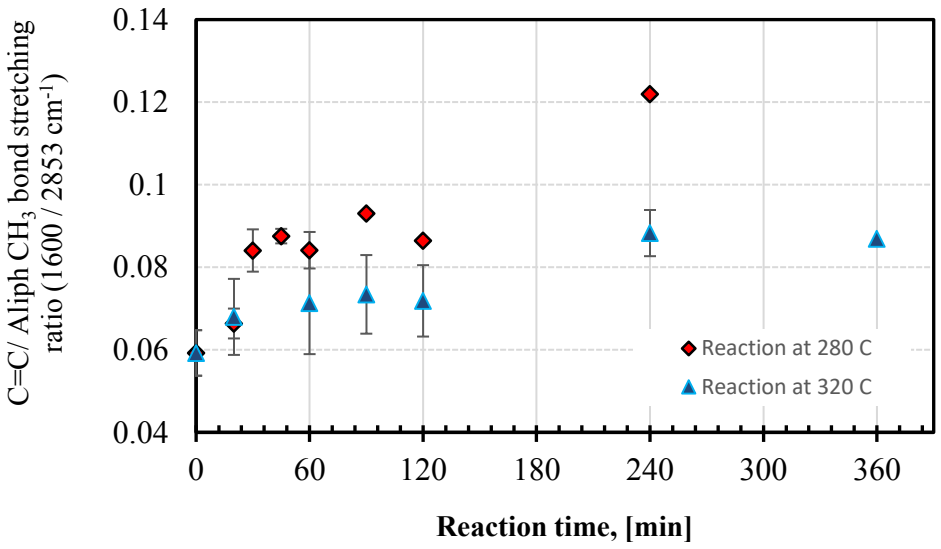

Figure 3-31. Ratio of aromatics C=C bonds to aliphatic methylene bonds stretching intensity of Thermal Conversion Products obtained under 280 °C and 320 °C, initial pressure of 3 MPa and different reaction times

3.4.4 Asphaltene content – Electron Spin resonance relationship

As it was mentioned in the previous section, the presence of the peak at about 720 cm^{-1} in the FTIR infrared spectrum provide indications that deasphalted oil contain polynuclear aromatic

systems with alkyl side chains attached [25]. That is also corroborated by considerable amount of gaseous products generated during thermal conversion. For example, after 240 min at 320 °C the gas yield is around 6 wt. %. On the other hand, Kapoor et al suggested that dealkylation of these polynuclear aromatics are considerable at low severity, promoting the condensation of pentane soluble materials (aromatics and resins) to create new asphaltenes [26].

This investigation is tracking changes in all of the products using multiple techniques. It was observed in Figure 3-14 and Figure 3-15 that the industrially deasphalted DAO is not completely asphaltenes free, and it contains 6.6 ± 0.5 wt. % *n*-pentane insoluble material as determined by precipitation at 40:1 solvent:DAO ratio in the laboratory.

Additionally, the presence of free radicals in the DAO was confirmed by electron spin resonance (ESR) spectrometry and corroborated previous studies of persistent free radicals in such materials [27]. The number of spins per gram of DAO was found around 1.3 x 10^{17}, which within the same order of magnitude reported for Athabasca and Cold Lake bitumen values (1 x 10^{17} spins/g), and one order of magnitude when it is compared with the values reported in previous studies for Athabasca and Cold Lake asphaltenes [27] [28] [29]. In addition, this value is one order of magnitude larger than the free radical concentration obtained by Schultz and Selucky [13] in petroleum resin fractions which suggest that there is a relationship between the organic free radical concentration and asphaltenes content.

From the *n*-pentane insoluble content (Figure 3-14 and Figure 3-15) and organic free radical concentration (Figure 3-21 and Figure 3-22) of the thermal conversion liquid product obtained after 280 and 320 °C, it seems that the presence of organic free radicals are mainly associated to petroleum asphaltenes.

Moreover, this data provide an indication of the changes in microstructure in the heavy oils as these changes are occurring in the reacting product, as well as show that the increase in the asphaltene content and organic free radical formation are not just a high temperature process, but take place also at the lowest temperature investigated, namely 280 °C.

This indicate that bitumen and their asphaltenes are not completely unreactive at the temperatures that will be experienced along the process pathway leading from steam assisted gravity drainage (SAGD) through solvent deasphalting. During this pathway, the bitumen will be exposed to temperature between 200 – 250 °C [30].

This approach is further supported by Storm et al [31] that suggested that polycondensed aromatic cores conducive to coke formation actually forms from non-asphaltenic fraction when it is heated above 285 °C.

3.5 Conclusions

Through experimental investigations on thermal conversion of deasphalted oil below 320 °C, the following observations were made:

a) At 280 °C, there is not significant change in viscosity and conversion (material with BP below 524°C) since there is limited amount of energy to occur chemical reactions. In the case of thermal conversion at 320 °C, a decrease in viscosity by about half order of magnitude compare with raw DAO, although there was not remarkable change in the amount of material in the liquid product with boiling point below 524 °C (< 6 wt. %). Thus, it is likely that most of this decrease in viscosity can be attributed to deaggregation and molecular rearrangement.

b) The thermal conversion of deasphalted oil below 320 °C, there is a mainly prevalence of dealkylation of side chains associated to polycondensed aromatics rings and dehydrogenation of naphthenic rings to aromatics.

c) There is an increase in the *n*-pentane insoluble content along reaction time for both temperature investigated, which suggest that new asphaltenes could form at low temperature and it is not just a high temperature process.

d) The presence of free radicals in the DAO was confirmed by electron spin resonance (ESR) spectrometry, showing also that those species are not completely unreactive at low temperature. It

also appears that the presence of organic free radicals are mainly associated to petroleum asphaltenes.

References

[1] Wang, L.; Zachariah, A.; Yang, S.; Prasad, V.; De Klerk, A. Visbreaking oilsands-derived bitumen in the temperature range of 340-400 °C. *Energy Fuels* **2014**, *28*, 5014-5022.

[2] Wang, L. Low temperature visbreaking. MSc Thesis, University of Alberta, Edmonton, AB, Canada, 2013.

[3] Yañez Jaramillo, L. M. Visbreaking of oilsands bitumen between 150 and 300 ˚C. MSc Thesis, University of Alberta, Edmonton, AB, Canada, 2016.

[4] Gary, J. H.; Handwerk, G. E. *Petroleum Refining: Technology and Economics*, 5th Edition; CRC Press: Boca Raton, 2007.

[5] Japanwala, M. S. Quality of distillates from coking of recycled residue. MSc Thesis, University of Alberta, Edmonton, AB, Canada, 2011.

[6] ASTM D7169-11: *Standard test method for boiling point distribution of samples with residues such as crude oils and atmospheric and vacuum residues by high temperature gas chromatography*; ASTM: West Conshohocken, PA, 2012.

[7] ASTM D6560-12: *Standard test method for determination of asphaltenes in crude petroleum and petroleum products*; ASTM: West Conshohocken, PA, 2012.

[8] ASTM D 70-09: *Standard test method for density of semi-solid bituminous materials (Pycnometer Method)*; ASTM: West Conshohocken, PA, 2009.

[9] Sharma, B. K.; Tyagi, O. S.; Aloopwan, M. K. S.; Bhagat, S. D. Spectroscopic characterization of solvent soluble fractions of petroleum vacuum residues. *Pet. Sci. Technol.* **2000**, *18*, 249-272.

[10] Yen, T. F.; Wu, W. H.; Chilingar, G. V. A study of the structure of petroleum asphaltenes and related substances by proton nuclear magnetic resonance. *Energy Sources*, **1984,** *7*(3), 275-304.

[11] Hauser, A.; AlHumaidan, F.; Al-Rabiah, H.; Halabi, M. A. Study on thermal cracking of Kuwaiti heavy oil (vacuum residue) and its SARA fractions by NMR spectroscopy. *Energy Fuels* **2014**, *28*(7), 4321-4332.

[12] Dehkissia, S.; Larachi, F.; Rodrigue, D.; Chornet, E. Characterization of Doba–Chad heavy crude oil in relation with the feasibility of pipeline transportation. *Fuel* **2004**, *83*(16), 2157-2168.

[13] Yen, T. F.; Tynan, E. C.; Vaughan, G. B.; Boucher, L. J. Electron spin resonance studies of petroleum asphaltics. In *Spectrometry of Fuels;* Friedel R.A. *Eds;* Springer, Boston, MA, **1970**, 187–201.

[14] Humphrey, B. J. *Electron Paramagnetic Resonance on Asphaltic Materials (No. NMERI-WA5-10-(SS-5.01))*; rep.; New Mexico Engineering Research Institute: New Mexico, 1987.

[15] Schultz, K. F.; Selucky, M. L. ESR measurements on asphaltene and resin fractions from various separation methods. *Fuel* **1981**, *60*(10), 951-956.

[16] Kotlyar, L. S.; Sparks, B. D.; Kodama, H.; Grattan-Bellew, P. E. Isolation and characterization of organic-rich solids present in Utah oil sand. *Energy & Fuels* **1988**, *2* (4), 589–593.

[17] Di Carlo, S.; Janis, B. Composition and visbreakability of petroleum residues. *Chem. Eng. Sci.* **1992**, *47*, 2695-2700.

[18] Akbar, M.; Geelen, H. Visbreaking uses soaker drum. *Hydrocarbon Process.* **1981**, *60*(5), 81-85.

[19] Fainberg, V.; Podorozhansky, M.; Hetsroni, G.; Brauch, R.; Kalchouck, H. Changes in the composition and properties of the vacuum residues as a result of visbreaking. *Fuel Sci. Technol. Int.* **1996**, *14* (6), 839.

[20] Brauch, R.; Fainberg, V.; Kalchouck, H.; Hetsroni, G. Correlations between properties of various feedstocks and products of visbreaking. *Fuel Sci. Technol. Int.* **1996**, *14*(6), 753-765.

[21] Gray, M. R. *Upgrading oilsands bitumen and heavy oil*; The University of Alberta Press: Edmonton, 2015.

[21] Speight, J. G. Thermal cracking of Athabasca bitumen, Athabasca asphaltenes, and Athabasca deasphalted heavy oil. *Fuel* **1970**, *49*(2), 134-145.

[23] Silverstein, R. M.; Webster, F. X.; Kiemle, D. J.; Bryce, D. L. *Spectrometric identification of organic compounds*; John Wiley & Sons: New York, 2014**.**

[24] Hardinger, S. Infrared Spectroscopy. http://www.chem.ucla.edu/harding/notes/notes_14C_IR.pdf (accessed Dec 15, 2017).

[25] Speight, J. G. *The Chemistry and Technology of Petroleum*; CRC press: Boca Raton, 2014.

[26] Kapoor, M. P.; Kothiyal, V.; Singh, I. D. Compositional and structural studies of visbroken residues. *Fuel Sci. Technol. Int.* **1993**, *11*(7), 975-989.

[27] Strausz, O. P.; Lown, E. M. *The Chemistry of Alberta Oil Sands, Bitumens and Heavy Oils*; Alberta Energy Research Institute: Calgary, **2003**.

[28] Elofson, R. M.; Schulz, K. F.; Hitchon, B. Geochemical significance of chemical composition and ESR properties of asphaltenes in crude oils from Alberta, Canada. *Geochim. Cosmochim. Acta* **1977**, *41*(5), 567-580.

[29] Scotti, R.; Montanari, L. Molecular structure and intermolecular interaction of asphaltenes by FT-IR, NMR, EPR. In *Structures and Dynamics of Asphaltenes*; Mullins, O. C., Sheu, E.Y. Eds.; Springer: Boston, 1998.

[30] Banerjee, D. K. *Oil Sands, Heavy Oil, & Bitumen: From Recovery to Refinery*; PennWell Corp.: Tulsa, Oklahoma, 2012.

[31] Storm, D. A.; Barresi, R. J.; Sheu, E. Y.; Bhattacharya, A. K.; De Rosa, T. F. Microphase behavior of asphaltic micelles during catalytic and thermal upgrading. *Energy Fuels* **1998**, *12*(1), 120-128.

4. THERMAL CONVERSION OF DEASPHALTED OIL AT 360 °C

4.1 Introduction

In Chapter 3, thermal conversion of deasphalted oil was performed below 320 °C. As it was expected, small changes and low conversion was found since there is limited amount of energy so that the homolytic scission which required lowest activation energy occurred first. Results were very interesting due to the reaction conditions that are seldom reported on in visbreaking literature. The data indicated that changes in the microstructure took place even at the lowest temperature investigated, namely 280 °C, in which an increase in the asphaltene content was observed. This suggest that bitumen and their asphaltenes are not completely unreactive at the temperatures that will be experienced along the process pathway (between 200-250 °C [1]) leading from steam assisted gravity drainage (SAGD) through solvent deasphalting.

At 360 °C, more significant changes and higher conversion of the deasphalted oil is expected to occur. This temperature was selected for study because it represents the temperature threshold for thermal decomposition to proceed at a significant rate [2]. Based on what was mentioned before, it was of interest to obtain a deeper understanding of those changes that deasphalted oil experiences during milder conversion, as well as the trade-off relationship between processing time and reaction temperature.

4.2 Experimental Section

4.2.1 Materials

Deasphalted vacuum residue oil from the Nexen Long Lake upgrader was used for the thermal conversion reactions. Deasphalted oil used in these experiments belongs to the same barrel as the bitumen samples employed on the previous experiments in Chapter 3. Nexen Long Lake deasphalted vacuum residue oil was characterized and the characterization is shown in Table 3-1.

The source and purity of nitrogen, methylene chloride, *n*-pentane, and toluene were described in Chapter 3. These materials were also used in this Chapter's experiments.

4.2.2 Equipment and Procedure

The experiments were performed in a batch reactor system, and the same experimental procedure employed in Chapter 3 was also used in this chapter's investigations. All the experiments in this chapter were conducted in triplicate at an internal reactor temperature of 360 °C, and results were reported as an average with one sample standard deviation.

4.2.3 Analysis

Analyses made in this chapter on the products as well as the description of the instruments and analysis procedures are the same used in the Chapter 3.

4.3 Results

4.3.1 Material Balance

The reaction products were obtained under these conditions: 360 °C, an initial pressure of 3 MPa N_2 and reaction time varying from 1 to 360 minutes. The reaction time of 0 min correspond to deasphalted vacuum residue sample (feed). The mass of each phase was determined individually. The overall material balance (Table 4-1) and the product yields of each phase at 360 °C (Table 4-2) were obtained for experiments that were performed in triplicate.

Table 4-1. Mass balance for thermal conversion at 360 °C for different reaction times

Balance Material [wt. %][a]		
Reaction temperature: 360 °C		
Reaction time [min]	**x**	**s**
20	100.02	0.50
30	99.51	1.23
45	100.05	1.42
60	99.43	0.58
90	99.46	0.05
120	100.52	0.10
240 [b]	97.71	--
360 [b]	100.00	--

[a] Average (x) and sample standard deviation (s) of three experiments are reported

[b] Single sample was performed at this condition

In all experiments, the average material balance closed to within 3 %, i.e. material balance was between 97 and 103 %.

After reaction, some observation were made during the phase separation. A significantly amount of gaseous products were obtained from the reaction in the first 20 minutes of reaction (> 1wt. %), mostly methane, ethane, propane, H_2S and CO_2 (See section 4.3.2.10 – gas chromatography).

Table 4-2. Product yield (wt. %) for thermal conversion at 360 °C for different reaction times

Material Balance [wt. %][a]						
Reaction temperature: 360 °C						
Time [min]	**Gas**		**Liquid**		**Solid**	
	x	**s**	**x**	**s**	**x**	**s**
20	2.55	0.49	96.86	0.30	0.63	0.27
30	2.99	0.39	96.46	0.17	0.55	0.32
45	4.53	0.29	94.86	0.10	0.61	0.23
60	5.93	0.56	93.44	0.67	0.63	0.11
90	6.62	0.99	92.02	0.64	0.83	0.41
120	7.61	0.49	91.95	0.44	0.44	0.17
240[b]	8.50	--	91.20	--	0.30	--
360[b]	10.46	--	82.62	--	6.92	--

[a] Average (x) and sample standard deviation (s) of three experiments are reported
[b] Single sample was performed at this condition

In the case of reaction at 360 °C, the liquid yield decreased progressively from the beginning as the yield of gas increased. As shown in the Table 4-2, the yield of liquid diminished within the first 240 min by about 9 wt. % without showing an increase in the amount of solid (coke formation). During this time, there is a trade-off between the gas yield and liquid yield, in which there was a considerable loss to gaseous products. This is significant mainly because it constitutes a loss of hydrogen from the product in the form of light hydrocarbons (C_1-C_5). These observations were corroborated by liquid product analyses, such as H:C molar ratio, refractive index and hydrogen distribution based on proton nuclear magnetic resonance spectroscopy.

On the other hand, after 360 min, a considerable increase in the amount of solid in the sample was observed.

As the experiments made for chapter 3, filtration of liquid products took a long time before solids were obtained and this was found for all experiments. It is likely that the solids in the feed were very fine, which was later confirmed by microscopy.

4.3.2 Product characterization

In order to have a better idea about the changes that took place during this mild thermal treatment. Products were characterized and analyzed. The three phases influenced each other; nevertheless, this work is mainly focused on those changes related to the liquid phase products.

4.3.2.1 Viscosity

In the light of support for the industrial development of a process for the partial upgrading of oil sands bitumen in smaller facilities closer to the point of bitumen recovery, the first and probably the main product property of this work is the viscosity measurements. Every measurement was performed at 4 different temperatures (30, 40, 50 and 60 °C), but shear rate was kept constant at 10 s^{-1} for all the temperatures except 30 °C (shear rate $1s^{-1}$). These results are shown in Table 4-3 for reaction temperature at 360 °C.

Table 4-3. Viscosity data to thermal conversion products under 360 °C and initial pressure 3 MPa

	Time reaction [min]								
	0	**20**	**30**	**45**	**60**	**90**	**120**	**240**	**360**
	Viscosity [Pa.s]								
Measured Temperature: 60 [°C]									
Average	131.23	47.77	45.84	29.63	16.14	8.00	4.67	0.83	0.81
Std. dev.	3.81	3.48	7.10	6.12	0.97	0.46	0.49	--[a]	--[a]
Measured Temperature: 50 [°C]									
Average	600.00	153.61	143.71	90.36	47.77	27.51	12.75	1.88	1.80
Std. dev.	13.40	12.11	22.96	22.96	3.94	1.53	1.59	--[a]	--[a]
Measured Temperature: 40 [°C]									
Average	3718.50	806.39	770.13	474.70	193.40	95.38	40.00	4.74	4.50
Std. dev.	293.93	18.63	120.65	27.02	4.25	6.31	6.65	--[a]	--[a]
Measured Temperature: 30 [°C]									
Average	--[b]	5156.20	4901.80	3071.00	1070.8	453.61	153.35	14.12	12.52
Std. dev.	--	121.22	776.00	54.55	13.35	34.16	26.67	--[a]	--[a]

[a] Single sample was performed at this condition

[b] Viscosity of the sample could not be determined (>10000 Pa.s)

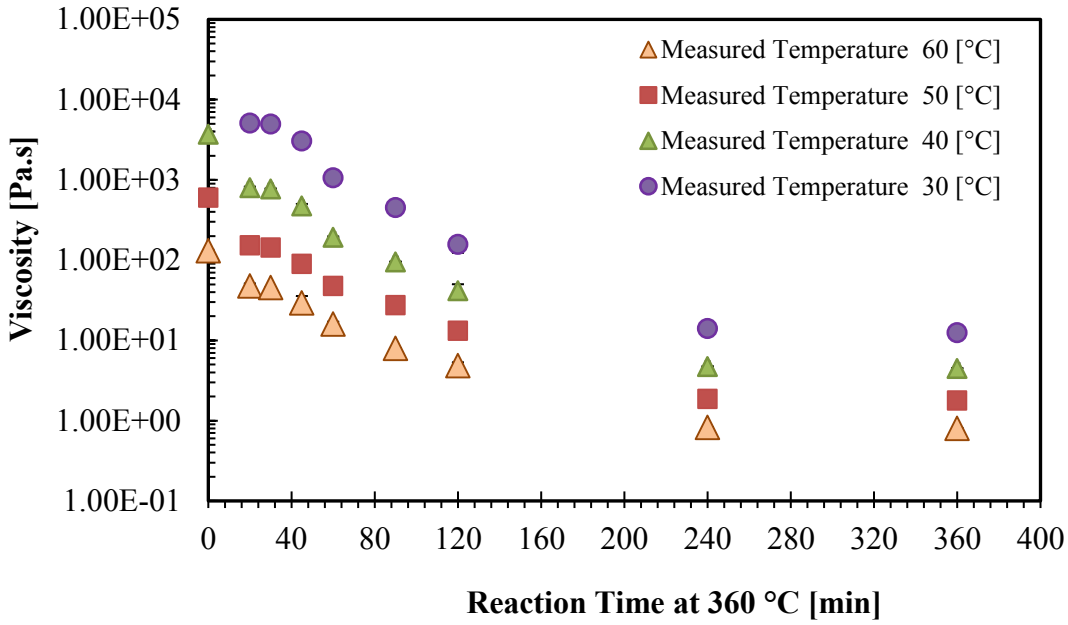

Figure 4-1. Viscosity of thermal conversion products obtained under 360 °C, initial pressure of 3 MPa and reaction time varying between 1 and 360 minutes. Measurements were performed at different temperature

After thermal treatment at 360 °C, the viscosity of the products at 40 °C was reduced by two to three orders of magnitude compared with the value of DAO from 0 min to 240 min without coke formation (Figure 4-1). Afterward, the viscosity of the products looks fairly constant, and there is not a further significantly reduction along the time.

4.3.2.2 Refractive index

The refractive index of every sample was obtained at 5 different temperatures (20, 30, 40, 50 and 60 °C), and in Table 4-4 is reported the refractive index of thermal conversion at 360 °C at different reaction times. In addition, Figure 4-2 shows the refractive index at 360 °C versus time in order to identify variation of this property over reaction time.

Table 4-4. Refractive Index measurements performed on thermal conversion products after 360 °C and initial pressure 3 MPa reaction

	Temperature [°C]	Time reaction [min]								
		0	20	30	45	60	90	120	240	360
		Refractive index [nD]								
Average	20	1.5921	1.5913	1.5928	1.5919	1.5915	1.5929	1.5928	1.5977	1.6026
Std. dev.		0.0001	0.0007	0.0006	0.0002	0.0007	0.0015	0.0023	--[a]	--[a]
Average	30	1.5883	1.5875	1.5889	1.5881	1.5877	1.5892	1.5890	1.5937	1.5985
Std. dev.		0.0000	0.0005	0.0007	0.0002	0.0007	0.0016	0.0022	--[a]	--[a]
Average	40	1.5846	1.5836	1.5853	1.5843	1.5838	1.5854	1.5851	1.5897	1.5945
Std. dev.		0.0001	0.0005	0.0006	0.0002	0.0008	0.0016	0.0023	--[a]	--[a]
Average	50	1.5808	1.5798	1.5816	1.5806	1.5800	1.5816	1.5813	1.5857	1.5910
Std. dev.		0.0001	0.0006	0.0007	0.0001	0.0009	0.0017	0.0024	--[a]	--[a]
Average	60	1.5773	1.5760	1.5785	1.5773	1.5765	1.5782	1.5780	1.5817	1.5869
Std. dev.		0.0001	0.0008	0.0006	0.0002	0.0007	0.0020	0.0029	--[a]	--[a]

[a] Single sample was performed at this condition

As it is shown in the Figure 4-2, the index of refraction remains fairly constant along the time until reaction time reach 60 minutes, after which the variable measured continually increase along the time. This behavior is an indication of the liquid product is being mildly more aromatic after reach 60 min at 360 °C.

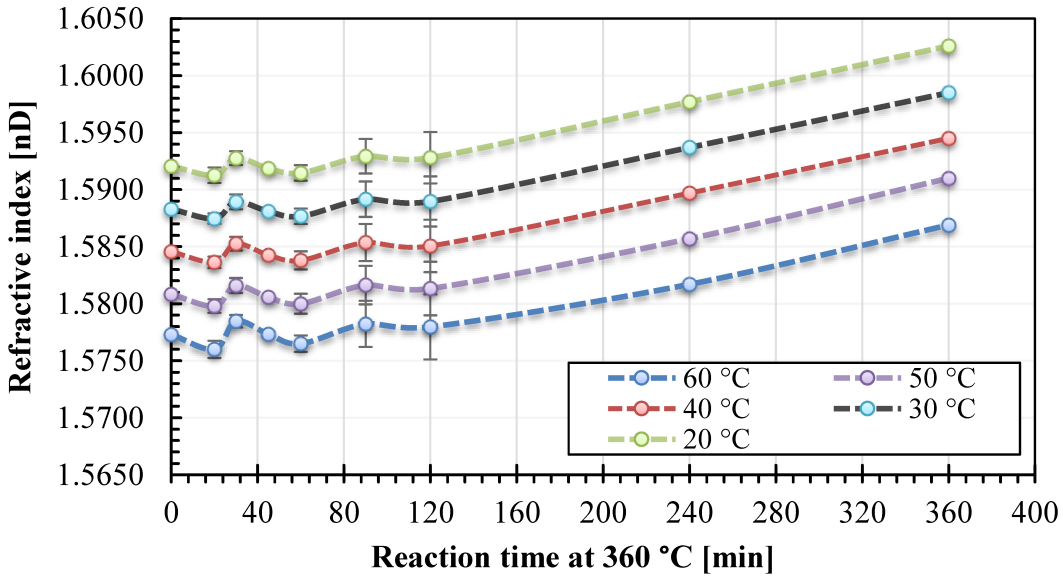

Figure 4-2. Refractive Index results for Thermal Conversion Products at 360 °C, initial pressure of 3 MPa and different reaction times: Refractive index vs Time

4.3.2.3 Liquid boiling point distribution (SimDist)

The liquid boiling point distribution of the thermal conversion products at 360 °C was determined following ASTM D7169 – 11 [3], and it is presented in Figure 4-3. The results of this analysis are shown in the following way: Temperature vs weight percent distilled.

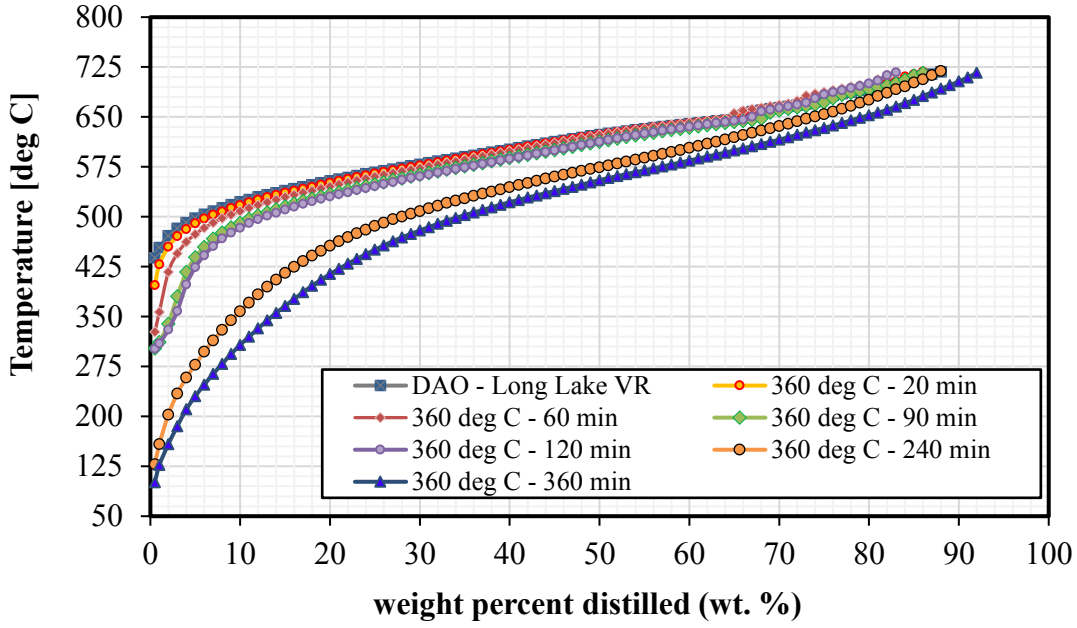

Figure 4-3. Liquid boiling point distribution of thermal conversion products after 360 °C, initial pressure of 3 MPa at different reaction times

In the case of thermal conversion at 360 °C, an increase in the amount of light boiling point compounds (BP < 524 °C) is observed after 20 minutes reaction time, although this increment is considerable after 240 minutes.

4.3.2.4 Elemental analysis

Elemental analysis of the products and deasphalted vacuum residue oil were obtained in order to track changes in the products such as hydrogen disproportionation. These results are reported in the Table 4-5 for reaction temperature at 360 °C. Moreover, the hydrogen/carbon molar ratio of the thermal conversion products at 360 °C were calculated, it is presented in Figure 4-4.

Table 4-5. Elemental analysis in wt. % of thermal conversion products after 360 °C, initial pressure of 3 MPa at different reaction times

Elemental analysis [wt. %][a]								
Time [min]	C		H		N		S	
	x	s	x	s	x	s	x	s
0	83.35	0.31	9.88	0.05	0.58	0.03	5.59	0.12
20	82.48	0.22	9.78	0.05	0.58	< 0.01	5.72	0.03
30	83.08	0.12	9.81	0.01	0.54	0.01	5.49	0.09
45	83.17	0.40	9.80	0.01	0.55	0.01	5.48	0.03
60	82.46	0.86	9.73	0.14	0.56	0.04	5.51	0.04
90	83.53	0.02	9.86	0.02	0.56	0.01	5.51	0.02
120	83.36	0.37	9.73	0.01	0.54	0.01	5.45	0.04

[a] Average (x) and sample standard deviation (s) of three experiments are reported

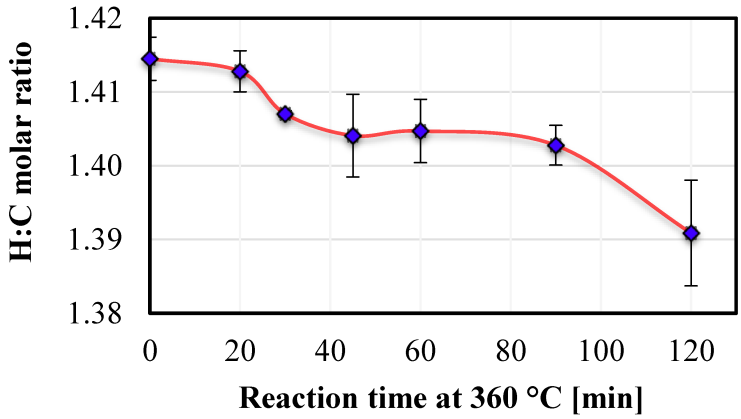

Figure 4-4. Hydrogen/carbon molar ratio of thermal conversion products after 360 °C, initial pressure of 3 MPa at different reaction time

From Figure 4-4, it can be observed that the H/C molar ratio decreases along time after reach 20 minutes of reaction, being more significantly after 90 min of reaction time.

4.3.2.5 Proton nuclear magnetic resonance ^{1}H NMR

Proton NMR analysis was utilized to determine aliphatic and aromatic content and observe how its proportions change under different reaction conditions. In Figure 4-5, is presented a) the NMR spectra of thermal conversion products to detect and track all the structural changes in the DAO if

there is any change, and b) the aliphatic hydrogen content of thermal conversion products at 360 °C against reaction time to track changes in the DAO related with the aliphatic hydrogen content. In order to convert the NMR data to obtain the aliphatic hydrogen content, some regions were identified and defined in the chapter 3 (section 3.3.2.5) based on data presented by Sharma et al [4], Yen et al [5], and Hauser et al [6]. Moreover, a peak was found between 5 and 5.5 ppm (ca. 5.3 ppm) which corresponds to the solvent used (methylene chloride) during the sample preparation. This shift value was also reported and attributed to methylene chloride by Dehkissia et al [7].

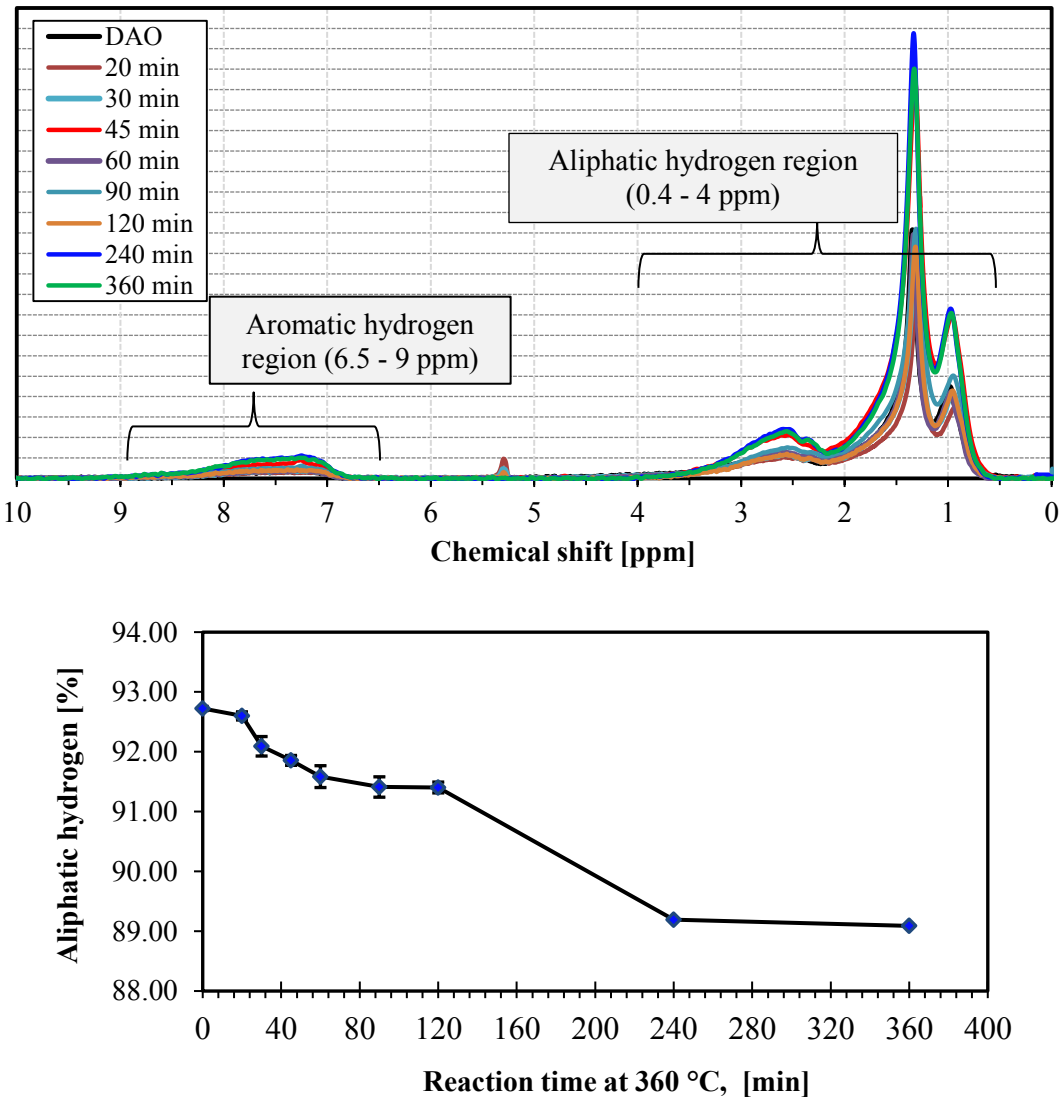

Figure 4-5. Proton NMR results of thermal conversion products after 360 °C, initial pressure of 3 MPa and different times; a) ^{1}H NMR spectra b) % Aliphatic hydrogen vs Time

Mnova NMR software was used the determination of peak area based on the hydrogen ranges mentioned before, and methylene chloride shift was ignored for the calculations.

At 360 °C, the aliphatic hydrogen content decrease constantly along time with the most pronounced decrease between 120 and 240 min reaction time. Afterward, from 240 min to 360 min, the aliphatic hydrogen content remains constant. This behavior is aligned with others measured variables such as C:H molar ratio, refractive index, and pentane insoluble material.

4.3.2.6 Pentane insoluble material (Asphaltene content)

The *n*-pentane precipitated asphaltenes content was determined following ASTM D6560-12 [8], it is reported in Table 4-6. Furthermore, the Figure 4-6 illustrated the *n*-pentane content in the thermal conversion products versus time at 360 °C so as to identify variation of this property over reaction time.

Table 4-6. Pentane insoluble content in wt. % of thermal conversion products after 360 °C, initial pressure of 3 MPa and different times

	Time reaction [min]								
	0	**20**	**30**	**45**	**60**	**90**	**120**	**240**	**360**
	***n*-Pentane insoluble [wt. %]**								
Average	6.56	8.12	8.53	8.48	9.12	8.45	9.69	12.30	13.10
Std. dev.	0.15	0.63	0.51	0.67	0.76	0.65	0.93	--[a]	--[a]

[a] Single sample was performed at this condition

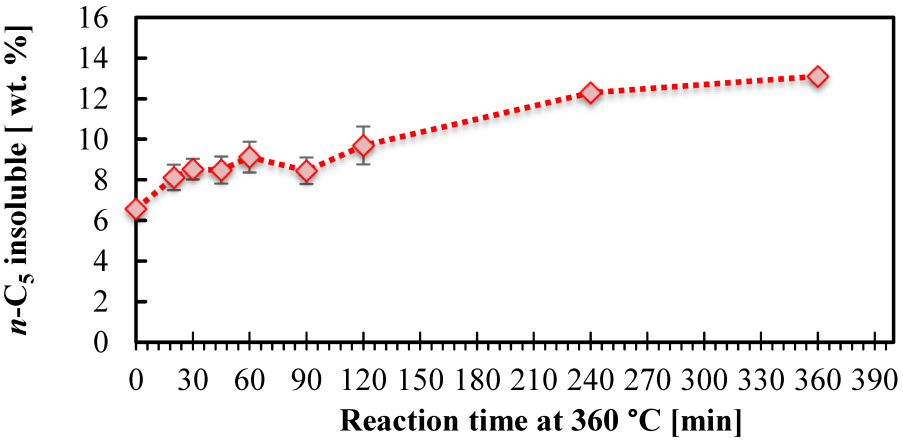

Figure 4-6. Pentane insoluble content of thermal conversion products after thermal conversion at 360 °C, initial pressure of 3 MPa and different times

4.3.2.7 FT-IR spectroscopy

In Figure 4-7, the FT-IR spectrum for every reaction time was plotted in order to obtain more information about changes of chemical groups in the liquid product during the thermal conversion at 360 °C.

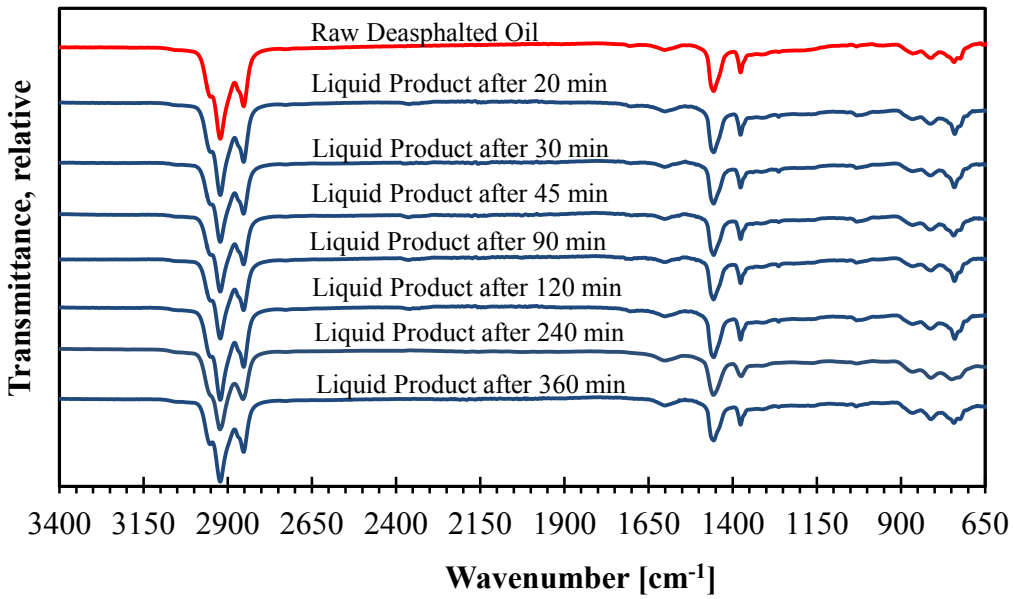

Figure 4-7. FTIR spectra of thermal conversion products after 360 °C, initial pressure of 3 MPa and different reaction times

4.3.2.8 Electron spin resonance (ESR) spectroscopy

The electron spin resonance (ESR) spectra of the liquid products and deasphalted vacuum residue oil were obtained in order to track the free radical species, mainly focused on organic radicals, and the first derivate ESR spectra are shown in Figure 4-8.

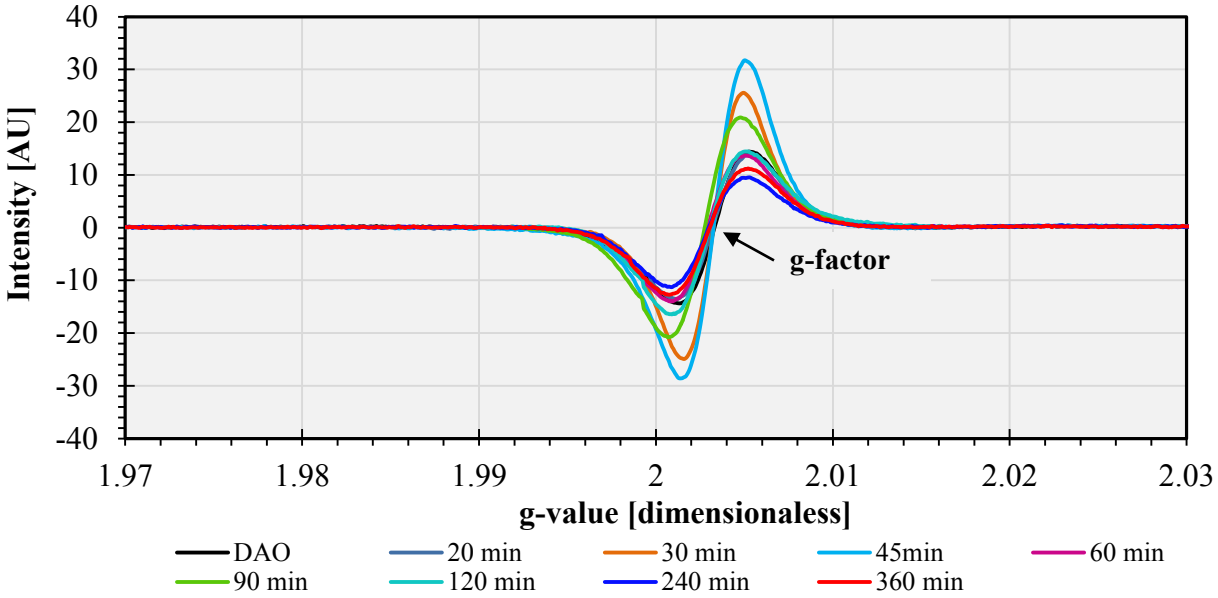

Figure 4-8. ESR spectrum of DAO and thermal conversion products after 360 °C, initial pressure of 3 MPa and different reaction times

Like it was observed in the chapter 3 for thermal conversion of DAO below 320 °C, a single peak between g-values of 1.99-2.01 (3440 - 3470 gauss), corresponding to the organic free radical, was found in the ESR spectrum for all the samples (Figure 4-8).

In the case of vanadium complexes (VO^{2+}), there is not well-defined peaks detected in the spectrum due to the low vanadium content in the feed (around 60 ppm) and the dilution factor used in this work.

The free radicals concentration were calculated by comparison of the double integrated intensity against the calibration curve built using 4-hydroxy TEMPO (see Figure 3-3 in chapter 3). The number of unpaired spins per gram and g-factor of the thermal conversion products at 360 °C were calculated, it is presented in Table 4-7.

In addition, Figure 4-9 shows the organic free radical concentration and g-factors of thermal conversion products at 360 °C versus time in order to identify variations in these properties over reaction time.

Table 4-7. ESR Parameters of thermal conversion products after 360 °C, initial pressure of 3 MPa and different reaction times

Time [min]	Double integrated intensity Area		Calculated organic free radical concentration		g-factor	
	x	s	x	s	x	s
0	14269	833	1.30×10^{17}	8.10×10^{15}	2.0032	0.0002
20	17471	385	1.61×10^{17}	3.74×10^{15}	2.0035	0.0002
30	17785	704	1.63×10^{17}	6.84×10^{15}	2.0033	<0.0001
45	19755	2063	1.83×10^{17}	2.00×10^{16}	2.0032	0.0002
60	21432	556	1.99×10^{17}	5.40×10^{15}	2.0032	0.0002
90	20799	724	1.93×10^{17}	7.03×10^{15}	2.0031	0.0003
120	23375	1319	2.18×10^{17}	1.28×10^{16}	2.0033	0.0001
240	12265	--[a]	1.10×10^{17}	--[a]	2.0030	--[a]
360	10375	--[a]	9.17×10^{16}	--[a]	2.0030	--[a]

[a] Single sample was performed at this condition

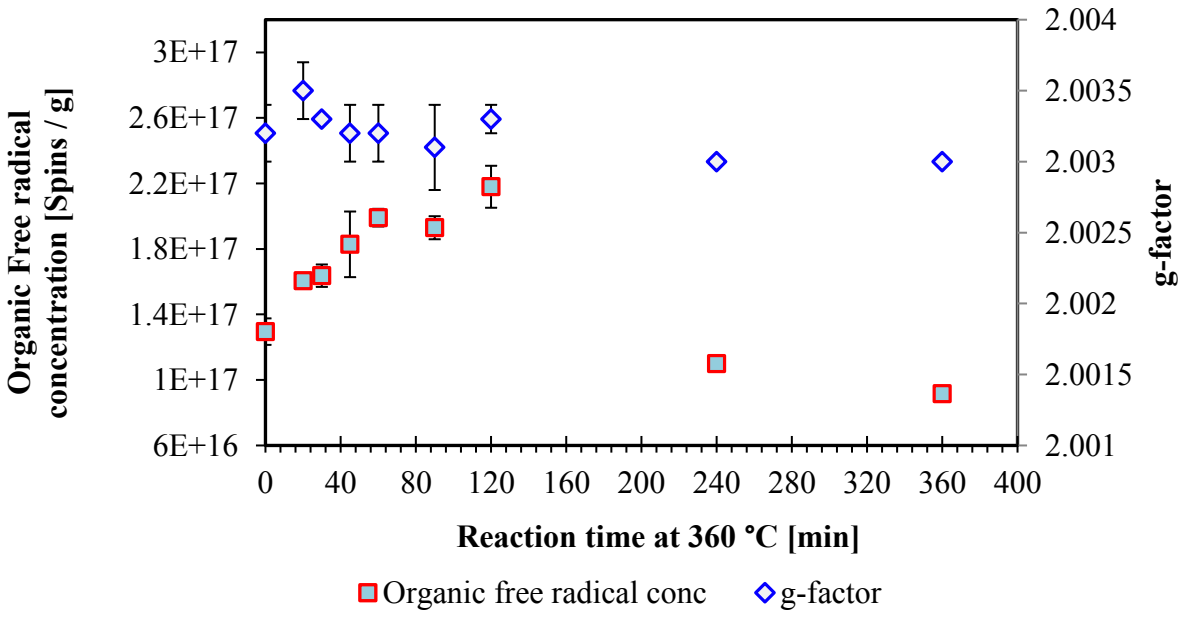

Figure 4-9. Organic free radical concentration and g-factors of thermal conversion products after 360 °C, initial pressure of 3 MPa and different reaction times

As remarked in the Chapter 3, the g-factor, a measure of the center of free radical absorption, obtained from the thermal conversion of DAO at 360 °C and agree with the values reported for

asphaltenes fractions obtained from bitumens by literature, falling in the range of 2.0027-2.0036 [9]. In addition, these g-factors did not show any significantly change along the reaction time.

4.3.2.9 Density

Density measurements of the liquid products and deasphalted vacuum residue oil were determined at two different temperatures, namely 20 and 40 °C. Samples must be heated up before being injected in the pycnometer. Density measurements is reported in Table 4-8 for thermal conversion products after reaction at 360 °C. In addition, density data is presented in Figure 4-10 in order to reveal any change over reaction time.

Table 4-8. Density measurements performed at two different temperatures: 20 and 40 °C to thermal conversion products after reaction at 360 °C

	Temperature [°C]	Time reaction [min]							
		0	20	30	45	60	90	120	360
		Density [kg/m³][b]							
Average	20	1057.3	1063.0	1054.0	1057.0	1058.4	1053.4	1055.2	1031.9
Std. dev.		3.6	0.4	2.2	0.7	1.8	3.9	1.4	--[a]
Average	40	1049.8	1055.5	1046.6	1049.5	1050.9	1046.0	1047.7	1018.9
Std. dev.		4.7	0.4	2.2	0.7	1.8	3.9	1.4	--[a]

[a] Single sample was performed at this condition
[b] There was not enough sample to measure the density at 240 min

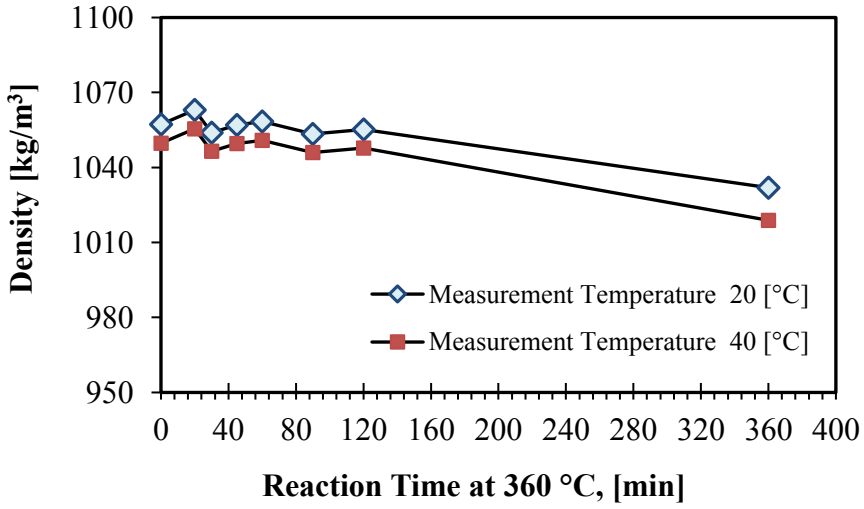

Figure 4-10. Density of thermal conversion products obtained under 360 °C, initial pressure of 3 MPa and different reaction times

In the case of reaction at 360 °C, the density of the liquid products after thermal conversion remains mostly constant along the time until 120 minutes of reaction time is reached. Afterward, there is a decrease in the density of the liquid product reported after 360 minutes (density reduction around 2.4% compared to initial DAO), which coincides with the increase in solids formation.

4.3.2.10 Gas Chromatography

Gas products associated the thermal conversion reactions were collected in a gas bag and injected in the gas chromatograph to be analyzed. The mole concentration obtained for every compound in the gaseous product associated with thermal conversion reactions at 360 °C is presented in Table 4-9.

Table 4-9. Gas products associated to thermal conversion of deasphalted vacuum residue oil after reaction at 360 °C and initial pressure 3 MPa

Reaction time at 360 °C; Gas product chromatography								
Compounds	**20 min**	**30 min**	**45 min**	**60 min**	**90 min**	**120 min**	**240 min**	**360 min**
[mole %]								
Methane	2.94	2.54	5.99	12.67	14.67	11.47	15.51	19.34
Ethylene	--	--	0.30	0.46	0.22	0.43	0.15	0.19
Ethane	1.96	0.57	4.28	8.00	9.02	8.35	8.44	13.04
Propylene	--	--	5.62	0.56	1.30	--	0.09	0.25
Propane	3.29	3.42	1.31	4.69	9.46	12.26	9.66	15.75
Iso-Butane	--	0.33	0.87	1.69	1.86	1.77	0.04	0.03
n-Butane	1.36	0.81	1.74	1.99	1.09	2.36	2.36	4.21
cis-2 Butane	2.01	1.90	3.87	5.38	4.62	6.04	5.13	9.66
Iso-Pentane	0.57	0.97	3.38	3.33	2.26	2.58	8.42	6.52
n-pentane	1.08	1.70	3.71	4.37	4.27	3.71	4.66	6.44
Iso-Hexane	0.22	--	1.50	0.29	4.06	1.18	6.77	2.61
n-Hexane	0.31	--	1.62	0.30	3.54	0.34	3.47	2.17
H_2S	0.15	0.11	0.20	0.13	0.40	0.38	0.41	0.09
CO_2	0.02	0.06	0.05	0.08	0.14	0.05	0.10	--
H_2	--	--	--	--	--	--	--	--
N_2	86.10	87.59	65.44	56.05	43.05	49.09	34.80	19.66
Total	**100.00**	**100.00**	**100.00**	**100.00**	**100.00**	**100.00**	**100.00**	**100.00**

Measurements of gas evolution at moderately low temperatures provided a key to the detection and monitoring of chemical changes which take place in the deasphalted heavy oil. Rigorous tracking and interpretation in the evolution of the each compound along the reaction time is not possible due to the use of gas bag for collecting the samples. This sampling method is a poor technique for collecting and analysis of gaseous compounds generated from batch reactor systems, and it is reflected in the data presented in the Table 4-9.

4.3.2.11 Solid content

In Figure 4-11, is shown images of the solids recovered from vacuum filtering step after thermal conversion of deasphalted oil at 360 °C. A milipore filter paper of 0.22 um was used and samples were left inside the fumehood for 2 days to dry. The total solid content obtained after thermal conversion were reported as part of the material balance (see Table 4-2).

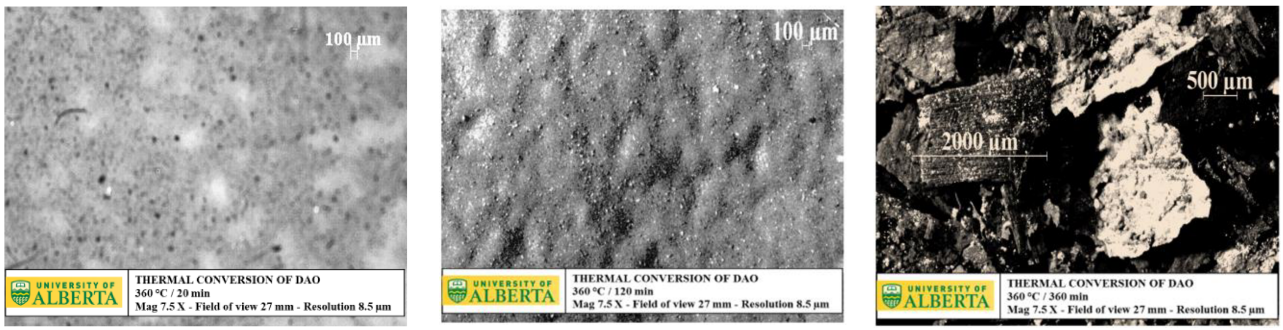

Figure 4-11. Images taken of 20 min, 120 min and 360 min reaction solids in StereoMicroscope V.20. Reaction conditions: 360 °C and 3 MPa (Mag 7.5x / Field of view 27 mm / Res 8.5 µm)

Some fine solids smaller than 100 microns were observed under the microscope during the first 240 min at 360 °C. Afterward, from 240 min to 360 min, some solids with approximate 2 mm were seen from the filtration of the thermal conversion product. In addition, some pictures were taken using a scanning electron microscope (SEM) in order to obtain further information about the solids change along the reaction time.

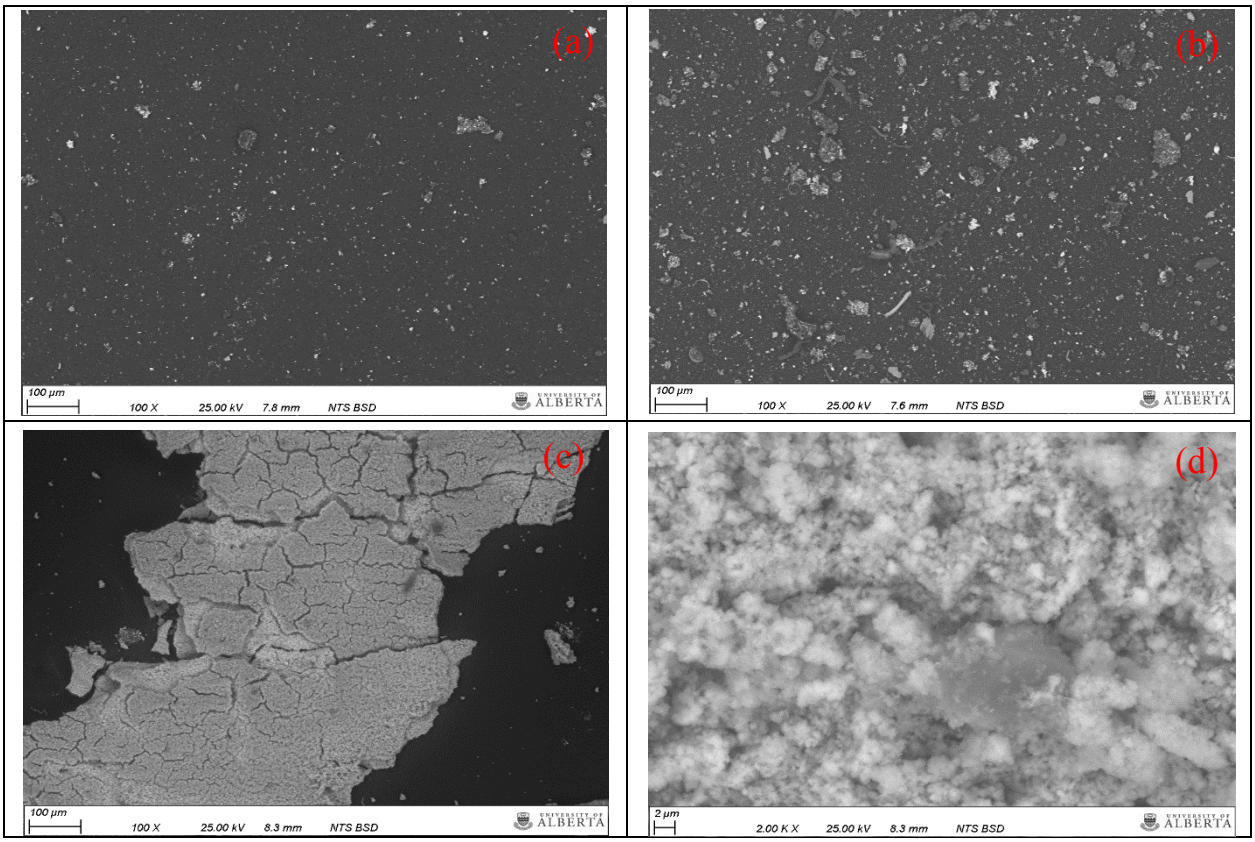

Figure 4-12. Images taken of 20 min (a), 120 min (b) and 360 min (c) (d) reaction solids in SEM. Reaction conditions: 360 °C and 3 MPa

Figure 4-12 illustrate the SEM images of the solid samples collected after reaction. As previously mentioned in the Chapter 3, dispersed fine solids with irregular shape smaller than 100 microns associated to mineral matter were observed under the microscope during the first 240 minutes of reaction time. This agree with the results of X-ray dispersive analysis (EDX) to the solid obtained from thermal conversion after 120 minutes of reaction time, which showed primarily the presence of S, Fe, Cl, Al, Si, and Mg (see Figure 4-13).

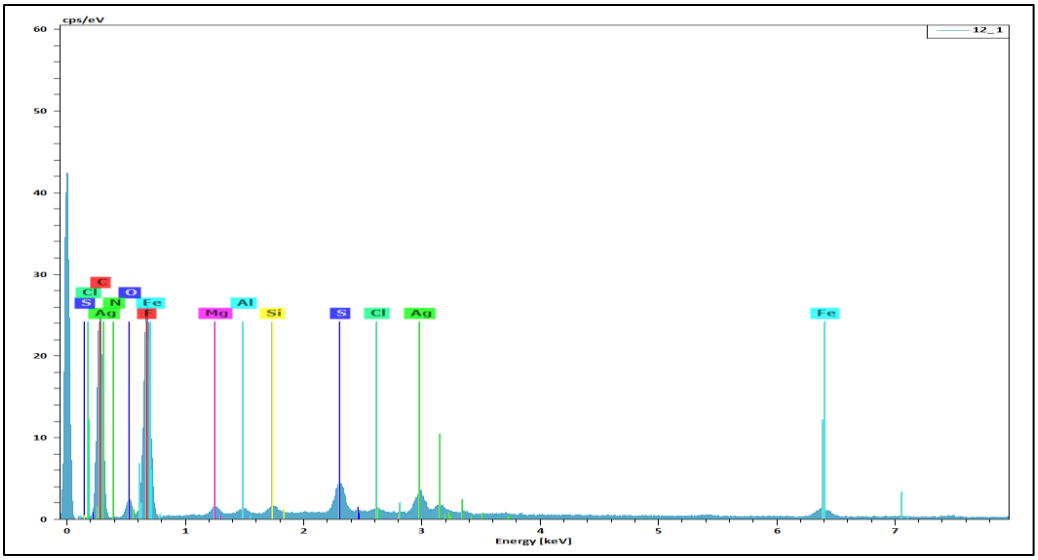

Figure 4-13. SEM-EDX spectra of solids obtained from thermal conversion of DAO under 360 °C after 120 minutes of reaction time

On the other hand, SEM images of solids obtained after 360 minutes (Figure 4-12c and Figure 4-12d) exhibited a change in the grain structure with the presence of agglomerated particles larger than 100 microns. The SEM-EDX spectra showed the predominantly presence of sulfur and iron (see Figure 4-14), which suggests that this particles are related to iron sulfide scale generated from the reaction between DAO and the reactor.

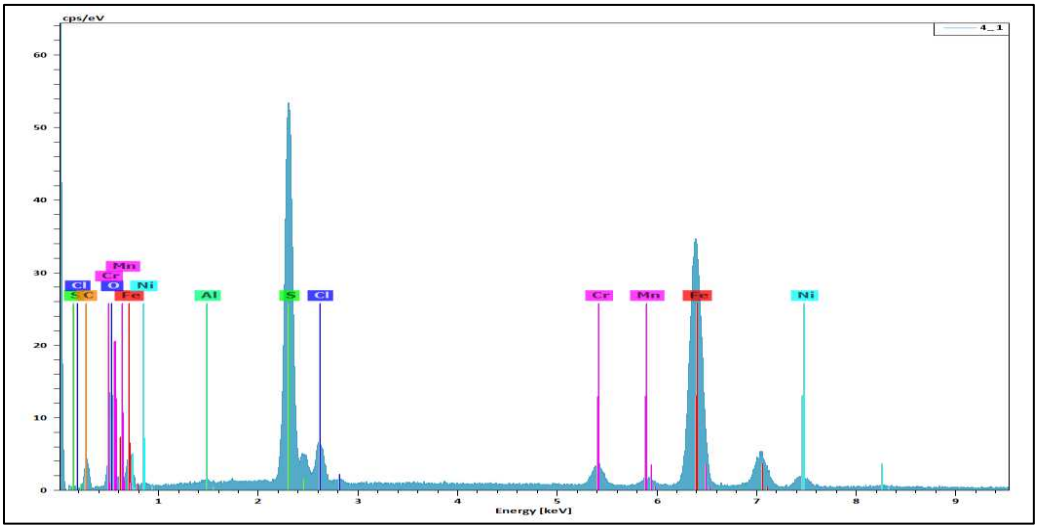

Figure 4-14. SEM-EDX spectra of solids obtained from thermal conversion of DAO under 360 °C after 360 minutes of reaction time

4.4 Discussion

4.4.1 Viscosity reduction and crackability of deasphalted oil at low temperature

In the case of thermal conversion at 360 °C, as the reaction time increases, a decrease in viscosity compared to the initial deasphalted oil was observed up to 240 min. The viscosity of the products at 40 °C was reduced by two to three orders of magnitude compared with the value of DAO from 0 min to 240 min without increase in the solid content (coke formation).

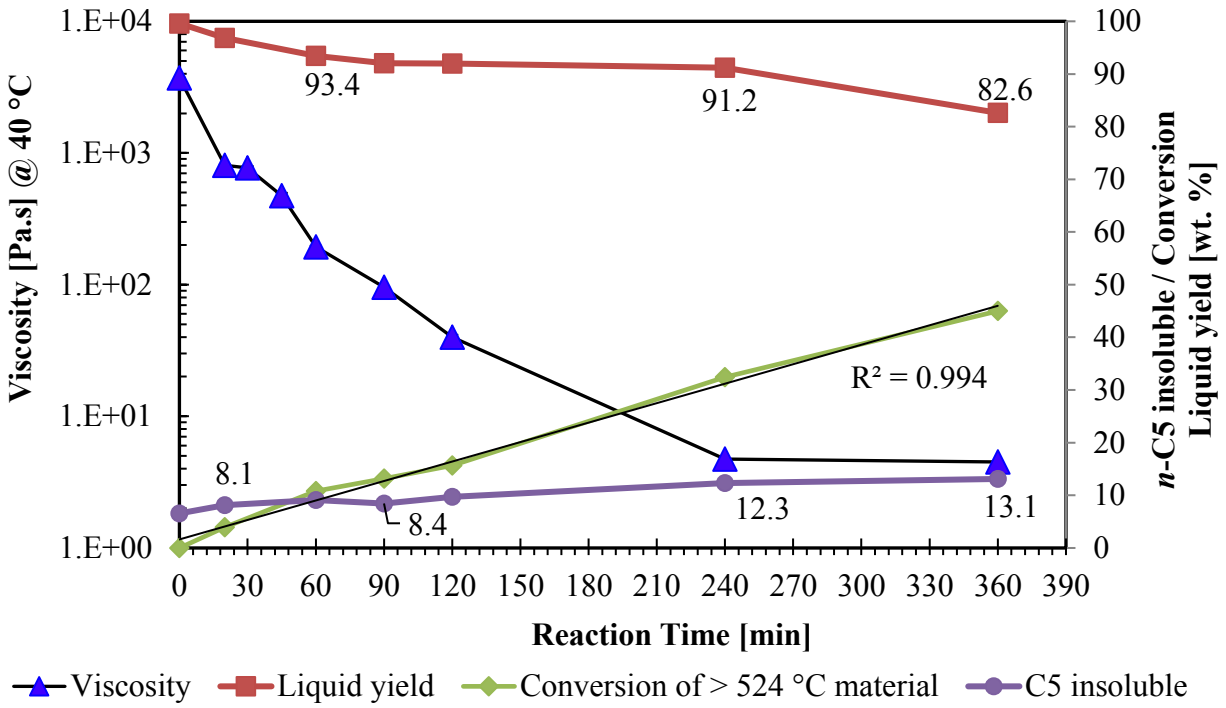

Figure 4-15. Viscosity reduction and crackability of DAO obtained under 360 °C, initial pressure of 3 MPa and reaction time varying between 1 and 360 minutes

After 240 minutes, the viscosity of the products remains fairly constant, and there is not a further significantly reduction along the time. Therefore, 240 min is considered the end of the coke induction time during the thermal conversion of DAO at 360 °C since the viscosity reached its minimum value and coke formation is initiated. In the visbreaking technology, the resident time for the thermal conversion is limited by this point (onset of coking) in order to avoid the coke formation in the furnace.

As it mentioned in Chapter 3 and shown in Figure 4-15, the viscosity reduction via thermal cracking increase with an increase in the conversion of high-molecular weight components to lighter material. However, this trend of viscosity reduction is considerable at low conversion and becomes relatively less pronounced at higher conversion. This could be ascribed to prevalence of addition reactions through condensation at higher conversion [10], as well as the interaction of aggregated asphaltenes in suspension which significantly increase the relative viscosity. Argiller et al. suggested that the colloidal behavior of asphaltenes play an important role in the viscosity of heavy oil, where the viscosity increase dramatically above a critical asphaltenes concentration (10 % by weight) [11].

4.4.2 Visbreaking kinetics

One of the objectives of the work was to extend the temperature range that can be used for the modelling of visbreaking of DAO. The challenge of describing cracking kinetics has always been one of describing conversion of a complex mixture.

It is worth to mention that the visbreaking kinetics was originally developed from pure compound paraffin cracking studies above 400 °C [12]. Cracking rate was described by a first order rate constant, k (s^{-1}), that followed an Arrhenius-type exponential relationship with inverse temperature, 1/T. The apparent first order kinetic relationship between residence time and temperature under typical visbreaking operating conditions led to the development of the concept of equivalent residence time (ERT), as described by Yan [13]. Using the same underlying assumptions, the residence time and reaction temperature have been treated to be interchangeable variables in order to achieve a certain process severity, as measured by conversion of heavy material, viscosity reduction or coke formation.

In the Figure 4-15, it is shown the conversion of residue boiling material based on the equation 1.

$$Conversion, X_{VR} = 1 - \frac{Mass\ of\ vacuum\ residue\ _{BP>524C,product}}{Mass\ of\ vacuum\ residue\ _{BP>524C,feed}} \quad (1)$$

From the figure, it was surprising to find that at 360 °C there was a linear increase in conversion with reaction time and that this relationship persisted to the onset of coking. This was a zero order kinetic relationship. Based on a previous study performed at lower visbreaking temperatures [14], it was suspected that the ERT concept might not be valid over the total temperature range of 280 to 400 °C.

4.4.3 Effects of hydrogen disproportionation

As described by Quignard and Kressmann [15], all the reactions that takes place during thermal conversion of heavy oil proceed by thermal activation and free radical steps; initiation step - the free radical is created by homolytic scission of bonds, and the most common bonds during primary upgrading is carbon-hydrogen (C-H), carbon-carbon (C-C), and carbon-sulfur (C-S); propagation step-the free radicals experience reactions of hydrogen transfer, decomposition and creation of new low molecular weight free radicals, cyclization, isomerization, condensation/polymerization; termination step, free radicals recombine together. These reactions depend on pressure, time and temperature.

Many previous studies [7][16][2] have reported that temperatures higher than 350 - 370 °C, the C-C, C-H and C-S bonds are broken in the vacuum residue at a significant rate producing reactive free radicals. However, vacuum residue and deasphalted oil derived bitumen have been found to have a higher reactivity than the conventional heavy oil fractions, even at low temperature [17][18].

In Chapter 3, it was observed that changes in the distribution of aliphatic and hydrogen content occurred, which is evidence of hydrogen transfer or hydrogen disproportionation that take place also at the lowest temperature investigated, namely 280 °C.

In order to obtain more information about changes that occurred during the thermal conversion of deasphalted oil at 360 °C, the hydrogen distribution can be determined from Figure 4-5a based on regions in the ^{1}H NMR spectrum defined in the previous Chapter 3.

The Figure 4-16 illustrates the changes in the hydrogen distribution in the thermal conversion liquid product along the time. It is observed that the amount of primary aliphatic (region between 0.4 and 1.1 ppm in the spectrum) decreases by 7.5 % relative to that feed after the first 20 minutes of reaction to then remains almost constant along the time. In the case of the amount of secondary hydrogen (region between 1.1 and 2 ppm in the ^{1}H NMR spectra) and benzylic (region between 2 and 4 ppm in the ^{1}H NMR spectra) remains narrowly constant during the first 60 minutes. From another stand point, the aromatic hydrogen content (region between 6 and 9 ppm in the spectra) show an increase that it may be associated to an increase in the proportion due to aliphatic hydrogen reduction.

After 60 minutes of reaction, a decrease in the secondary aliphatic hydrogen content is observed meanwhile the aromatic, primary, and benzylic hydrogen content increases along the reaction time. This increase in the rest of the hydrogen content may be ascribed to an increase in the proportion due to secondary aliphatic hydrogen reduction.

This latter behavior in the reduction of secondary aliphatic hydrogen content along with the increase in the aromaticity of the liquid product after 60 minutes observed by the increase in the density and refractive index values suggest that dehydrogenation of naphthenic rings to aromatics (C-H $_{sec}$, BDE: 95 kcal mol^{-1}) is taking place.

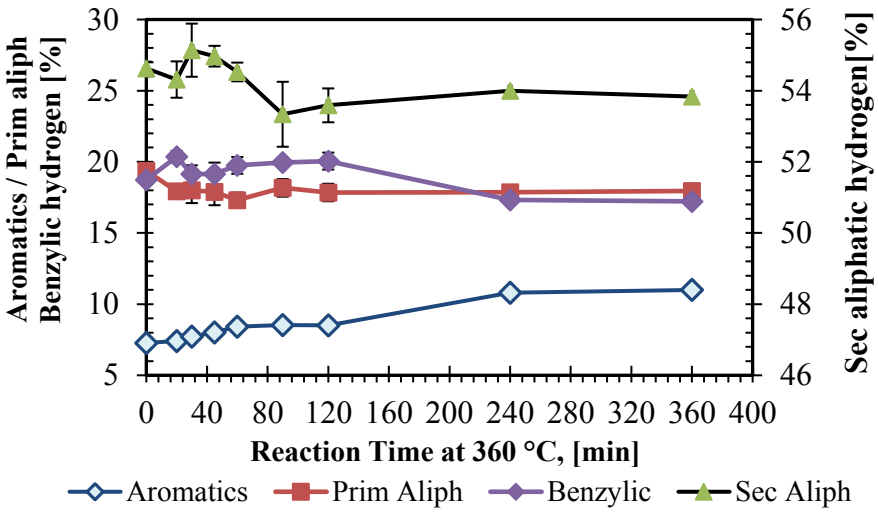

Figure 4-16. Area under the curve extracted from the NMR spectra, comparing the amount of the type of hydrogen found in the thermal conversion liquid product after 360 °C reaction

This reduction in the total aliphatic hydrogen (see Figure 4-5b), mainly associated to primary and secondary aliphatic, content along the reaction time shows that hydrogen transfer or hydrogen disproportionation reactions is taking place along time. From this it may be also suggested that dealkylation reactions of side chains in the polycondensed aromatics rings are occurring, being more predominant at low conversion. This inference is also supported by 1) gas products analysis where there was a considerable loss of hydrogen from the product in the form of light hydrocarbons (mainly methane and propane) generated since the first 20 minutes of reaction. 2) The liquid boiling point distribution (Simdist) of the thermal conversion liquid products where an increase in the amount of light boiling point compounds was observed along the reaction time (see Figure 4-3). For example, after 60 min at 360 °C the conversion of the vacuum residue fraction to lighter liquid products is around 16 wt. % (see Figure 4-15), where more than 70 % of the material converted goes into the gas and naphtha fraction (B.P below 350 °C), giving yields around 6 and 2.3 wt. % respectively.

These observations were also corroborated by liquid product analyses, such as H:C molar ratio, where a decrease of the ratio is observed along the time after the first 20 minutes.

The decrease in the amount of benzylic hydrogen after 120 minutes suggest an increase in rate in the aromatization of naphthenic components through hydrogen transfer are presented to the thermal conversion of DAO. The prevalence of dehydrogenation of naphthenic rings to aromatics after 120 minutes may explain why there is not additional viscosity reduction with more time, as it is shown in the Figure 4-16.

This behavior was also found previously by Di Carlo el at. [19] and Kapoor el at. [10], and reported that feedstocks rich in polynuclear aromatic cores with alkyl side chains attached (such as asphaltenes, resins, and polar compounds typically present in vacuum residues) undergoes predominantly to dealkylation reactions of the aromatics and resins (C_{ar}-C_{ali}, BDE: 78 kcal mol^{-1}) to give a higher selectivity towards gas and naphtha over gasoil (B.P between 350-524 °C), with parallel dehydrogenation of the naphthenic rings (C-H_{sec}, BDE: 95 kcal mol^{-1}) to produce coke at high severity via condensation.

4.4.4 FT-IR Hints

The FT-IR spectra were analyzed and interpreted in the same way as described in Chapter 3. In the Figure 4-17 is shown the ratio of aromatics C=C bonds to aliphatic methylene bonds stretching intensity [measured as the ratio of 1600 cm^{-1}/ 2853 cm^{-1} band] vs reaction time in order to track the aromaticity of the liquid product along the time. As it was reported in the Chapter 3, an increase in the aromatic: aliphatic methylene ratio is observed along the time, inferring an increment in the aromatic content caused by addition reactions.

In addition, a peak emerging between 720 -725 cm^{-1} was observed in all the samples for thermal conversion of DAO at 360 °C, which is associated to alkyl side chains possessing four and more methylene groups attached to aromatic rings [4].

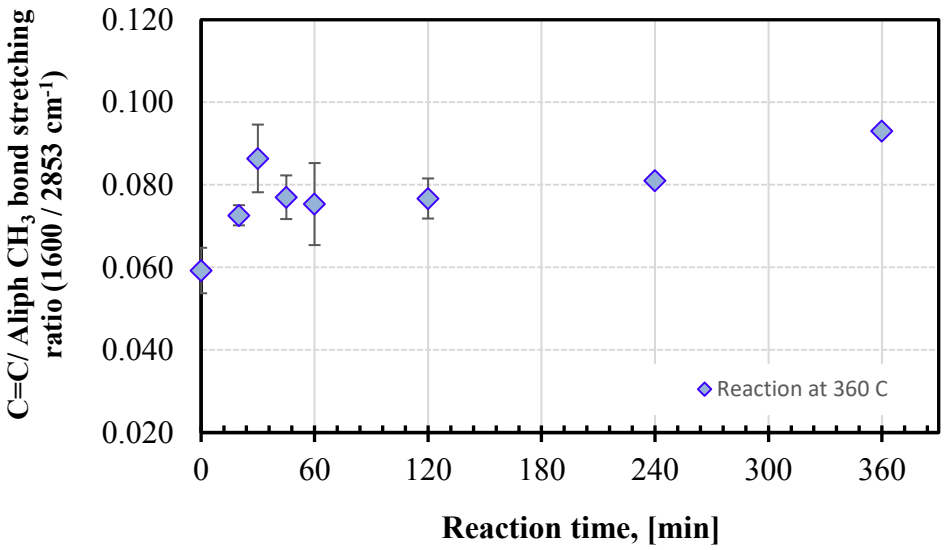

Figure 4-17. Ratio of aromatics C=C bonds to aliphatic methylene bonds stretching intensity of Thermal Conversion Products obtained under 360 °C, initial pressure of 3 MPa and different reaction times

4.4.5 Asphaltene content – Electron Spin resonance relationship

The presence of some asphaltenes (6.6 ± 0.5 wt. % *n*-pentane insoluble material) as well as stable organic free radicals in the DAO was confirmed in the Chapter 3. It was also suggested that the presence of organic free radicals are mainly associated to petroleum asphaltenes.

In addition, the *n*-pentane insoluble content (Figure 4-6) and organic free radical concentration (Figure 4-9) of the thermal conversion liquid product obtained after 360 °C seems to follow the same behavior reported for thermal conversion below 320 °C. Similar values of free radical concentration, approximately 2 x 10^{17} spins/g – which is 50 % higher than reported for untreated DAO, and *n*-pentane insoluble content (circa 10 wt. %) were obtained after 120 min of reaction time for 280, 320, and 360 °C experiments. This increase in the free radical might be associated to the cleavage of weakly bonded sulfur compounds.

Moreover, the free organic radical concentration decreased after reaching 120 min in all three set of experiments. The latter might indicate that the rate of radical recombination via condensation reactions and/or hydrogen transfer occurred at a greater rate than the rate of free radical formation.

This behavior was previously reported by Khulbe et al. [20] that observed an initial increase in the concentration of free radical concentration in the Athabasca bitumen during the heating of the samples at temperature below 350 °C, reaching a maximum free radical concentration which was followed by a continuous decline.

It is believed that this free radicals are reactive species located within polycondensed aromatic systems associated to asphaltenes. Their persistence at ambient temperature could be explained by "cage effect", in which they are protected against the possible free radical-radical or hydrogen transfer reactions by other polycyclic aromatic hydrocarbons in aggregates [21]. Thus, the tendency of asphaltenes to form aggregates will enhance the stability of the free radical itself.

Although Rahimi et al. [22] suggested that with increasing temperature at about 300 °C during thermal treatment of heavy oil, the 'caging' effect decrease due to dissociation of aggregates and breakup of the protective resin layer. Hence, the free radical type reactions would be enabled due to the asphaltene cores that become exposed.

On the other hand, Yen et al [5] suggested that the reactivity or stability of polycondensed aromatic systems is predominately led by the forms and behavior of free radicals evolved in the thermal conversion process.

In the case of the industrial DAO, the thermal decomposition of this polynuclear aromatic systems with alkyl side chains attached proceeds even a low temperature with dealkylation and aromatization of naphthenic fraction leading to addition reactions within the pentane soluble materials (aromatics and resins) via free radical type reactions to create new asphaltenes, and eventually coke formation.

In addition, Rahimi et al. [23] suggests that the structure of asphaltenes themselves are also changed during thermal conversion, increasing their aromaticity due to the side chain fragmentation and dehydrogenation reactions. These reactions make the subsequent decomposition more difficult, as well as decrease their solubility approaching to the reaction limit of the asphaltene aromatic core [24]. Once the solubility limit of the asphaltene core is reached, a second liquid phase is created which is lean in donor hydrogen and asphaltene radical recombination is possible causing an irreversible rapid reaction to form solid coke [22].

The latter might explain the reduction in the organic free radical concentration after 120 minutes of reaction time.

Finally, it was expected that some trend in g-factors obtained in the ESR results would be apparent as the nature of the radical should change with increasing system aromaticity and the asphaltene content. However, the thermal conversion of DAO did not show any marked change in g-factors in relation to molecular size along the reaction time in this work.

4.5 Conclusions

Through experimental investigations on thermal conversion of deasphalted oil at 360 °C, the following observations were made:

a) There is significant reduction in viscosity of the liquid product after thermal conversion at 360 °C, decreasing by two to three orders of magnitude compared with the value of DAO from 0 min to 240 min without increase in the solid content (coke formation). During this reaction time, the viscosity reduction via thermal cracking was considerable at low conversion and became relatively slow at higher conversion, possible to prevalence of addition reactions at higher conversion.

b) As observed at temperature below 320 °C, there is a predominance of dealkylation of side chains associated to polycondensed aromatics rings and dehydrogenation of naphthenic rings to aromatics.

c) Thermal conversion of DAO at 360 °C resulted in a linear increase in cracking conversion with reaction time, which means that the cracking kinetics at 360 °C was zero order.

d) There is a continual increase in the *n*-pentane insoluble content along reaction time, which suggest that addition reactions to create new asphaltenes take place even at low temperature.

e) An increase in the free radical concentration was observed during the thermal conversion of DAO at 360 °C, reaching a maximum free radical concentration which was followed by a continuous decline in the concentration. This could suggest that organic free radical are not completely unreactive.

f) There also appears to be a correlation between the asphaltenes content and the concentration of unpaired electrons observed in the products during the first 120 minutes of reaction time. After 120 minutes, an increase in the aromaticity and reduction in the free radical concentration of the product may suggest free radical recombination in the asphaltene fraction is occurring.

References

[1] Banerjee, D. K. *Oil sands, heavy oil & bitumen: from Recovery to Refinery.* PennWell Corporation: Tulsa, Okla, 2012.

[2] Speight, J. G.; Ozum, B. *Petroleum refining processes*; CRC press: Boca Raton, 2001.

[3] ASTM D7169 – 11: Standard test method for boiling point distribution of samples with residues such as crude oils and atmospheric and vacuum residues by high temperature gas chromatography; ASTM: West Conshohocken, PA, 2012.

[4] Sharma, B. K.; Tyagi, O. S.; Aloopwan, M. K. S.; & Bhagat, S. D. Spectroscopic characterization of solvent soluble fractions of petroleum vacuum residues. *Petroleum science and technology*, **2000**, *18*(3-4), 249-272.

[5] Yen, T. F.; Wu, W. H.; Chilingar, G. V. A study of the structure of petroleum asphaltenes and related substances by proton nuclear magnetic resonance. *Energy Sources*, **1984,** *7*(3), 275-304.

[6] Hauser, A.; AlHumaidan, F.; Al-Rabiah, H.; Halabi, M. A. Study on thermal cracking of Kuwaiti heavy oil (vacuum residue) and its SARA fractions by NMR spectroscopy. *Energy Fuels* **2014**, *28*(7), 4321-4332.

[7] Dehkissia, S.; Larachi, F.; Rodrigue, D.; Chornet, E. Characterization of Doba–Chad heavy crude oil in relation with the feasibility of pipeline transportation. *Fuel* **2004**, *83*(16), 2157-2168.

[8] ASTM D6560-12: *Standard test method for Determination of Asphaltenes in Crude Petroleum and Petroleum Products*; ASTM: West Conshohocken, PA, 2012.

[9] Yen, T. F.; Tynan, E. C.; Vaughan, G. B.; Boucher, L. J. Electron spin resonance studies of petroleum asphaltics. In *Spectrometry of Fuels;* Friedel R.A. *Eds;* Springer, Boston, MA, **1970**; 187–201.

[10] Kapoor, M. P.; Kothiyal, V.; Singh, I. D. Compositional and structural studies of visbroken residues. *Fuel Sci. Technol. Int.* **1993**, *11*(7), 975-989.

[11] Argillier, J.-F.; Coustet, C.; Henaut, I. Heavy oil rheology as a function of asphaltene and resin content and temperature. *Proceedings of SPE International Thermal Operations and Heavy Oil Symposium and International Horizontal Well Technology Conference* **2002**.

[12] Sachanan, A. N. Conversion of petroleum. *Production of motor fuels by thermal and catalytic processes*, 2ed; Reinhold: New York, 1948.

[13] Yan, T. Y. Characterization of visbreaker feeds. Fuel **1990**, *69*, 1062-1064.

[14] Wang, L.; Zachariah, A.; Yang, S.; Prasad, V.; De Klerk, A. Visbreaking oilsands-derived bitumen in the temperature range of 340-400 °C. Energy Fuels **2014**, *28*, 5014-5022.

[15] Huc, A. Y. *Heavy crude oils, from geology to upgrading: an overview*; Editions Technip: Paris, 2011.

[16] Gray, M. R. *Upgrading oilsands bitumen and heavy oil*; The University of Alberta Press: Edmonton, 2015.

[17] Bianco, A. D.; Panariti, N.; Anelli, M.; Beltrame, P.; Carniti, P. Thermal cracking of petroleum residues. *Fuel* **1993**, *72* (1), 75–80

[18] Speight, J. G. Thermal cracking of Athabasca bitumen, Athabasca asphaltenes, and Athabasca deasphalted heavy oil. *Fuel* **1970**, *49*(2), 134-145.

[19] Di Carlo, S.; Janis, B. Composition and visbreakability of petroleum residues. *Chem. Eng. Sci.* **1992**, *47*, 2695-2700.

[20] Khulbe, K.; Mann, R.; Lamarche, G.; Lamarche, A. Electron spin resonance study of the thermal decomposition of solvent extracted Athabasca tar sand bitumen. *Fuel Processing Technology* **1992**, 31 (2), 91–103

[21] Mujica, V.; Nieto, P.; Puerta, L.; Acevedo, S. Caging of molecules by asphaltenes. A model for free radical preservation in crude oils. *Energy Fuels* **2000**, 14(3), 632-639.

[22] Rahimi, P. M.; Gentzis, T. The chemistry of bitumen and heavy oil processing. In *Practical Advances in Petroleum Processing;* Hsu C.S.; Robinson P.R. Eds; Springer, New York, NY**, 2006**; Volume 2, 597–634

[23] Rahimi, P. M.; Teclemariam, A.; Taylor, E.; Debruijn, T.; Wiehe, I. A. Thermal processing limits of Athabasca bitumen during visbreaking using solubility parameters. *ACS Symposium Series Heavy Hydrocarbon Resources* **2005**, *895*, 183–196

[24] Wiehe, I.A. *Process chemistry of petroleum macromolecules*. Baton Raton: CRC Press, 2008.

5. THERMAL CONVERSION OF DEASPHALTED OIL AT 400 °C

5.1 Introduction

In previous Chapters, thermal conversion of deasphalted oil was performed below the intended thermal cracker temperature of operation and was selected specifically to provide information about the changes taking place at lower conversion. At that temperature range, small and analogous changes in the microstructure were found since there is limited amount of energy so the homolytic scission which required lowest activation energy first occurs. Despite of the limited amount of energy, it seems that polycondensed cyclic species in the DAO are thermally driven, being enable to create new asphaltenes, even at low temperature. This will significantly affect the properties of the thermal conversion product. In addition, it appears that there was a correlation between the asphaltenes content and the concentration of unpaired electrons observed in the products.

From literature findings [1] 2] [3] and the results obtained thus far, it is evident that asphaltenes content of the feed significantly impacts the thermal cracking of heavy oil.

On the other hand, it is known that as the temperature and/or reaction time increase, more energy is added to reach the level of energy for certain type of reaction happen. Based on that, it was of interest to gain understanding about the reactivity of deasphalted heavy oil (DAO), as well as the formation of pentane insoluble asphaltenes at moderate temperature, namely 400°C.

5.2 Experimental Section

5.2.1 Materials

Deasphalted vacuum residue oil from the Nexen Long Lake upgrader was utilized for the thermal conversion reactions. Deasphalted oil used in these experiments belongs to the same barrel as the heavy oil samples employed on the previous Chapters. Nexen Long Lake deasphalted vacuum residue oil was characterized and the characterization is shown in Chapter 3, Table 3-1.

The source and purity of nitrogen, methylene chloride, *n*-pentane, and toluene were described in Chapter 3. These materials were also used in this Chapter's experiments.

5.2.2 Equipment and Procedure

The experiments were conducted in a closed reactor system using the same experimental procedure previous described in Chapter 3. All the experiments in this chapter were performed in triplicate at an internal reactor temperature of 400 °C, and results were reported as an average with one sample standard deviation.

5.2.3 Analysis

Analyses made in this chapter on the products as well as the description of the instruments and analysis procedures are the same used in the Chapter 3.

5.3 Results

5.3.1 Material Balance

The reaction products were obtained under these conditions: 400 °C, an initial pressure of 3 MPa N_2 and reaction time varying from 10 to 90 minutes. The reaction time of 0 min correspond to deasphalted vacuum residue sample (feed). The mass of each phase was determined individually. The overall material balance (Table 5-1) and the product yields of each phase at 400 °C (Table 5-2) were obtained for experiments that were performed in triplicate or more.

Table 5-1. Mass balance for thermal conversion at 400 °C for different reaction times

Balance Material [wt. %][a]			
Reaction temperature: 400 °C			
Reaction time [min]	**x**	**s**	**n [b]**
10	98.98	0.37	3
30	99.72	0.46	4
45	99.91	0.61	3
60	100.00	0.77	3
90	99.45	0.10	4

[a] Average (x) and sample standard deviation (s) of number (n) of experiments are reported
[b] Number of samples performed at this condition

In all experiments, the average material balance closed to within 2 %, i.e. material balance was between 98 and 102 %.

Table 5-2. Product yield (wt. %) for thermal conversion at 400 °C for different reaction times

Material Balance [wt. %][a]						
Reaction temperature: 400 °C						
Time [min]	**Gas**		**Liquid**		**Solid**	
	x	**s**	**x**	**s**	**x**	**s**
10	7.78	1.05	91.61	1.37	0.61	0.11
30	10.33	0.51	89.04	0.67	0.64	0.26
45	10.74	1.00	88.60	1.03	0.66	0.10
60	10.99	0.45	88.39	0.59	0.63	0.19
90	12.17	0.64	87.14	2.21	1.84	1.07

[a] Average (x) and sample standard deviation (s) of three experiments are reported

From the product yield for thermal conversion of DAO at 400 reported in Table 5-2, there is a trade-off between the yields of liquid and gas from 0 min to 60 min. As it was reported in the previous Chapters, a significant amount of gaseous products were obtained from the reaction in the first 10 minutes of reaction.

In addition, after 90 min, it was observed that there was an increase in the amount of solid in the sample. Therefore, 60-90 min may be considered as the break-down point (end of the induction time) of deasphalted oil thermal conversion at the processing temperature of 400 °C as coke formed.

As the experiments made in previous chapters, filtration of liquid products took a long time before solids were obtained and this was found for all experiments. It is likely that the solids in the feed were very fine, which was later confirmed by microscopy.

5.3.2 Product characterization

Products were characterized and analyzed so that have a better idea about the changes that occurs during mild thermal treatment at 400 °C.

5.3.2.1 Viscosity

Viscosity measurements were performed at 5 different temperatures (7.5, 20, 30, 40 and 50 °C), but shear rate was kept constant at 20 s^{-1} for all the temperatures except 7.5 °C (shear rate 10 s^{-1}). These results are reported in Table 5-3.

Table 5-3. Viscosity data to thermal conversion products under 400 °C and initial pressure 3 MPa

	Time reaction [min]					
	0	**10**	**30**	**45**	**60**	**90**
	Viscosity [Pa.s]					
Measured Temperature: 50 [°C]						
Average	600.0	17.4	2.0	0.7	0.8	0.5
Std. dev.	13.0	9.4	0.2	0.3	0.3	0.2
Measured Temperature: 40 [°C]						
Average	3646.4	52.5	4.7	1.7	2.0	1.1
Std. dev.	242.5	26.6	1.3	0.8	0.9	0.5
Measured Temperature: 30 [°C]						
Average	--[a]	209.6	13.8	4.7	5.6	2.8
Std. dev.	--	104.5	4.3	2.6	2.7	1.4
Measured Temperature: 20 [°C]						
Average	--[a]	1369.8	47.5	15.0	17.6	8.4
Std. dev.	--	689.9	15.1	9.1	9.9	4.6
Measured Temperature: 7.5 [°C]						
Average	--[a]	12806	397.4	86.9	106.8	47.5
Std. dev.	--	6373.8	10.0	61.0	68.0	29.7

[a] Viscosity of the sample could not be determined (>10000 Pa.s)

In addition, Figure 5-1 illustrated the viscosity measurements of thermal conversion products at 400 °C versus time in order to identify variation of this property over reaction time.

After thermal cracking at 400 °C, the viscosity of the products at 40 °C dropped by three orders of magnitude compared with the value of the raw DAO from 0 min to 45 min without coke formation (Figure 5-1). Afterward the viscosity of the products looks fairly constant, showing that any difference falls within the experimental error and it is not a further significantly reduction along the time. Although the changes after 45 min reaction time are within experimental uncertainty,

there was an increase in viscosity before onset of coking, as was found in the earlier study carried out by Wang et al. [4].

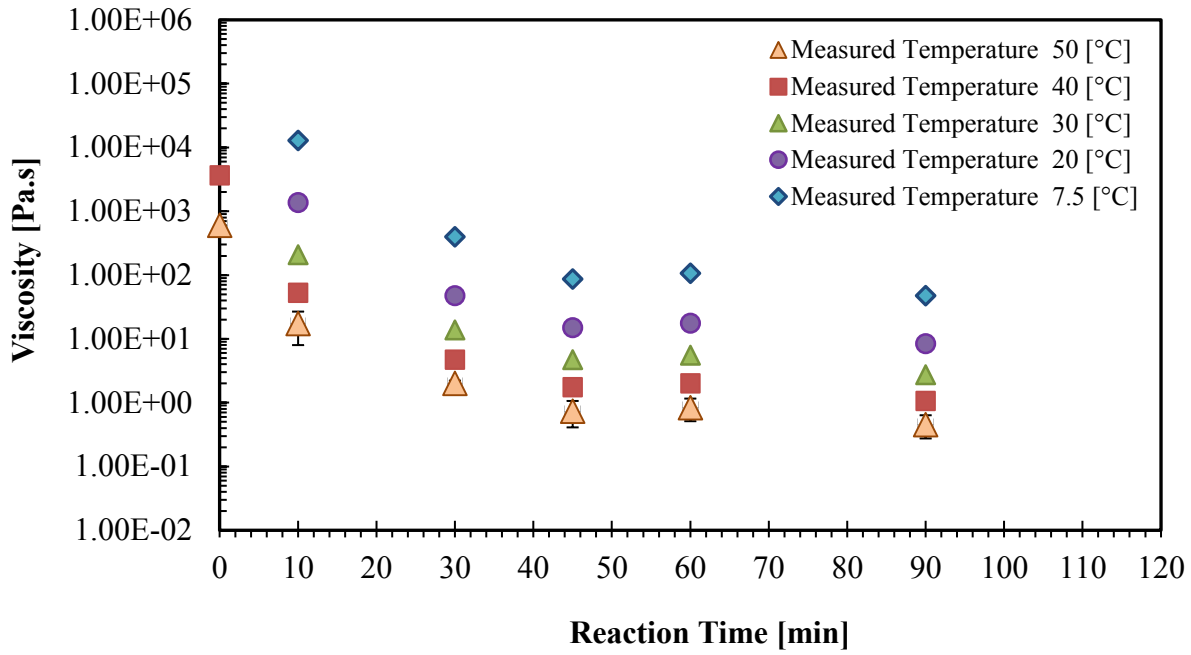

Figure 5-1. Viscosity of thermal conversion products obtained under 400 °C, initial pressure of 3 MPa and reaction time varying between 10 and 90 minutes. Measurements were performed at different temperature

It is worth mentioning that all the 5 measured temperatures followed the same trend in the viscosity measurements of the thermal conversion product obtained under 400 °C along the different reaction time.

5.3.2.2 Refractive index

The refractive index of every sample was determined at 5 different temperatures (20, 30, 40, 50 and 60 °C), and in Table 5-4 the results are tabulated for the refractive index at 400 °C at different reaction times. Furthermore, Figure 5-2 shows the refractive index at 400 °C versus time in order to identify variation of this property over reaction time.

Table 5-4. Refractive Index measurements performed on thermal conversion products after 400 °C and initial pressure 3 MPa reaction

	Temperature [°C]	Time reaction [min]					
		0	10	30	45	60	90
		Refractive index [nD]					
Average	20	1.5921	1.5917	1.5957	1.5967	1.5949	1.6122
Std. dev.		0.0001	0.0007	0.0005	0.0007	0.0007	0.0043
Average	30	1.5883	1.5878	1.5915	1.5925	1.5908	1.6080
Std. dev.		0.0000	0.0010	0.0005	0.0005	0.0006	0.0044
Average	40	1.5846	1.5840	1.5670	1.5881	1.5867	1.6038
Std. dev.		0.0001	0.0010	0.0009	0.0003	0.0006	0.0045
Average	50	1.5808	1.5801	1.5830	1.5826	1.5823	1.5996
Std. dev.		0.0001	0.0010	0.0004	0.0005	0.0004	0.0045
Average	60	1.5773	1.5765	1.5793	1.5775	1.5780	1.5952
Std. dev.		0.0001	0.0012	0.0004	0.0005	0.0002	0.0047

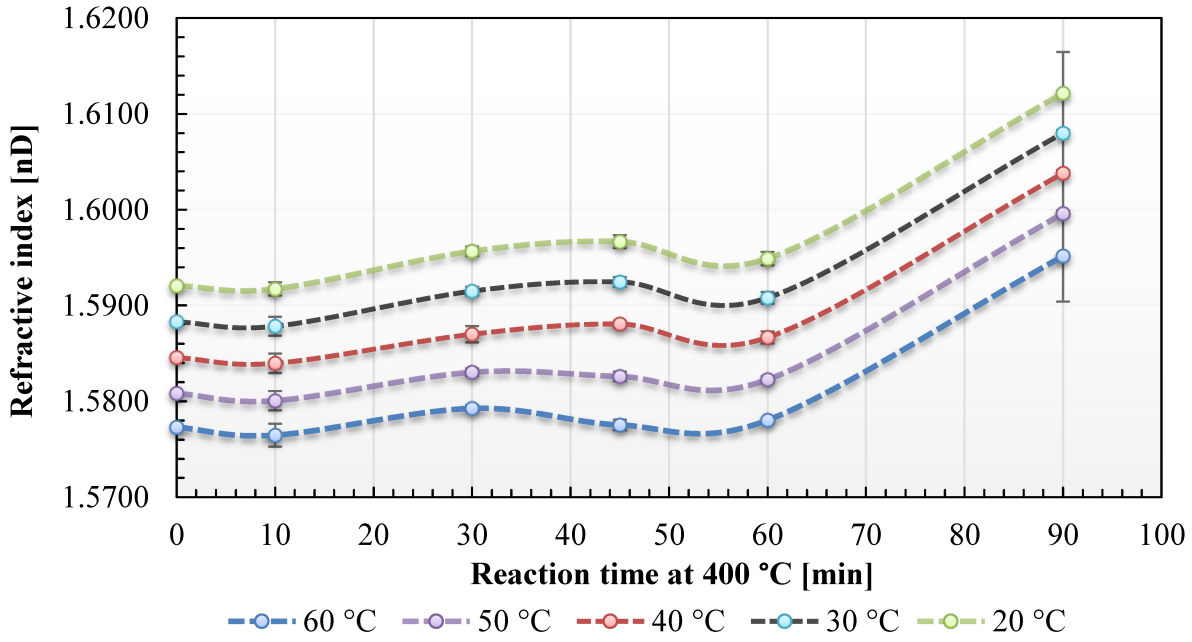

Figure 5-2. Refractive Index results for Thermal Conversion Products at 400 °C, initial pressure of 3 MPa and different reaction times: Refractive index vs Time

From the figure, it is shown that the refractive index increase slightly after 10 minutes reaction time, to then remain almost constant until reaching 60 minutes. Thereafter, it is followed by an

increase in the measurement. This behavior is an indication of the liquid product is being more aromatic.

5.3.2.3 Liquid boiling point distribution (SimDist)

The liquid boiling point distribution of the thermal conversion products at 400 °C was determined, and it is presented in Figure 5-3. The results of this analysis are shown in the following way: Temperature vs weight percent distilled.

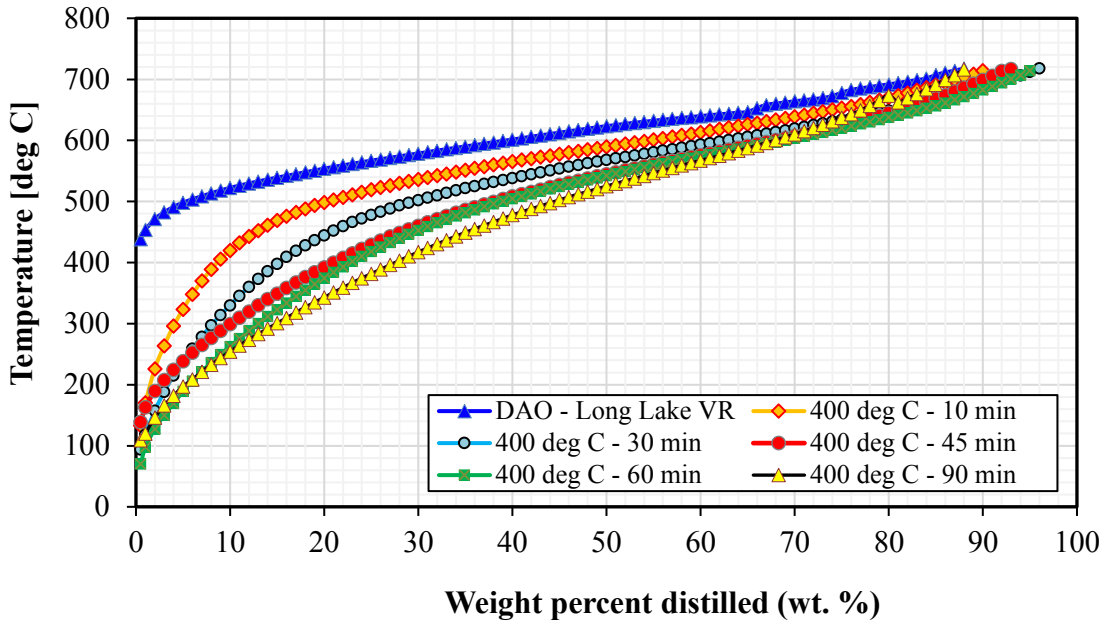

Figure 5-3. Liquid boiling point distribution of thermal conversion products after 400 °C, initial pressure of 3 MPa at different reaction times

In the case of reaction at 400 °C, there is a considerable increase in the amount of light boiling point compounds (BP < 524 °C) during the first 45 minutes of reaction, to then it is observed that there is mostly an over cracking of the light compounds and increase in the amount of heavy compounds (BP > 700 °C). A better approach can be observed in the Figure 5-4 where a decrease in the weight average boiling point (WABP) is shown along the reaction time until reaching 45 minutes. Afterward, the WABP keeps relatively constant until reaching 90 minutes.

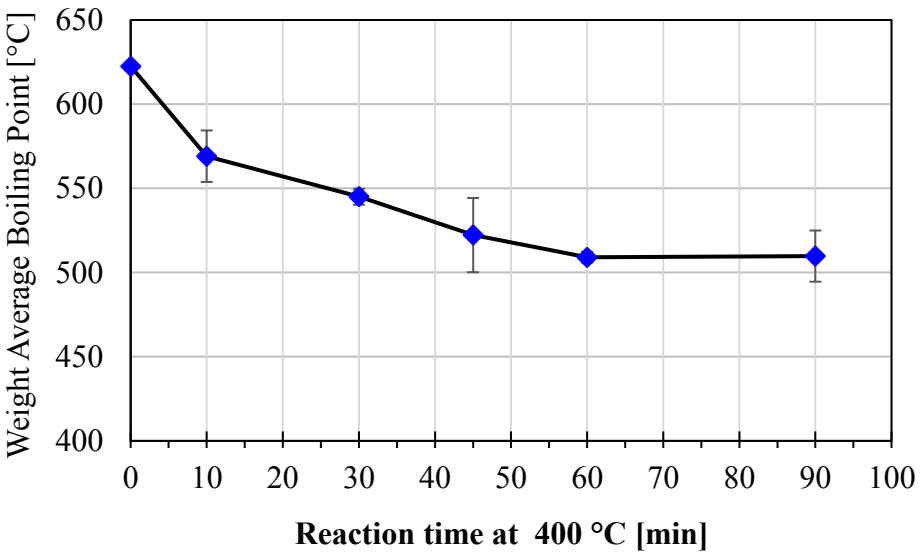

Figure 5-4. Weight average boiling point (WABP) of the liquid thermal conversion products after 400 °C, initial pressure of 3 MPa at different reaction times

5.3.2.4 Proton nuclear magnetic resonance ^{1}H NMR

As in previous chapters, aliphatic and aromatic hydrogen content was determined using proton NMR analysis. In Figure 5-5, the following data is presented a) the NMR spectra of liquid products during thermal conversion of the DAO at 400 °C in order to detect and track all the structural changes, and b) the aliphatic hydrogen content of thermal conversion products at 400 °C against reaction time thereby tracking changes in the DAO related with the aliphatic hydrogen content.

Some regions in the NMR data were identified and defined in the chapter 3 (section 3.3.2.5) so as to obtain hydrogen aliphatic content based on data presented by Sharma et al [5], Yen et al [6], and Hauser et al [7]. Mnova NMR software was used the determination of peak area based on the hydrogen ranges.

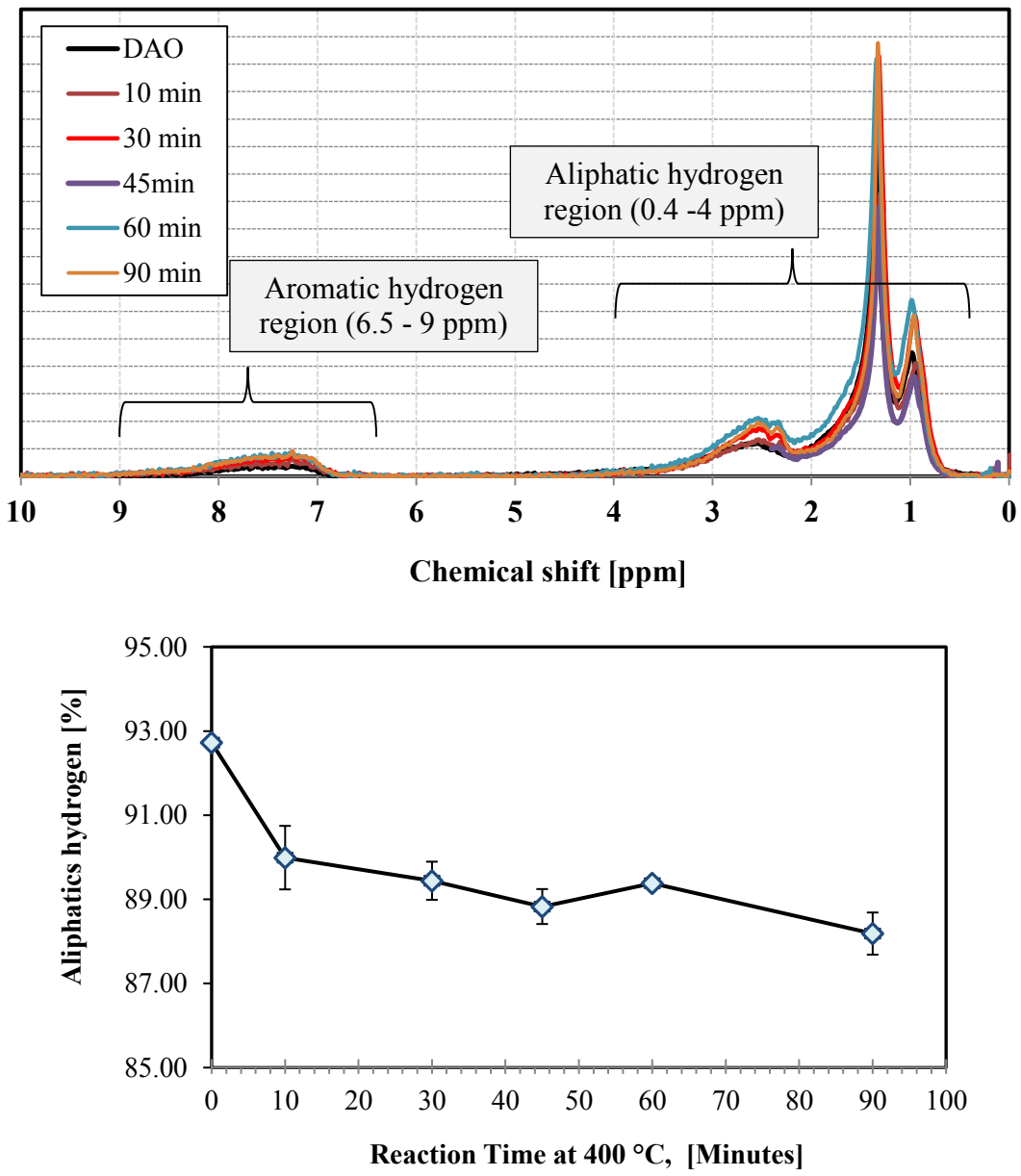

Figure 5-5. Proton NMR results of thermal conversion products after 400 °C, initial pressure of 3 MPa and different times; a) ^{1}H NMR spectra b) % Aliphatic hydrogen vs Time

At 400 °C, the aliphatic hydrogen content decreased significantly after the first 10 minutes, to then it was observed a slightly decrease along the reaction time.

5.3.2.5 Pentane insoluble (Asphaltene content)

The *n*-pentane precipitated asphaltenes content in the thermal conversion product was obtained by ASTM D6560-12 [8] and it is reported in Table 5-5. In addition, Figure 5-6 illustrated the *n*-pentane content in the thermal conversion products versus time at 400 °C so as to identify variation of this property over reaction time.

Table 5-5. Pentane insoluble content in wt. % of thermal conversion products under 400 °C, initial pressure of 3 MPa and different times

	Time reaction [min]					
	0	**10**	**30**	**45**	**60**	**90**
	***n*-Pentane insoluble [wt. %]**					
Average	6.56	10.53	12.35	12.53	16.00	20.81
Std. dev.	0.15	0.21	0.35	1.28	0.32	3.07

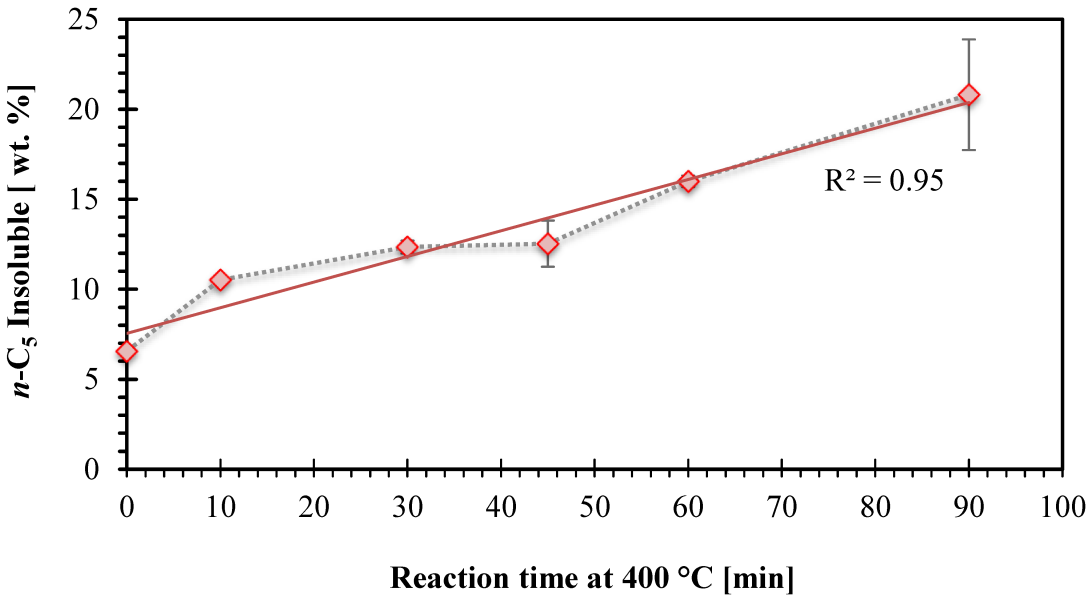

Figure 5-6. Pentane insoluble of thermal conversion products under 400 °C, initial pressure of 3 MPa and different times

From Figure 5-6, it can be observed that there was an increase in *n*-pentane insoluble asphaltenes content along the reaction time, being more significantly during the first 10 minutes of reaction.

5.3.2.6 FT-IR spectroscopy

FT-IR spectroscopy enables the detection of chemical groups in materials. In the case of raw deasphalted oil, as bitumen, it is a complex mixture that contains many compounds, thereby this method help to support and confirm hypothesis about changes during the thermal conversion. In Figure 5-7, the spectra for every reaction time was plotted.

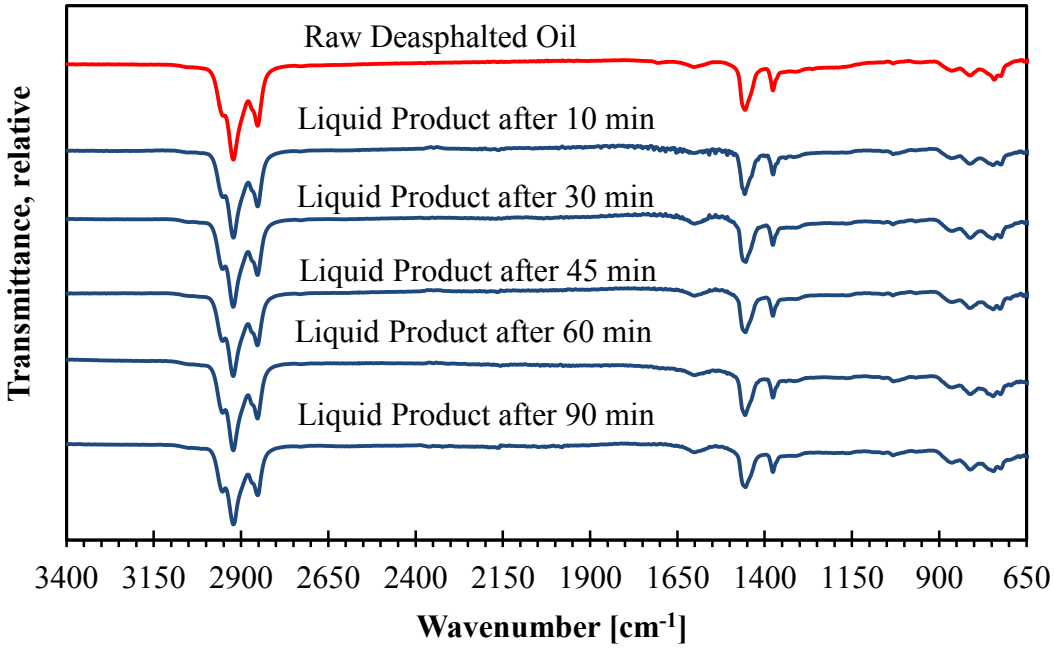

Figure 5-7. FTIR spectra of thermal conversion products after 400 °C, initial pressure of 3 MPa and different reaction times

5.3.2.7 Electron spin resonance (ESR)

The electron spin resonance (ESR) spectra of the liquid products and deasphalted vacuum residue oil were obtained in order to track the organic free radical species, thereby offering insights into the nature and amount of free radical during thermal conversion of heavy oil. The ESR spectra were recorded as first derivative curves, and they are shown in Figure 5-8.

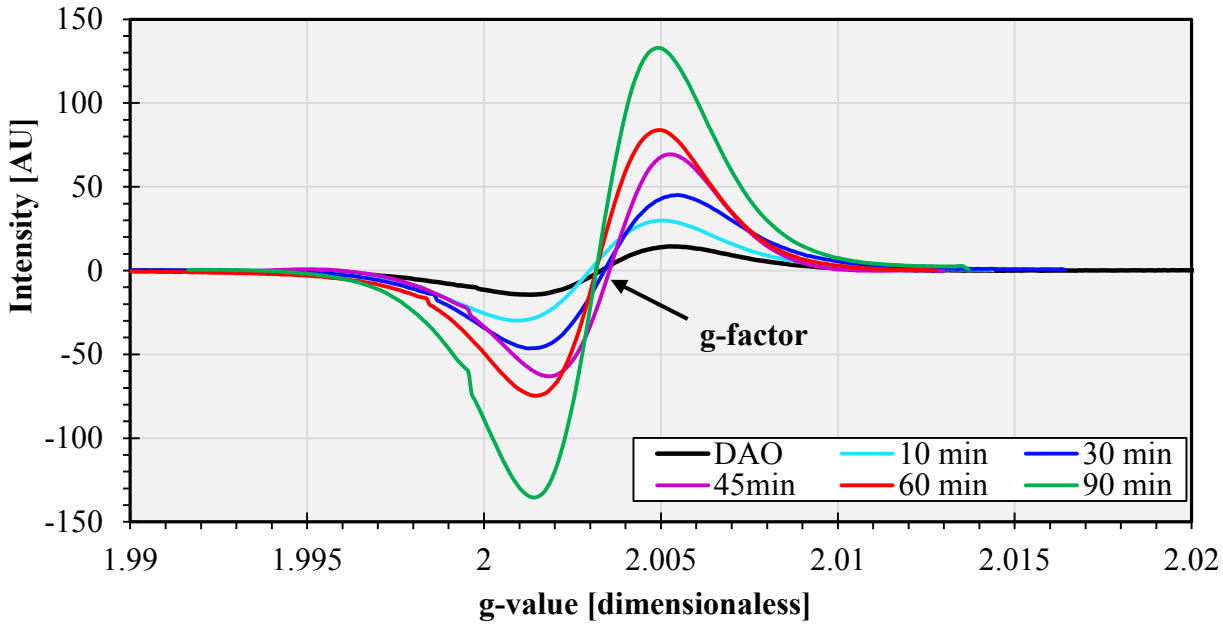

Figure 5-8. ESR spectrum of DAO and thermal conversion products after 400 °C, initial pressure of 3 MPa and different reaction times

As in previous chapters, the samples were diluted at 30 wt.% in toluene and the organic free radicals concentration were obtained by comparison of the double integrated intensity against the calibration curve built using 4-hydroxy TEMPO (see Figure 3-3 in chapter 3). The number of unpaired spins per gram and g-factor (a measure of the center of free radical absorption) of the thermal conversion products at 400 °C were calculated, the results are presented in Table 5-7.

Table 5-6. ESR Parameters of thermal conversion products after 400 °C, initial pressure of 3 MPa and different reaction times

Time [min]	Double integrated intensity Area		Calculated organic free radical concentration [spins/g]		g-factor	
	x	s	x	s	x	s
0	14269	833	1.30×10^{17}	8.10×10^{15}	2.0032	0.0002
10	19261	4193	1.78×10^{17}	4.07×10^{16}	2.0029	0.0003
30	26150	2409	2.45×10^{17}	2.34×10^{16}	2.0030	0.0002
45	31680	2293	2.99×10^{17}	2.23×10^{16}	2.0031	0.0004
60	37526	3903	3.55×10^{17}	3.80×10^{16}	2.0032	0.0001
90	47812	3099	4.55×10^{17}	3.01×10^{16}	2.0030	0.0003

In addition, the Figure 5-9 shows the organic free radical concentration and g-factors of thermal conversion products at 400 °C versus time in order to identify variation of this property over reaction time.

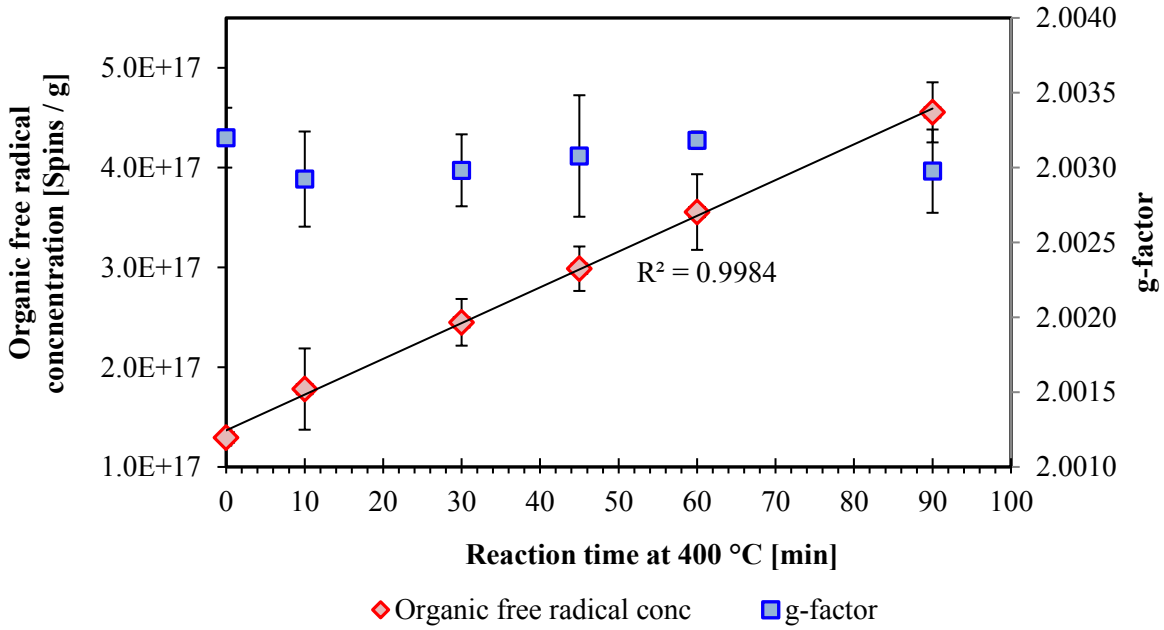

Figure 5-9. Organic free radical concentration of thermal conversion products after 400 °C, initial pressure of 3 MPa and different reaction times

5.3.2.8 Density

Density measurements of the liquid products and deasphalted vacuum residue oil were determined at two different temperatures at 20 and 40 °C, respectively. Samples must be heated up before being injected in the pycnometer. Density data is reported in Table 5-8.

Table 5-7. Density measurements performed at two different temperatures: 20 and 40 °C to thermal conversion products after reaction at 400 °C

	Temperature [°C]	Time reaction [min]					
		0	10	30	45	60	90
		Density [kg/m^3]					
Average	20	1057.3	1035.2	1019.6	1016.8	1027.0	1036.7
Std. dev.		3.6	2.0	1.0	3.9	4.5	3.7
Average	40	1049.8	1020.2	1006.6	1003.3	1014.4	1023.8
Std. dev.		4.7	1.9	1.0	4.2	5.2	4.4

In Figure 5-10, the density measurements versus reaction time is shown so that reveal any change in the liquid product density along reaction time.

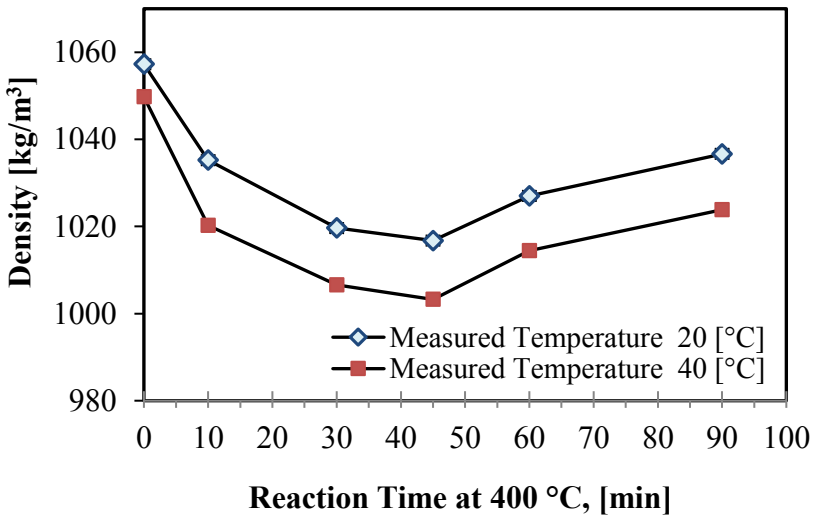

Figure 5-10. Density of thermal conversion products obtained under 400 °C, initial pressure of 3 MPa and different reaction times

At 400 °C, there is a decrease in the density of the products along reaction time until 45 minutes of reaction time, showing that some compounds with lighter molecular weight are generated from the thermal conversion. After 45 minutes, there is an increase in the density of the liquid product that it might be related to addition reactions are occurring at this time.

5.3.2.9 Gas Chromatography

Gas products generated from the thermal conversion reactions were collected in a gas bag and injected in the gas chromatograph to be analyzed. The gaseous product analyses are reported in Table 5-8 for thermal conversion reactions at 400 °C, which presents the mole concentration obtained for every compound between C_1 to C_6 in the sample.

Table 5-8. Gas products associated to thermal conversion of DAO after reaction at 400 °C

Compounds	**10 min**	**30 min**	**45 min**	**60 min**	**90 min**
[mole %]					
Methane	2.94	2.54	5.99	12.67	14.67
Ethylene	--	--	0.30	0.46	0.22
Ethane	1.96	0.57	4.28	8.00	9.02
Propylene	--	--	5.62	0.56	1.30
Propane	3.29	3.42	1.31	4.69	9.46
Iso-Butane	--	0.33	0.87	1.69	1.86
n-Butane	1.36	0.81	1.74	1.99	1.09
Cis-2 Butane	2.01	1.90	3.87	5.38	4.62
Iso-pentane	0.57	0.97	3.38	3.33	2.26
n-pentane	1.08	1.70	3.71	4.37	4.27
Iso-Hexane	0.22	--	1.50	0.29	4.06
N-Hexane	0.31	--	1.62	0.30	3.54
H_2S	0.15	0.11	0.20	0.13	0.40
CO_2	0.02	0.06	0.05	0.08	0.14
H_2	--	--	--	--	--
N_2	86.10	87.59	65.44	56.05	43.05
Total	**100.00**	**100.00**	**100.00**	**100.00**	**100.00**

[a] H_2S was observed at very low concentration

Measurements of gas evolution at moderately low temperatures provided a key to the detection and monitoring of chemical changes which take place in the deasphalted heavy oil.

As mentioned in previous chapters, a rigorous tracking and interpretation in the evolution of the each compound along the reaction time is not possible due to the use of gas bag for collecting the samples. Although, an increase in the amount of methane is observed along the reaction time.

5.3.2.10 Solid content

In Figure 5-11, is exhibited images of the solids recovered from vacuum filtering step after thermal treatment of DAO at 400 °C. A milipore filter paper of 0.22 um was employed and samples were left inside the fumehood for 2 days to dry. The total solid content obtained after thermal conversion were reported as part of the material balance (see Table 5-2).

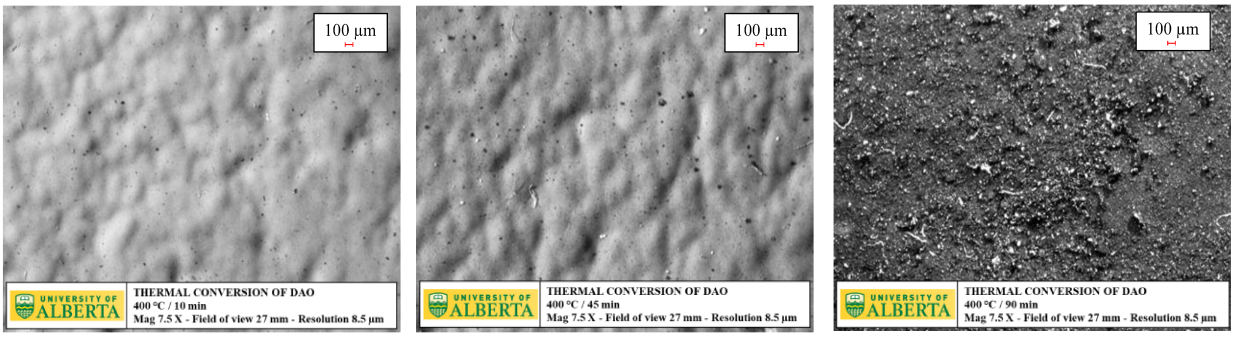

Figure 5-11. Images taken of 10 min, 45 min and 90 min reaction solids in StereoMicroscope V.20. Reaction conditions: 400 °C and 3 MPa (Mag 7.5x / Field of view 27 mm / Res 8.5 µm)

Some fine solids smaller than 100 microns were observed under the microscope during the first 45 min at 400 °C. Afterward, solids with approximate 200 microns were seen from the filtration of the thermal conversion product after 90 minutes of reaction time.

Moreover, some pictures were taken using a scanning electron microscope (SEM) with the purpose of obtaining additional information about the solids change along the reaction time.

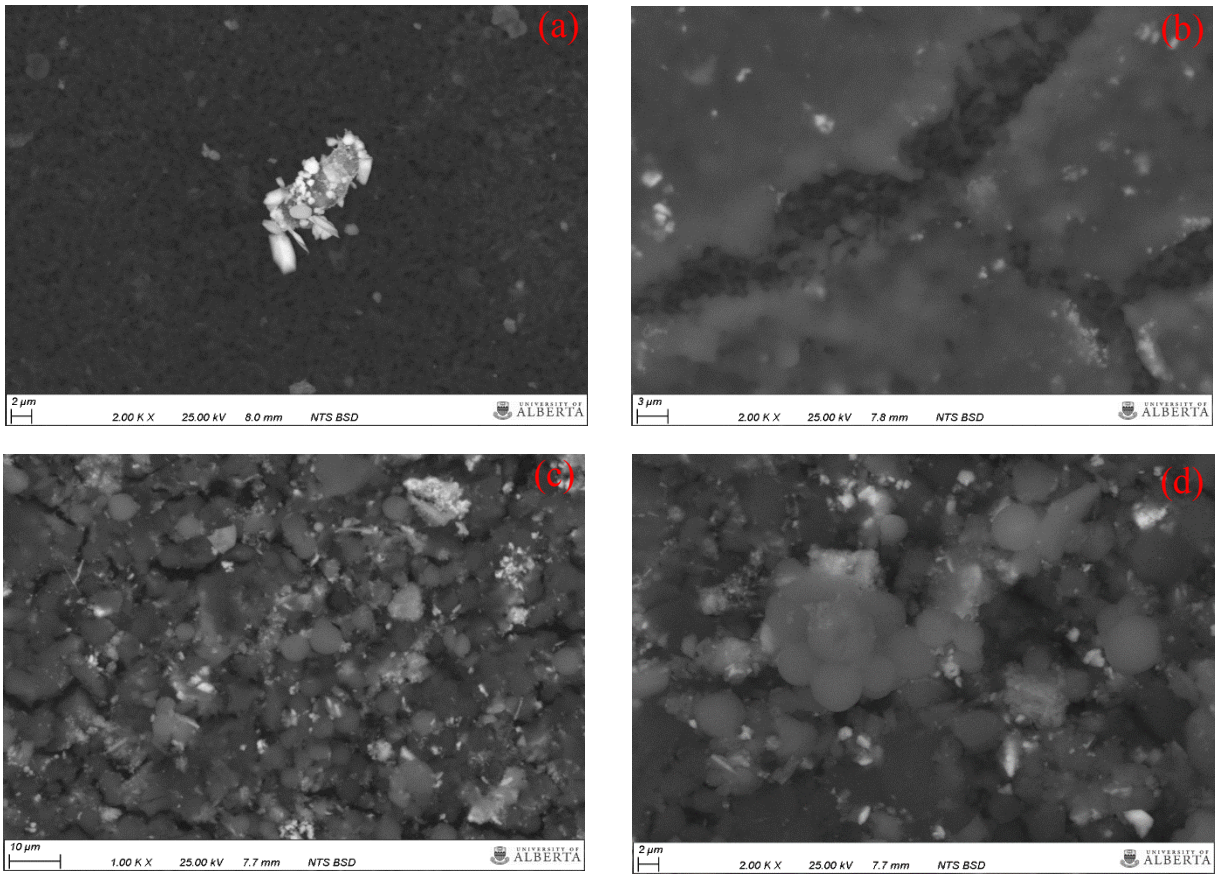

Figure 5-12. Images taken of 10 min (a), 45 min (b) and 90 min (c) (d) reaction solids in SEM. Reaction conditions: 400 °C and 3 MPa

Figure 5-12 shows the SEM images of the solid samples collected after reaction. As previously mentioned in the Chapter 3, dispersed fine solids with irregular shape smaller than 100 microns associated to mineral matter were observed under the microscope during the first 30 minutes of reaction time. In accordance with the results of X-ray dispersive analysis (EDX), it showed primarily the presence of C, O, Fe, S, Cl, and Al (see appendix B – figure B.14).

Moreover, SEM images of solids obtained after 45 minutes (Figure 5-12b) exhibits a change in the grain structure. The SEM-EDX spectra reported the predominantly presence of carbon, oxygen, sulfur, and iron (see Figure 5-14). The latter suggests that some particles are related to iron sulfide scale generated from the reaction between DAO and the reactor.

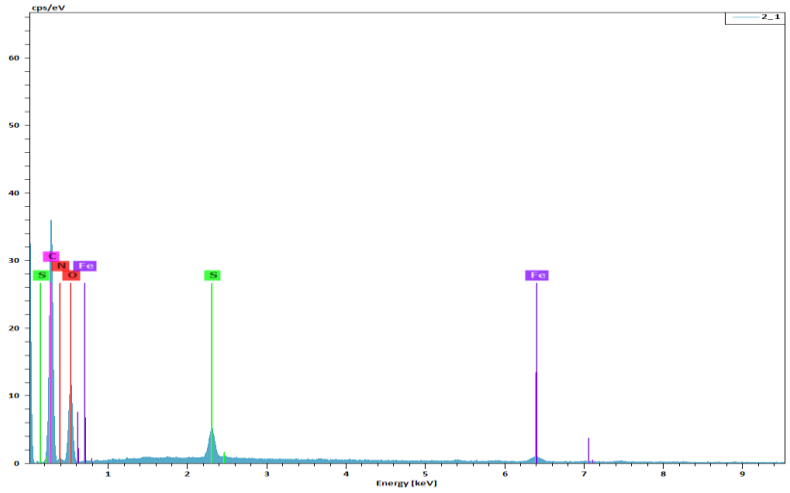

Figure 5-13. SEM-EDX spectra of solids obtained from thermal conversion of DAO under 400 °C after 45 minutes of reaction time

In the case of the solids obtained from thermal conversion after 90 minutes, the SEM images shows a more complex and denser structure with the presence of particles that exhibits greater opacity and brittle shape composed with smaller rounded particles tending toward spherical. Most of the particles are on the order of 5 µm in diameter. The SEM-EDX spectra showed the predominately presence of carbon, sulfur, iron, and chromium in this particles. The latter may be associated to vanadium instead which generates characteristic signal around 5 keV. This morphology is characteristic of the carbon-rich material (coke) obtained after thermal cracking at higher temperature [1] [9] [10].

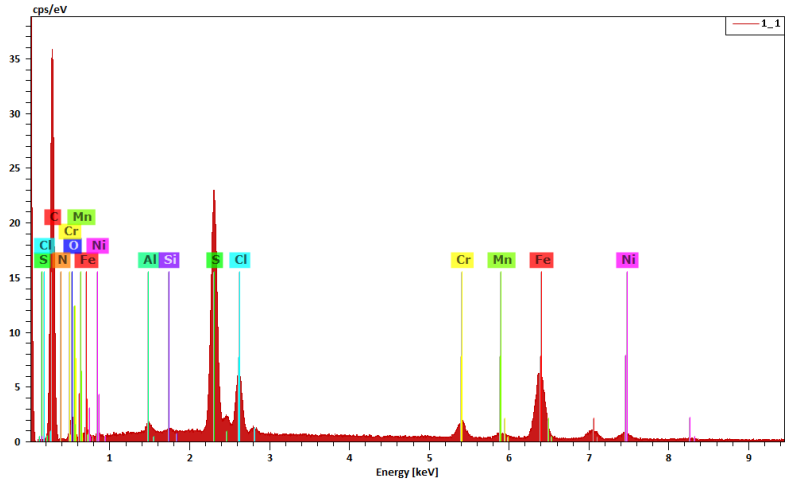

Figure 5-14. SEM-EDX spectra of solids obtained from thermal conversion of DAO under 400 °C after 90 minutes of reaction time

5.4 Discussion

5.4.1 Viscosity reduction and crackability of deasphalted oil at low temperature

The thermal cracking of vacuum residue derived from bitumen have shown the high reactivity of this fraction when it is exposed to temperature higher than 400 °C [1] [2] [11]. This high reactivity allows significant viscosity reduction of the product during a visbreaking process. However, the extent of viscosity reduction via thermal cracking is mainly governed by the degree of conversion to lighter material achieved [2]. Previous authors also suggest that the presence of asphaltenes in the feed limit the achievement of increased conversion in thermal cracking process owing to their instability during moderate severity condition [12][13]. Moreover, Cabrales-Navarro and Pereira-Almao shown that creation of new asphaltenes was significant during the thermal cracking of the deasphalted oil fraction at temperature between 380 - 423 °C [14].

In the case of thermal conversion at 400 °C, as the reaction time increases, a continually decrease in viscosity compared to the initial deasphalted oil was found until reaching 45 minutes of reaction. In Figure 5-15 shows that the kinematic viscosity of the products at 50 °C was reduced by three orders of magnitude compared with the value of DAO from 0 min to 45 min without increase in the solid content (coke formation), remaining slightly constant thereafter.

There also seems a relationship among the viscosity reduction trend, conversion of high-molecular weight components (Conversion = ($VR_{feed\ BP>524\ °C}$ - $VR_{product\ BP>524\ °C}$)/ ($VR_{feed\ BP>524\ °C}$) x 100) to lighter material, and the creation of new asphaltenes. Three evident trends for viscosity reduction were observed as a result of conversion, which are directly related to the severity of the reaction, as can be seen in Figure 5-15. A noticeable viscosity reduction was shown in the first 10 minutes of reaction associated to the breakage of the most reactive bonds in the DAO, followed by a more moderate viscosity reduction and conversion of high-molecular weight (around 45% conversion of material with B.P >524 °C) was reported after 45 minutes reaction time. During this time, the rate or slope associated to creation of new asphaltenes maintained lower than the slope related to the conversion of high-molecular weight into lighter material. Afterward, there was an additional decrease in the slope of conversion into lighter material due to as time reaction increase, more energy is required to break the less reactive bonds (with higher energies bond dissociation) that remains in the high molecular weight fraction. However, the slope associated to asphaltenes

content shown steady increase after 45 minutes, while the viscosity in the thermal conversion product remains fairly constant thereafter.

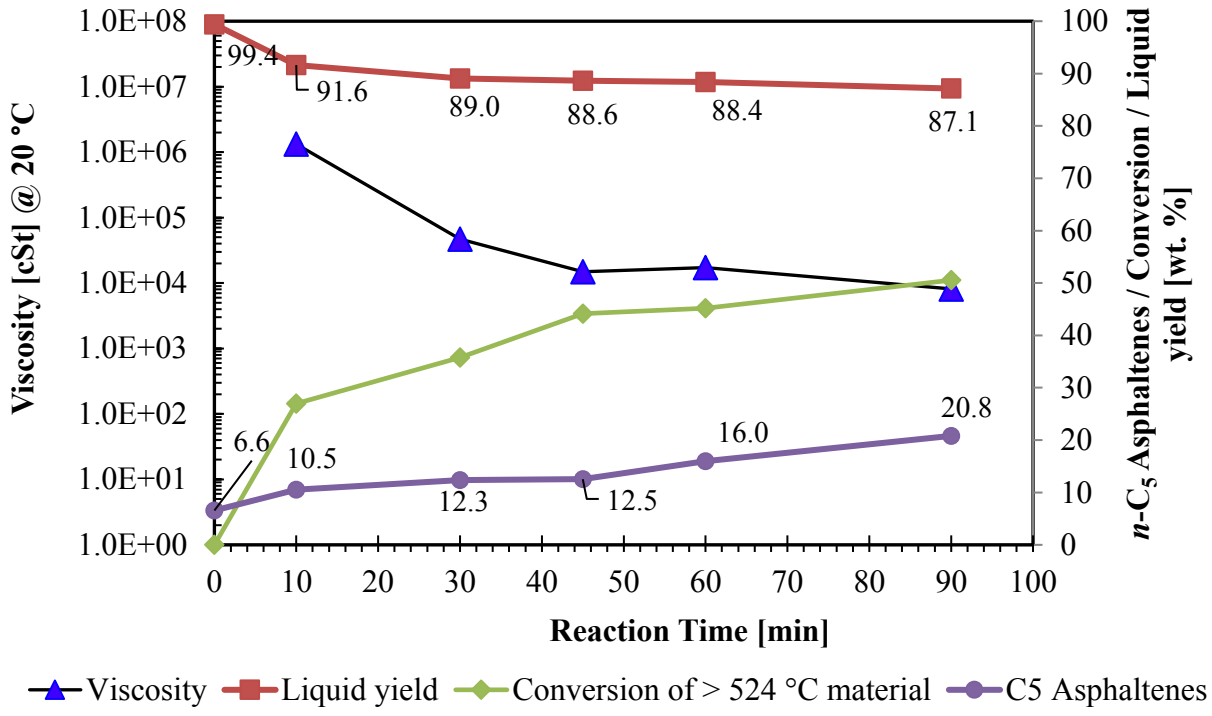

Figure 5-15. Viscosity reduction and crackability of DAO obtained under 400 °C, initial pressure of 3 MPa and reaction time varying between 10 and 90 minutes

5.4.2 Visbreaking kinetics

In the previous chapter 4, it was observed that thermal conversion of DAO at 360 °C resulted in a linear increase in cracking conversion with reaction time, suggesting that the cracking kinetics at 360 °C was zero order.

At 400 °C, the relationship between time and conversion (Figure 5-15) was less straightforward to interpret. The data approximated a first-order kinetic relationship better than zero order kinetic relationship. The high conversion within 10 min in relation to the increase in conversion at longer reaction times indicated that the description had to be of a non-zero kinetic order.

When combining the observations at 360 and 400 °C (Figures 16 and 24), it pointed to a rate expression with a zero order term and a non-zero order term. The non-zero order term became the dominant term as temperature increased from 360 to 400 °C. When extending the kinetic description of DAO visbreaking to lower temperatures, it would therefore require a different description for the rate expression than a simple first-order relationship.

5.4.3 Effects of hydrogen disproportionation

As it was observed in previous chapters, hydrogen disproportion changes the distribution of aliphatic hydrogen content. It is a favorable reaction during the thermal conversion of vacuum residue derived from bitumen as a result of the abundancy of weak C–H bonds in the hydro aromatics, alkyl side chains, and alkyl bridges that are common in this fraction.

In order to obtain more information about changes that occurred during the thermal conversion of deasphalted oil at 400 °C, the hydrogen distribution can be determined based on regions in the ^{1}H NMR spectra (see Figure 5-5a) defined in Chapter 3.

The Figure 5-16 illustrates the changes in the hydrogen distribution in the thermal conversion liquid product along the time.

It is observed that the content of primary (region between 0.4 and 1.1 ppm in the spectra) and secondary aliphatic hydrogen (region between 1.1 and 2 ppm in the ^{1}H NMR spectra) decreases by 5.3 % and 12.7 % relative to the feed after the first 45 minutes of reaction, the decrease being more pronounced during the first 10 minutes. On the other hand, the amount of benzylic aliphatic (α-methyl and α-methylene substitution, region between 2 and 4 ppm in the ^{1}H NMR spectra) and aromatic hydrogen (region between 6.5 and 9 ppm in the spectra) show an increase that it may be associated to an increase in the proportion due to primary and secondary aliphatic hydrogen reduction.

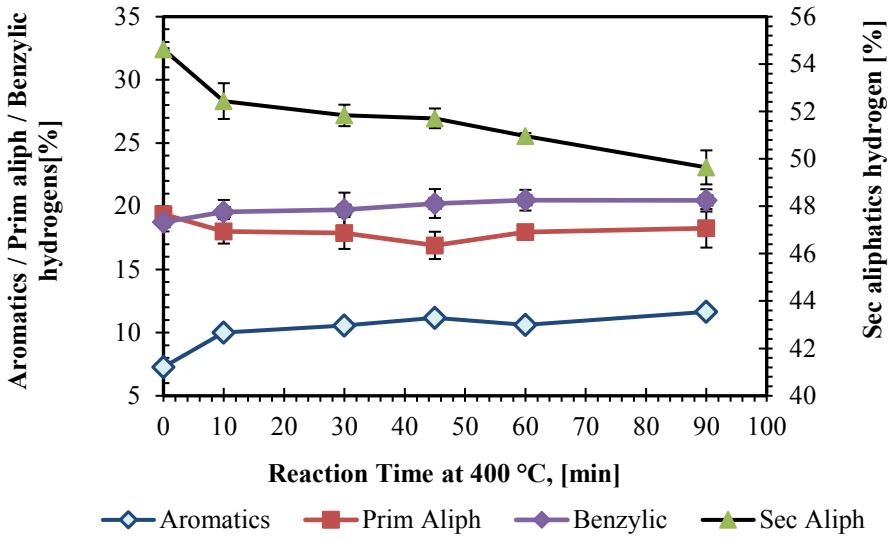

Figure 5-16. Area under the curve extracted from the NMR spectra, comparing the amount of the type of proton found in the thermal conversion liquid product after 400 °C reaction

This behavior is characteristic during the thermal conversion of vacuum residue derived from bitumen where dealkylation of side chains associated to aromatics and resins will result first due to their low bond dissociation energy (C_{ar} -C_{ali}, BDE: 89 kcal mol^{-1} [1]), giving high yield of gas and lower carbon molecules (naphtha). This could explain the decrease observed in the total aliphatic hydrogen content after 10 minutes of reaction time (see Figure 5-5b), which shows that hydrogen transfer or hydrogen disproportionation reactions is taking place along time. These observations were corroborated by 1) gas products analysis where there was a considerable loss of hydrogen from the product in the form of light hydrocarbons (C_1-C_5) generated since the first 10 minutes of reaction (gas yield; 7.8 wt. %), 2) The liquid boiling point distribution (Simdist) of the thermal conversion liquid products where an increase in the amount of light boiling point compounds was observed during the first 45 minutes of reaction.

After 45 minutes of reaction, an additional decrease in the secondary aliphatic hydrogen content is observed meanwhile the aromatic, primary, and benzylic hydrogen content increases along the reaction time until 90 minutes. This increase in the rest of the hydrogen content may be ascribed to an increase in the proportion due to secondary aliphatic hydrogen reduction.

This latter behavior in the reduction of secondary aliphatic hydrogen content along with the increase in the aromaticity of the liquid product after 45 minutes observed by the increase in the density and refractive index values suggest that dehydrogenation of naphthenic rings to aromatics (C-H $_{sec}$, BDE: 95 kcal mol^{-1}) is taking place. This may explain why there is not additional viscosity reduction with more time, as shown in Table 5-3.

Similar results using ^{1}H and ^{13}C NMR spectroscopy have been obtained by Kapoor et al [15] and Hauser et al [7] during the thermal cracking of different vacuum residues, suggesting that alkyl groups scission or dealkylation reaction is dominant at low conversion. Both studies reported a reduction in the alkyl substituent length, estimated as the ratio between the total aliphatic hydrogen and benzylic hydrogen content, with increasing reaction time. Based on before mentioned, the Figure 5-17 shows a decrease in the calculated alkyl substituent length (n) of thermal conversion products under 400 °C along the reaction time.

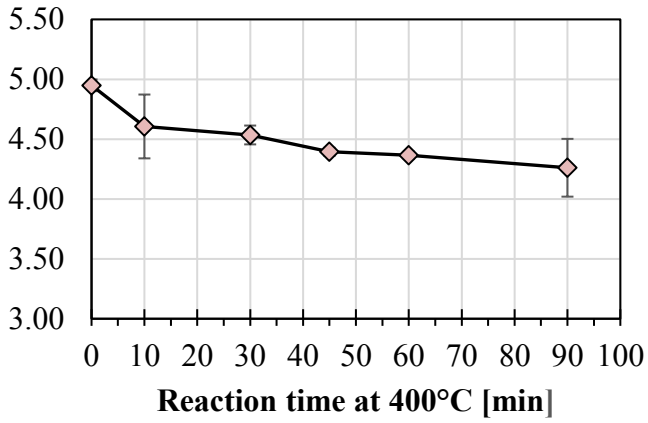

Figure 5-17. Calculated alkyl substituent length (n) of thermal conversion products under 400 °C, based on ^{1}H NMR average structural parameter

5.4.4 FT-IR Hints

FT-IR spectroscopy was employed in order to obtain more information about the changes that deasphalted vacuum residue experiences during milder conversion treatment.

As presented in previous chapters, in Figure 5-18 is shown the ratio of aromatics C=C bonds to aliphatic methylene bonds stretching intensity [measured as the ratio of 1600 cm^{-1}/ 2853 cm^{-1}

band] vs reaction time in order to track the aromaticity of the liquid product along the reaction time.

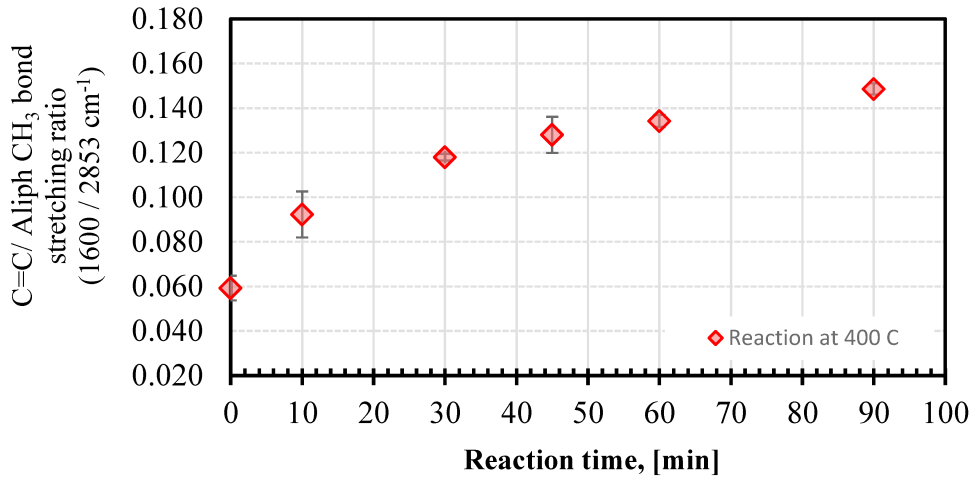

Figure 5-18. Ratio of aromatics C=C bonds to aliphatic methylene bonds stretching intensity of Thermal Conversion Products obtained under 400 °C, initial pressure of 3 MPa and different reaction times

In Figure 5-15, an increase in the aromatic: aliphatic methylene ratio and it is inferred that it is due to an increment in the aromatic content caused by addition reactions. This pattern correspond with others measured variables such as refractive index, ^{1}H NMR, and *n*-pentane insoluble content.

In addition, all samples shows a group of peaks in the 900-700 cm^{-1} region of the FT-IR spectra that are associated with out-of plane C-H and ring bending vibration of one isolated aromatic C-H bond (870 cm^{-1}), two or three adjacent aromatic C-H bonds (815 cm^{-1}) and four aromatic adjacent aromatic bonds (745 cm^{-1}) [5]. In Figure 5-19, it can be seen that there is an increase in the intensity of the peaks at 870 cm^{-1} and 815 cm^{-1} in all the thermal conversion products compared with the raw DAO, where a more significantly increase in the intensity of those peaks and the peak at 745 cm^{-1} is obtained after 90 minutes of reaction time. This also indicate an increase in the aromaticity of the products as well as suggest that addition reactions take place along the reaction time leading to the creation of new asphaltenes.

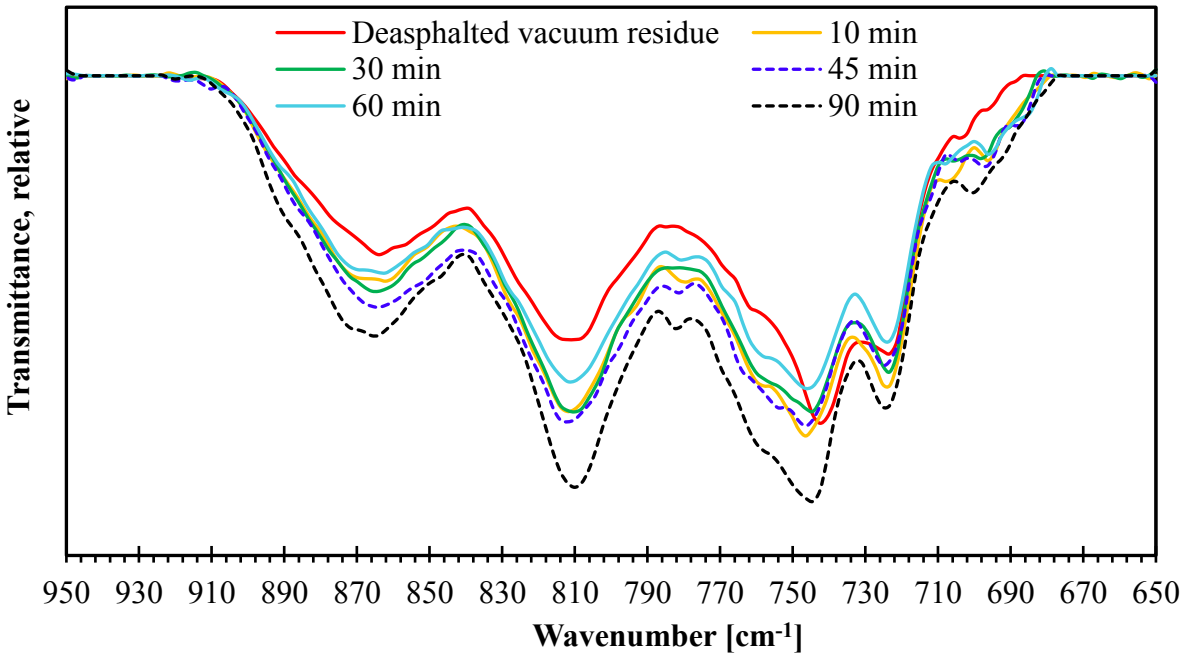

Figure 5-19. FTIR region 650-950 cm^{-1} spectra of thermal conversion products after 400 °C, initial pressure of 3 MPa and different reaction times

5.4.5 Asphaltene content – Electron Spin resonance relationship

As mentioned in the previous chapters, the existence of an absorption peak at about 720 cm^{-1} in the FTIR spectra (see Figure 5-19) provide indications that deasphalted oil contains polycyclic aromatic systems with alkyl side chains attached [11]. Furthermore, Kapoor et al. suggest that dealkylation of these polycyclic aromatics promotes addition reactions between aromatics and resins in the pentane soluble materials to create new asphaltenes [15].

On the other hand, the presence of some asphaltenes (6.6 ± 0.5 wt. % *n*-pentane insoluble material) as well as stable organic free radicals in the DAO was reported in Chapter 3. There was also suggested in this work that the asphaltenes content and the concentration of organic free radicals in the thermal conversion products show a relationship between each other. In the same order of idea, Yen et al [16] reported that the presence of organic free radicals are mainly associated to polycyclic aromatic systems in petroleum asphaltenes.

In the case of thermal conversion at 400 °C, important changes in microstructure in the deasphalted vacuum residue (DAO) are occurring along the reaction time, observing a relatively linear increase in the C_5 asphaltene content and the organic free radical concentration.

In agreement with the results in this work, Storm et al. also obtained a linear increase in the C_5 asphaltenes content along the reaction time after heated up during 60 minutes at 400 °C samples of heptane soluble deasphalted vacuum residue with a residual content of around 6 wt. % pentane insoluble material [17]. In addition, Wiehe suggests that this linear correlation (or zero order rate constant) disappear once significant coke begins to form (>3%) [13].

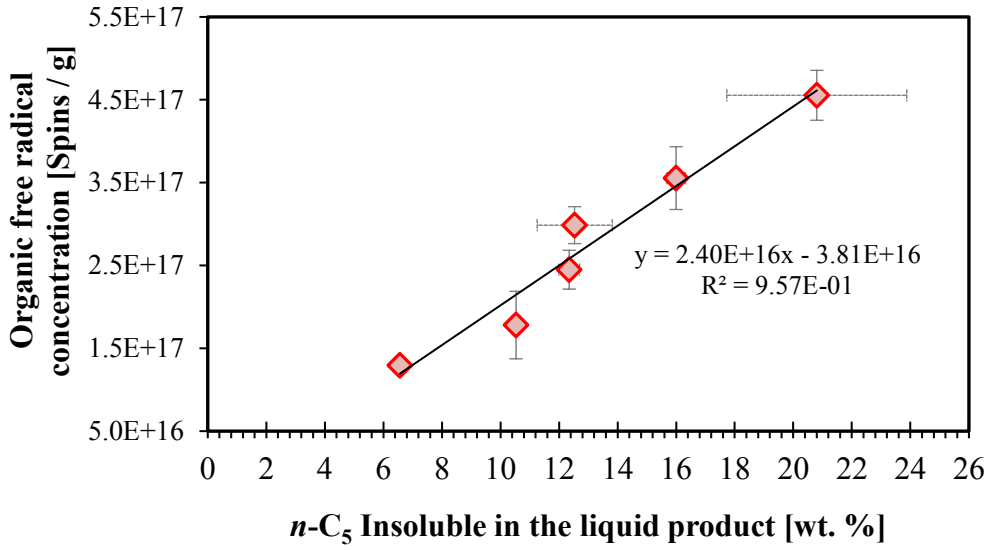

Figure 5-20. Pentane insoluble vs organic free radical concentration of thermal conversion products under 400 °C, initial pressure of 3 MPa

Additionally, Figure 5-20 is shown the relationship between the organic free radical concentration and *n*-pentane insoluble content in the liquid product obtained after thermal conversion at 400 °C. The data seems to correlate well (R^2 =0.957), suggesting a linear relationship between both variables.

Moreover, similar values of free radical concentration (approximately 1.7 x 10^{17} spins/g) corresponding to *n*-pentane insoluble content in the liquid product (circa 10 wt. %) were obtained in previous chapters.

The data indicate that the free radical sites are mainly associated with the aromatic rings of the asphaltenes fraction. Schultz and Selucky suggested that *n*-pentane precipitation of asphaltenes obtained from bitumen is the result of separation by number of spins per gram, where this value is not a simple relationship with the size of the species, but it seems that size determine whether a species is precipitated in the asphaltene fraction or remains in the resins [18].

Finally, as it was observed in previous chapters, the g-factor did not show any marked trend along the reaction time during the thermal conversion of DAO at 400 °C.

5.5 Conclusions

Through experimental investigations on thermal conversion of deasphalted oil at 400 °C, the following observations were made:

a) There is significant reduction in viscosity of the liquid product after thermal conversion of deasphalted vacuum residue at 400 °C, decreasing by three orders of magnitude compared with the value of DAO from 0 min to 45 min without increase in the solid content (coke formation). The viscosity reduction via thermal cracking was considerable during the first 10 minutes and became relatively slow at higher conversion, possible to prevalence of addition reactions at higher conversion. During this reaction time, a conversion of 45 % of material with B.P > 524 °C into lighter material was reached.

b) A significantly amount of gaseous products were obtained from the reaction in the first 10 minutes of reaction, this could suggest that there is considerable loss of hydrogen from the deasphalted vacuum residue in the form of light hydrocarbons (C_1-C_5), even at low conversion.

c) There is a predominance of dealkylation of side chains associated to polycondensed aromatics rings and dehydrogenation of naphthenic rings to aromatics during the thermal conversion of deasphalted vacuum residue based on gas yield, ^{1}H NMR, FTIR, density, and refractive index analysis in the product.

d) There is a relatively linear increase in the *n*-pentane insoluble content along reaction time, which suggest that addition reactions to create new asphaltenes following a zero order rate constant during the coke induction period.

e) A linear increase in the free radical concentration was also observed during the thermal conversion of DAO at 400 °C. This increase together with the increase in the *n*-pentane insoluble material could suggest that organic free radical sites are mainly associated with the aromatic rings of the asphaltenes fraction. There also appears to be a linear correlation between the *n*-pentane asphaltenes content and the concentration of unpaired electrons observed in the products.

References

[1] Gray, M. R. *Upgrading oilsands bitumen and heavy oil*; The University of Alberta Press: Edmonton, 2015.

[2] Di Carlo, S.; Janis, B. Composition and visbreakability of petroleum residues. *Chem. Eng. Sci.* **1992**, *47*, 2695-2700.

[3] Rahimi, P. M.; Gentzis, T. The chemistry of bitumen and heavy oil processing. In *Practical Advances in Petroleum Processing;* Hsu C.S.; Robinson P.R. Eds; Springer, New York, NY**,** **2006**; Volume 2, 597–634.

[4] Wang, L.; Zachariah, A.; Yang, S.; Prasad, V.; De Klerk, A. Visbreaking oilsands-derived bitumen in the temperature range of 340-400 °C. *Energy Fuels* **2014**, *28*, 5014-5022.

[5] Sharma, B. K.; Tyagi, O. S.; Aloopwan, M. K. S.; Bhagat, S. D. Spectroscopic characterization of solvent soluble fractions of petroleum vacuum residues. *Pet. Sci. Technol.* **2000**, *18*, 249-272.

[6] Yen, T. F.; Wu, W. H.; Chilingar, G. V. A study of the structure of petroleum asphaltenes and related substances by proton nuclear magnetic resonance. *Energy Sources*, **1984,** *7*(3), 275-304.

[7] Hauser, A.; AlHumaidan, F.; Al-Rabiah, H.; Halabi, M. A. Study on thermal cracking of Kuwaiti heavy oil (vacuum residue) and its SARA fractions by NMR spectroscopy. *Energy Fuels* **2014**, *28*(7), 4321-4332.

[8] ASTM D6560-12: *Standard test method for determination of asphaltenes in crude petroleum and petroleum products*; ASTM: West Conshohocken, PA, 2012.

[9] Millette, J. R.; Brown, R. S.; Kyle, J. P.; Turner Jr, W.; Hill, W.; Boltin, W. R. Distinguishing coal, coke and other black particles. *The microscope* **2009**, *57*(2), 51.

[10] Rahmani, S.; McCaffrey, W.; Elliott, J. A.; & Gray, M. R. Liquid-phase behavior during the cracking of asphaltenes. *Industrial & engineering chemistry research*, **2003**, *42*(17), 4101-4108.

[11] Speight, J. G. *The Chemistry and Technology of Petroleum*; CRC press: Boca Raton, 2014.

[12] Fainberg, V.; Podorozhansky, M.; Hetsroni, G.; Brauch, R.; Kalchouck, H. Changes in the composition and properties of the vacuum residues as a result of visbreaking. *Fuel Sci. Technol. Int.* **1996**, *14* (6), 839.

[13] Wiehe, I.A. *Process chemistry of petroleum macromolecules*. Baton Raton: CRC Press, 2008.

[14] Cabrales-Navarro, F. A.; Pereira-Almao, P. Reactivity and comprehensive kinetic modeling of deasphalted vacuum residue thermal cracking. *Energy & Fuels* **2017**, *31* (4), 4318–4332.

[15] Kapoor, M. P.; Kothiyal, V.; Singh, I. D. Compositional and structural studies of visbroken residues. *Fuel Sci. Technol. Int.* **1993**, *11*(7), 975-989.

[16] Yen, T. F.; Tynan, E. C.; Vaughan, G. B.; Boucher, L. J. Electron spin resonance studies of petroleum asphaltics. In *Spectrometry of Fuels;* Friedel R.A. *Eds;* Springer, Boston, MA, **1970**; 187–201.

[17] Storm, D. A.; Barresi, R. J.; Sheu, E. Y.; Bhattacharya, A. K.; De Rosa, T. F. Microphase behavior of asphaltic micelles during catalytic and thermal upgrading. *Energy Fuels* **1998**, *12*(1), 120-128.

[18] Schultz, K. F.; Selucky, M. L. ESR measurements on asphaltene and resin fractions from various separation methods. *Fuel* **1981**, *60*(10), 951-956.

6. THERMAL CONVERSION OF DEASPHALTED OIL AT 408 °C

6.1 Introduction

In this chapter, a set of reactions were performed at 408°C and 11.43 min, and the results are presented so that there will be a point of reference to account for difference in the reactor configuration and absence of steam during the micro-batch testing and the laboratory pilot testing. This will enable the present study to be integrated with the proprietary industrial investigations being conducted. Although this latter results are not discussed or compared in this chapter.

6.2 Experimental Section

6.2.1 Materials

Deasphalted vacuum residue oil from the Nexen Long Lake upgrader was utilized for the thermal conversion reactions, and it belongs to the same barrel as the heavy oil samples used on the previous Chapters. Nexen Long Lake deasphalted vacuum residue oil was characterized and the characterization is shown in Chapter 3, Table 3-1.

The source and purity of nitrogen, methylene chloride, *n*-pentane, and toluene were described in Chapter 3. These materials were also used in this Chapter's experiments.

6.2.2 Equipment and Procedure

The experiments in this chapter were carried out in a closed reactor system at an internal reactor temperature of 408 °C and 11.43 minutes. The results were reported as an average with one sample standard deviation.

6.2.3 Analysis

Analyses made in this chapter on the products as well as the description of the instruments and analysis procedures are the same used in the Chapter 3.

6.3 Results

6.3.1 Material Balance

The reaction products were obtained under these conditions: 408 °C, an initial pressure of 3 MPa N_2 and reaction time of 11.43 minutes. The mass of each phase was determined individually. The overall material balance (Table 6-1) and the product yields of each phase at 408 °C (Table 6-2) were calculated for experiments that were performed in triplicate.

Table 6-1. Mass balance for thermal conversion at 408 °C, and reaction time of 11.43 minutes

Balance Material [wt. %][a]		
Reaction temperature: 408 °C		
Reaction time [min]	**x**	**s**
11.43	98.97	1.64

[a] Average (x) and sample standard deviation (s) of number (n) of experiments are reported

In all experiments, the average material balance closed to within 3 %, i.e. material balance was between 97 and 103 %.

Table 6-2. Product yield (wt. %) for thermal conversion at 408 °C, and reaction time of 11.43 minutes

Material Balance [wt. %][a]						
Reaction temperature: 408 °C						
Time [min]	**Gas**		**Liquid**		**Solid**	
	x	**s**	**x**	**s**	**x**	**s**
11.43	8.68	1.08	90.72	1.25	0.42	0.03

[a] Average (x) and sample standard deviation (s) of three experiments are reported

As it was reported in the previous Chapters, a significantly amount of gaseous products were obtained from the reaction.

As the experiments made in previous chapters, filtration of liquid products took a long time before solids were obtained and this was found for all experiments. It is likely that the solids in the feed were very fine, which was later confirmed by microscopy.

6.3.2 Product characterization

Products were characterized and analyzed so that have a better idea about the changes that occurs during mild thermal treatment at 408 °C.

6.3.2.1 Viscosity

Viscosity measurements were performed at 5 different temperatures (7.5, 20, 40, 50 and 60 °C), but shear rate was kept constant at 20 s^{-1} for all the temperatures except 7.5 °C (shear rate 10 s^{-1}). These results are reported in Table 6-3 for set of reaction at 408 °C. The shear rate for this measurements were increased compared with previous chapters in order to work within the appropriate sensitivity range due to the low values of viscosity obtained at 408 °C

Table 6-3. Viscosity data to thermal conversion products under 408 °C and reaction time of 11.43 minutes

	Time reaction [min]	
	Raw DAO	**11.43**
	Viscosity [Pa.s]	
Measured Temperature: 60 [°C]		
Average	131.23	2.70
Std. dev.	3.81	0.99
Measured Temperature: 50 [°C]		
Average	600.00	10.43
Std. dev.	13.40	1.00
Measured Temperature: 40 [°C]		
Average	3718.50	31.87
Std. dev.	293.93	4.04
Measured Temperature: 20 [°C]		
Average	--[a]	513.31
Std. dev.	--	60.42
Measured Temperature: 7.5 [°C]		
Average	--[a]	5710
Std. dev.	--	1645

[a] Viscosity of the sample could not be determined (>10000 Pa.s)

After thermal cracking at 408 °C and reaction time of 11.43 min, the viscosity of the products at 40 °C dropped by three orders of magnitude compared with the value of the raw DAO.

6.3.2.2 Refractive index

The refractive index of every sample was determined at 5 different temperatures (20, 30, 40, 50 and 60 °C), and in the Table 6-4 is tabulated the refractive index at 408 °C and reaction time of 11.43 minutes.

Table 6-4. Refractive Index measurements performed on thermal conversion products after 408 °C, initial pressure 3 MPa reaction, and reaction time of 11.43 minutes

	Temperature [°C]	**Time reaction [min]**	
		Raw DAO	**11.43**
Average	20	1.5921	1.5958
Std. dev.		0.0001	0.0003
Average	30	1.5883	1.5918
Std. dev.		0.0001	0.0003
Average	40	1.5846	1.5878
Std. dev.		0.0001	0.0003
Average	50	1.5808	1.5838
Std. dev.		0.0001	0.0003
Average	60	1.5773	1.5799
Std. dev.		0.0001	0.0003

From the table, is shown that the refractive index of the liquid product increase after thermal conversion at 408 C and a reaction time of 11.43 minutes. This behavior is an indication of the liquid product is being more aromatic.

6.3.2.3 Liquid boiling point distribution (SimDist)

The liquid boiling point distribution after thermal conversion at 408 °C and a reaction time of 11.43 minutes was determined, and it is shown in Figure 6-1. The results of this analysis are shown in the following way: Temperature vs weight percent distilled.

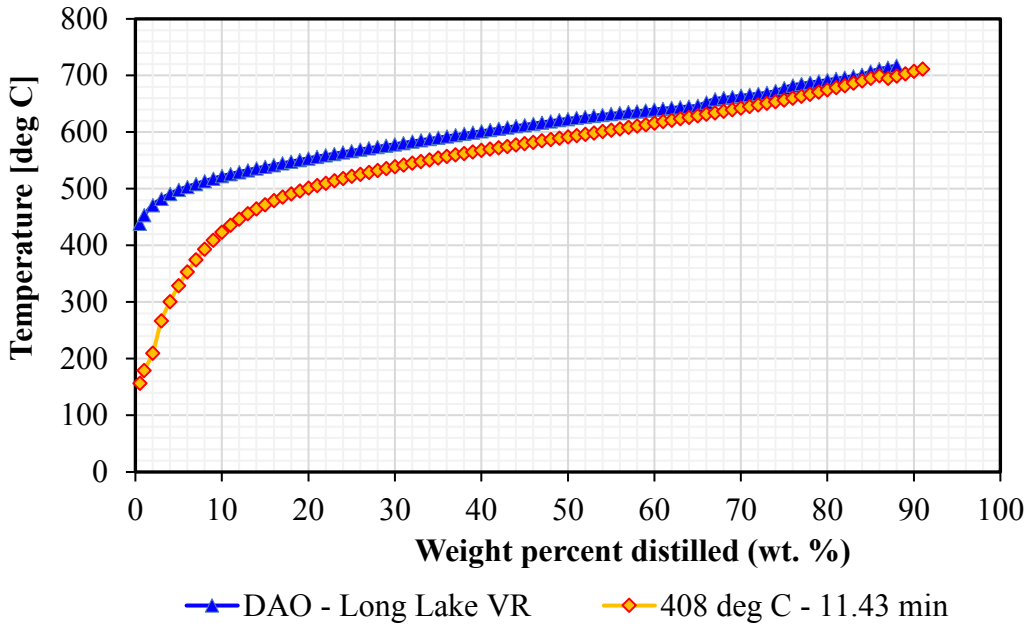

Figure 6-1. Liquid boiling point distribution of thermal conversion products after 408 °C, initial pressure of 3 MPa, and a reaction time of 11.43 minutes

In the case of reaction at 408 °C, there is a considerable increase in the amount of light boiling point compounds (BP < 524 °C), where the conversion of high-molecular weight components to lighter material was 24.10 ± 2.08 wt. % (conversion = ($VR_{feed\ BP>524\ °C}$ - $VR_{product\ BP>524\ °C}$) / ($VR_{feed\ BP>524\ °C}$) x 100 [1]). The weight average boiling point (WABP) in the liquid product decrease from 623 to 579 °C.

6.3.2.4 Proton nuclear magnetic resonance ^{1}H NMR

As in previous chapters, aliphatic and aromatic hydrogen content was obtained using proton NMR analysis so that observing how its proportions change under thermal conversion at 408 °C. In Figure 6-2, the NMR spectra of the feed and liquid products after thermal conversion of the DAO at 408 °C are presented in order to detect and track all the structural changes.

Some regions in the NMR data were identified and defined in the chapter 3 (section 3.3.2.5) in order to obtain hydrogen aliphatic content based on data presented by Sharma et al. [2], Yen et al.

[3], and Hauser et al. [4]. Mnova NMR software was used the determination of peak area based on the hydrogen ranges.

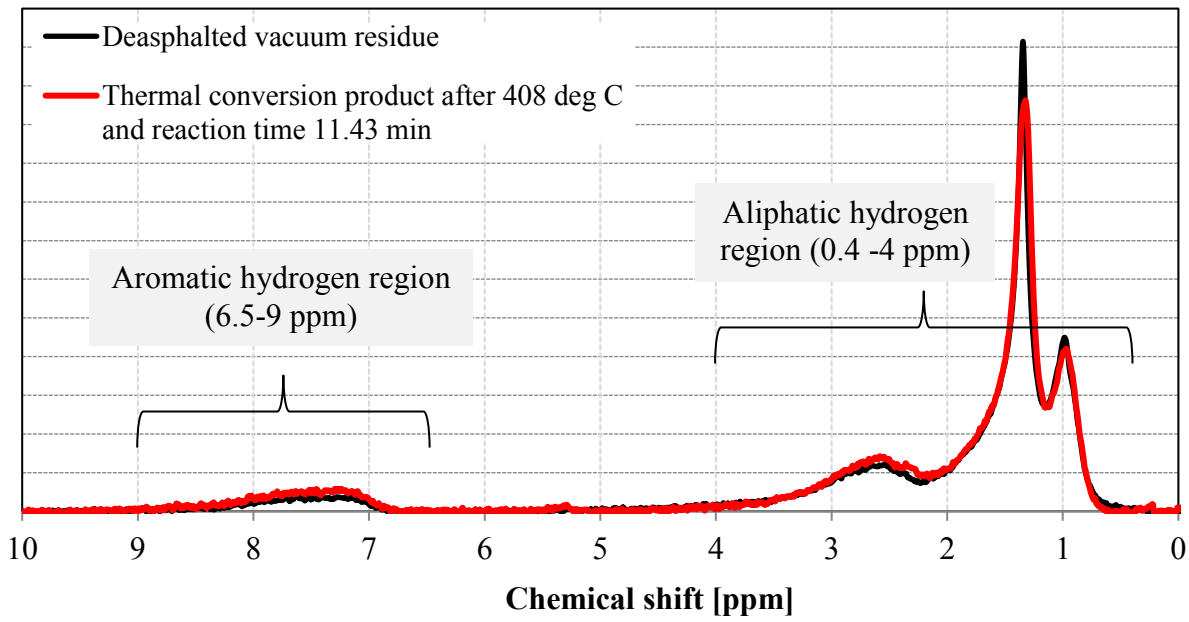

Figure 6-2. Proton NMR spectra of deasphalted vacuum residue oil and thermal conversion product after 408 °C, initial pressure of 3 MPa, and a reaction time of 11.43 minutes

In addition, the aliphatic hydrogen content of liquid products after thermal conversion at 408 °C is reported in Table 6-5.

Table 6-5. Aliphatic hydrogen content of liquid product determined by ^{1}H NMR analysis after thermal conversion of DAO at 408 °C, and a reaction time of 11.43 minutes

	Time reaction [min]	
	Raw DAO	**11.43**
	Aliphatic hydrogen content [%]	
Average	92.72	90.26
Std. dev.	0.05	0.23

At 408 °C, the aliphatic hydrogen content decrease approximately 2.7 % compared with the value of the raw DAO.

6.3.2.5 Pentane insoluble (Asphaltene content)

The *n*-pentane precipitated asphaltenes content in the thermal conversion product was obtained ASTM D6560-12 [5], it is reported in Table 6-6. From the table, it was observed that there was an increase in *n*-pentane insoluble asphaltenes content at the thermal conversion conditions, showing that new asphaltenes were created.

Table 6-6. Pentane insoluble content in wt. % of liquid product analysis after thermal conversion of DAO at 408 °C, and a reaction time of 11.43 minutes

	Time reaction [min]	
	0	**11.43**
	***n*-Pentane insoluble [wt. %]**	
Average	6.56	11.37
Std. dev.	0.15	0.62

6.3.2.6 FT-IR spectroscopy

In Figure 6-3, the spectra of the DAO and liquid product after thermal conversion at 408 °C were plotted.

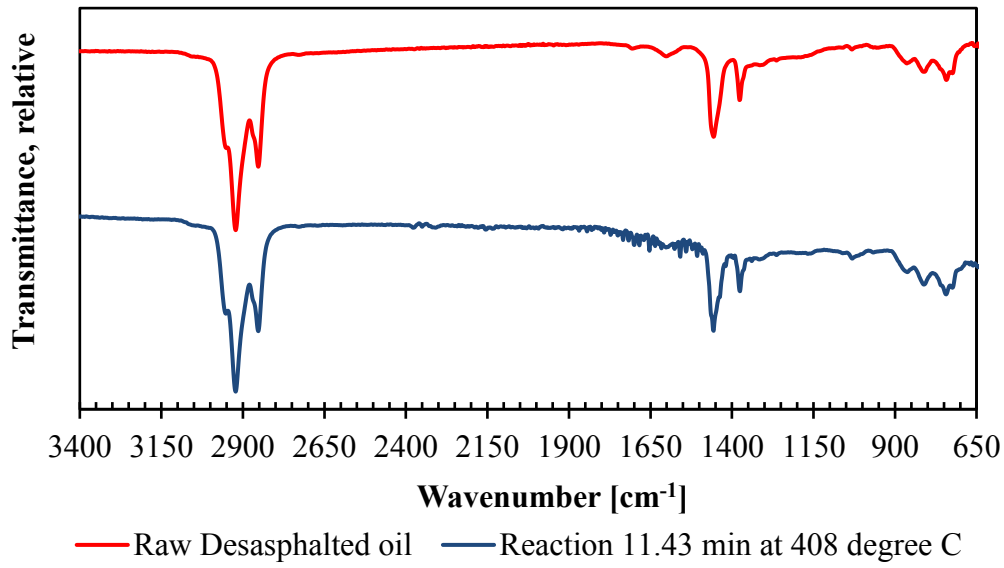

Figure 6-3. FTIR spectra of liquid product analysis after thermal conversion of DAO at 408 °C, and a reaction time of 11.43 minutes

6.3.2.7 Electron spin resonance (ESR)

The ESR spectra of the DAO and reaction product were recorded as first derivative curves, and they are shown in Figure 6-4.

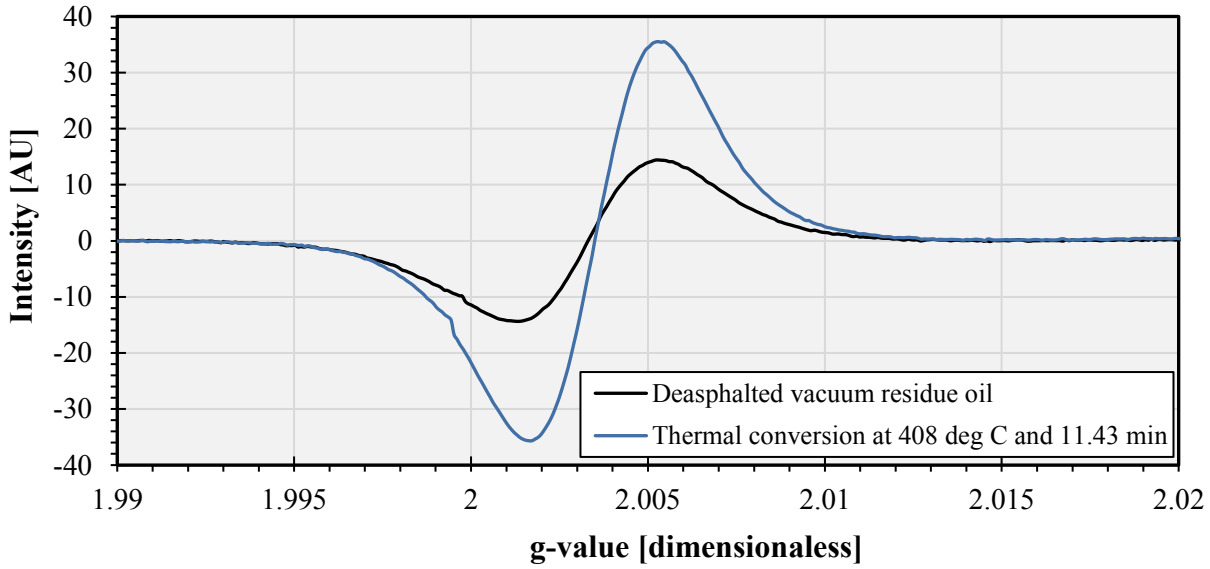

Figure 6-4. ESR spectra of DAO and liquid product after thermal conversion of DAO at 408 °C, and a reaction time of 11.43 minutes

As previous chapters, the samples were diluted at 30 wt.% in toluene and the organic free radicals concentration were obtained by comparison of the double integrated intensity against the calibration curve built using 4-hydroxy TEMPO (see Figure 3-3 in chapter 3). The number of unpaired spins per gram and g-factor (a measure of the center of free radical absorption) of liquid product analysis after thermal conversion of DAO at 408 °C, and a reaction time of 11.43 minutes were calculated, it is presented in Table 6-7.

Table 6-7. ESR Parameters of liquid product analysis after thermal conversion of DAO at 408 °C, and a reaction time of 11.43 minutes

Time [min]	Double integrated intensity Area		Calculated organic free radical concentration [spins/g]		g-factor	
	x	s	x	s	x	s
0	14269	833	1.30×10^{17}	8.10×10^{15}	2.0032	0.0002
11.43	25070	1871	2.34×10^{17}	1.82×10^{16}	2.0032	0.0004

6.3.2.8 Density

Density measurements of the liquid products and deasphalted vacuum residue oil were determined at two different temperatures at 20 and 40 °C, respectively. Samples must be heated up before being injected in the pycnometer. Density data is reported in Table 5-8.

Table 6-8. Density measurements performed at two different temperatures: 20 and 40 °C to thermal conversion product after reaction at 408 °C, and a reaction time of 11.43 minutes

	Temperature [°C]	**Time reaction [min]**	
		Raw DAO	**11.43**
		Density [kg/m^3]	
Average	20	1057.3	1036.4
Std. dev.		3.6	3.0
Average	40	1049.8	1021.4
Std. dev.		4.7	2.9

At 408 °C, there is a decrease in the density of the product after thermal conversion of DAO at 408°C, showing that some compounds with lighter molecular weight are generated from the thermal conversion reaction.

6.3.2.9 Gas Chromatography

Gas products generated from the thermal conversion reactions were collected in a gas bag and injected in the gas chromatograph to be analyzed. The gaseous product analyses are shown in Table 6-9 for thermal conversion reaction at 408 °C, which presents the mole concentration obtained for every compound between C_1 to C_6 in the sample.

Table 6-9. Gas products associated to thermal conversion of deasphalted vacuum residue oil after reaction at 408 °C, and a reaction time of 11.43 minutes

Reaction time at 408 °C; Gas product chromatography		
Compounds	**Reaction time** 11.43 min	
	Average	Std. dev.
[mole %]		
Methane	17.85	1.49
Ethylene	0.36	0.31
Ethane	12.70	0.59
Propylene	3.13	0.74
Propane	14.56	0.27
Iso-Butane	3.11	0.69
n-Butane	2.79	1.20
Cis-2 Butane	8.62	0.54
Iso-pentane	3.52	0.37
n-pentane	4.95	0.74
Iso-Hexane	0.98	0.17
N-Hexane	1.30	1.11
H_2S	0.75	0.11
CO_2	0.07	0.02
N_2	25.24	1.58
Total	**100.00**	

6.3.2.10 Solid content

In Figure 6-5, is exhibited images of the solids recovered from vacuum filtering step after thermal treatment of DAO at 400 °C. A milipore filter paper of 0.22 um was employed and samples were left inside the fumehood for 2 days to dry. The total solid content obtained after thermal conversion were reported as part of the material balance (see Table 6-2).

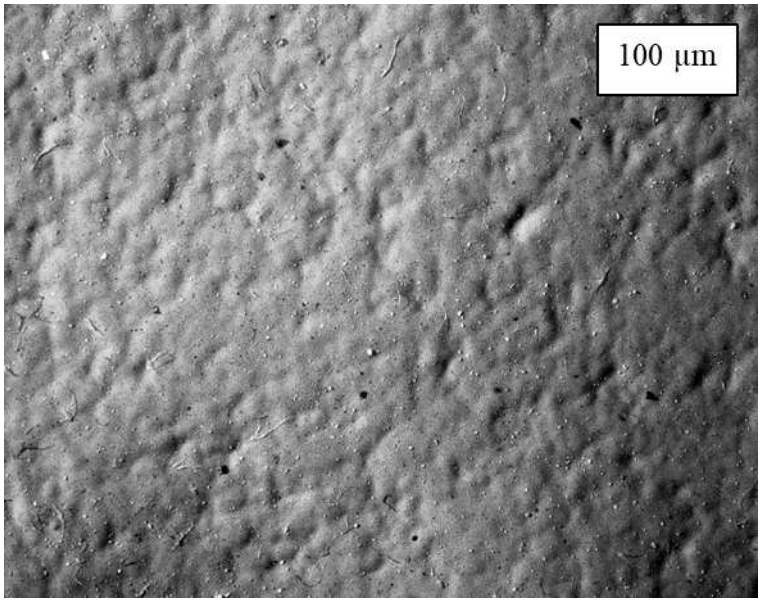

Figure 6-5. Images taken of 11.43 min reaction solids in StereoMicroscope V.20. Reaction conditions: 408 °C and 3 MPa (Mag 7.5x / Field of view 27 mm / Res 8.5 µm)

Some fine solids smaller than 100 microns were observed under the microscope after thermal treatment at 408 °C. As mentioned in previous Chapters, this dispersed fine solids with irregular shape smaller than 100 microns may be associated to mineral matter based on the SEM analysis.

References

[1] Gray, M. R. *Upgrading oilsands bitumen and heavy oil*; The University of Alberta Press: Edmonton, 2015.

[2] Sharma, B. K.; Tyagi, O. S.; Aloopwan, M. K. S.; Bhagat, S. D. Spectroscopic characterization of solvent soluble fractions of petroleum vacuum residues. *Pet. Sci. Technol.* **2000**, 18, 249-272.

[3] Yen, T. F.; Wu, W. H.; Chilingar, G. V. A study of the structure of petroleum asphaltenes and related substances by proton nuclear magnetic resonance. *Energy Sources*, **1984,** 7(3), 275-304.

[4] Hauser, A.; AlHumaidan, F.; Al-Rabiah, H.; Halabi, M. A. Study on thermal cracking of Kuwaiti heavy oil (vacuum residue) and its SARA fractions by NMR spectroscopy. *Energy Fuels* **2014**, 28(7), 4321-4332.

[5] ASTM D6560-12: *Standard test method for Determination of Asphaltenes in Crude Petroleum and Petroleum Products*; ASTM: West Conshohocken, PA, 2012.

7. CONCLUSIONS

Vacuum residue deasphalted oil derived from Athabasca bitumen was thermally converted at 280, 320, 360 and 400 °C. For the purpose of partial upgrading, only reaction at 360 and 400 °C resulted in substantial cracking conversion and viscosity reduction to facilitate pipeline transport.

7.1 MAJOR CONCLUSIONS

a) Thermal conversion reactions were performed in order to evaluate the deasphalted vacuum residue viscosity reduction at low temperature. Based on the results obtained in this work, the range of temperature used shows interesting changes in the microstructure of deasphalted oil during the thermal conversion. Although there was not significant change in viscosity at thermal conversion reactions at 280 °C, an increase in the asphaltene content was observed. This suggest that bitumen and their asphaltenes are not completely unreactive and detrimental reactions can occurs at the temperatures that will be experienced along the process pathway (between 200-250 °C) leading from steam assisted gravity drainage (SAGD) through solvent deasphalting.

b) At 320 °C, a decrease in viscosity by about half order of magnitude compare with raw DAO was observed, although there was not remarkable change in the amount of material in the liquid product with boiling point below 524 °C (< 6 wt. %). Thus, it is likely that most of this decrease in viscosity can be attributed to deaggregation and molecular rearrangement.

c) The presence of free radicals in the deasphalted vacuum residue was confirmed by electron spin resonance (ESR) spectrometry, showing also that those species are not completely unreactive at low temperature.

d) A significantly amount of gaseous products were obtained from the thermal conversion reactions above 320 °C, this could suggest that there is considerable loss of hydrogen from the deasphalted vacuum residue in the form of light hydrocarbons (C_1-C_5), even at low conversion.

e) There is significant reduction in viscosity of the liquid product after thermal conversion at 360 °C, decreasing by two to three orders of magnitude compared with the value of DAO without increase in the solid content (coke formation).

f) Vacuum residue conversion at 360 °C increased linearly with time, which indicated zero order kinetics. Vacuum residue conversion at 400 °C was non-zero order. This study showed that thermal cracking at 360–400 °C is better described by a rate equation with two terms, and the equivalent residence time (ERT) description of visbreaking was an inadequate approximation of thermal conversion at 400 °C and below.

g) At 400 °C, a more significant changes occurred during the thermal conversion of DAO, corroborating the literature findings about this topic. The viscosity of the liquid product after thermal conversion at 400 °C decreased about three orders of magnitude compared with the value of DAO after 45 min without increase in the solid content

h) A linear increase in the organic free radical concentration was observed during the thermal conversion of DAO at 400 °C. This increase together with the increase in the *n*-pentane insoluble material could suggest that organic free radical sites are mainly associated with the aromatic rings of the asphaltenes fraction. There also appears to be a linear correlation between the *n*-pentane asphaltenes content and the concentration of unpaired electrons observed in the products.

7.2 FUTURE WORK

This work provided interesting results. However, there are some points that could be studied in more detail.

a) Visbreaking in a narrow reaction time range close to onset coking should be studied. Previous studies carried out in the group, as well as in this work showed an increase in the viscosity before the onset of coking. This viscosity response of heavy oil during thermal conversion could be useful for the understanding of bitumen behavior and their fractions.

b) Visbreaking reactions after remove the residual C_5 asphaltenes content in the DAO should be studied. This could provide the opportunity to measure of organic free radicals concentration present in the maltenes fraction, and determine if the relationship between asphaltene content and free radical concentration is maintained along the thermal cracking.

Bibliography

ASTM D70-09: *Standard test method for density of semi-solid bituminous materials (Pycnometer Method)*; ASTM: West Conshohocken, PA, 2009.

ASTM D7169 – 11: *Standard test method for boiling point distribution of samples with residues such as crude oils and atmospheric and vacuum residues by high temperature gas chromatography*; ASTM: West Conshohocken, PA, 2012.

ASTM D6560-12: *Standard test method for determination of asphaltenes in crude petroleum and petroleum products*; ASTM: West Conshohocken, PA, 2012.

Adams, J.; Altgelt. K.; LeTourneau, L.; Lindeman, P. Free radical concentration in gel permeation fractions of asphaltenes from different crude oils. *Am. Chem. Soc. Div. Petrol. Chem. Preprints* **1966**, *11*, B-140.

Akbar, M.; Geelen, H. Visbreaking uses soaker drum. *Hydrocarbon Processing.* **1981**, *60* (5), 81-85.

Ancheyta, J. *Modeling of processes and reactors for upgrading of heavy petroleum;* CRC Press: Boca Raton, 2013.

Argillier, J.-F.; Coustet, C.; Henaut, I. Heavy oil rheology as a function of asphaltene and resin content and temperature. *Proceedings of SPE International Thermal Operations and Heavy Oil Symposium and International Horizontal Well Technology Conference* **2002**.

Avid, B.; Sato, S.; Takanohashi, T.; Saito, I. Effect of *n*-pentane and *n*-heptane insolubles on the pyrolysis of vacuum residue. *Energy & Fuels* **2006**, *20* (6), 2475–2477.

Banerjee, D. K. *Oil Sands, Heavy oil, & bitumen: from recovery to refinery*; PennWell Corp.: Tulsa, Oklahoma, 2012.

Bauquis, P. R. A Reappraisal of energy supply and demand in 2050. *Oil & Gas Science and Technology* **2001**, *56* (4), 389–402.

Bianco, A. D.; Panariti, N.; Anelli, M.; Beltrame, P.; Carniti, P. Thermal cracking of petroleum residues. *Fuel* **1993**, *72* (1), 75–80

Brauch, R.; Fainberg, V.; Kalchouck, H.; Hetsroni, G. Correlations between properties of various feedstocks and products of visbreaking. *Fuel Sci. Technol. Int.* **1996**, *14*(6), 753-765.

Brons, G.; Yu, J. M. Solvent deasphalting effects on whole Cold Lake bitumen. *Energy Fuels* 1995, *9* (4), 641–647.

Cabrales-Navarro, F. A.; Pereira-Almao, P. Reactivity and comprehensive kinetic modeling of deasphalted vacuum residue thermal cracking. *Energy Fuels* **2017**, *31*(4), 4318-4332.

Canadian Association of Petroleum Producers. 2017 CAPP Crude oil forecast, markets & transportation [Online access]. Publication # 2017-0009. http://www.capp.ca/ publications-and-statistics/publications/303440.

Canadian Energy Research Institute (CERI). Canadian economic impacts of new and existing oil sands development in Alberta, 2014, Calgary, Alberta, Canada.

Castaneda, L.; Munoz, J.; Ancheyta, J. Current situation of emerging technologies for upgrading of heavy oils. *Catal. Today* **2014**, 220-222, 248-273.

Chilingarian, G. V. *Bitumens, asphalts, and tar sands, Volume 7;* Ed.; Elsevier, 2011.

Dehkissia, S.; Larachi, F.; Rodrigue, D.; Chornet, E. Characterization of Doba–Chad heavy crude oil in relation with the feasibility of pipeline transportation. *Fuel* **2004**, *83*(16), 2157-2168.

De Klerk, A.; Reques, N. G. Z.; Xia, Y.; Omer, A. A. (Nexen Energy ULC). Integrated central processing facility (CPF) in oil field upgrading (OFU). U.S. Patent 2014/0138287, May 22, 2014.

Di Carlo, S.; Janis, B. Composition and visbreakability of petroleum residues. *Chem. Eng. Sci.* **1992**, *47*, 2695-2700.

Elofson, R. M.; Schulz, K. F.; Hitchon, B. Geochemical significance of chemical composition and ESR properties of asphaltenes in crude oils from Alberta, Canada. *Geochim. Cosmochim. Acta* **1977**, *41*(5), 567-580.

Eshraghian, A.; Husein, M. M. Thermal cracking of Athabasca VR and bitumen and their maltene fraction in a closed reactor system. *Fuel* **2017**, *190*, 396–408.

Fainberg, V.; Podorozhansky, M.; Hetsroni, G.; Brauch, R.; Kalchouck, H. Changes in the composition and properties of the vacuum residues as a result of visbreaking. *Fuel Sci. Technol. Int.* **1996**, *14* (6), 839.

Gary, J. H.; Handwerk, G. E. *Petroleum refining: technology and economics*, 5th Edition; CRC Press: Boca Raton, 2007.

Guedes, C. L. B.; Di Mauro, E.; Mangrich, A. S.; Ramoni, M.; Antunes, V. Study of the photodegradation of oil by electronic paramagnetic resonance. *Cienc.-Tec.-Pet., Sec. Quim.* **2001**, *3*, 145-154.

Gray, M. R. *Upgrading oilsands bitumen and heavy oil*; The University of Alberta Press: Edmonton, 2015.

Hardinger, S. Infrared Spectroscopy. http://www.chem.ucla.edu/harding/notes/notes_14C_IR.pdf (accessed Dec 15, 2017).

Hauser, A.; AlHumaidan, F.; Al-Rabiah, H.; Halabi, M. A. Study on thermal cracking of Kuwaiti heavy oil (vacuum residue) and its SARA fractions by NMR spectroscopy. *Energy Fuels* **2014**, *28* (7), 4321-4332.

Huc, A. Y. *Heavy crude oils, from geology to upgrading: an overview*; Editions Technip: Paris, 2011.

Humphrey, B. J. *Electron paramagnetic resonance on asphaltic materials (No. NMERI-WA5-10-(SS-5.01))*; rep.; New Mexico Engineering Research Institute: New Mexico, 1987.

Japanwala, M. S. Quality of distillates from coking of recycled residue. MSc Thesis, University of Alberta, Edmonton, AB, Canada, 2011.

Joshi, J. B.; Pandit, A. B.; Kataria, K. L.; Kulkarni, R. P.; Sawarkar, A. N.; Tandon, D.; Ram, Y.; Kumar, M. M. Petroleum residue upgrading via visbreaking: A review. *Ind. Eng. Chem. Res.* **2008**, *47*, 8960-8988.

Karlsson, R.; Isacsson, U. Application of FTIR-ATR to Characterization of bitumen rejuvenator diffusion. *J. Mater. Civ. Eng.* **2003**, *15*(2), 157-165.

Kariznovi, M.; Nourozieh, H.; Abedi, J. Measurement and correlation of viscosity and density for compressed Athabasca Bitumen at temperatures up to 200ºC. *Journal of Canadian Petroleum Technology* **2014**, *53* (06), 330–338.

Kissin, Y. V. Free-radical reactions of high molecular weight isoalkanes. Ind. *Eng. Chem*. Res. **1987**, *26*, (8), 1633–1638.

Kapoor, M. P.; Kothiyal, V.; Singh, I. D. Compositional and structural studies of visbroken residues. *Fuel Sci. Technol. Int.* **1993**, *11*(7), 975-989.

Kotlyar, L. S.; Sparks, B. D.; Kodama, H.; Grattan-Bellew, P. E. Isolation and characterization of organic-rich solids present in Utah oil sand. *Energy & Fuels* **1988**, *2* (4), 589–593.

Khulbe, K.; Mann, R.; Lamarche, G.; Lamarche, A. Electron spin resonance study of the thermal decomposition of solvent extracted Athabasca tar sand bitumen. *Fuel Processing Technology* **1992**, *31* (2), 91–103

Liang, W.; Que, G.; Chen, Y.; Liu, C. Chapter 10. Chemical composition and characteristics of residues of Chinese crude oils. *Developments in Petroleum Science Asphaltenes and Asphalts, 2* **2000**, 281–304

Mujica, V.; Nieto, P.; Puerta, L.; Acevedo, S. Caging of molecules by asphaltenes. A model for free radical preservation in crude oils. *Energy Fuels* **2000**, *14*(3), 632-639.

Millette, J. R.; Brown, R. S.; Kyle, J. P.; Turner Jr, W.; Hill, W.; Boltin, W. R. Distinguishing coal, coke and other Black Particles. *The microscope* **2009**, *57*(2), 51.

Parsons, A. F. *An introduction to free radical chemistry*; Wiley-Blackwell: United Kingdom, 2000, p. 16.

Piccinato, M. T.; Guedes, C. L. B.; Di Mauro, E. Crude oil by EPR. *In crude oil emulsions-composition stability and characterization*; InTech: Brazil, 2012.

Rahimi, P. M.; Gentzis, T. The chemistry of bitumen and heavy oil processing. In *Practical Advances in Petroleum Processing;* Hsu C.S.; Robinson P.R. Eds; Springer, New York, NY**,** **2006**; Volume 2, 597–634

Rahimi, P. M.; Teclemariam, A.; Taylor, E.; Debruijn, T.; Wiehe, I. A. Thermal processing limits of Athabasca bitumen during visbreaking using solubility parameters. *ACS Symposium Series Heavy Hydrocarbon Resources* **2005**, *895*, 183–196

Rahmani, S.; McCaffrey, W.; Elliott, J. A.; & Gray, M. R. Liquid-phase behavior during the cracking of asphaltenes. *Industrial & Engineering Chemistry Research*, **2003**, *42*(17), 4101-4108.

Sharma, B. K.; Tyagi, O. S.; Aloopwan, M. K. S.; & Bhagat, S. D. Spectroscopic characterization of solvent soluble fractions of petroleum vacuum residues. *Petroleum science and technology*, **2000**, *18*(3-4), 249-272.

Scotti, R.; Montanari, L. Molecular structure and intermolecular interaction of asphaltenes by FT-IR, NMR, EPR. In *Structures and Dynamics of Asphaltenes*; Mullins, O. C., Sheu, E.Y. Eds.; Springer: Boston, 1998.

Silverstein, R. M.; Webster, F. X.; Kiemle, D. J.; Bryce, D. L. *Spectrometric identification of organic compounds*; John Wiley & Sons: New York, 2014**.**

Strausz, O. P.; Lown, E. M. *The chemistry of Alberta oil sands, bitumens and heavy Oils*; Alberta Energy Research Institute: Calgary, **2003**.

Silverstein, R. M.; Webster, F. X.; Kiemle, D. J.; Bryce, D. L. *Spectrometric identification of organic compounds*; John Wiley & Sons: New York, 2014**.**

Schultz, K. F.; Selucky, M. L. ESR measurements on asphaltene and resin fractions from various separation methods. *Fuel* **1981**, *60*(10), 951-956.

Speight, J.G. *The chemistry and technology of petroleum*, 4th Edition; Taylor & Francis Group: Boca Raton, FL, 2007.

Speight, J. G. Visbreaking: A technology of the past and the future. *Sci. Iran.* **2012**, *19*(3), 569-573.

Speight, J. G.; Ozum, B. *Petroleum Refining Processes*; Marcel Dekker, Inc.: New York, 2001, p. 348.

Speight, J. G. Thermal cracking of Athabasca bitumen, Athabasca asphaltenes, and Athabasca deasphalted heavy oil. *Fuel* **1970**, *49*(2), 134-145.

Storm, D. A.; Barresi, R. J.; Sheu, E. Y.; Bhattacharya, A. K.; De Rosa, T. F. Microphase behavior of asphaltic micelles during catalytic and thermal upgrading. *Energy Fuels* **1998**, *12*(1), 120-128.

Stratiev, D.; Shishkova, I.; Tsaneva, T.; Mitkova, M.; Yordanov, D. Investigation of relations between properties of vacuum residual oils from different Origin, and of their deasphalted and asphaltene fractions. *Fuel* **2016**, *170*, 115–129.

Takamura, K. Microscopic structure of Athabasca oil sand. *Can. J. Chem. Eng.* **1982**, *60*, 538.

Wang, L.; Zachariah, A.; Yang, S.; Prasad, V.; De Klerk, A. Visbreaking oilsands-derived bitumen in the temperature range of 340-400 °C. *Energy Fuels* **2014**, *28*, 5014-5022.

Wang, L. Low Temperature Visbreaking. MSc Thesis, University of Alberta, Edmonton, AB, Canada, 2013.

Wiehe, I.A. *Process Chemistry of Petroleum Macromolecules*. Baton Raton: CRC Press, 2008.

Wiehe, I. A. Tutorial on resid conversion and coking, Proc. 2nd Intl. Conf. on refinery processing, AIChE 1999 Spring National Meeting, Houston, TX, March 14-18, 499-505.

Yan, Y. T. Characterization of visbreaker feeds. *Fuel* **1990**, *69*, (8), 1062–1064.

Yañez Jaramillo, L. M. Visbreaking of Oilsands Bitumen between 150 and 300 ˚C. MSc Thesis, University of Alberta, Edmonton, AB, Canada, 2016.

Yen, T. F.; Erdman, J. G.; Saraceno, A. J. Investigation of the nature of free radicals in petroleum asphaltenes and related substances by electron spin resonance. *Anal. Chem.* **1962**, *34*(6), 694-700.

Yen, T. F.; Wu, W. H.; Chilingar, G. V. A study of the structure of petroleum asphaltenes and related substances by proton nuclear magnetic resonance. *Energy Sources*, **1984,** *7*(3), 275-304.

Yen, T. F.; Tynan, E. C.; Vaughan, G. B.; Boucher, L. J. Electron spin resonance studies of petroleum asphaltics. In *Spectrometry of Fuels;* Friedel R.A. *Eds;* Springer, Boston, MA, **1970**; 187–201.

Yen, T. F.; Sprang, S. R. Contribution of ESR analysis toward diagenic mechanisms in bituminous deposits. *Geochim. Cosmochim. Acta* **1977**, *41*(8), 1007-1018.

APPENDICESS

APPENDIX A. Calculation of the deasphalted vacuum residue oil and thermal conversion product density using a 5 mL (+/- 0.03) Thomas Specific gravity bottle (glass pycnometer – Gay-Lussac type).

Measurements were performed following the standard test method for Density of Semi-Solid Bituminous Materials (ASTM D 70 – 09).

Sample name; Thermal conversion liquid product after 360 minutes at 320 °C (Sample Number 93)

Weigh of the empty Thomas Specific gravity bottle pycnometer; 12.1145 grams

Weigh of the sample; 2.072 grams

Total volume of the pycnometer; 5 ml

Calculation of Oil density at 20 °C

Total weigh of the pycnometer (oil+ de-ionized water+ empty pycnometer) at 20 °C; 17.2701 grams

Total weigh of the mixture = 17.2701 - 12.1145 = 5.1556 grams

$$\text{Density of the mixture (oil + deionized water) @ 20 °C} = \frac{Total\ weigh\ of\ the\ pycnometer - weigh\ of\ the\ empty\ pycnometer}{Total\ volume\ of\ the\ pycnometer}$$

$$\text{Density of the mixture (oil + deionized water) @ 20 °C} = \frac{17.2701 - 12{,}1145\ grams}{5\ ml}$$

$$\text{Density of the mixture (oil + deionized water) @ 20 °C} = 1.0155\ \text{g/ml}$$

Density of the deionized water at 20 °C; 0.9982 g/ml (from *Handbook of Chemistry and Physics 53rd Edition*. Chemical Rubber Pub)

Based on;

$$\text{Density of the mixture} = \rho_{oil} \times weight\ fraction\ of\ oil + \rho_{water} \times weight\ fraction\ of\ water \quad (1)$$

So the density of the oil can be calculated from equation 1,

$$\rho_{liquid\ conversion\ product\ @\ 20\,°C} = \frac{(\rho_{total} - \frac{weigh\ of\ deoinized\ water}{total\ weigh\ of\ the\ mixture} \times \rho_{water})}{\frac{weigh\ of\ oil}{Total\ weigh\ of\ the\ mixture}}$$

$$\rho_{liquid\ conversion\ product\ @\ 20\ °C} = \frac{(1.0155 - \frac{5.1556 - 2.072}{5.1556} \times\ 0.9982\ )}{\frac{2.072}{5.1556}}$$

$$\rho_{liquid\ conversion\ product\ @\ 20\ °C} = 1.0801 \frac{g}{ml} = 1080.1\ kg/m3$$

Calculation of Oil density at 40 °C

Density of the deionized water at 40 °C; 0.9922 g/ml (from *Handbook of Chemistry and Physics 53rd Edition*. Chemical Rubber Pub)

Total weigh of the pycnometer (oil+ de-ionized water+ empty pycnometer) at 40 °C; 17.2296 grams

Total weigh of the mixture = 17.2296 - 12.1145 = 5.1151 grams

$$\text{Density of the mixture (oil + deionized water) @ 40 °C} = \frac{Total\ weigh\ of\ the\ pycnometer - weigh\ of\ the\ empty\ pycnometer}{Total\ volume\ of\ the\ pycnometer}$$

$$\text{Density of the mixture (oil + deionized water) @ 40 °C} = \frac{17.2296 - 12{,}1145\ grams}{5\ ml}$$

$$\text{Density of the mixture (oil + deionized water) @ 40 °C} = 1.023\ \text{g/ml}$$

$$\rho_{liquid\ conversion\ product\ @\ 40\ °C} = \frac{(1.023 - \frac{5.1151 - 2.072}{5.1151} \times\ 0.9922\ )}{\frac{2.072}{5.1151}}$$

$$\rho_{liquid\ conversion\ product\ @\ 40\ °C} = 1.0683\ \frac{g}{ml} = 1068.3\ kg/m3$$

APPENDIX B. Scanning electron microscope results (SEM)

- Images taken and EDS results of 10 min, 60 min and 240 min reaction solids obtained during thermal conversion of DAO at 280 °C

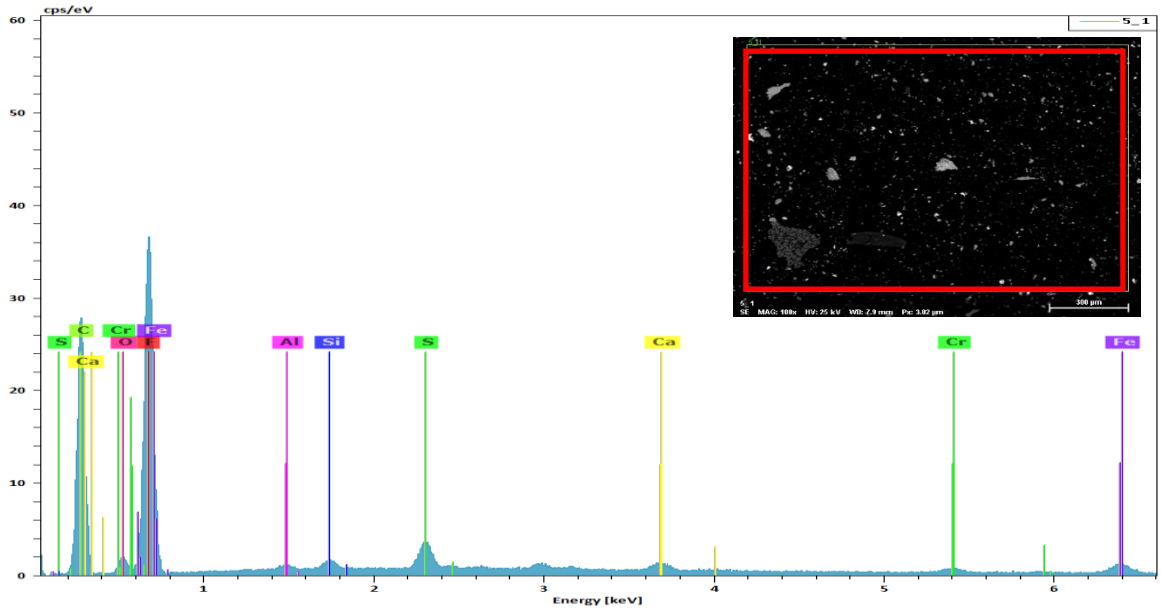

Spectrum	C	N	O	F	Na	Mg	Al	Si	S	Cl	Ca	Cr	Mn	Fe	Ni	Ag
5_ 1.spx (%)	49.85		3.69	43.54			0.17	0.23	0.90		0.38	0.30		0.93		

Figure B.1 SEM-EDX spectra of solids obtained from thermal conversion of DAO after 20 minutes at 280 °C. Magnification 100x

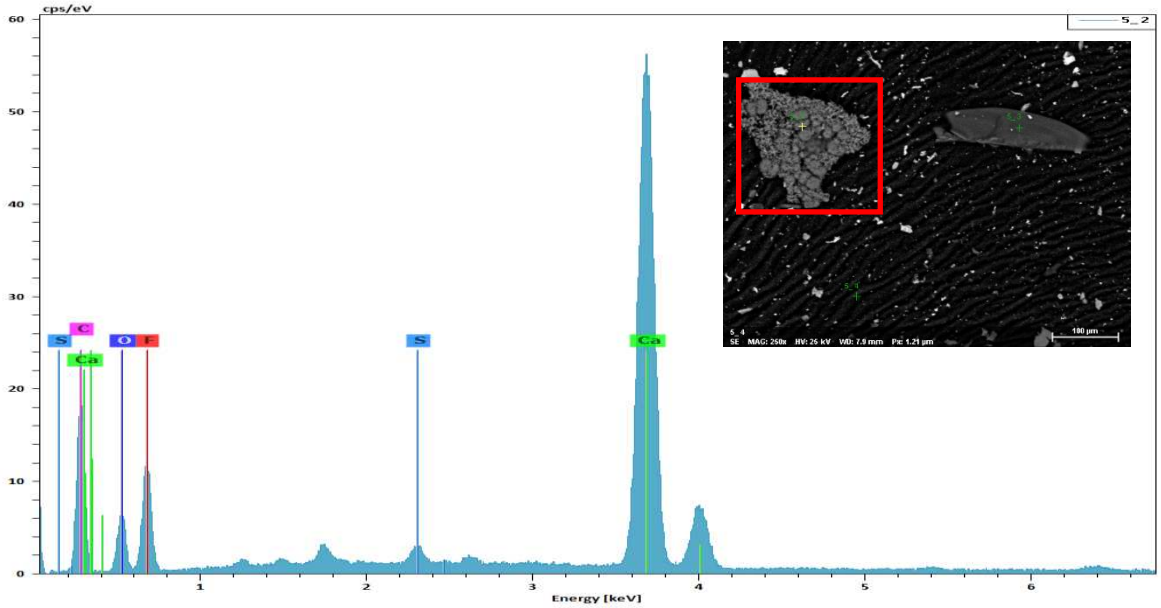

Spectrum	C	N	O	F	Na	Mg	Al	Si	S	Cl	Ca	Cr	Mn	Fe	Ni	Ag
5_ 2.spx (%)	32.48		18.66	24.37					0.53		23.97					

Figure B.2 SEM-EDX spectra of solids obtained from thermal conversion of DAO after 20 minutes at 280 °C. Magnification 250x

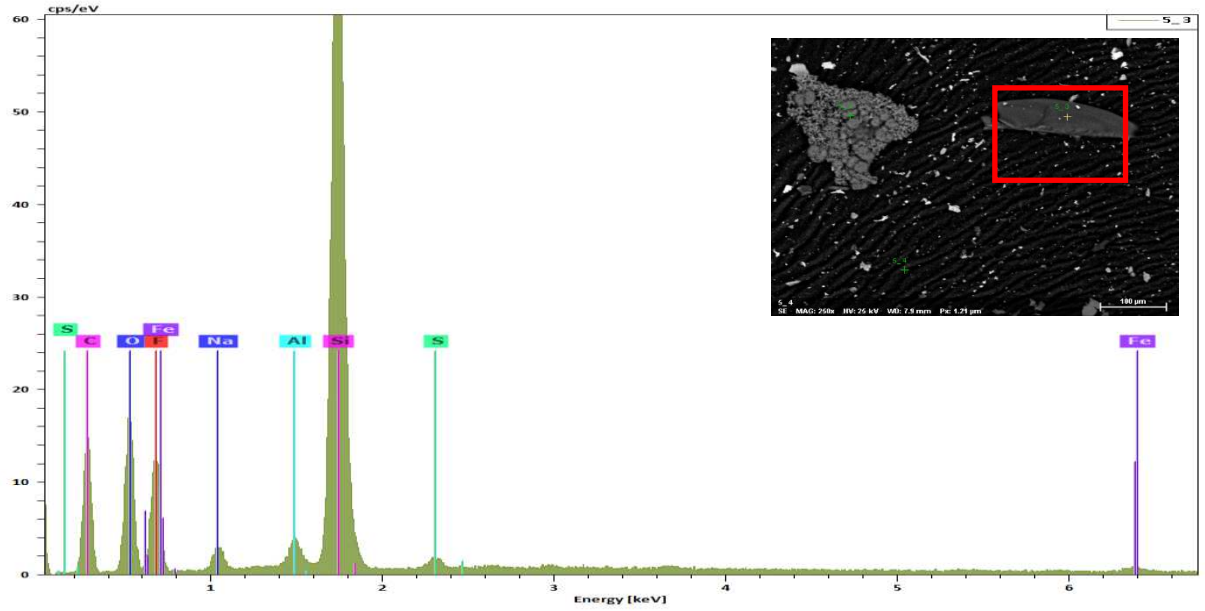

Spectrum	C	N	O	F	Na	Mg	Al	Si	S	Cl	Ca	Cr	Mn	Fe	Ni	Ag
5_ 3.spx (%)	36.74		26.01	17.87	1.43		0.80	16.42	0.41					0.31		

Figure B.3 SEM-EDX spectra of solids obtained from thermal conversion of DAO after 20 minutes at 280 °C. Magnification 250x

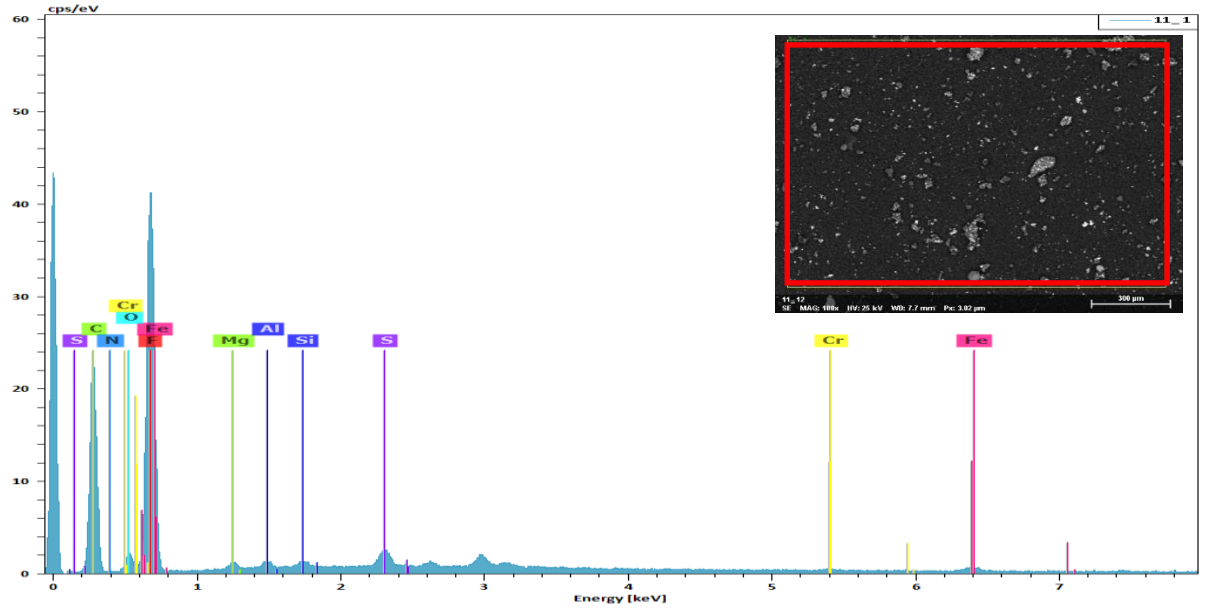

Spectrum	C	N	O	F	Na	Mg	Al	Si	S	Cl	Ca	Cr	Mn	Fe	Ni	Ag
11_ 1.spx (%)	44.21	1.81	4.24	47.88		0.38	0.26	0.17	0.57			0.11		0.38		

Figure B.4 SEM-EDX spectra of solids obtained from thermal conversion of DAO after 60 minutes at 280 °C. Magnification 100x

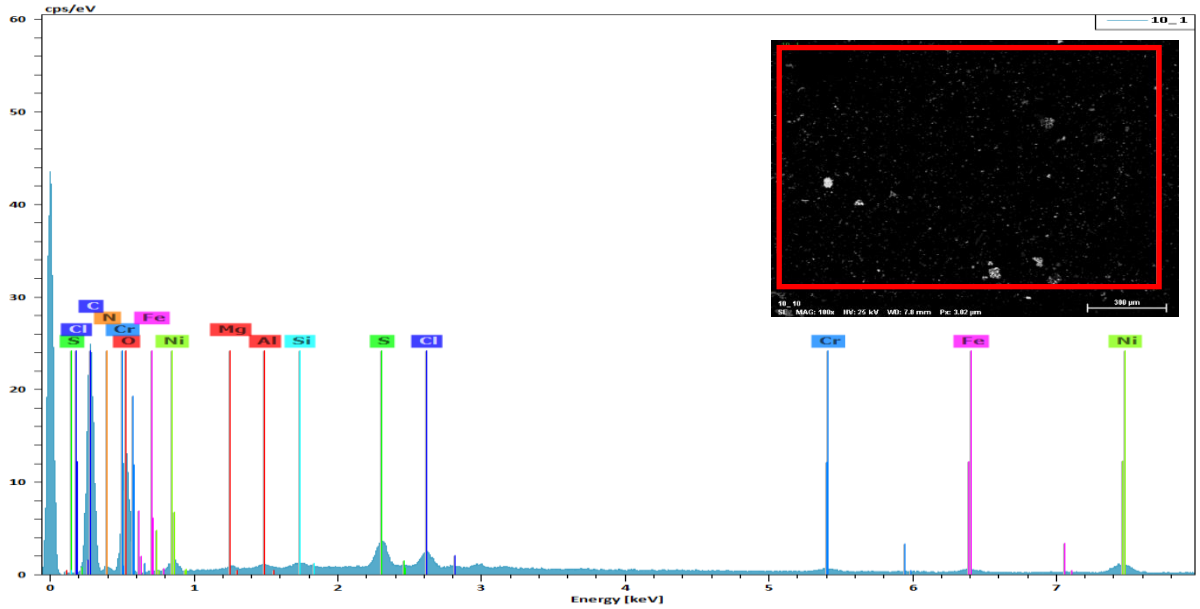

Spectrum	C	N	O	F	Na	Mg	Al	Si	S	Cl	Ca	Cr	Mn	Fe	Ni	Ag
10_ 1.spx (%)	43.90	2.23	21.16	16.61					5.20	0.41		1.28		6.19	3.03	

Figure B.5 SEM-EDX spectra of solids obtained from thermal conversion of DAO after 240 minutes at 280 °C. Magnification 100x

- Images taken and EDS results of 20 min, 120 min and 360 min reaction solids obtained during thermal conversion of DAO at 320 °C

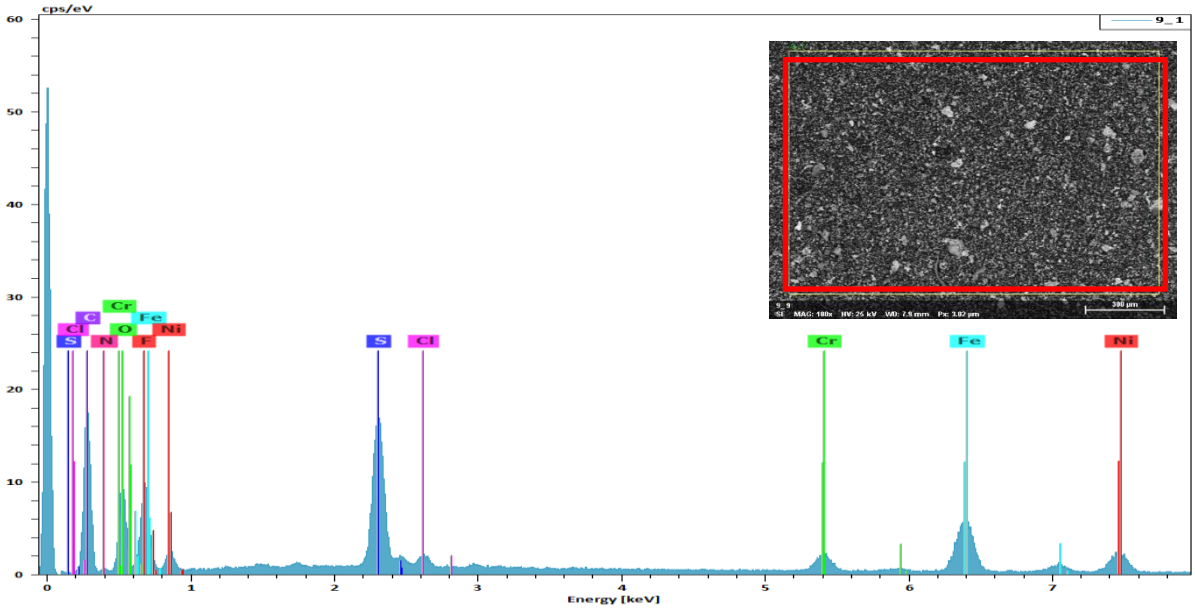

Spectrum	C	N	O	F	Na	Mg	Al	Si	S	Cl	Ca	Cr	Mn	Fe	Ni	Ag
9_ 1.spx (%)	43.90	2.23	21.16	16.61					5.20	0.41		1.28		6.19	3.03	

Figure B.6 SEM-EDX spectra of solids obtained from thermal conversion of DAO after 20 minutes at 320 °C. Magnification 100x

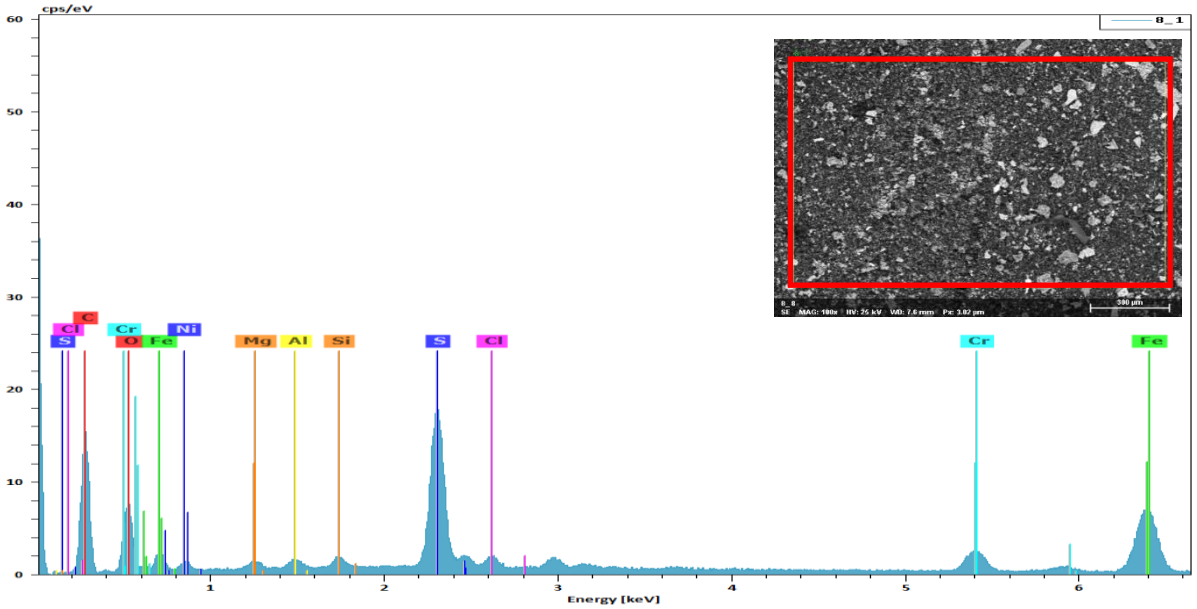

Spectrum	C	N	O	F	Na	Mg	Al	Si	S	Cl	Ca	Cr	Mn	Fe	Ni	Ag
8_ 1.spx (%)	52.47		24.38			0.59	0.57	0.38	6.70	0.50		2.16		10.00	2.25	

Figure B.7 SEM-EDX spectra of solids obtained from thermal conversion of DAO after 120 minutes at 320 °C. Magnification 100x

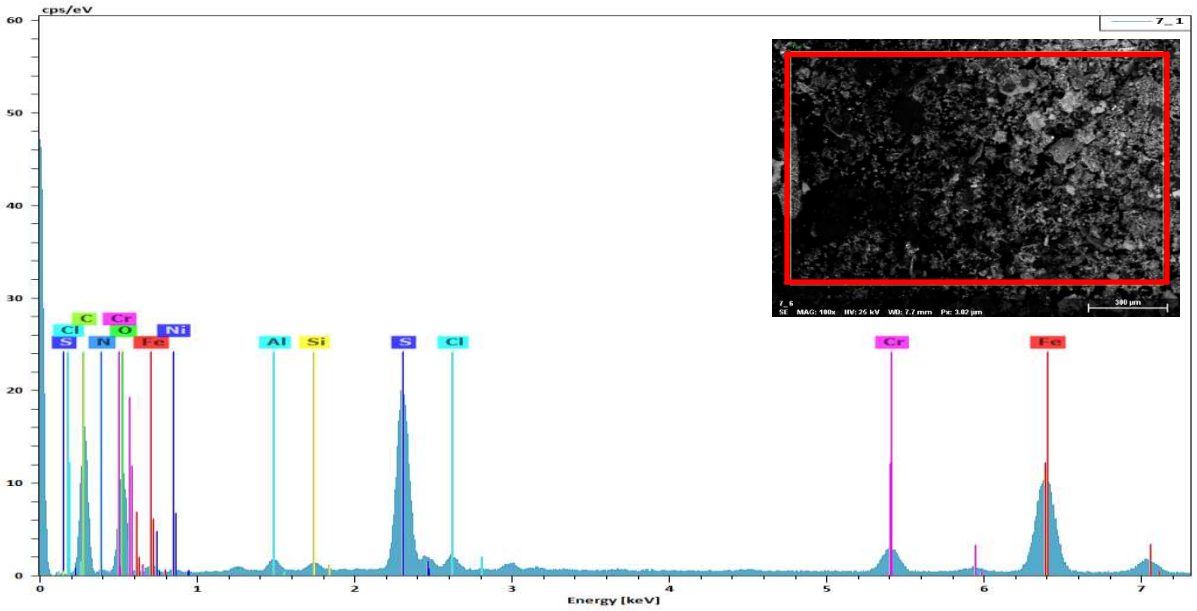

Spectrum	C	N	O	F	Na	Mg	Al	Si	S	Cl	Ca	Cr	Mn	Fe	Ni	Ag
7_ 1.spx (%)	44.04	3.48	28.47				0.64	0.27	8.05	0.61		1.73		11.17	1.53	

Figure B.8 SEM-EDX spectra of solids obtained from thermal conversion of DAO after 360 minutes at 320 °C. Magnification 100x

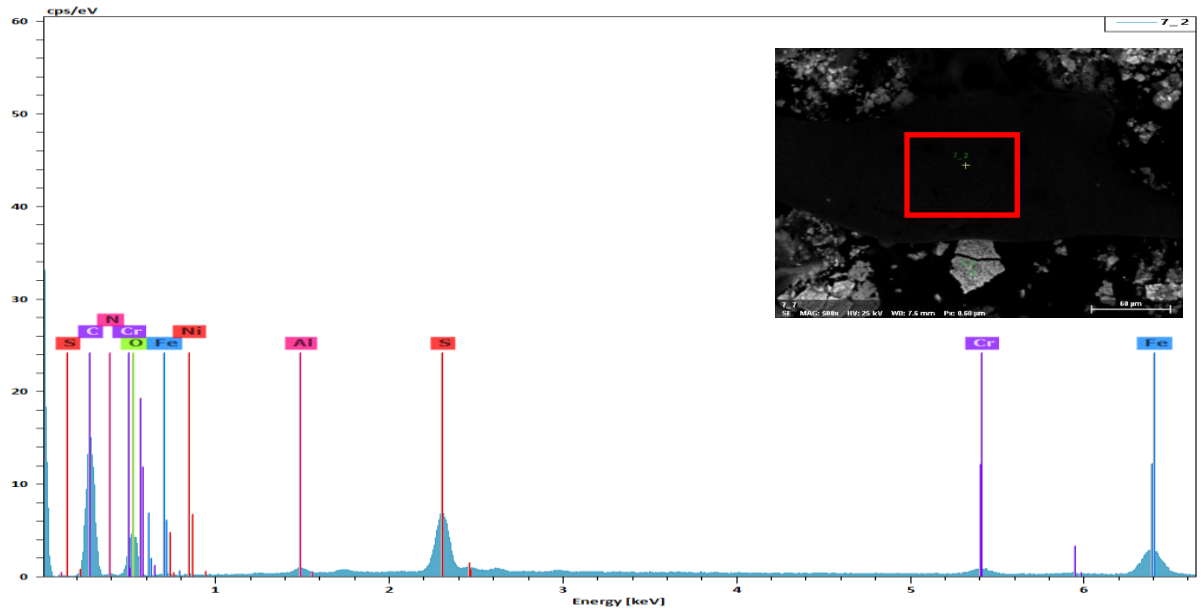

Spectrum	C	N	O	F	Na	Mg	Al	Si	S	Cl	Ca	Cr	Mn	Fe	Ni	Ag
7_2.spx (%)	57.17	3.54	27.50				0.62		4.40			0.74		5.26	0.78	

Figure B.9 SEM-EDX spectra of solids obtained from thermal conversion of DAO after 360 minutes at 320 °C. Magnification 500x

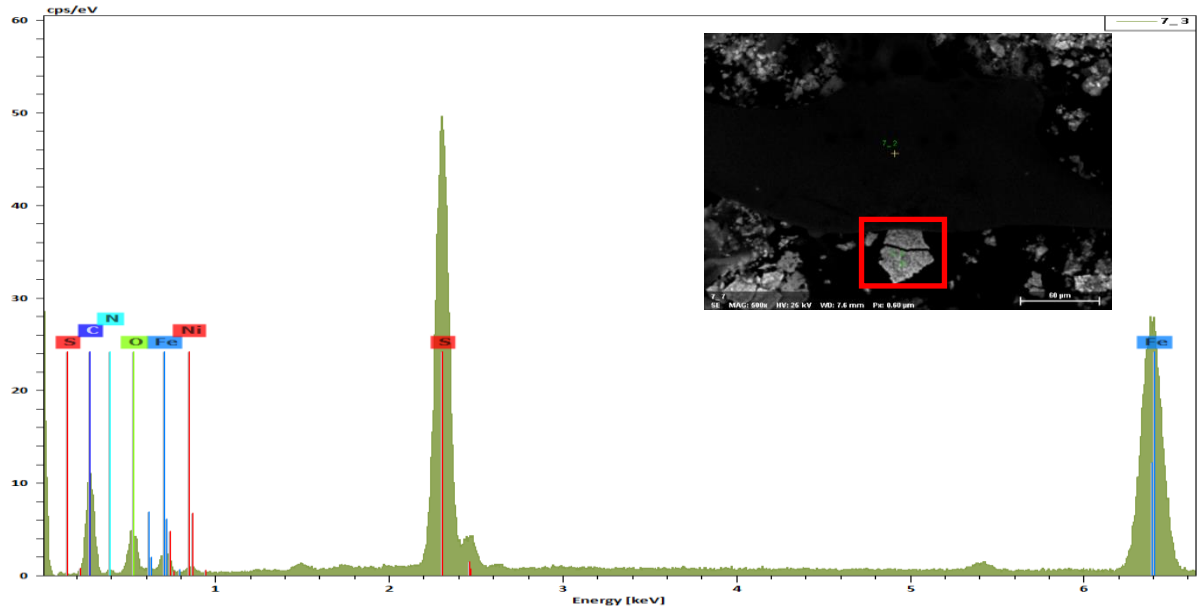

Spectrum	C	N	O	F	Na	Mg	Al	Si	S	Cl	Ca	Cr	Mn	Fe	Ni	Ag
7_3.spx (%)	40.36	1.23	11.04						19.26					25.14	2.98	

Figure B.10 SEM-EDX spectra of solids obtained from thermal conversion of DAO after 360 minutes at 320 °C. Magnification 500x

- Images taken and EDS results of 20 min, 120 min and 360 min reaction solids obtained during thermal conversion of DAO at 360 °C

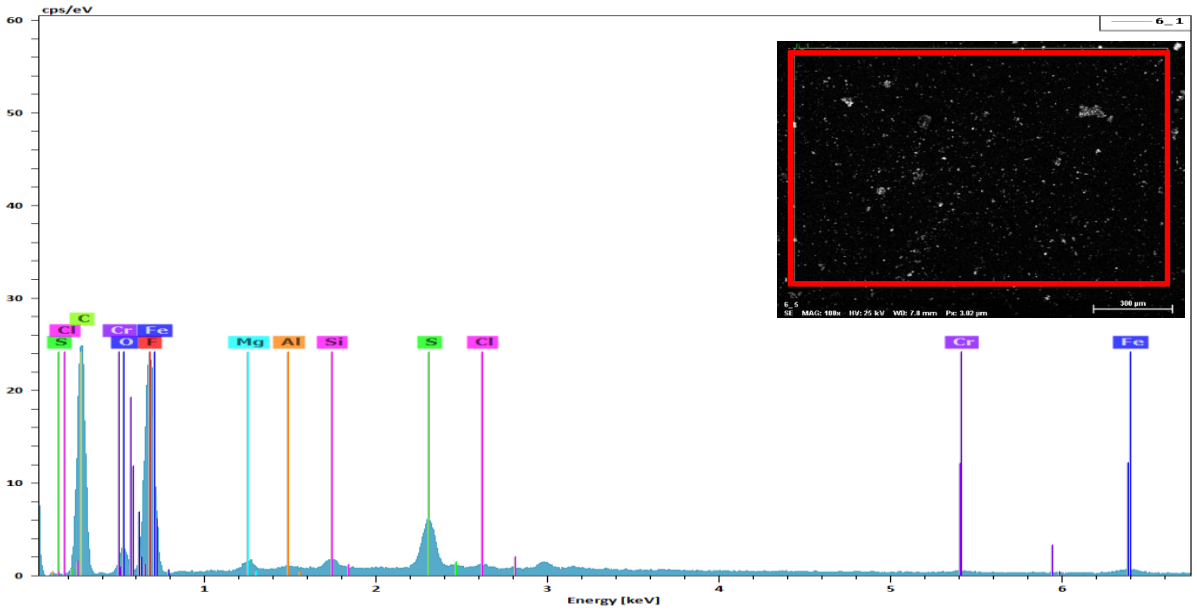

Spectrum	C	N	O	F	Na	Mg	Al	Si	S	Cl	Ca	Cr	Mn	Fe	Ni	Ag
6_ 1.spx (%)	52.67		7.54	36.46		0.45	0.11	0.23	1.85	0.16		0.12		0.42		

Figure B.11 SEM-EDX spectra of solids obtained from thermal conversion of DAO after 20 minutes at 360 °C. Magnification 100x

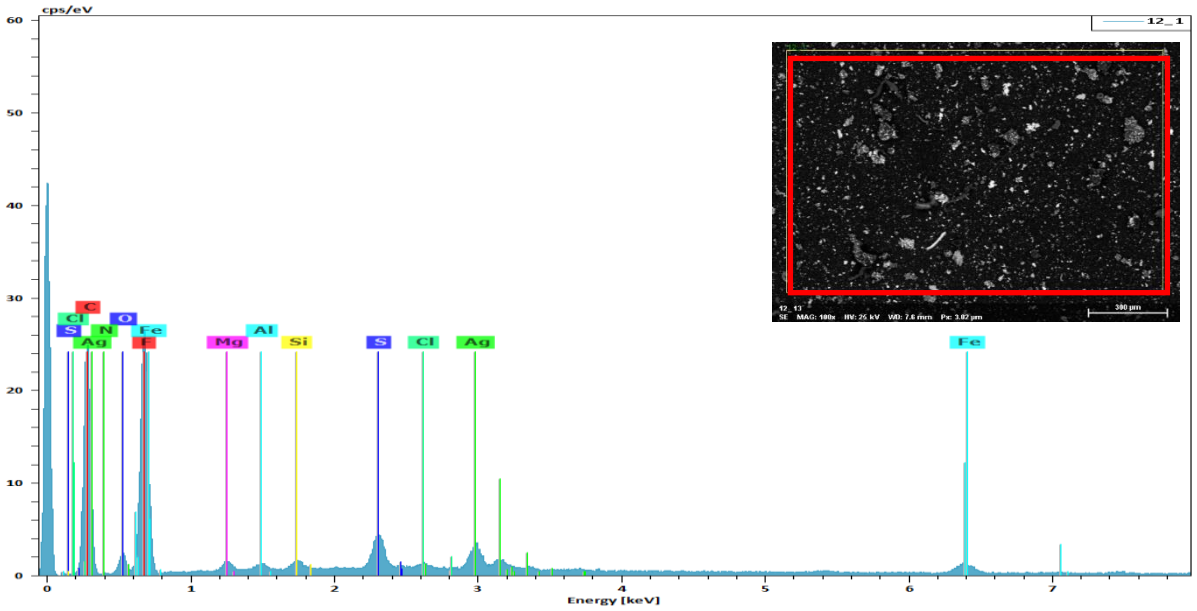

Spectrum	C	N	O	F	Na	Mg	Al	Si	S	Cl	Ca	Cr	Mn	Fe	Ni	Ag
12_ 1.spx (%)	48.40	1.63	5.21	38.24		0.56	0.31	0.27	1.45	0.18				1.25		2.51

Figure B.12 SEM-EDX spectra of solids obtained from thermal conversion of DAO after 120 minutes at 280 °C. Magnification 100x

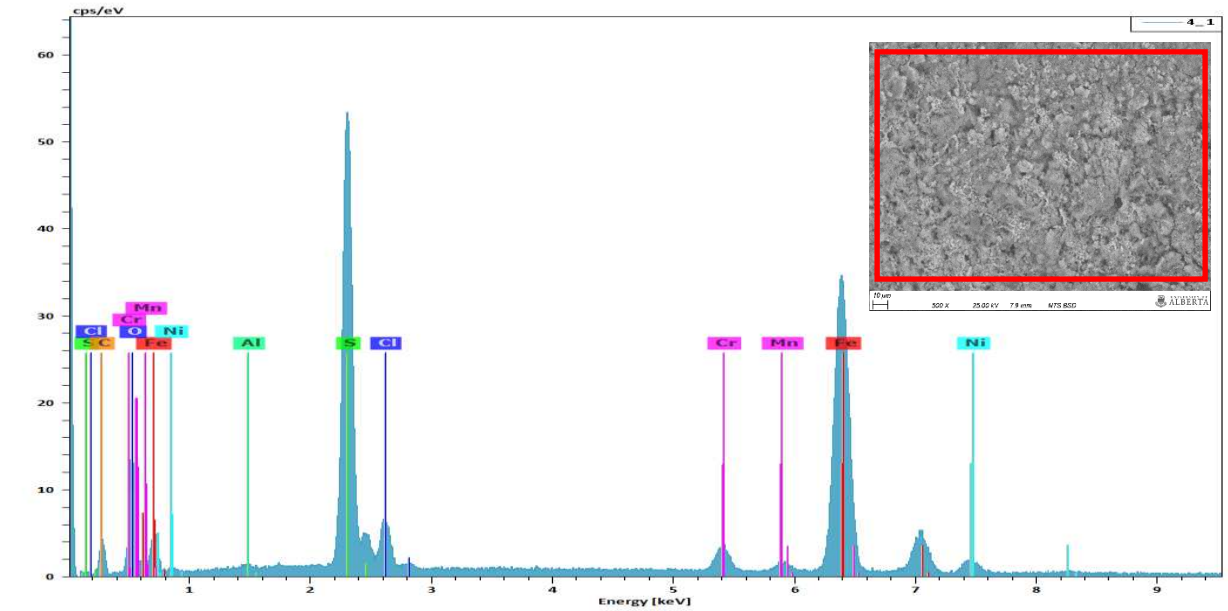

Spectrum	C	N	O	F	Na	Mg	Al	Si	S	Cl	Ca	Cr	Mn	Fe	Ni	Ag
4_ 1.spx (%)	16.25		21.80				0.21		19.51	2.66		1.98	0.47	34.89	2.22	

Figure B.13 SEM-EDX spectra of solids obtained from thermal conversion of DAO after 360 minutes at 280 °C. Magnification 500x

- Images taken and EDS results of 10 min, 45 min and 90 min reaction solids obtained during thermal conversion of DAO at 400 °C

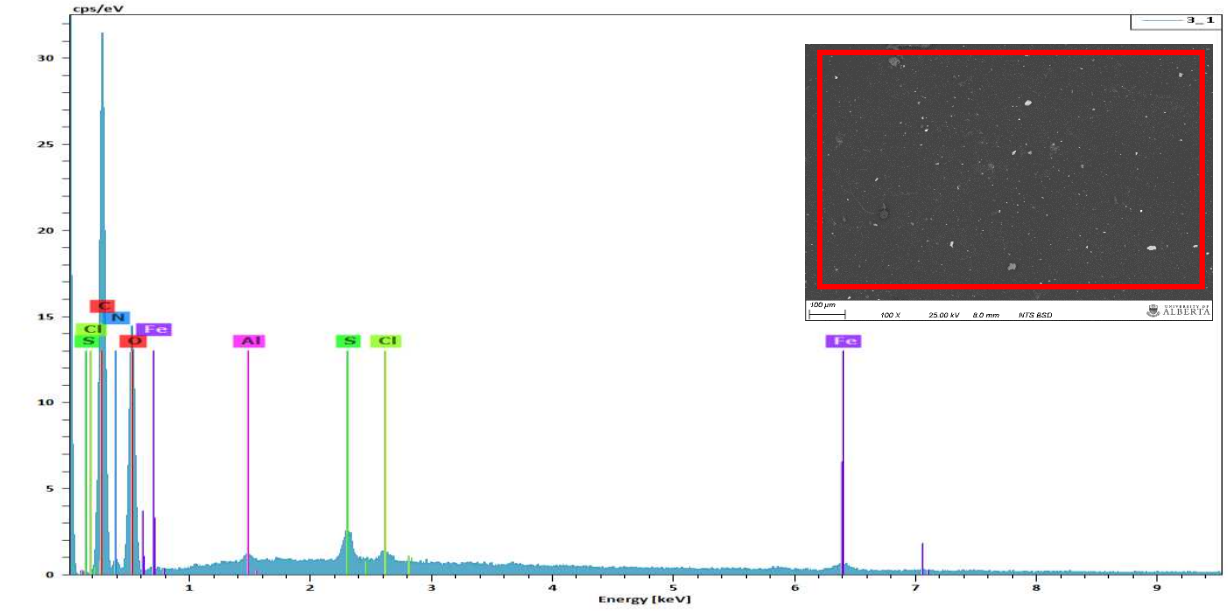

Spectrum	C	N	O	F	Na	Mg	Al	Si	S	Cl	Ca	Cr	Mn	Fe	Ni	Ag
3_ 1.spx (%)	49.15	6.83	42.59				0.14		0.63	0.24				0.43		

Figure B.14 SEM-EDX spectra of solids obtained from thermal conversion of DAO after 10 minutes at 400 °C. Magnification 100x

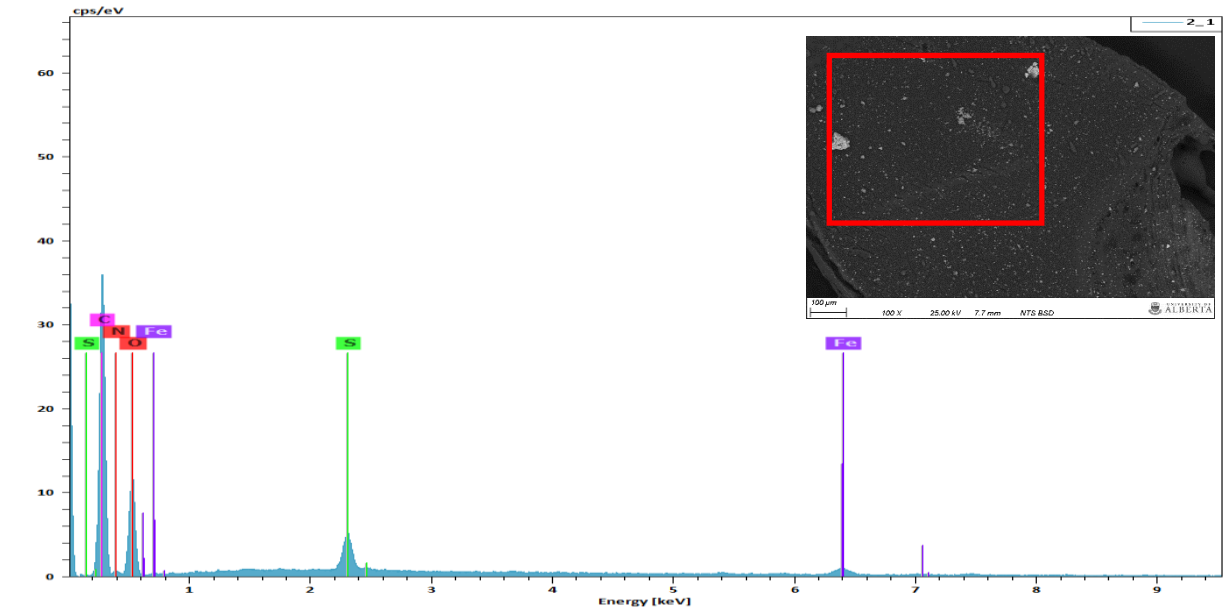

Spectrum	C	N	O	F	Na	Mg	Al	Si	S	Cl	Ca	Cr	Mn	Fe	Ni	Ag
2_1.spx (%)	55.54	5.93	36.26						1.39					0.88		

Figure B.15 SEM-EDX spectra of solids obtained from thermal conversion of DAO after 45 minutes at 400 °C. Magnification 100x

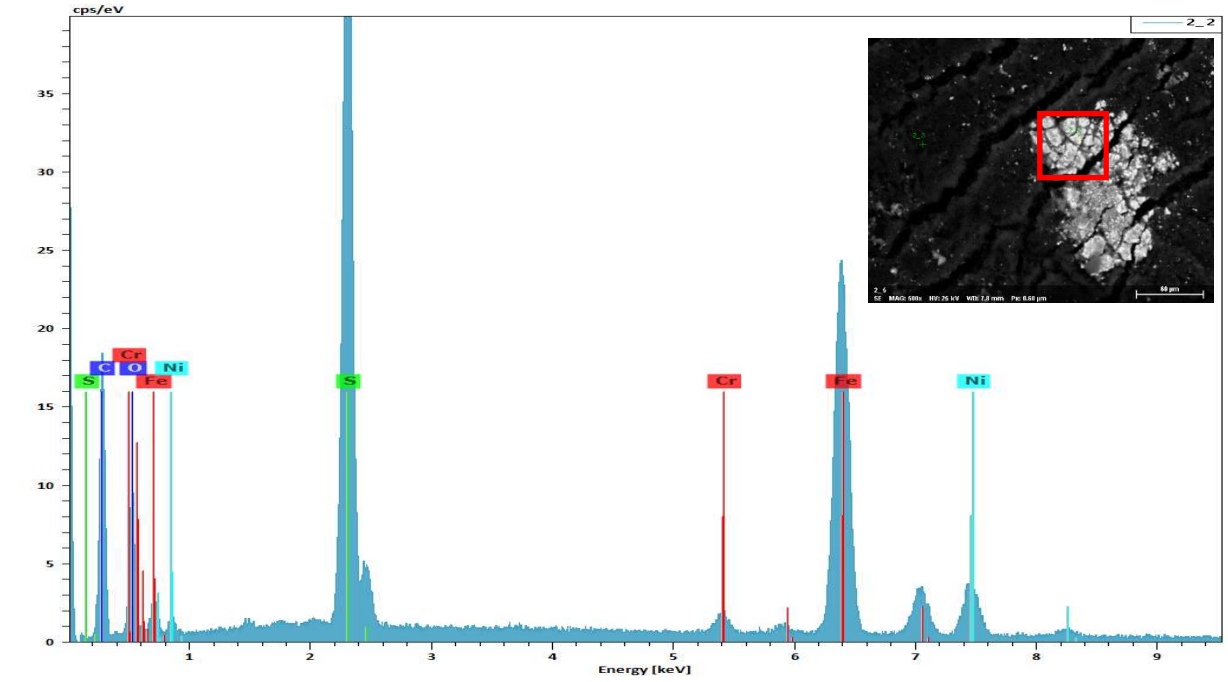

Spectrum	C	N	O	F	Na	Mg	Al	Si	S	Cl	Ca	Cr	Mn	Fe	Ni	Ag
2_2.spx (%)	45.56		17.05						14.06			0.61		19.07	3.65	

Figure B.16 SEM-EDX spectra of solids obtained from thermal conversion of DAO after 45 minutes at 400 °C. Magnification 500x

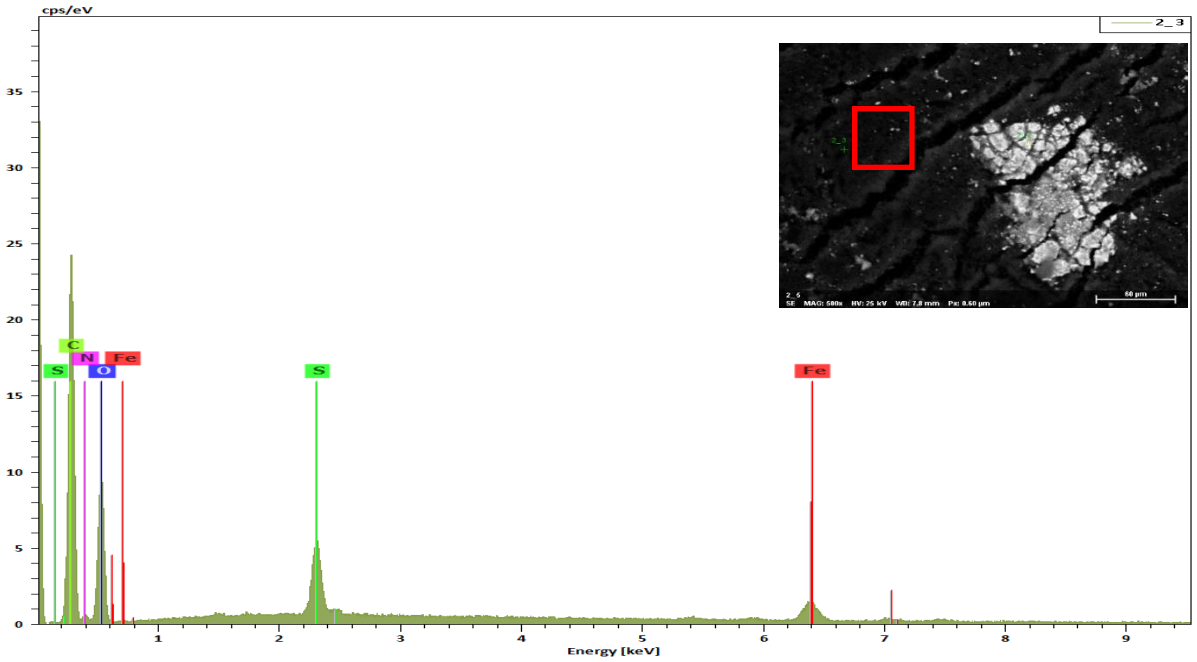

Spectrum	C	N	O	F	Na	Mg	Al	Si	S	Cl	Ca	Cr	Mn	Fe	Ni	Ag
2_ 3.spx (%)	52.81	6.39	36.90						2.18					1.72		

Figure B.17 SEM-EDX spectra of solids obtained from thermal conversion of DAO after 45 minutes at 400 °C. Magnification 500x

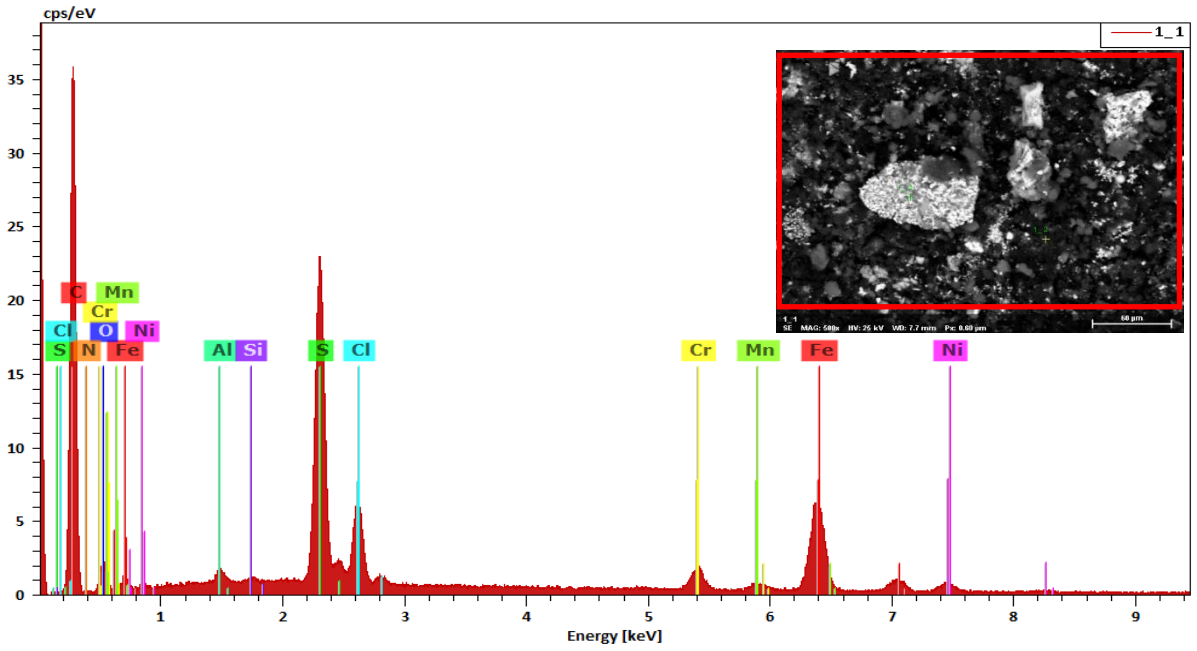

Spectrum	C	N	O	F	Na	Mg	Al	Si	S	Cl	Ca	Cr	Mn	Fe	Ni	Ag
1_ 1.spx (%)	74.09	3.05	6.75				0.25	0.04	5.66	1.82		0.96	0.17	6.44	0.77	

Figure B.18 SEM-EDX spectra of solids obtained from thermal conversion of DAO after 90 minutes at 400 °C. Magnification 100x

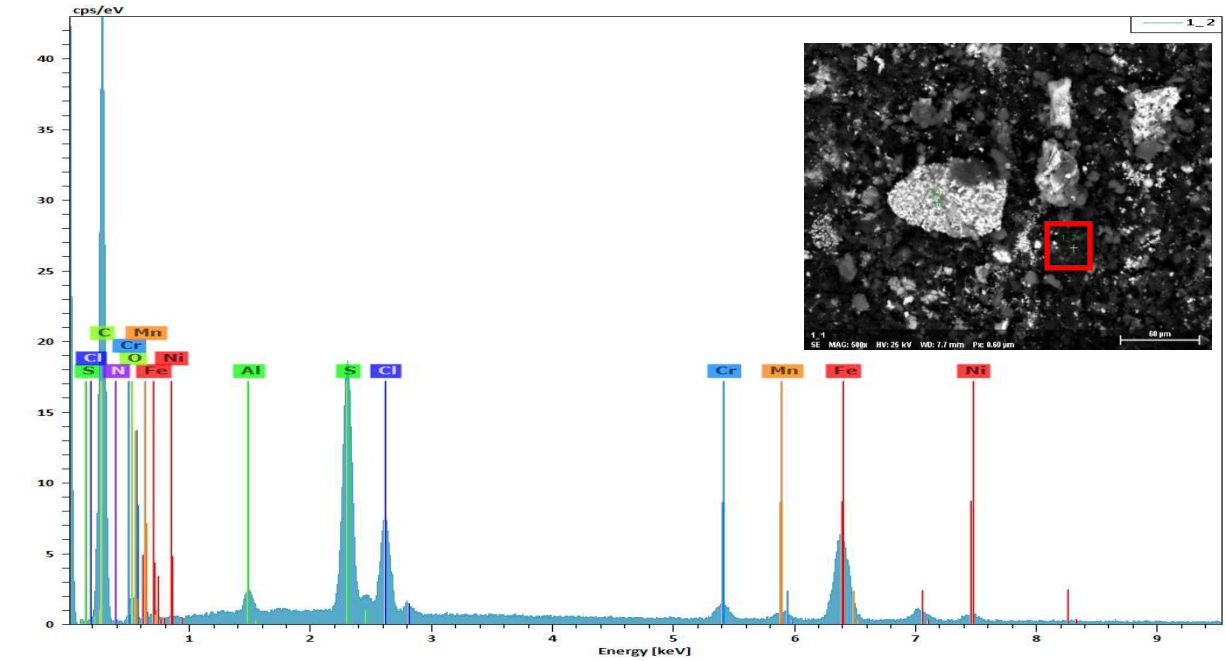

Spectrum	C	N	O	F	Na	Mg	Al	Si	S	Cl	Ca	Cr	Mn	Fe	Ni	Ag
1_ 2.spx (%)	76.71	2.96	6.11				0.46		4.35	2.04		0.66	0.27	5.86	0.57	

Figure B.19 SEM-EDX spectra of solids obtained from thermal conversion of DAO after 90 minutes at 400 °C. Magnification 500x

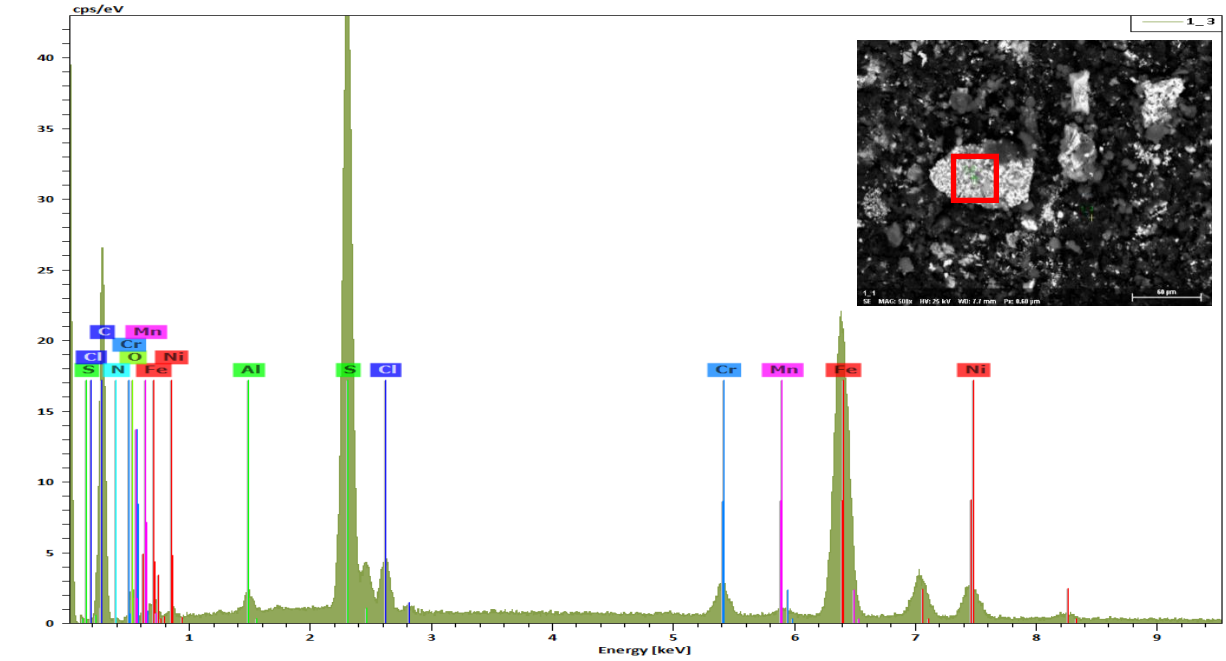

Spectrum	C	N	O	F	Na	Mg	Al	Si	S	Cl	Ca	Cr	Mn	Fe	Ni	Ag
1_ 3.spx (%)	60.32	1.32	4.89				0.49		12.23	1.18		1.07	0.15	15.89	2.45	

Figure B.20 SEM-EDX spectra of solids obtained from thermal conversion of DAO after 90 minutes at 400 °C. Magnification 500x

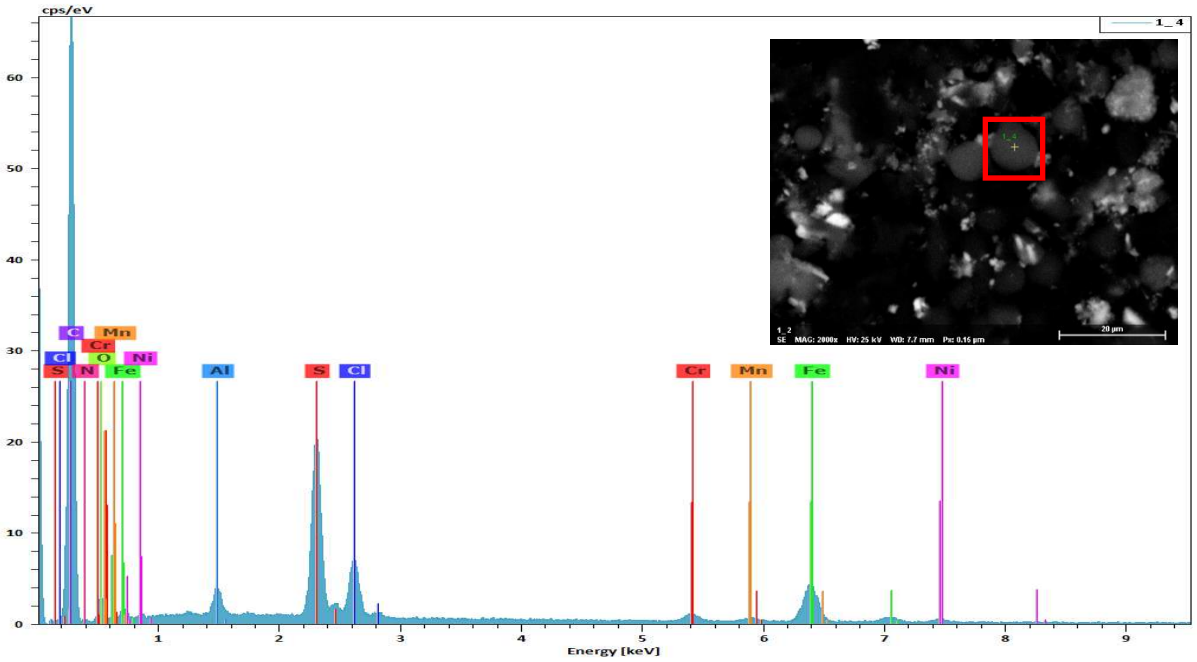

Spectrum	C	N	O	F	Na	Mg	Al	Si	S	Cl	Ca	Cr	Mn	Fe	Ni	Ag
1_ 4.spx (%)	79.99	3.70	7.27				0.48		3.56	1.41		0.36	0.14	2.81	0.28	

Figure B.21 SEM-EDX spectra of solids obtained from thermal conversion of DAO after 90 minutes at 400 °C. Magnification 2000x

APPENDIX C. ESR calculations

ESR calculations were made using the calculation spreadsheet elaborated by Dr. Arno De Klerk.

PROPERTY DATA

Name of calibration substance	**4-Hydroxy - TEMPO**
Properties of calibration substance:	
molecular mass (g/mol)	**172.25**
number of radicals per molecule	**1**
purity of substance (%)	**98**
Name of solvent for dilution	**toluene**
Properties of solvent for dilution:	
liquid density (g/mL)	**0.867**

Table C.1. ESR Calibration curve calculations using TEMPOL diluted in toluene

Mass of substance (mg)	Mass of solvent (g)		Concentration of substance (mg/mL)	Paramagnetic concentration (spins/mL)	Double integral area of spectrum (ESR area)
0.12	**86.70**		0.001	3.96E+15	**1793.0**
0.23	**86.70**		0.002	7.88E+15	**3322.7**
0.46	**86.70**		0.005	1.58E+16	**7038.3**
5.03	**86.70**		0.050	1.72E+17	**73524.7**
25.00	**86.70**		0.250	8.57E+17	**319561.7**
50.10	**86.70**		0.501	1.72E+18	**617214.6**
66.70	**86.70**		0.667	2.29E+18	**867443.6**

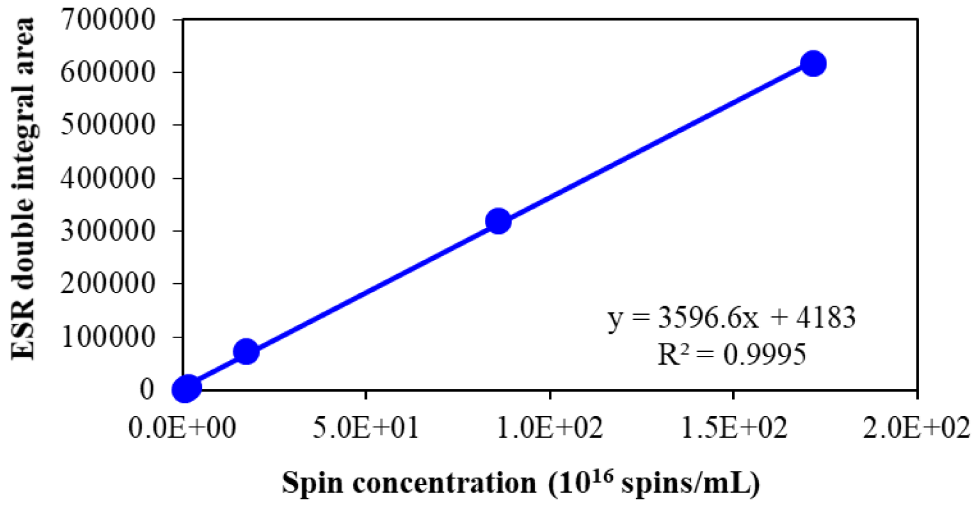

Figure C.1 Calibration curve double integral area vs free radical concentration; built using 4-hydroxy TEMPO, free radical (98+ %) at different concentrations diluted in toluene

The calibration curve is shown in a separate sheet. Although it was intuitive to plot the area obtained on the y-axis and the concentration that was the controlled variable on the x-axis, it is not the most useful way to express the calibration for determining unknown samples. The following format will therefore be adopted:

(spins/mL) = a.(ESR double integral area) + b	
Correlation coefficient, r^2	0.9989
Slope, a	2.69E+12
Intercept, b	-2.51E+15

The intercept has special meaning, because it is an estimate of the detection limit of the instrument. Thus, when no ESR signal is observed, it means that the concentration of paramagnetic species is below that limit.

The electron spin resonance (ESR) of the samples were obtained using an Active Spectrum' Micro ESR TM Electron Spin Resonance Spectrometer operating a nominal frequency 9.7 GHz. The figure C.1 shown the snapchat of Active Spectrum Micro – ESR software used to obtain the value of area in the spectrum related to the organic free radical after baseline correction.

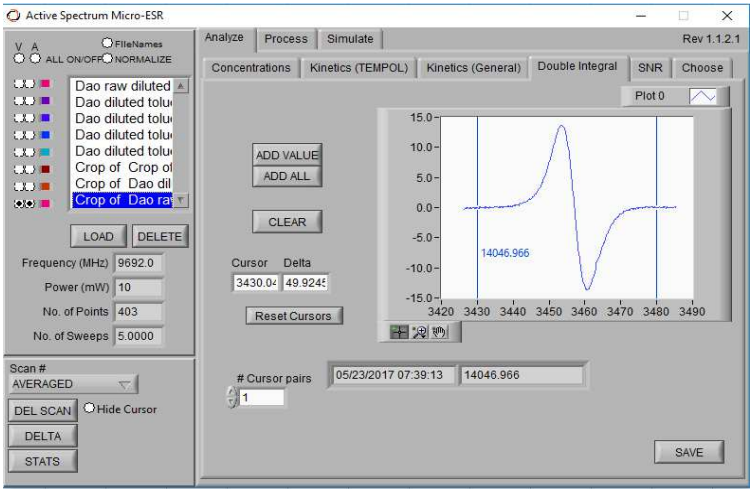

Figure C.2. Snapchat of Active Spectrum Micro- ESR software – Double integral calculation; Sample DAO diluted at 30 wt. % in toluene

Name of analyte	**Nexen Long Lake vacuum residue deasphalted oil**					
Name of solvent for dilution	**toluene**			Solute density (g/ml	**1.057**	
Properties of solvent for dilution: liquid density (g/mL)	**0.867**					
Mass of substance (mg)	Mass of solvent (g)	Concentration of analyte (mg/mL)	Double integral area of spectrum (ESR area)	Calculated spin concentration (spins/mL)	Analyte spin content (spins/g)	
254.23	**0.589**	276.479	**14046.97**	3.52E+16	1.27E+17	